Optimized Geometric and Electronic Wavefront Shaping with Line Source Arrays for Large-Scale Sound Reinforcement

vorgelegt von
Dipl.-Ing.
Florian Straube
geb. in Zerbst

von der Fakultät I – Geistes- und Bildungswissenschaften
der Technischen Universität Berlin
zur Erlangung des akademischen Grades

Doktor der Naturwissenschaften
- Dr. rer. nat. -

genehmigte Dissertation

Promotionsausschuss:

Vorsitzender:	Prof. Dr. Thorsten Roelcke
Gutachter:	Prof. Dr. Stefan Weinzierl
Gutachter:	Prof. Dr. Anselm Goertz
Gutachter:	Dr. Stefan Feistel

Tag der wissenschaftlichen Aussprache: 28.11.2018

Berlin 2019

Abstract

Line Source Arrays (LSAs) are used for large-scale sound reinforcement aiming at the synthesis of homogeneous wavefronts for the whole audio bandwidth. The deployed loudspeaker cabinets are rigged with different tilt angles and/or are electronically controlled in order to provide the intended coverage of the audience zones and to avoid radiation towards reflective ceilings, sidewalls or residential areas. In this thesis, different frequency domain optimization schemes for the geometric and electronic wavefront shaping with LSAs are revisited, compared and enhanced. For that purpose, an analytical approach for finding appropriate tilt angles of the LSA cabinets, denoted as polygonal audience line curving (PALC), and a mixed analytical-numerical approach for optimizing the individual loudspeakers' driving functions, referred to as line source array venue slice drive optimization (LAVDO), are introduced. LAVDO is meant to overcome the non-smooth frequency responses resulting from purely numerical frequency domain approaches without additional frequency-connecting constraints.

A mathematically explicitly formulated framework serves as basis for all calculations. This incorporates a modified complex-directivity point source (CDPS) model for ideal as well as measured loudspeaker data providing realistic sound pressure levels, an enclosed geometric model in order to exactly specify the source and receiver positions of the LSA configurations and the consideration of practical loudspeaker multiway designs with respect to the frequency crossover filters. Both straight and curved LSA configurations are analyzed for exemplary sound reinforcement venues. The results are evaluated with the help of a comprehensive set of graphical representations and technical quality measures for sound field as well as source-related characteristics. Finally, the conversion from optimized driving functions to practical finite impulse response (FIR) filters is considered.

Zusammenfassung

Line Source Arrays (LSAs) werden heutzutage typischerweise für Großbeschallungsaufgaben (z. B. bei Open-Air-Veranstaltungen, in Arenen und Stadien) eingesetzt, um möglichst homogene Wellenfronten im gesamten Audio-Frequenzbereich zu generieren. Die verwendeten Lautsprecherboxen werden zueinander angewinkelt und/oder geeignet elektronisch angesteuert, um wie beabsichtigt die Zuhörerbereiche zu beschallen und die Abstrahlung in Richtung reflektierenden Decken, Wänden und bewohnten Gebieten zu vermeiden. In dieser Dissertation werden verschiedene Verfahren im Frequenzbereich zur Optimierung der Geometrie und der elektronischen Ansteuerung von LSAs untersucht, verglichen und erweitert. Dazu werden ein analytischer Ansatz zum Finden geeigneter Neigungswinkel der LSA-Boxen, der als Polygonal Audience Line Curving (PALC) bezeichnet wird, und ein gemischt analytisch-numerischer Ansatz zum Optimieren der Treiberfunktionen der einzelnen Lautsprecher eingeführt. Das zuletzt genannte Verfahren wird Line Source Array Venue Slice Drive Optimization (LAVDO) genannt und soll glatte Frequenzgänge garantieren, die mit rein numerischen Frequenzbereichsmethoden ohne zusätzliche frequenzverbindende Randbedingungen in der Regel nicht oder nur mit erhöhtem Rechenaufwand realisiert werden können.

Ein mathematisch explizites Formelwerk dient als Grundlage für alle Berechnungen. Es umfasst ein angepasstes Complex-Directivity-Point-Source-Modell für ideale und gemessene Lautsprecherdaten, das realistische Schalldruckpegel liefert, sowie ein geschlossenes geometrisches Modell, um die Quellen- und die Empfängerpositionen der LSA-Anordnungen exakt zu spezifizieren, und es berücksichtigt den Mehrwegeaufbau von existierenden Lautsprechern in Form der Frequenzübergangsfilter. Sowohl gerade als auch gekrümmte LSA-Konfigurationen werden für typische Beschallungssituationen untersucht. Die jeweiligen Ergebnisse werden mit Hilfe einer umfassenden Sammlung von graphischen Darstellungen und technischen Qualitätsmaßen evaluiert, die sowohl Schallfeld- als auch quellenbezogene Eigenschaften zeigen. Auch die Überführung der optimierten Treiberfunktionen in einsetzbare Finite-Impulse-Response-Filter wird betrachtet.

List of Included Publications

This thesis is a cumulative dissertation. It contains the following publications that were authored and co-authored by the doctoral candidate given in chronological publishing order:

[1] Straube, Florian; Schultz, Frank; Weinzierl, Stefan (2015): "On the Effect of Spatial Discretization of Curved Line Source Arrays." In: *Fortschritte der Akustik: Tagungsband d. 41. DAGA*. Nuremberg, Germany, pp. 459 – 462.

[2] Schultz, Frank; Straube, Florian; Spors, Sascha (2015): "Discussion of the Wavefront Sculpture Technology Criteria for Straight Line Source Arrays." In: *Proc. of the 138th Audio Eng. Soc. Conv.*, Warsaw, Poland, #9323 --- peer-reviewed. Winner of the Audio Eng. Soc. 138th Convention Best Peer-Reviewed Paper Award.

[3] Straube, Florian; Schultz, Frank; Makarski, Michael; Spors, Sascha; Weinzierl, Stefan (2015): "Evaluation Strategies for the Optimization of Line Source Arrays." In: *Proc. of the 59th Audio Eng. Soc. Int. Conf. on Sound Reinforcement*, Montreal, Canada --- peer-reviewed.

[4] Straube, Florian; Schultz, Frank; Makarski, Michael; Weinzierl, Stefan (2016): "Optimized Driving Functions for Curved Line Source Arrays Using Modeled and Measured Loudspeaker Data." In: *Fortschritte der Akustik: Tagungsband d. 42. DAGA*. Aachen, Germany, pp. 1136 – 1139.

[5] Lemke, Mathias; Straube, Florian; Sesterhenn, Jörn; Weinzierl, Stefan (2017): "Adjungierten-basierte Schallfeldsynthese und Beschallung." In: *Fortschritte der Akustik: Tagungsband d. 43. DAGA*. Kiel, Germany, pp. 1422 – 1425.

[6] Straube, Florian; Bonillo, David Albanés; Schultz, Frank; Weinzierl, Stefan (2017): "Zur Optimierung der Kruemmung von Line Source Arrays." In: *Fortschritte der Akustik: Tagungsband d. 43. DAGA*. Kiel, Germany, pp. 1418 – 1421.

[7] Straube, Florian; Schultz, Frank; Bonillo, David Albanés; Weinzierl, Stefan (2017): "An Analytical Approach for Optimizing the Curving of Line Source Arrays." In: *Proc. of the 142nd Audio Eng. Soc. Conv.*, Berlin, Germany, #9699 --- peer-reviewed. Winner of the Audio Eng. Soc. 142nd Convention Best Peer-Reviewed Paper Award.

[8] Lemke, Mathias; Straube, Florian; Schultz, Frank; Sesterhenn, Jörn; Weinzierl, Stefan (2017): "Adjoint-Based Time Domain Sound Reinforcement." In: *Proc. of the 3rd Audio Eng. Soc. Int. Conf. on Sound Reinforcement – Open Air Venues*, Struer, Denmark --- peer-reviewed.

[9] Straube, Florian; Schultz, Frank; Bonillo, David Albanés; Weinzierl, Stefan (2018): "An Analytical Approach for Optimizing the Curving of Line Source Arrays." In: *J.*

Audio Eng. Soc., vol. 66, no. 1/2, pp. 4 – 20 (January/February), doi: https://doi.org/10.17743/jaes.2017.0043 --- peer-reviewed.

[10] Straube, Florian; Schultz, Frank; Makarski, Michael; Weinzierl, Stefan (2018): "Mixed Analytical-Numerical Filter Design for Optimized Electronic Control of Line Source Arrays." In: *J. Audio Eng. Soc.*, vol. 66, no. 9, pp. 690 – 702 (September), doi: https://doi.org/10.17743/jaes.2018.0043 --- peer-reviewed.

Content

1 Introduction

In this overview section, it is intended to summarize and link the research which is presented in the different scientific publications. Sec 1.1 contains the basic motivation for dealing with line source arrays for sound reinforcement within academic activities. Large-scale sound reinforcement fundamentals are revisited in Sec. 1.2. The individual scientific publications are connected in Sec. 1.3. In Sec. 1.4 the main objectives of this thesis are considered. A summary of achievements accomplished within the framework of the studies is incorporated in Sec. 1.5. Future research perspectives are discussed in Sec. 1.6.

1.1 Motivation

Line Source Arrays (LSAs) are used for large-scale sound reinforcement aiming at the synthesis of homogeneous wavefronts for the whole audio bandwidth. The deployed loudspeaker cabinets are rigged with different tilt angles and/or are electronically controlled in order to provide the intended coverage of the audience zones and to avoid radiation towards reflective ceilings, sidewalls or residential areas. For the optimization of the curving and the electronic control of LSAs for advanced sound reinforcement there is no standard procedure.

In practice both, a pure geometric and pure electronic wavefront shaping as well as combinations thereof are realized. Even state-of-the-art line array systems with extensive beam steering capabilities differ considerably (Scheirman, 2015). Since they comprise several individually controlled, small drivers, beam steering is nowadays feasible up to high audio frequencies. While the cabinets of some array systems are curved in addition to the beam steering, the cabinets of other systems are rigged as a straight line.

Before starting this dissertation work, there has been no enclosed theoretical framework to the author's knowledge which covered geometric and electronic wavefront shaping with respect to LSAs and large-scale sound reinforcement. Besides patents (Martin Audio Limited, 2006a, Martin Audio Limited, 2006b and SDA Software Design Ahnert GmbH, 2013), technical details for the wavefront shapings are only rarely published in some scientific contributions. From the author's point of view, a public scientific exchange would strongly contribute to find advanced and theoretically substantiated solutions using analytical and numerical optimization approaches for the geometric and electronic wavefront shaping. This is also due to strong similarities to related tasks such as multi-zone sound field synthesis or designing antenna arrays. Note that this dissertation does not deal with the loudspeaker cabinet engineering. It is presupposed that the performance quality of a single loudspeaker cabinet is well-engineered (Button, 2002).

This thesis was motivated by Schultz, 2016. Therein, it is intended to unify two approaches for characterizing the radiation of loudspeaker arrays which are aimed at generating homogeneous sound fields. This includes Wave Field Synthesis (WFS, Berkhout et al., 1992a and Berkhout et al., 1992b) for synthesizing the wavefronts of virtual sources based on the Helmholtz-Kirchhoff integral equation and the Wavefront Sculpture Technology (WST, Heil and Urban, 1992 and Urban et al., 2003) for reducing destructive interference and increasing

constructive interference between multiple loudspeakers based on the Fresnel approach and analytical derivations of the diffraction theory.

There was also the will for a mathematically formulated model based on analytical considerations which can be used as a basis for comparing different methods and for enhancements. With the intention to find analytical solutions as far as possible, this framework should cover the calculation model for sound field prediction, geometric and electronic wavefront shaping as well as the inclusion of modeled and measured loudspeaker data. Numerical techniques may only refine an analytically predetermined solution space excluding physically unfeasible solutions in advance and allowing for comprehensive control of the optimization parameters.

1.2 Large-Scale Sound Reinforcement

Large-scale sound reinforcement typically deals with large audiences, large venues and large loudspeaker setups. Since the number of considered audience positions is larger than the number of individual sources, an ill-posed inverse problem must be solved (Deschamps and Cabayan, 1972, Nelson, 2001 and Kim and Nelson, 2004). The sound field predictions are usually performed by means of the complex-directivity point source (CDPS) model (Feistel et al., 2009 and Meyer, 1984 and Meyer and Schwenke, 2003) of baffled piston far-field radiation patterns. Assuming that the horizontal radiation of the LSAs is convenient anyway, it is a common approach to reduce the considered venues to a two-dimensional slice representation for vertical radiation containing audience and non-audience positions.

The established Wavefront Sculpture Technology (WST) (Heil and Urban, 1992 and Urban et al., 2003) for grating lobe-free arrayability of sound sources incorporates five criteria how to create a homogeneous wavefront based on geometric LSA shaping. Thus, they are the fundamentals for proper beam shaping. They are based on the Fresnel approach and analytical derivations of the diffraction theory. WST includes the spatial sampling condition specifying the maximum allowed distance between adjacent sources and the Active Radiating Factor (ARF) theorem specifying the maximum relation of the pistons' dimensions to the fixed distance between the acoustic centers of adjacent sources. A further criterion defines the maximum allowed wavefront curvature at a waveguide's exit for high frequency radiation. The remaining criteria define the maximum allowed splay angle between adjacent LSA cabinets and an optimal array curvature to provide a homogenous and frequency independent sound pressure level (SPL) loss over the audience using an appropriate wavefront shape.

Gain and delay are the parameters – sometimes called excitation coefficients, feeding coefficients or driving functions/signals – which have to be ascertained for electronic optimization of the LSA radiation in frequency domain optimizations. They are typically computed separately for each frequency. These two parameters can be mathematically considered as the amplitude and as the phase of a complex frequency-dependent driving function. Approaches which disregard the phases are known as amplitude shadings such as Kaiser (Schmidmaier and Meyer, 1992) or Legendre shadings. The latter are established as constant beam width transducers (CBTs) in the context of curved loudspeaker arrays (Rogers

and Buren, 1978 and Keele, 2000). In favor of rather simple and easily applicable driving functions, however with limitations in the specification of the desired sound fields, the computational complexity is quite small. It also requires an adequate geometric adjustment, i.e., appropriate curving of the LSA boxes, in order to reinforce only the intended sections.

Least-squares optimization algorithms with Tikhonov regularization are frequently used in sound field synthesis applications for determining the loudspeakers' driving functions. They include methods such as the loudspeaker weight energy (LWE) method minimizing the spatial average error between the desired and the synthesized sound field imposing an energy constraint on the loudspeaker weights (Betlehem and Withers, 2012).

In the field of multi-zone sound field synthesis (MZSFS), the minimization of the spatial average error often comes along with an LWE-like constraint and is linked to the minimization of the sound pressure in the dark zone. The dark zone corresponds to the non-audience zone and the bright zone to the audience zone in large-scale sound reinforcement. These methods are denoted as pressure matching or spatial error optimization with brightness control (BC). Alternatively, the error minimization is linked to the acoustic contrast control (ACC), i.e., maximizing the ratio of the average sound pressure in the bright and in the dark zones (Choi and Kim, 2002, Cai et al., 2014 and Coleman et al., 2014). Although these approaches incorporate the deviant array radiation depending on the different zones, the driving functions of each loudspeaker cannot be individually controlled. So far, they have been widely used for small arrays as well as for small receiver areas with simple segmentations of the bright and the dark zones and without the need of providing high SPLs over a large area.

In the context of LSA optimization, a least-squares algorithm has been extended by spatial weighting for the control positions and measures to make the driving robust against small deviations of the LSA characteristics. The precise procedure, however, has not been documented (Beuningen and Start, 2000).

Genetic algorithms have also been used for calculating appropriate loudspeaker driving signals (Terrell and Sandler, 2010). These schemes suffer from a reduced solution space as they are based on predetermined sets of parameters. Depending on the extent of these sets, however, they provide rather non-complex solutions and exhibit very low computational load.

Recent – mostly proprietary – software such as Martin Audio Display, EAW Resolution 2, d&b ArrayCalc and AFMG's FIRmaker offer (numerical) optimization schemes for the electronic drive as well as automatic splay methods for the LSA curving. These approaches yield considerable improvements with respect to homogeneous audience coverage and/or avoidance of high side lobe energy compared to manually adjusted setups. However, the algorithms and their parametrization are rarely publicly documented in research papers (Thompson, 2008, Thompson 2009, Thompson et al., 2011 and Feistel et al., 2013). In the cited research papers, approaches with several optimization objectives are used. These different objectives can either be summed including specified weights – which results in a scalar objective function – or they can be written as vector, also with specified weights for the

different objectives, e.g., within the multiobjective goal attainment approach (Gembicki and Haimes, 1975). The objectives are multivariable functions incorporating the loudspeakers' drives as variables. They comprise the optimization goals, such as the error between the desired and the generated sound field or the ratio of the SPLs in the audience and in the non-audience zones.

Patents contain technical details on the general optimization scheme and the objective functions (Martin Audio Limited, 2006a, Martin Audio Limited, 2006b and SDA Software Design Ahnert GmbH, 2013). In Koehler, 2013 the whole optimization scheme following a pre-stage of SDA Software Design Ahnert GmbH, 2013 is described and analyzed. Optimization results based on simulations and measurement are presented.

Wave field synthesis (WFS) as an approach for synthesizing wavefronts within a target listening plane using a contour of loudspeakers has also been proposed as a large-scale sound reinforcement technique (Berkhout et al., 1992a, Vries et al., 1994, Start, 1996 and Vries, 1996). Recently, in Firtha et al., 2017 the referencing schemes of so called traditional WFS (Vries, 1996 and Start, 1997) and revisited WFS (Spors et al., 2008 and Ahrens, 2012) were classified into a unified framework for the derivation of 2.5D WFS driving functions, i.e., the individual loudspeakers' driving functions. Using this framework, the derivation of arbitrary referencing functions and thus reference curves is feasible also for curved loudspeaker contours, such as LSAs.

In Schultz, 2016, WFS is reintroduced as a wavefront shaping control technique using LSAs for large-scale sound reinforcement. WFS of a virtual directional point source with a far-field radiation pattern (FRP) adapted to the intended SPL coverage together with referencing to a specific audience position is regarded for straight and curved LSAs (Schultz, 2016, Ch. 4.). By applying the reference curve to the desired audience line and by applying the FRP of the virtual source to the audience line, the sound field homogeneity can be further improved (Schultz et al., 2017).

Regarding the curving of LSAs, the performance and the characteristics of the standard curving schemes straight, arc, J and progressive are discussed in Ureda, 2001 and Ureda, 2004. In Thompson, 2006, Thompson, 2009 and Thompson et al., 2011, the LSA cabinet tilt angles are determined by numerical optimization methods, cf., Martin Audio Limited, 2006a, Martin Audio Limited, 2006b, which are also applied for the electronic optimization.

1.3 Geometric and Electronic Wavefront Shaping with Line Source Arrays

In this section, the scientific work of the author is discussed, interpreted and linked on the basis of the published conference, convention and journal articles. Due to the practical engineering orientation of the topic at hand and the main origin of the reference literature, the papers and articles were primarily submitted to the Audio Engineering Society. Additional studies were also presented at the annual meeting of the German Acoustical Society. The section is thematically divided into the electronic wavefront shaping, the geometric wavefront

shaping and additional research on the Wavefront Sculpture Technology criteria as well as the adjoint-based approach.

1.3.1 Electronic Wavefront Shaping

"On the Effect of Spatial Discretization of Curved Line Source Arrays" [1] was the initial publication in March 2015. In this contribution, it is examined whether the widely accepted CDPS model for sound field prediction is applicable for the examination of geometric and electronic optimization approaches. Based on the CDPS calculations, the results for two LSA setups with modeled circular and line pistons are compared with respect to the spatial discretization and the tilt effects of a curved, uniformly driven LSA. One LSA uses rather large waveguides for high frequency (HF) radiation and the other one consists of a larger amount of sources which are smaller. The evaluation is performed by means of position index plots (PIPs) and far-field radiation patterns (FRPs).

It is concluded that CDPS with modeled data is suitable for developing and analyzing different optimization approaches although there may be other models or even measured LSA data closer matching actual LSA sound fields. More visualizations and technical quality measures are demanded for a comprehensive and more profound evaluation of the LSA loudspeaker and the generated sound field characteristics. In this paper [1], also generalized formulae for the positioning of the LSA boxes and loudspeakers are given. They are based on the formulae for the progressive curved arrays (Ureda, 2001 and Ureda, 2004) which are revised for convenient usage.

For the 59th Audio Engineering Society International Conference on Sound Reinforcement in July 2015, enhanced visualization techniques and adequate technical quality measures for characterizing the performance of LSAs are recommended in [3]. Least-squares optimizations with Tikhonov regularization following the loudspeaker weight energy (LWE, Betlehem and Withers, 2012) method are conducted for determining the individual loudspeakers' driving functions. This approach which is known from sound field synthesis applications is deployed for one common concert venue geometry and for two fictitious LSA setups differing in the number of sources for high frequency radiation. The calculations are based on CDPS with modeled piston data.

In addition to the PIP and the FRP from [1], the LSA and the sound field characteristics are visualized by means of the sound pressure level distribution over space for certain frequencies (SPLxy), the frequency responses of all audience positions (FAP) as well as the driving function index plots (DFIPs) as magnitude and group delay spectra for the driving functions of each loudspeaker. The proposed technical quality measures comprise (i) the absolute and (ii) the relative error between the synthesized and the desired sound field, (iii) the relation of the obtained average sound pressure levels of the audience and the non-audience zones, also known as acoustic contrast, (iv) a frequency dependent distribution measure of the level difference between the desired and the obtained sound field as well as (v) two source related distribution measures specifying the frequency- and the source-dependent load balance of the individual loudspeakers.

The LWE optimizations unveil obvious drawbacks of this approach. Since it is not possible to set constraints on the individual loudspeakers' driving functions, only on the squared sum of several driving functions, the loudspeakers are unevenly controlled. It is recommended to present and discuss the proposed visualizations and technical quality measures in combination for a full, in-depth and convenient interpretation of sound reinforcement with LSAs. The suggested technical quality measures should be included as goals and constraints for future optimization approaches.

Measured loudspeaker data are incorporated in [4] which was presented at the annual meeting of the German Acoustical Society in 2016. The multiobjective goal attainment approach (Gembicki and Haimes, 1975) is used for optimizing the individual driving functions of modeled and measured loudspeakers. To include the loudspeaker data from vertical directivity and sensitivity measurements and to consider multiway loudspeaker cabinets, the CDPS model is adapted. The sound field prediction is explicitly divided into separate frequency bands for the low, the mid and the high frequency range with frequency crossover filters as a part of the driving functions. A loudspeaker sensitivity standardization – considering the sound pressure levels in 1 m distance of the single sources – is introduced in order to obtain realistic sound pressure levels for the CDPS predictions with modeled and measured loudspeaker data and in order to allow their comparison. One LSA setup is analyzed for a typical concert venue geometry.

With the help of the PIPs, the FRPs and the DFIPs for the magnitudes, the advantages of the multiobjective goal attainment approach over the least-squares optimization with Tikhonov regularization are shown. This multiobjective optimization method allows to pursue different optimization goals and to set linear as well as non-linear constraints on the individual amplitudes and phases of the driving functions. Since the optimization results are quite similar for the modeled and the measured loudspeaker data, it is concluded that modeled LSA data are more beneficial for the design and the evaluation of appropriate LSA optimization strategies than measured directivities. For further improvement, the authors propose additional goals and constraints for the multiobjective goal attainment approach and/or subsequent post-processing in order to obtain smooth magnitude frequency and smooth phase frequency responses for the practical finite impulse response (FIR) filter design. Also numerical refinement of initial solutions, in this case amplitude shadings, has already been considered as a possible future solution.

A mixed analytical-numerical approach, referred to as line source array venue slice drive optimization (LAVDO), is, thus introduced in [10] for determining the individual loudspeakers' driving functions. It is meant to overcome the non-smooth frequency responses resulting from purely numerical frequency domain optimization approaches without additional frequency-connecting constraints. Therefore different numerical optimization schemes for the driving functions are compared including the least-squares optimization with Tikhonov regularization already used in [3], the multiobjective goal attainment approach already used in [4] and the proposed LAVDO. The CDPS model with measured loudspeaker data is utilized for one LSA setup in straight and in curved configuration for an elementary

concert venue. Goals for the optimizations are set for the control positions within the vertical radiation plane of an LSA representing audience and non-audience positions. A collection of the previously deployed visualizations and technical quality measures serve as basis for the evaluation.

The introduced LAVDO approach consists of finding adequate initial solutions based on analytical far-field considerations and of a subsequent numerical refinement by means of the multiobjective goal attainment approach optimizing curve fitting parameters across broad frequency ranges. LAVDO ensures smooth frequency responses as the magnitudes and the phases are separately fitted to predetermined curves before the numerical stage. Since the numerical refinement does not operate frequency-wise and since the calculation of the initial solutions is based on analytical considerations excluding physically unfeasible solutions in advance and allowing broad parameter control, extensive post-processing or re-optimizations can be avoided. Therefore, LAVDO is more application-oriented, more robust and lower computational than the considered least-squares optimization with Tikhonov regularization and the pure multiobjective goal attainment approach.

Comparing the generated sound fields of the straight and of the curved LSA setup, the optimization results show that the desired sound fields can be realized for both configurations. If the array is not geometrically adapted to the audience zone, small source distances – i.e., a large amount of small sources – are, however, necessary for allowing beam steering up to the highest audio frequencies. Therefore, it is reasonable to find a meaningful mix of geometric and electronic wavefront shaping using LSAs for practical realizations with respect to technical and economical reasons. The electronic influence and hence the applied optimization algorithms can be kept to a manageable level if the LSA is appropriately geometrically adapted to the sound reinforcement area.

The article [10] also covers the transform from the calculated individual loudspeakers' driving functions to practical FIR filters considering linearly-spaced measurement frequency vectors and logarithmically-spaced optimization frequency vectors. Smooth amplitude and smooth phase frequency responses are necessary in order to obtain moderate filter lengths and to deal with uncertainties of the measurement data (Feistel and Ahnert, 2007) and of the geometric source-receiver configuration.

As future work, it is indicated to add further LAVDO optimization goals and to combine all the goals within the numerical computation so that an absolute weighting between the different goals is possible. WFS based initial solutions instead of the initial solutions found by far-field considerations and verification by means of hands-on measurements are also mentioned as successive tasks.

1.3.2 Geometric Wavefront Shaping

The geometric wavefront shaping using LSAs for sound reinforcement is considered in contribution [6] which was presented at the 2017 meeting of the German Acoustical Society and in [7] which was presented at the 142nd Audio Engineering Society Convention in May

2017. Since the latter was decorated with the AES 142nd convention best peer-reviewed paper award, the paper was extended for publication in the Journal of the Audio Engineering Society [9].

For finding appropriate LSA cabinet tilt angles with respect to the geometry of the receiver area and the intended coverage, the analytical polygonal audience line curving (PALC) is introduced. The positions of the audience zones in the vertical LSA radiation plane are mathematically interpreted as polygonal line. PALC can be previously applied to a numerical optimization of the individual loudspeakers' driving functions or could also be applied for uniformly driven LSAs. Furthermore, it can be used with different objectives, such as a constant interaction between adjacent LSA cabinets with respect to the receiver geometry, or by additionally considering source-receiver amplitude attenuation characteristics.

While [6] is a preliminary study without detailed explanation of the PALC algorithm, only focusing on the PIPs of the standard curving schemes arc and progressive as well as the technical quality measures for one concert venue, PALC is elaborately described and compared with different standard LSA curving schemes and a commercially available numerical method for two receiver geometries in [7]. The evaluation of the sound fields is based on the PIPs and two technical quality measures: the acoustic contrast and a homogeneity measure. This homogeneity measure is introduced as the frequency dependent standard deviation of the distance compensated SPLs of all audience positions. For the sound field predictions, the CDPS model is utilized for one uniformly driven LSA configuration with different tilt angles, i.e., different curvings.

PALC is a robust and easily applicable approach offering flexible adaptability with respect to the receiver geometry and being less computational than numerical methods. It is concluded that PALC is superior to the standard curving schemes as it allows direct adaptation to the present receiver geometry. PALC is also faster and more efficient than the evaluated numerical method. A final comparative statement regarding accuracy is not made as identical specifications for the PALC algorithm and the evaluated numerical optimization approach cannot be ensured. It is predicted that PALC can be easily extended so that it only seeks from a discrete set of tilt angle values as it is required for practical realizations.

For publishing this study in the Journal of the Audio Engineering Society [9], it was extended by additional graphics for easier comprehension and by discussing links to the Wavefront Sculpture Technology criterion #4. Since WST comprises criteria for the arrayability of sound sources, the results of the proposed PALC algorithm for optimizing the tilt angles of LSA cabinets are compared with the LSA curvatures derived from WST. It is found that PALC provides results being in accordance with the demand from WST #4 for a constant product of the intersplay angles and the respective source-to-receiver distances.

1.3.3 Wavefront Sculpture Technology Criteria and the Adjoint-based Approach

In cooperation with the Institute of Communications Engineering from the University of Rostock, paper [2] was submitted for the Audio Engineering Society Convention in May

2015. In this contribution, the Wavefront Sculpture Technology (Heil and Urban, 1992 and Urban et al., 2003) and its criteria are revisited for straight arrays on the basis of a signal processing model from sound field synthesis. It contains a detailed analysis of the first three WST criteria dealing with reducing or even avoiding grating lobes resulting from the discretization of practical loudspeaker configurations. The Active Radiating Factor (ARF) specifying the relation of the pistons' dimensions to the fixed distance between adjacent piston centers is correctly adapted for circular pistons. A line piston model for wavefront curvature is introduced.

For the 3rd Audio Engineering Society International Conference on Sound Reinforcement with focus on open-air venues in August 2017, [8] was submitted resulting from a cooperation of the Computational Fluid Dynamics Group and the Audio Communication Group from TU Berlin. The used adjoint-based approach (Lemke, 2015) can be applied for determining both the driving functions and the positions of the sources for the synthesis of a desired sound field. The method operates in the time domain and is based on the Euler equations and the corresponding adjoint which are solved by means of computational aeroacoustic techniques. It allows considering geometric boundary constraints, for including such as the room influence, and base flows, for including such as wind.

The fundamentals and the features of the method together with two validation examples with three monopole sources are presented in [8]. The second example incorporates a base flow. It is found that the adjoint-based method is suitable to identify predetermined driving functions for the selected examples and that it provides reasonable driving functions when considering a base flow. A preliminary study with two loudspeakers is also included in [5].

In order to deploy the adjoint-based approach as alternative for the common frequency domain techniques for acoustic problems and for practical sound reinforcement setups, an efficient implementation is required. Also the conversion from the adjoint-based solutions to driving functions has to be analyzed in detail.

1.4 Summary of Original Achievements

In line with this thesis, the complex-directivity point source (CDPS) model which is typically used for sound field prediction with line source arrays (LSAs) was modified in order to provide realistic sound pressure levels based on modeled loudspeaker data and based on measured loudspeaker directivity and sensitivity data. Also an enclosed geometric model was developed in order to exactly specify the source and receiver positions of modeled and measured LSA configurations.

Evaluation criteria for assessing the performance of geometrically adapted and electronically controlled LSAs were recommended. These criteria include comprehensive graphical representations and technical quality measures of sound field as well as source related characteristics. They are both technically and economically motivated.

The analytical polygonal audience line curving (PALC) approach was introduced for finding appropriate LSA cabinet tilt angles with respect to the geometry of the receiver area and the intended coverage. Its advantages regarding sound field homogeneity, target-oriented radiation and computational efficiency were presented in comparison with typical standard LSA curving schemes and a commercially available numerical method.

For the electronic control of the individual LSA loudspeakers, different numerical optimization approaches from the research literature were implemented and evaluated. In order to overcome the non-smooth frequency responses resulting from purely numerical frequency domain approaches without additional frequency-connecting constraints, the line source array venue slice drive optimization (LAVDO) method was proposed. This mixed analytical-numerical approach is aim-oriented and low-computational. The numerical stage does not operate separately for various frequencies. It optimizes curve fitting parameters for the individual loudspeakers' driving functions across a broad frequency range.

To the author's knowledge, there has been no in-depth consideration of the finite impulse response (FIR) filter design from (numerically) optimized loudspeakers' driving functions for large-scale sound reinforcement in the literature before. A complete procedure with respect to the different frequency vectors and resolutions and the windowing was presented.

For the first time, the adjoint-based approach operating in the time domain was applied for basic sound reinforcement configurations in order to determine the loudspeakers' driving functions. It allows considering geometric boundary constraints, such as the room influence, and base flows, such as wind.

1.5 Outlook

For the future, it is intended to enhance the proposed algorithms for the geometric as well as for the electronic wavefront shaping, to specify generally accepted evaluation criteria and to continue the perceptual studies with respect to audible phase effects.

The polygonal audience line curving (PALC) algorithm for finding the tilt angles of the individual LSA cabinets can be easily extended so that it only seeks from a discrete set of tilt angle values as it is required for practical realizations. This should be completed before providing this method as an open-access web application with visual user interaction.

It is planned to consider additional goals for the electronic optimization of the individual loudspeakers' driving functions by means of the introduced line source array venue slice drive optimization (LAVDO). The goals of all optimization cases are to be combined within the numerical refinement step so that an absolute weighting between these goals is possible. Additionally, the calculated LAVDO results should be verified by means of hands-on measurements and informal listening tests. Different initial solutions instead of far-field considerations should also be analyzed.

For both the introduced geometric and electronic optimization methods, PALC and LAVDO, a thorough comparison with the optimization results of the approaches from the patents

Martin Audio Limited, 2006a, Martin Audio Limited, 2006b and SDA Software Design Ahnert GmbH, 2013 is desirable. This requires a well-defined specification of the entire optimization setting with the same optimization goals and constraints.

Alternatively, other optimization methods should be considered. This includes the adjoint-based approach which is known from fluid mechanics and operates in the time domain. Its fundamentals and features have already been examined with basic validation examples, cf., publications [5, 8]. Further steps comprise an efficient implementation for acoustic problems and for practical sound reinforcement setups as well as an adequate adaption framework for the adjoint-based solutions in order to transfer them directly to driving functions.

Based on the evaluation strategies presented in [3], generally accepted evaluation criteria with respect to technical, economical and perceptual matters are sought. An expert focus group consisting of developers of loudspeakers and line array systems, production engineers of large-scale sound reinforcement systems and live sound operators could be called.

Another issue is the common restriction of the optimization goals to the magnitudes. Phase optimization constraints may be revealed by additional listening tests investigating the perception of phase shifts in the sound pressure spectrum when moving through sound fields generated by (numerically) optimized LSAs.

1.6 References

Ahrens, J. (2012): *Analytic Methods of Sound Field Synthesis* (Springer, Heidelberg), 1st ed.

Berkhout, A.J.; Vogel, P.; de Vries, D. (1992a): “Use of Wave Field Synthesis for Natural Reinforced Sound.” In: *Proc. of the 92nd Audio Eng. Soc. Conv.*, Vienna, #3299.

Berkhout, A.J.; de Vries, D.; Vogel, P. (1992b): “Wave Front Synthesis: A New Direction In Electroacoustics.” In: *Proc. of the 93rd Audio Eng. Soc. Conv.*, San Francisco, #3379.

Betlehem, T.; Withers, C. (2012): “Sound Field Reproduction with Energy Constraint on Loudspeaker Weights.” In: *IEEE Trans. on Audio, Speech, and Language Process.*, vol. 20, no. 8, pp. 2388 – 2392 (October).

Beuningen, G.W. van; Start, E.W. (2000): “Optimizing Directivity Properties of DSP Controlled Loudspeaker Arrays.” In: *Proc. of the Inst. of Acoustics: Reproduced Sound*, vol. 22, no. 6, pp. 17 – 37.

Button, D. (2002): “High Frequency Components for High Output Articulated Line Arrays.” In: *Proc. of 113th Audio Eng. Soc. Conv.*, Los Angeles, #5684.

Cai, Y.; Wu, M.; Yang, J. (2014): “Sound Reproduction in Personal Audio Systems Using the Least-Squares Approach with Acoustic Contrast Control Constraint.” In: *J. Acoust. Soc. Am.*, vol. 135, no. 2, pp. 734 – 741 (February).

Choi, J.-W.; Kim, Y.-H. (2002): “Generation of an Acoustically Bright Zone with an Illuminated Region Using Multiple Sources.” In: *J. Acoust. Soc. Am.*, vol. 111, no. 4, pp. 1695 – 1700 (April).

Coleman, P.; Jackson, P.J.; Olik, M.; Møller, M.; Olsen, M.; Pedersen, J.A. (2014): “Acoustic Contrast, Planarity and Robustness of Sound Zone Methods Using a Circular Loudspeaker Array.” In: *J. Acoust. Soc. Am.*, vol. 135, no. 4, pp. 1929 – 1940 (April).

Deschamps, G.A.; Cabayan, H.S. (1972): “Antenna Synthesis and Solution of Inverse Problems by Regularization Methods.” In: *IEEE Trans. on Antennas and Propagation*, vol. 20, no. 3, pp. 268 – 274 (May).

Feistel, S.; Thompson, A.; Ahnert, W. (2007): “Modeling of Loudspeaker Systems Using High-Resolution Data.“ In: *J. Audio Eng. Soc.*, vol. 55, no. 7/8, pp. 571 – 597 (July/August).

Feistel, S.; Thompson, A.; Ahnert, W. (2009): “Methods and Limitations of Line Source Simulation.“ In: *J. Audio Eng. Soc.*, vol. 57, no. 6, pp. 379 – 402 (June).

Feistel, S.; Sempf, M.; Köhler, K.; Schmalle, H. (2013): “Adapting Loudspeaker Array Radiation to the Venue using Numerical Optimization of FIR Filters.” In: *Proc. of the 135th Audio Eng. Soc. Conv.*, New York, #8937.

Firtha, G.; Fiala, P.; Schultz, F.; Spors, S. (2017): “Improved Referencing Schemes for 2.5D Wave Field Synthesis Driving Functions.” In: *IEEE/ACM Trans. Audio, Speech, Language Process.*, vol. 25, no. 5, p. DOI10.1109/TASLP.2017.2689245 (May).

Gembicki, F.W.; Haimes, Y.Y. (1975): “Approach to Performance and Sensitivity Multiobjective Optimization: The Goal Attainment Method.” In: *IEEE Trans. on Automatic Control*, vol. 20, no. 6, pp. 769 – 771 (December).

Heil, C.; Urban, M. (1992): “Sound Fields Radiated by Multiple Sound Sources Arrays.” In: *Proc. of the 92nd Audio Eng. Soc. Conv.*, Vienna, #3269.

Keele, D. (2000): “The Application of Broadband Constant Beamwidth Transducer (CBT) Theory to Loudspeaker Arrays.” In: *Proc. of the 109th Audio Eng. Soc. Conv.*, Los Angeles, #5216.

Kim, Y.; Nelson, P. (2004): “Optimal Regularisation for Acoustic Source Reconstruction by Inverse Methods.” In: *J. of Snd. Vibr.*, vol. 275, no. 3, pp. 463 – 487 (August).

Koehler, K. (2013): *Praxisorientierte Optimierungsalgorithmen für digital gesteuerte Beschallungssysteme.* Master’s Thesis, TU Berlin.

Lemke, M. (2015): *Adjoint Based Data Assimilation in Compressible Flows with Application to Pressure Determination from PIV Data.* Ph.D. thesis, TU Berlin.

Martin Audio Limited (2006a): “UK Patent 2 456 113, Speaker Configuration.” Priority Date 16.10.2006.

Martin Audio Limited (2006b): “US Patent 8 750 542 B2, Speaker Configuration.” Priority Date 16.10.2006.

Meyer, D.G. (1984): “Computer Simulation of Loudspeaker Directivity.” In: *J. Audio Eng. Soc.*, vol. 32, no. 5, pp. 294 – 315 (May).

Meyer, P.; Schwenke, R. (2003): “Comparison of the Directional Point Source Model and BEM Model for Arrayed Loudspeakers.” In: *Proc. of the Inst. of Acoustics*, vol. 25, no. 4.

Nelson, P.A. (2001): “A Review of Some Inverse Problems in Acoustics.” In: *J. Acoust. and Vibr.*, vol. 6, no. 3, pp. 118 – 134 (September).

Rogers, P.H.; Buren, A.V. (1978): “New Approach to a Constant Beamwidth Transducer.” In: *J. Acoust. Soc. Am.*, vol. 64, no. 1, pp. 38 – 43 (July).

Scheirman, D. (2015): “Large-Scale Loudspeaker Arrays: Past, Present and Future (Part Two – Electroacoustic Considerations.” In: *Proc. of the 59th Audio Eng. Soc. Int. Conf. on Sound Reinforcement*, Montreal.

Schmidmaier, R.; Meyer, D.G. (1992): “Dynamic Amplitude Shading of Electronically Steered Line Source Arrays.” In: *Proc. of the 92nd Audio Eng. Soc. Conv.*, Vienna, #3272.

Schultz, F. (2016): *Sound Field Synthesis for Line Source Array Applications in Large-Scale Sound Reinforcement*. Ph.D. thesis, University of Rostock.

Schultz, F.; Firtha, G.; Fiala, P.; Spors, S. (2017): “Wave Field Synthesis Driving Functions for Large-Scale Sound Reinforcement Using Line Source Arrays.” In: *Proc. of the 142nd Audio Eng. Soc. Conv.*, Berlin, #9722.

SDA Software Design Ahnert GmbH (2013): “European Patent 2 965 538, Verfahren zum Bestimmen einer Konfiguration für eine Lautsprecheranordnung zum Beschallen eines Raums und Computerprogrammprodukt.“ Priority Date 08.03.2013.

Spors, S.; Rabenstein, R.; Ahrens, J. (2008): “The Theory of Wave Field Synthesis Revisited.” In: *Proc. of the 124th Audio Eng. Soc. Conv.*, Amsterdam, #7358.

Start, E.W. (1996): “Application of Curved Arrays in Wave Field Synthesis.” In: *Proc. of the 100th Audio Eng. Soc. Conv.*, Copenhagen, #4143.

Start, E.W. (1997): *Direct Sound Enhancement by Wave Field Synthesis*. Ph.D. thesis, Delft University of Technology.

Terrell, M.; Sandler, M. (2010): “Optimising the Controls of a Homogenous Loudspeaker Array.” In: *Proc. of the 129th Audio Eng. Soc. Conv.*, San Francisco, #8159.

Thompson, A. (2006): “Line Array Splay Angle Optimisation.” In: *Proc. of the Inst. of Acoustics*, vol. 28, no. 8.

Thompson, A. (2008): “Real World Line Array Optimization.” In: *Proc. of the Inst. of Acoustics*, vol. 30, no. 6.

Thompson, A. (2009): “Improved Methods for Controlling Touring Loudspeaker Arrays.” In: *Proc. of the 127th Audio Eng. Soc. Conv.*, New York, #7828.

Thompson, A.; Baird, J.; Webb, B. (2011): “Numerically Optimised Touring Loudspeaker Arrays – Practical Applications.” In: *Proc. of the 131st Audio Eng. Soc. Conv.*, New York, #8511.

Urban, M.; Heil, C.; Bauman, P. (2003): “Wavefront Sculpture Technology.” In: *J. Audio Eng. Soc.*, vol. 51, no. 10, pp. 912 – 932 (October).

Ureda, M.S. (2001): “Line Arrays: Theory and Applications.” In: *Proc. of the 110th Audio Eng. Soc. Conv.*, Amsterdam, #5304.

Ureda, M.S. (2004): “Analysis of Loudspeaker Line Arrays.” In: *J. Audio Eng. Soc.*, vol. 52, no. 5, pp. 467 – 495 (May).

Vries, D. de; Start, E.W; Valstar, V.G. (1994): “The Wave Field Synthesis Concept Applied to Sound Reinforcement: Restrictions and Solutions.” In: *Proc. of the 96th Audio Eng. Soc. Conv.*, Amsterdam, #3812.

Vries, D. de (1996): “Sound Reinforcement by Wavefield Synthesis: Adaptation of the Synthesis Operator to the Loudspeaker Directivity Characteristics.” In: *J. Audio Eng. Soc.*, vol. 44, no. 12, pp. 1120 – 1131 (December).

2 Publications

This section includes the publications that were authored and co-authored by the doctoral candidate in the following order:

[1] Straube, Florian; Schultz, Frank; Weinzierl, Stefan (2015): "On the Effect of Spatial Discretization of Curved Line Source Arrays." In: *Fortschritte der Akustik: Tagungsband d. 41. DAGA*. Nuremberg, Germany, pp. 459 – 462, ISBN: 978-3939296089. Preprint.

[2] Schultz, Frank; Straube, Florian; Spors, Sascha (2015): "Discussion of the Wavefront Sculpture Technology Criteria for Straight Line Source Arrays." In: *Proc. of the 138th Audio Eng. Soc. Conv.*, Warsaw, Poland, #9323, url: http://www.aes.org/e-lib/browse.cfm?elib=17747. Publisher's Version.

[3] Straube, Florian; Schultz, Frank; Makarski, Michael; Spors, Sascha; Weinzierl, Stefan (2015): "Evaluation Strategies for the Optimization of Line Source Arrays." In: *Proc. of the 59th Audio Eng. Soc. Int. Conf. on Sound Reinforcement*, Montreal, Canada, url: http://www.aes.org/e-lib/browse.cfm?elib=17829. Publisher's Version.

[4] Straube, Florian; Schultz, Frank; Makarski, Michael; Weinzierl, Stefan (2016): "Optimized Driving Functions for Curved Line Source Arrays Using Modeled and Measured Loudspeaker Data." In: *Fortschritte der Akustik: Tagungsband d. 42. DAGA*. Aachen, Germany, pp. 1136 – 1139, ISBN: 978-3939296102. Preprint.

[5] Lemke, Mathias; Straube, Florian; Sesterhenn, Jörn; Weinzierl, Stefan (2017): "Adjungierten-basierte Schallfeldsynthese und Beschallung." In: *Fortschritte der Akustik: Tagungsband d. 43. DAGA*. Kiel, Germany, pp. 1422 – 1425, ISBN: 978-3939296126. Preprint.

[6] Straube, Florian; Bonillo, David Albanés; Schultz, Frank; Weinzierl, Stefan (2017): "Zur Optimierung der Kruemmung von Line Source Arrays." In: *Fortschritte der Akustik: Tagungsband d. 43. DAGA*. Kiel, Germany, pp. 1418 – 1421, ISBN: 978-3939296126. Preprint.

[7] Straube, Florian; Schultz, Frank; Bonillo, David Albanés; Weinzierl, Stefan (2017): "An Analytical Approach for Optimizing the Curving of Line Source Arrays." In: *Proc. of the 142nd Audio Eng. Soc. Conv.*, Berlin, Germany, #9699, url: http://www.aes.org/e-lib/browse.cfm?elib=18577. Publisher's Version.

[8] Lemke, Mathias; Straube, Florian; Schultz, Frank; Sesterhenn, Jörn; Weinzierl, Stefan (2017): "Adjoint-Based Time Domain Sound Reinforcement." In: *Proc. of the 3rd Audio Eng. Soc. Int. Conf. on Sound Reinforcement – Open Air Venues*, Struer, Denmark, url: http://www.aes.org/e-lib/browse.cfm?elib=19178. Publisher's Version.

[9] Straube, Florian; Schultz, Frank; Bonillo, David Albanés; Weinzierl, Stefan (2018): "An Analytical Approach for Optimizing the Curving of Line Source Arrays." In: *J. Audio Eng. Soc.*, vol. 66, no. 1/2, pp. 4 – 20 (January/February), doi: https://doi.org/10.17743/jaes.2017.0043. Publisher's Version.

[10] Straube, Florian; Schultz, Frank; Makarski, Michael; Weinzierl, Stefan (2018): "Mixed Analytical-Numerical Filter Design for Optimized Electronic Control of Line Source Arrays." In: *J. Audio Eng. Soc.*, vol. 66, no. 9, pp. 690 – 702 (September), doi: https://doi.org/10.17743/jaes.2018.0043. Publisher's Version.

On the Effect of Spatial Discretization of Curved Line Source Arrays

Florian Straube[1], Frank Schultz[2], Stefan Weinzierl[1]

[1] *Audio Communication Group, TU Berlin, 10587, Berlin, Germany, E-mail: florian.straube@tu-berlin.de*

[2] *Institute of Communications Engineering, University of Rostock, 18119, Rostock, Germany*

Introduction

Line Source Arrays (LSAs) are used for sound reinforcement of large listening areas aiming at sound fields which are as homogenous as possible for the whole audio bandwidth. This contribution presents the analysis of a complex-directivity point source model (CDPS) with respect to spatial discretization as well as tilting effects when employing a curved, uniformly driven LSA setup for a common concert venue. The CDPS-based calculations include far-field radiation patterns of baffled line and circular pistons for the modeling of multi-way cabinets with varying discretization between adjacent drivers. The results are discussed by means of position index plots (PIPs), i. e. sound pressure level spectra for all selected receiver points, and far-field radiation patterns (FRPs) as isobar plots. As expected, it will be shown that sound fields generated by typical LSAs using rather large waveguides are corrupted by spatial aliasing. This can be avoided by applying small individually driven pistons resulting in an increased spatial aliasing frequency.

Spiral Curved LSA

Following [1, 2] generalized formulae for the positioning of the LSA elements were developed based on the spiral curved sources, also known as progressive sources. The main principle of the respective mathematic analysis is that a segment between two points of the spiral is defined by a straight line with the length ΔL, the n-th segment having the tilt angle γ_n with $n = 1, 2, ..., N$. This is depicted for $\Delta L = \Lambda_{y,\mathrm{LSA}}$ in Fig. 1. In case of the progressive source, the tilt angle of a segment results from the tilt angle of the preceding segment and a preset angle increment, i. e. $\gamma_n = \gamma_{n-1} + (n-1)\ \Delta\gamma$. The top segment ($n = 1$) can have an initial tilt angle γ_0 equivalent to a tilt offset of the whole spiral. Hence, the tilt angles can be calculated explicitly by

$$\gamma_n = \gamma_0 + \sum_{\eta=1}^{\eta=n} (\eta - 1)\ \Delta\gamma = \gamma_0 + \frac{n}{2}\ (n-1)\ \Delta\gamma. \quad (1)$$

The terminal angle of the spiral then reads

$$\gamma_{\mathrm{final}} = \gamma_N = \gamma_0 + \frac{N}{2}\ (N-1)\ \Delta\gamma \quad (2)$$

which is equal to the tilt angle of the N-th spiral segment. As prefigured above, the generalized positioning formulae of the top and bottom coordinates can thus be written as

$$\begin{pmatrix} x_{\mathrm{t},n} \\ y_{\mathrm{t},n} \end{pmatrix} = \begin{pmatrix} x_{\mathrm{H}} \\ y_{\mathrm{H}} \end{pmatrix} - \sum_{\mu=1}^{\mu=n-1} \Delta L \begin{pmatrix} \sin\gamma_\mu \\ \cos\gamma_\mu \end{pmatrix}, \quad (3)$$

$$\begin{pmatrix} x_{\mathrm{b},n} \\ y_{\mathrm{b},n} \end{pmatrix} = \begin{pmatrix} x_{\mathrm{H}} \\ y_{\mathrm{H}} \end{pmatrix} - \sum_{\mu=1}^{\mu=n} \Delta L \begin{pmatrix} \sin\gamma_\mu \\ \cos\gamma_\mu \end{pmatrix} \quad (4)$$

using $(x_{\mathrm{H}}, y_{\mathrm{H}})$ as the initial top position of the first segment, i. e. $(x_{\mathrm{t},1}, y_{\mathrm{t},1}) = (x_{\mathrm{H}}, y_{\mathrm{H}})$.

LSA Setup

Not only the LSA setup but also the geometry under discussion is schematically depicted in Fig. 1. A total number of $N = 16$ LSA cabinets is used. $\Lambda_{y,\mathrm{LSA}}$ denotes the front grille's height of a single LSA cabinet and is chosen to $\Lambda_{y,\mathrm{LSA}} = 0.372$ m. Note that $\Lambda_{y,\mathrm{LSA}}$ equals the straight line length ΔL from the former section and the front grille top and bottom coordinates of the individual LSA cabinets equal the top $(x_{\mathrm{t}}, y_{\mathrm{t}})$ and bottom coordinates $(x_{\mathrm{b}}, y_{\mathrm{b}})$ of the respective spiral segments in this case.

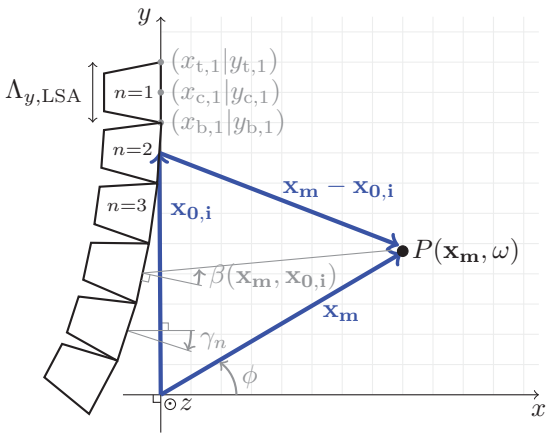

Figure 1: Sketch of the LSA setup under discussion. A total of $N = 16$ LSA cabinets of the height $\Lambda_{y,\mathrm{LSA}} = 0.372\,\mathrm{m}$ are used.

The LSA is built from multi-way cabinets with L_{LF}, L_{MF} and L_{HF} vertically-stacked circular pistons for the low (LF) and mid (MF), as well as line pistons for the high frequency range (HF). Ideal crossover filters with the cut frequencies $f_{\mathrm{LF,MF}} = 400$ Hz and $f_{\mathrm{MF,HF}} = 1.5$ kHz are deployed. A modified Active Radiating Factor (ARF) [3, Sec. 3.2], [4, Sec. 3] is used to specify the piston dimensions – i. e. the circular piston radius R and the line piston length Λ_y – related to the fixed distance between adjacent piston centers Δy. The ARF of a line piston

reads [4, (21)], [3, Sec. 3.2]

$$\mathrm{ARF}_{\mathrm{line}} = \alpha = \frac{\Lambda_y}{\Delta y} \qquad 0 \leq \alpha \leq 1, \tag{5}$$

whereas the ARF for a circular piston can be written as [4, (26)], [4, (27)]

$$\mathrm{ARF}_{\mathrm{circ}} = \frac{\pi}{4}\,\alpha^2 = \frac{\pi}{4}\left(\frac{2\,R}{\Delta y}\right)^2 \qquad 0 \leq \alpha \leq 1. \tag{6}$$

α is chosen to 0.82 for both the circular and the line piston – meeting the Wave Front Sculpture Technology (WST) criterion 1 (cf. [3, p. 917]). Considering the characteristics of multi-way cabinets, different piston sensitivities are assumed for the sources in order to obtain realistic sound pressure levels. Two LSA configurations

$$\mathrm{LSA}_1 = \begin{cases} L_{\mathrm{LF}} = 1 \text{ (12 in)} \\ L_{\mathrm{MF}} = 2 \text{ (6 in)} \\ L_{\mathrm{HF}} = 1 \text{ (12 in)} \end{cases} \qquad \mathrm{LSA}_2 = \begin{cases} L_{\mathrm{LF}} = 1 \text{ (12 in)} \\ L_{\mathrm{MF}} = 4 \text{ (3 in)} \\ L_{\mathrm{HF}} = 10 \text{ (1.2 in)} \end{cases}$$

with two different sets of the tilt angles γ_n fixed according to the intended audience coverage are examined. The first set is compliant to the WST criterion 5 (cf. [3, p. 929]), whereas the second set does not fulfill this condition for the maximum relative tilt angle (between adjacent LSA cabinets) that amounts to ca. 5.5 deg for the used setup and geometry. In Tab. 1 the chosen tilt angles can be found.

LSA cab.	1	2	3	4	5	6	7	8
$\gamma_{n,1}$ / deg	-3	-1	1	3	5	7	10	12
$\gamma_{n,2}$ / deg	-3	-2	-1	-0.5	1	3	5	7

LSA cab.	9	10	11	12	13	14	15	16
$\gamma_{n,1}$ / deg	15	18	21	24	27	30	34	38
$\gamma_{n,2}$ / deg	8	10	12	15	19	26	33	40

Table 1: Tilt angles of the LSA cabinets for the geometry used (Fig. 1).

With (3) and (4) the front grille center position of the i-th driver of the LSA is given as

$$\mathbf{x_{0,i}} = \begin{pmatrix} x_{0,i} \\ y_{0,i} \end{pmatrix} = \begin{pmatrix} x_{\mathrm{t},n} \\ y_{\mathrm{t},n} \end{pmatrix} + \frac{l - 0.5}{L} \begin{pmatrix} x_{\mathrm{b},n} - x_{\mathrm{t},n} \\ y_{\mathrm{b},n} - y_{\mathrm{t},n} \end{pmatrix}, \tag{7}$$

using $l = 1, 2, ..., L$ and $i = (n-1) \cdot L + l$ for $L = \{L_{\mathrm{LF}}, L_{\mathrm{MF}}, L_{\mathrm{HF}}\}$ with respect to the different frequency bands.

Venue Geometry

An arena with audience and non-audience sections, i. e. zones to be covered and zones to be avoided, is chosen as the concert venue following a practical example presented in [5, Sec. 6.1]. The venue is modeled by a two dimensional slice representation within the xy-plane considering vertical radiation as depicted in Fig. 2, cf. [5–7]. $M = 29\,525$ receiver points with $m = 1, 2, ..., M$ are taken into account. This corresponds to a distance of 0.005 m between the receiver points ensuring a discretization which approximately equals one fourth of the wave length at 17.2 kHz.

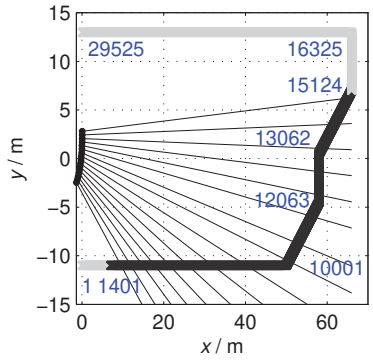

Figure 2: Venue Slice within the xy-plane with audience (black) as well as non-audience/ avoid (gray) zones. The LSA curving is depicted for the first set of tilt angles.

Calculation Model

Based on a complex-directivity point source model of baffled piston far-field radiation patterns, the sound field prediction equation reads [8, (11)], [9, Sec. 1.1]

$$P(\mathbf{x_m}, \omega) = \sum_{i=1}^{L\,N} D(\mathbf{x_{0,i}}, \omega) \times \underbrace{H_{\mathrm{post}}(\beta(\mathbf{x_m}, \mathbf{x_{0,i}}), \omega) \frac{\mathrm{e}^{-\mathrm{j}\,\frac{\omega}{c}\,\|\mathbf{x_m} - \mathbf{x_{0,i}}\|_2}}{4\,\pi\,\|\mathbf{x_m} - \mathbf{x_{0,i}}\|_2} \frac{\Lambda_{y,\mathrm{LSA}}}{L}}_{G(\mathbf{x_m}, \mathbf{x_{0,i}}, \omega)} \tag{8}$$

using the $\mathrm{e}^{+\mathrm{j}\,\omega\,t}$ time convention. $P(\mathbf{x_m}, \omega)$ denotes the sound pressure spectrum at the receiver position $\mathbf{x_m}$ with $[P(\mathbf{x_m}, \omega)] = 1\,\mathrm{Pa/Hz}$. The complex driving function spectrum $D(\mathbf{x_{0,i}}, \omega)$ with $[D(\mathbf{x_{0,i}}, \omega)] = 1\,\mathrm{Pa/Hz}$ of the i-th source is directly proportional to the source's velocity spectrum. Terming the acoustic transfer function (ATF) from the i-th source to the receiver points, $G(\mathbf{x_m}, \mathbf{x_{0,i}}, \omega)$ is composed of the free-field 3D Green's function (i. e. the spherical monopole) $\frac{\mathrm{e}^{-\mathrm{j}\,\frac{\omega}{c}\,\|\mathbf{x_m} - \mathbf{x_{0,i}}\|_2}}{4\pi\|\mathbf{x_m} - \mathbf{x_{0,i}}\|_2}$, a specific far-field radiation pattern $H_{\mathrm{post}}(\beta(\mathbf{x_m}, \mathbf{x_{0,i}}), \omega)$ and the distance $\Delta y = \Lambda_{y,\mathrm{LSA}}/L$ between adjacent piston centers (discretization step) for L sources per LSA cabinet. The far-field radiation pattern of the baffled circular piston with the radius R and with a constant surface velocity is [10, (26.42)]

$$H_{\mathrm{post,circ}}(\beta, \omega) = \frac{2\,J_1\left(\frac{\omega}{c} R \sin\beta\right)}{\frac{\omega}{c} R \sin\beta}, \tag{9}$$

denoting the cylindrical Bessel function of 1st kind of 1st order as $J_1(\cdot)$ [11, (10.2.2)]. Modeling an ideal waveguide for the HF band the far-field radiation pattern of the line piston with the length Λ_y can be written as [10, (26.44)]

$$H_{\mathrm{post,line}}(\beta, \omega) = \frac{\sin\left(\frac{\omega}{c}\frac{\Lambda_y}{2}\sin\beta\right)}{\frac{\omega}{c}\frac{\Lambda_y}{2}\sin\beta}. \tag{10}$$

In line with this modeling, air absorption is neglected, a constant velocity of sound ($c = 343$ m/s), infinite, straight baffles and a constant surface velocity are assumed. Note that the sound field prediction equation

(8) correctly synthesizes the collective Fresnel and Fraunhofer region of the whole array if the respective receiver point is located in the far-field of the individual pistons [4]. This does not impose any practical limitations, as the audience is typically located in some meters distance from the individual LSA cabinets. Precise rearward and low-frequency prediction are not feasible by means of this model.

Uniformly Driven LSAs

According to the spatial sampling theorem spatial aliasing can already occur for discretization steps which are larger than half of the wavelength. For the examination of these unwanted effects, the PIPs and the FRPs of the uniformly driven LSAs 1 and 2 are depicted in Fig. 3. An uniformly driven LSA corresponds to an array with sound field adjustment only by geometrical curving and without additional electronic control. Considering the number of individual pistons, the LSA_1 design complies with typical LSAs of the first generation, whereas LSA_2 complies with more recent designs with a larger number of pistons in the MF and HF band.

Discussion

The sound field of the LSA_1 is severely corrupted by spatial aliasing in the whole HF band, whereas the uniformly driven LSA_2 produces considerable aliasing above ca. 9 kHz (theoretical aliasing frequency: 4.61 kHz). The ratio of the audience and non-audience coverage does not turn out to be satisfactory for the LF and the lower frequencies of the MF bands because of the rather non-directed radiation. This ratio is acceptable for the HF band of the LSA_2 up to the frequency the spatial aliasing occurs. Since the effect of the different curving, i. e. the tilt angle sets one and two, can be noticed in the PIPs and FRPs in a very similar way, just the FRPs of the LSA designs with the non-WST5-compliant curving are visualized in the third row of Fig. 3. It can be clearly observed for the high frequencies and in the vertical angle range of ca. -20 deg to -40 deg, as anticipated, that distinct radiation gaps occur for this kind of LSA curving because of the seven-degree relative tilt angles between the last four LSA cabinets.

Conclusion

The presented model is judged to be applicable for the subsequent examination of optimization schemes despite the mentioned assumptions as well as drawbacks and although BEM models and measured LSA data likely provide results that closer match actual LSA sound fields but the latter presumably corrupt the fields so that the influence of optimization effects and inherent imperfections cannot be definitely distinguished. As expected, applying very small individual driven pistons results in an increased spatial aliasing frequency but the reduced power output of smaller pistons must also be taken into account. Additional electronic control is necessary for producing more homogenous sound fields. For a more profound investigation of the sound fields' characteristics and the radiation behavior, it may be advisable not to restrict the graphical evaluation to PIPs and FRPs but also consider e. g. the sound pressure level distribution in the whole vertical plane in order to gain more comprehensive insight not only into selected extracts but also into the entire LSA near-field as the audience is typically located at the widespread near-field. Furthermore, it may be helpful for the comparison and evaluation of different setups and different driving functions to introduce technical quality measures in the context of LSA design, for example a ratio of the average sound pressure levels of the audience and the non-audience zones, following a more quantitative-based and objective approach of assessment that can make it more convenient to set optimization parameters for electronic control.

References

[1] Ureda, M.S. (2001): "Line arrays: Theory and applications." In: *Proc. of 110th Audio Eng. Soc. Conv., Amsterdam*, #5304.

[2] Ureda, M.S. (2004): "Analysis of loudspeaker line arrays." In: *J. Audio Eng. Soc.*, **52**(5):467–495.

[3] Urban, M.; Heil, C.; Bauman, P. (2003): "Wavefront Sculpture Technology." In: *J. Audio Eng. Soc.*, **51**(10):912–932.

[4] Schultz, F.; Straube, F.; Spors, S. (2015): "Discussion of the Wavefront Sculpture Technology criteria for straight line arrays." In: *Proc. of the 138th Audio Eng. Soc. Conv., Warsaw*, #9323.

[5] Thompson, A.; Baird, J.; Webb, B. (2011): "Numerically optimised touring loudspeaker arrays - Practical applications." In: *Proc. of the 131st Audio Eng. Soc. Conv., New York*, #8511.

[6] Thompson, A. (2009): "Improved methods for controlling touring loudspeaker arrays." In: *Proc. of the 127th Audio Eng. Soc. Conv., New York*, #7828.

[7] Feistel, S.; Sempf, M.; Köhler, K.; Schmalle, H. (2013): "Adapting loudspeaker array radiation to the venue using numerical optimization of FIR filters." In: *Proc. of the 135th Audio Eng. Soc. Conv., New York*, #8937.

[8] Feistel, S.; Thompson, A.; Ahnert, W. (2009): "Methods and limitations of line source simulation." In: *J. Audio Eng. Soc.*, **57**(6):379–402.

[9] Meyer, P.; Schwenke, R. (2003): "Comparison of the directional point source model and BEM model for arrayed loudspeakers." In: *Proc. of the Institute of Acoustics*, vol. 25, part 4.

[10] Skudrzyk, E. (1971): *The Foundations of Acoustics. Basic Mathematics and Basic Acoustics*. New York, Vienna: Springer.

[11] Olver, F.W.J.; Lozier, D.W.; Boisvert, R.F.; Clark, C.W. (2010): *NIST Handbook of Mathematical Functions*. Cambridge University Press, 1. ed.

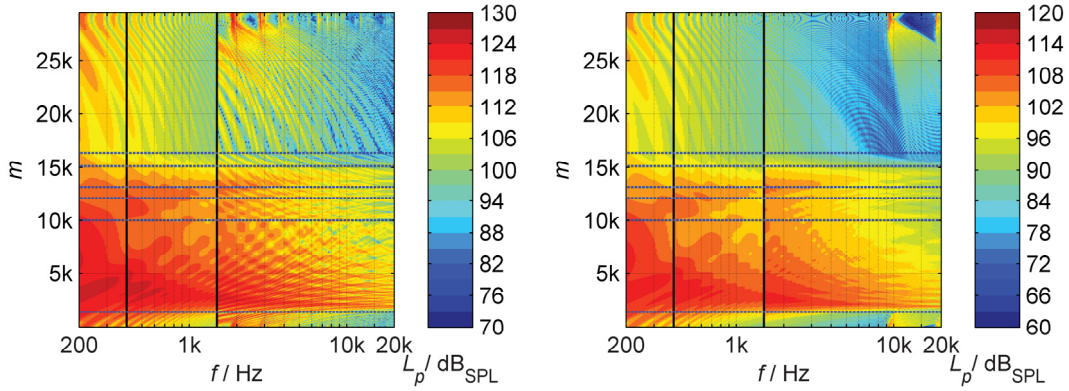

(a) PIP LSA_1 – WST5 compliant

(b) PIP LSA_2 – WST5 compliant

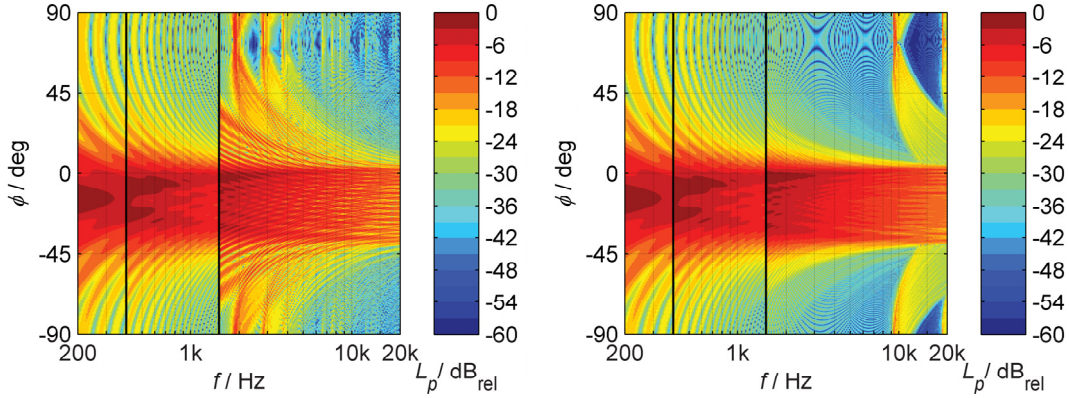

(c) FRP LSA_1 – WST5 compliant

(d) FRP LSA_2 – WST5 compliant

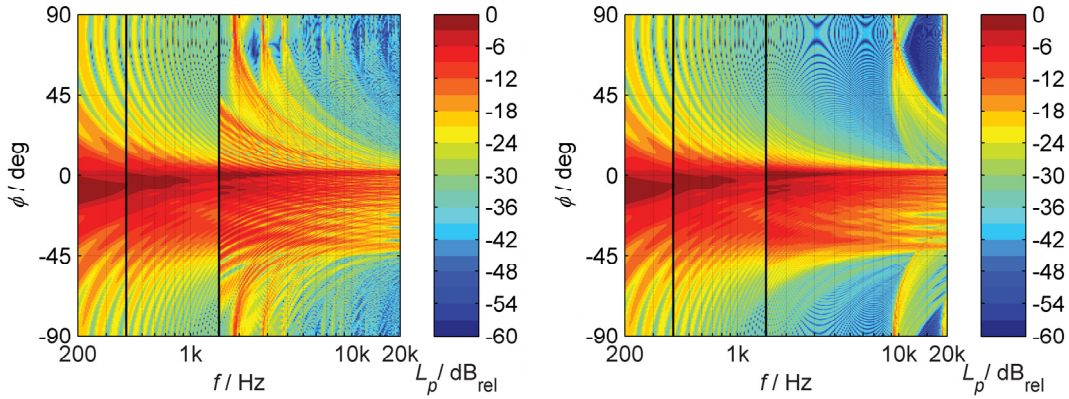

(e) FRP LSA_1 – not WST5 compliant

(f) FRP LSA_2 – not WST5 compliant

Figure 3: Position Index Plots (PIPs, first row) and Far-Field Radiation Patterns (FRPs, second row) of LSA_1 (left) and LSA_2 (right) – WST5 compliant, i. e. the relative tilt angles (between adjacent LSA cabinets) do not exceed a particular maximum depending on the setup and geometry, in this case: ca. 5.5 deg. Far-Field Radiation Patterns (third row) of LSA_1 (left) and LSA_2 (right) – not WST5 compliant, i. e. at least one of the relative tilt angles exceeds the aforementioned maximum.

Winner of the *AES 138th Convention Best Peer-Reviewed Paper Award*

Audio Engineering Society

Convention Paper 9323

Presented at the 138th Convention
2015 May 7–10 Warsaw, Poland

Discussion of the Wavefront Sculpture Technology Criteria for Straight Line Arrays

Frank Schultz[1], Florian Straube[2], and Sascha Spors[1]

[1] *Institute of Communications Engineering, University of Rostock, Germany*

[2] *Audio Communication Group, TU Berlin, Germany*

Correspondence should be addressed to Frank Schultz (`frank.schultz@uni-rostock.de`)

ABSTRACT

Wavefront Sculpture Technology introduced line source arrays for large scale sound reinforcement, aiming at the synthesis of highly spatial-aliasing free sound fields for full audio bandwidth. The paper revisits this technology and its criteria for straight arrays using a signal processing model from sound field synthesis. Since the latest array designs exhibit very small driver distances, the sampling condition for grating lobe free electronic beam forming regains special interest. Furthermore, a discussion that extends the initial derivations of the spatial lowpass characteristics of circular and line pistons, and line pistons with wavefront curvature applied in subarrays is given.

1. INTRODUCTION

In [1, 2] we started to revisit the Wavefront Sculpture Technology[1] (WST) [3, 4, 5] that constitutes the fundamentals of line array technology for full audio bandwidth public address. An acoustic signal processing model initially developed for sound field synthesis (SFS) [6, 7, 8, 9] was utilized, that is also well known in array processing and antenna theory [10, 11]. In essence, the first three WST criteria deal with the avoidance or attenuation of grating lobes in the farfield radiation pattern of straight line source arrays (LSA), which consequently avoids or reduces spatial aliasing in the Fresnel and Fraunhofer region. In this paper we revisit these WST criteria and give some extended analysis. The WST criteria under discussion are summarized as, cf. [5, p.929]:

The *active radiating factor* (ARF) criterion

$$\text{WST \#1:} \qquad \text{ARF} = \frac{l}{\Delta y} \geq 0.82 \qquad (1)$$

for a uniformly driven, straight LSA relates the discretization step Δy between adjacent line pistons

[1] Wavefront Sculpture Technology® is a registered trademark of L-ACOUSTICS US, LLC. We omit the labeling in the remainder of the paper and will only use the relevant research results.

with individual length l and a tolerated grating lobe level (i.e. the occurrence of spatial aliasing). The criterion ensures, that the maximum grating lobe level does not exceed -13.5 dB relative to the intended main lobe and holds for a large number of active line pistons. The criterion aims at avoiding or reducing spatial aliasing by utilizing the spatial lowpass characteristics of highly directive sources, i.e. waveguides.

The 2nd WST criterion

$$\text{WST \#2:} \qquad \Delta y < \frac{\lambda_{\min}}{2} \tag{2}$$

is the general spatial baseband sampling condition. It ensures complete grating lobe avoidance for electronically steered arrays built from spherical monopoles with the highest operating frequency $f_{\max} = c/\lambda_{\min}$ denoting the speed of sound $c = 343\,\mathrm{m/s}$ and the wave length λ in m. In [5, p.917] the criterion was derived in order to avoid strong off-axis lobes for a uniformly driven LSA. The criterion limits the temporal frequency bandwidth – matching the spatial base band – of the loudspeaker's driving function in order to avoid spatial aliasing.

The 3rd WST criterion relates an occurring wavefront curvature of horns, i.e. the arc in Fig. 1 and a tolerated grating lobe level for an LSA built without gaps between the horns. For the so called sagitta S

$$\text{WST \#3:} \qquad S < \frac{\lambda_{\min}}{4}, \tag{3}$$

must hold in order that the LSA exhibits a grating lobe attenuation larger than 10 dB relative to the intended main lobe, cf. [5, Fig. 9,10], [12, Fig. 19]. This criterion also aims at reducing spatial aliasing by utilizing the spatial lowpass characteristics of the sources that construct the LSA.

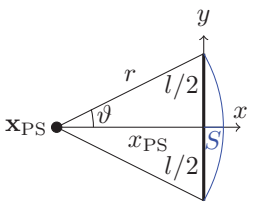

Fig. 1: Geometry for the wavefront curvature model, cf. [5, Fig. 8], [13, Fig. 38].

2. WST SIGNAL PROCESSING MODEL

For convenience the WST signal processing model is shortly revisited here, the nomenclature and conventions of [2] are used. The model is depicted in Fig. 2, given in the temporal and spatio-temporal Fourier spectrum domain. The spatio-temporal spectrum $P(k_y, \omega)$ of a sound pressure function over space and time $p(y, t)$ is given by the Fourier transform

$$P(k_y, \omega) = \int_{-\infty}^{+\infty} \int_{-\infty}^{+\infty} p(y, t)\, \mathrm{e}^{+\mathrm{j}\, k_y\, y}\, \mathrm{d}y\, \mathrm{e}^{-\mathrm{j}\, \omega\, t}\, \mathrm{d}t, \tag{4}$$

its inverse reads

$$p(y, t) = \frac{1}{4\,\pi^2} \int_{-\infty}^{+\infty} \int_{-\infty}^{+\infty} P(k_y, \omega)\, \mathrm{e}^{-\mathrm{j}\, k_y\, y}\, \mathrm{d}k_y\, \mathrm{e}^{+\mathrm{j}\, \omega\, t}\, \mathrm{d}\omega. \tag{5}$$

In the remainder only temporal, e.g. $P(x, y, \omega)$ and spatio-temporal spectra, e.g. $P(x, k_y, \omega)$ are considered. A monochromatic propagating sound field with angular temporal frequency ω_0 and corresponding wave length $\lambda_0 = \frac{2\,\pi\,c}{\omega_0}$ is assumed. Thus, the term $2\,\pi\,\delta(\omega - \omega_0)$ is omitted in all temporal and spatio-temporal spectra.

The LSA is located on the y-axis with y_0 indicating a position within the array. The xy-plane for $x > 0$ is considered as the the sound field synthesis region, thereby ignoring the horizontal radiation characteristics of the LSA, cf. [14, Sec. 4].

Following the signal processing model, the spatio-temporal spectrum of the sound pressure $P(x, k_y, \omega)$ can be obtained by different driving functions' spatio-temporal spectra

$$P(x, k_y, \omega) = \left\{ \begin{matrix} D(k_y, \omega) \\ D_w(k_y, \omega) \\ D_{w,\mathrm{S}}(k_y, \omega) \\ D_{w,\mathrm{S},H}(k_y, \omega) \end{matrix} \right\} \cdot G_0(x, k_y, \omega). \tag{6}$$

$D(k_y, \omega)$ models an infinite, continuous LSA; $D_w(k_y, \omega)$ a finite length, continuous LSA; $D_{w,\mathrm{S}}(k_y, \omega)$ a finite length, discretized LSA built from spherical monopoles and $D_{w,\mathrm{S,H}}(k_y, \omega)$ a finite length, discretized LSA built from identical baffled pistons.

$G_0(x, k_y, \omega)$ is the spatio-temporal spectrum of the 3D free-field Green's function

$$G(\mathbf{x}, \mathbf{x_0}, \omega) = \frac{1}{4\,\pi}\, \frac{\mathrm{e}^{-\mathrm{j}\, \frac{\omega}{c}\, \|\mathbf{x} - \mathbf{x_0}\|}}{\|\mathbf{x} - \mathbf{x_0}\|} \tag{7}$$

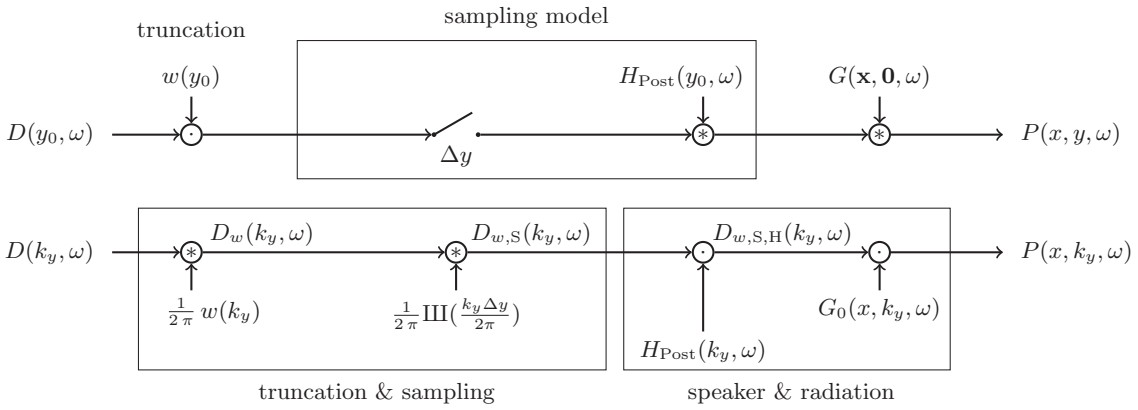

Fig. 2: WST signal processing model. Representation in temporal (top) and spatio-temporal spectrum domain (bottom). Convolution w.r.t. y is denoted by $\circledast$ (not to be confused with the circular convolution), multiplication w.r.t. k_y by $\odot$.

of the Helmholtz equation, placed at the origin $\mathbf{x_0} = \mathbf{0}$ [15, (52)].

The initial derivations of the WST criteria consider a uniformly driven and rectangular truncated LSA. Thus, with unity gain normalization, the driving function for an infinite, continuous LSA reads

$$D(y_0) = 1 \;\circ\!\!-\!\!\bullet\; D(k_y,\omega) = 2\,\pi\,\delta(k_y), \tag{8}$$

indicating the spatial Fourier transform with the $\circ\!\!-\!\!\bullet$ symbol. Spatial truncation with the rectangular window

$$w(y_0) = \begin{cases} \frac{1}{L} & \text{for } |y_0| \le \frac{L}{2} \\ 0 & \text{else} \end{cases} \;\circ\!\!-\!\!\bullet$$

$$w(k_y) = \begin{cases} \frac{\sin(k_y\,\frac{L}{2})}{k_y\,\frac{L}{2}} & \text{for } k_y \neq 0 \\ 1 & \text{for } k_y = 0, \end{cases} \tag{9}$$

leads to the driving function of a finite length, continuous LSA

$$D_w(y_0) = \begin{cases} \frac{1}{L} & \text{for } |y_0| \le \frac{L}{2} \\ 0 & \text{else} \end{cases} \;\circ\!\!-\!\!\bullet$$

$$D_w(k_y,\omega) = \begin{cases} \frac{\sin(k_y\,\frac{L}{2})}{k_y\,\frac{L}{2}} & \text{for } k_y \neq 0 \\ 1 & \text{for } k_y = 0. \end{cases} \tag{10}$$

Equidistant spatial sampling of the driving function w.r.t. the discretization step Δy with $\nu, \mu \in \mathbb{Z}$

$$\underbrace{\sum_{\nu=-\infty}^{+\infty} \delta(y_0 - \nu\,\Delta y)}_{=:\,\frac{1}{\Delta y}\mathrm{III}(\frac{y_0}{\Delta y})} \;\circ\!\!-\!\!\bullet\; \underbrace{\frac{2\,\pi}{\Delta y} \sum_{\mu=-\infty}^{+\infty} \delta\left(k_y - \mu\frac{2\,\pi}{\Delta y}\right)}_{=:\,\mathrm{III}(\frac{k_y\,\Delta y}{2\pi})} \tag{11}$$

and spatial truncation leads to the driving function of the finite length, discretized array built from an odd number N of spherical monopoles

$$D_{w,\mathrm{S}}(y_0) = \sum_{\nu=-\frac{N-1}{2}}^{+\frac{N-1}{2}} \frac{1}{N} \cdot \delta(y_0 - \nu\,\Delta y) \;\circ\!\!-\!\!\bullet$$

$$D_{w,\mathrm{S}}(k_y,\omega) = \begin{cases} \frac{\sin\left(k_y\,\Delta y\,\frac{N}{2}\right)}{N\,\sin\left(k_y\,\Delta y\,\frac{1}{2}\right)} & \text{for } k_y \neq \frac{2\,\pi}{\Delta y}\,\mu \\ 1 & \text{for } k_y = \frac{2\,\pi}{\Delta y}\,\mu. \end{cases} \tag{12}$$

$D_{w,\mathrm{S}}(k_y,\omega)$ is the so called aliased sinc function. For odd N it is periodic with the spatial sampling frequency $k_{y,\mathrm{S}} = \frac{2\,\pi}{\Delta y}$ and exhibits spectral repetitions of the 'base band' $|k_y| \le \frac{\pi}{\Delta y}$. For $\mu = 0$ the main lobe is obtained, for all other μ grating lobes of the same level as the main lobe occur. This LSA configuration exhibits an equivalent length $L = \Delta y\,N$, that a continuous, finite length LSA would have.

The sampling model requires a spatial reconstruction filter to suppress the spectral repetitions. This

filter has to be applied in the acoustic domain. As spatial reconstruction filter $H_{\mathrm{Post}}(k_y, \omega)$, the line piston on y-axis with length l

$$H_{\mathrm{Rect}}(y_0) = \begin{cases} \frac{1}{l} & \text{for } |y_0| \leq \frac{l}{2} \\ 0 & \text{else} \end{cases} \quad \circ\!\!-\!\!\bullet$$

$$H_{\mathrm{Rect}}(k_y, \omega) = \begin{cases} \frac{\sin(k_y \frac{l}{2})}{k_y \frac{l}{2}} & \text{for } k_y \neq 0 \\ 1 & \text{for } k_y = 0 \end{cases} \tag{13}$$

and the circular piston within the yz-plane with radius r_0

$$H_{\mathrm{Circ}}(y_0, z_0) = \begin{cases} \frac{1}{\pi\, r_0^2} & \text{for } y_0^2 + z_0^2 \leq r_0^2 \\ 0 & \text{else} \end{cases} \quad \circ\!\!-\!\!\bullet$$

$$H_{\mathrm{Circ}}(k_y, \omega) = \begin{cases} \frac{2\, J_1(k_y\, r_0)}{k_y\, r_0} & \text{for } k_y \neq 0 \\ 1 & \text{for } k_y = 0 \end{cases} \tag{14}$$

were considered for the derivation of the first WST criterion, denoting the cylindrical Bessel function of 1^{st} kind of 1^{st} order [16, §10.2] with $J_1(\cdot)$. Under the assumption that the LSA is built from identical pistons, the driving function's spatio-temporal spectrum

$$D_{w,\mathrm{S,H}}(k_y, \omega) = D_{w,\mathrm{S}}(k_y, \omega) \cdot H_{\mathrm{Post}}(k_y, \omega) \tag{15}$$

follows as a consequence of the product or pattern multiplication theorem [17, p.174], [10, Ch. 2.8].

Note that all driving function and postfilter Fourier transform pairs are chosen for amplitude normalization at $k_y = 0$, such that the main lobes exhibit unity gain. In doing so, relative grating and side lobe amplitudes can be conveniently discussed in terms of their absolute values.

The propagating part of $G_0(x, k_y, \omega)$ is bounded and thus bandlimited to the region where $|k_y| < \frac{\omega_0}{c}$ allows propagating wave synthesis. This is referred to as the *visible region* [10, Ch. 2.3] or *physical region* [3] of the array. Evanescent wave radiation occurs for $|k_y| > \frac{\omega_0}{c}$, this part of the spectrum is not bandlimited, however it is decaying rapidly for increased x. By restricting the spatio-temporal spectra of the driving functions to the visible region $-\frac{\omega_0}{c} < k_y < +\frac{\omega_0}{c}$, the nonlinear mapping between k_y and the propagating wave radiation angle ϕ

$$k_y = \frac{\omega_0}{c}\, \sin\phi \tag{16}$$

leads to the farfield radiation patterns $D_w(\phi)$, $D_{w,\mathrm{S}}(\phi)$ and $D_{w,\mathrm{S,H}}(\phi)$ of finite length LSAs for a given temporal frequency ω_0. $D_{w,\mathrm{S}}(\phi)$ is usually referred to as the *array factor* [10, p.45] or the *form factor* [3, II.2.a], whereas $D_{w,\mathrm{S,H}}(\phi)$ is termed *final array factor*, e.g. [18]. Those exclusively trigger the propagating part of the Green's function spatio-temporal spectrum [15, (52)]

$$G_0(x, k_y, \omega) = -\frac{\mathrm{j}}{4}\, H_0^{(2)}\left(\sqrt{\left(\frac{\omega}{c}\right)^2 - k_y^2} \cdot x\right), \tag{17}$$

denoting the 0^{th} order cylindrical Hankel function of 2^{nd} kind [16, §10.2] as $H_0^{(2)}(\cdot)$. The propagating contributions of the sound field can be consequently obtained by inverse spatial Fourier transform

$$P(x, y, \omega) = \frac{1}{2\,\pi} \times \int_{-\frac{\omega_0}{c}}^{+\frac{\omega_0}{c}} \underbrace{D_{w,\mathrm{S,H}}(k_y, \omega)\, G_0(x, k_y, \omega)}_{P(x, k_y, \omega)}\, \mathrm{e}^{-\mathrm{j}\, k_y\, y}\, \mathrm{d}k_y, \tag{18}$$

which is known as the 'method of decomposition into wavelengths' [19, Ch. 13.5.4] and correctly synthesizes the sound fields of the Fresnel and Fraunhofer region. In (18) the LSA is exemplarily modeled with $D_{w,\mathrm{S,H}}(k_y, \omega)$ but any other LSA model can be employed with another driving function's spatio-temporal spectrum, cf. [2, (24,45)].

Grating lobes within the array factor that enter the visible region of the array are the most critical contributions to spatial aliasing. If not sufficiently suppressed, those contributions interfere with the intended main lobe beam. This results in a heavily corrupted Fresnel region, that was referred to as the *chaotic region* of an LSA [3, Fig. 16]. The sound field in this region is not amenable for equalization, since the sound pressure is highly dependent on the listener point and the frequency. The grating lobes furthermore are included in the farfield radiation pattern, as discussed above, which describes the Fraunhofer region of the LSA.

The first three WST criteria introduced different approaches for LSA applications (i) to completely avoid grating lobes within the visible region (WST#2) or (ii) to attenuate them, if entering into the visible region cannot be avoided (WST#1,#3).

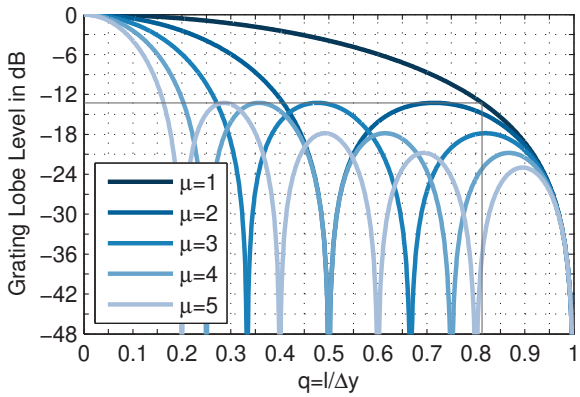

(a) Line piston LSA, ARF $= q$, the ratio $q = 0.812797$ with a resulting 1st grating lobe attenuation of 13.26 dB is indicated with lines.

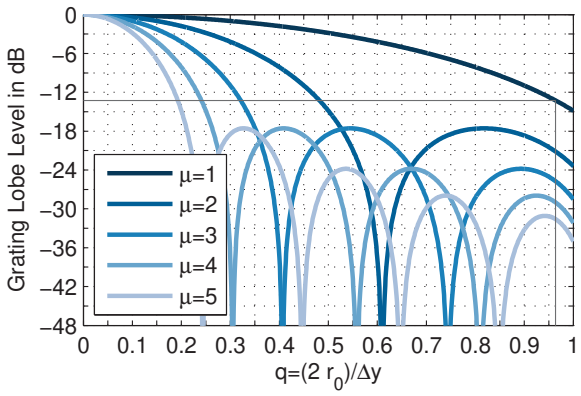

(b) Circular piston LSA, ARF $= \frac{\pi}{4} q^2$, the ratio $q = 0.9635792$ with a resulting 1st grating lobe attenuation of 13.26 dB is indicated with lines.

Fig. 3: Grating lobe level vs. q for (a) a line piston LSA and (b) a circular piston LSA. Relative grating lobe levels for $k_y = \mu \frac{2\pi}{\Delta y}$, $1 \leq \mu \leq 5$ are given. Only for a large number N of pistons this level corresponds to the real local maxima/minima of (19) and (25).

3. DISCUSSION OF WST #1:

The maximum tolerated grating lobe level of -13.5 dB relative to the intended main lobe can be understood as the essence of the 1st WST criterion (1). [3, 4, 5] concluded that this is only realizable with line pistons, i.e. waveguides. We present a discussion for both, the line and the circular piston for completeness.

3.1. The ARF for a Line Piston LSA

The initial derivation of the ARF-theorem [3, (8)], [5, Sec. 3.2] was performed by defining a continuous, uniformly driven, finite length line source and a polarity-inverted *disruption grid* and thus, by inherently modeling a line piston LSA. We give another, yet consistent derivation using the product theorem (15) with (12) and (13)

$$D_{w,\mathrm{S,H}}(k_y, \omega) = \frac{1}{N} \frac{\sin(k_y\, \Delta y\, N/2)}{\sin(k_y\, \Delta y/2)} \cdot \frac{\sin\left(k_y \frac{l}{2}\right)}{k_y \frac{l}{2}}. \tag{19}$$

Finding the local minima and maxima, especially of grating lobes

$$\frac{\mathrm{d}D_{w,\mathrm{S,H}}(k_y, \omega)}{\mathrm{d}k_y} = 0, \tag{20}$$

besides the main lobe, in order to minimize its largest occurring magnitude does not lead to a general closed form solution, which also holds for $D_w(k_y)$ and $D_{w,\mathrm{S}}(k_y)$. However, for large N the grating lobe maxima are approximately located at $k_y = \mu \frac{2\pi}{\Delta y}$, $\mu \in \mathbb{Z}, \neq 0$ in (19). The grating lobes decrease in level – except for the case $l = 0$ – for increasing $|k_y|$ due to the spatial lowpass characteristic of (13). Hence, the first grating lobes at $|\mu| = 1$ determine the maximum occurring and tolerated level of grating lobes. With the initial definition [5, p.917]

$$\mathrm{ARF} = q = \frac{l}{\Delta y} \qquad 0 \leq q \leq 1 \tag{21}$$

(19) is evaluated at $k_y = \Delta k_y = \frac{2\pi}{\Delta y}$ to

$$A(q) = D_{w,\mathrm{S,H}}(k_y = \Delta k_y, \omega) = \frac{\sin(\pi\, q)}{\pi\, q}, \tag{22}$$

for which $A(q) \in \mathbb{R}^+$ is valid for the given range of q. For $q = 0$ a linear array built from spherical monopoles is modeled, due to the limit $H_{\mathrm{Rect}} = 1$. All grating lobes will not be suppressed – $D_{w,\mathrm{S,H}}(k_y = \mu\, \Delta k_y, \omega) = 1$ – due to the missing spatial lowpass characteristic of a monopole. The limit $q = 1$ perfectly suppresses all grating lobes –

$D_{w,\mathrm{S,H}}(k_y = \mu\,\Delta k_y, \omega) = 0$ for $\mu \neq 0$ –, which furthermore leads to

$$D_w(k_y, \omega) = D_{w,\mathrm{S}}(k_y, \omega) \cdot H_{\mathrm{Rect}}(k_y, \omega)\big|_{l=\Delta y}, \quad (23)$$

i.e. the reconstruction towards the driving function's spectrum of the continuous, finite length LSA (10). Note that this perfect reconstruction holds only for $\Delta y = l$ and the WST driving function (12), i.e. for wave radiation perpendicular to the LSA. Note also, that in this case the reconstruction is independent of the temporal frequency and of the chosen length $\Delta y = l$. The maximum tolerated grating lobe level thus can be controlled between 0 dB and $-\infty$ dB by setting $0 \leq \mathrm{q} \leq 1$. This is depicted in Fig. 3a.

In [3, 5] the maximum tolerated level of grating lobes was set to the largest occurring relative side lobe level of -13.26 dB[2] of a uniformly driven, continuous linear array, i.e. the maximum side lobe level of a continuous rectangular window. Therefore solving (22) for $A(q) = 10^{-13.26/20}$ numerically, the ARF is given as

$$\mathrm{ARF} = q \approx 0.812797. \quad (24)$$

This is in accordance with [5, p.917], where the approximation ARF ≥ 0.82 for large N is given. Note that (22) is independent of N in first instance. A discussed above, only for large N (19) exhibits also the local maximum at exactly $k_y = \Delta k_y$.

The ARF is a temporal frequency independent measure since the derivation was performed in the k_y-domain. The occurrence of (attenuated) grating lobes depends on the visible region $-\frac{\omega_0}{c} < k_y < +\frac{\omega_0}{c}$ of the LSA. This indicates that if (2) can be fulfilled, the ARF criterion is of secondary importance and conversely, if (2) cannot be met, the grating lobe suppression is heavily dependent on the characteristics of the spatial reconstruction filter. An LSA with smaller Δy and smaller ARF may produce a better spatial-aliasing-free sound field for an intended frequency range, than an LSA with larger Δy and larger ARF. This is important realizing when aiming for electronic beam steering, that was initially not intended for the first LSA generation.

3.2. The ARF for a Circular Piston LSA

A treatment similar to Sec. 3.1 is given for the circular piston LSA. Applying the circular piston's postfilter characteristics (14) and the driving function (12) to the product theorem (15) yields

$$D_{w,\mathrm{S,H}}(k_y, \omega) = \frac{1}{N} \frac{\sin(k_y\,\Delta y\,N/2)}{\sin(k_y\,\Delta y/2)} \cdot \frac{2\,J_1(k_y\,r_0)}{k_y\,r_0}, \quad (25)$$

We define a ratio of lengths

$$q = \frac{d_0}{\Delta y} \qquad 0 \leq q \leq 1, \quad (26)$$

by introducing the piston's diameter $d_0 = 2\,r_0$. The ARF can be deduced to

$$\mathrm{ARF} = \frac{\pi\,r_0^2}{\Delta y^2} = \frac{\pi\,\left(\frac{q}{2}\,\Delta y\right)^2}{\Delta y^2} = \frac{\pi}{4}\,q^2, \quad (27)$$

by modeling a quadratic enclosure of side length Δy. Note that the ARF here is truly a ratio of surface areas (ARF $\neq q$), whereas for the line piston a ratio of line lengths is defined (ARF $= q$). Therefore, care must be taken when comparing the definitions of the ARF and q and its implications.

Evaluating (25) at $k_y = \Delta k_y = \frac{2\,\pi}{\Delta y}$ yields the relative level of the first grating lobe

$$A(q) = D_{w,\mathrm{S,H}}(k_y = \Delta k_y, \omega) = \frac{2\,J_1(\pi\,q)}{\pi\,q}. \quad (28)$$

The level of the first grating lobe ($\mu = 1$) over q is depicted in Fig. 3b. For $q = 1$ the maximum possible ARF $= \pi/4$ is obtained for directly adjacent pistons $\Delta y = d_0$. This yields the maximum possible attenuation of grating lobes. For the first grating lobe (28) is evaluated to

$$A(q = 1) = \frac{2\,J_1(\pi)}{\pi} \approx 0.181192, \quad (29)$$

which corresponds to -14.84 dB. This is in contrast to the line piston, for which perfect suppression ($-\infty$ dB) of the first grating lobe (and all others) is achieved for $q = 1$. This due to the fact that the first zero of the Bessel function cannot be coincidentally located to $k_y = \Delta k_y$ without overlapping pistons, which is physically not meaningful.

Regarding the initial intention of the 1st WST criterion, solving (28) for $A(q) = 10^{-13.26/20}$ yields

$$q = 0.9635792 \qquad \mathrm{ARF} = \frac{\pi}{4}\,q^2 = 0.72923. \quad (30)$$

[2] To be precise, [3] uses -12dB and [5] uses -13.5 dB

Hence, the circular piston postfilter is also able to attenuate the first grating lobe by 13.26 dB and therefore would be WST #1-compliant. This deduction is in contrast to that given in [3, 5]. In fact, the postfilter of the circular piston has a better spatial lowpass characteristic than the line piston since the Bessel function has a larger amplitude decay for increasing arguments than the $\sin(x)/x$ function. This can also be graphically deduced in Fig. 3. Only for $q \approx 1$ the grating lobe suppression for a line piston LSA is superior to a circular one.

While this discussion provides the whole picture of the ARF theorem from a theoretical viewpoint, LSAs nevertheless should be designed with waveguides for high audio frequencies due to the following reasons: (i) The circular piston model assumes a constant velocity over the membrane surface which is in practice much more demanding than designing an appropriate waveguide with an intended wavefront curvature; (ii) LSAs aim at a frequency independent horizontal coverage. This is much easier to control with the design of an appropriate waveguide than using circular pistons, i.e. electrodynamic loudspeakers.

4. DISCUSSION OF WST #2:

Some recent LSA designs exhibit a very small source spacing Δy for high audio frequencies to shift spatial aliasing to very high audio frequencies and to relax the ARF requirements. Those LSA designs can be fixed straightly and aim at electronic beam forming and -steering, instead of controlling the LSA radiation characteristics with geometric curving. The most simple beam steering method is the delay-and-sum approach [10, Ch. 2.5], for which [17, p.175]

$$\Delta y < \frac{\lambda_{\min}}{2} \frac{N-1}{N} \tag{31}$$

ensures that no grating lobe beams enter the visible region for all possible steering angles $|\phi_{\text{Steer}}| < 90°$ of a rectangular windowed LSA built from spherical monopoles. For a very large source number N (31) merges into (2). Instead of using the spatial lowpass characteristics to avoid or attenuate spatial aliasing, this criterion relies on the limitation of the excitation signal's temporal frequency bandwidth. The condition (31) may be relaxed if only a limited steering angle $|\phi_{\text{Steer}}| < |\phi_{\text{Steer,max}}|$ is allowed. For an infinite linear array [20, (10)], [15, (38)]

$$\Delta y < \frac{\lambda_{\min}}{1 + |\sin \phi_{\text{Steer,max}}|} \tag{32}$$

is known from SFS of a plane wave, as well as from antenna design [10, (2.129)]. For a finite length, rectangular windowed array with N spherical monopoles the condition reads

$$\Delta y < \frac{\lambda_{\min}}{1 + |\sin \phi_{\text{Steer,max}}|} \frac{N-1}{N}, \tag{33}$$

which is consistent with the result given in [21, (12)] for $\phi_{\text{Steer}} = 0$. Note that due to the non-linear mapping of $k_y \leftrightarrow \phi$ the beamwidth broadens for increased ϕ_{Steer} [10, Ch. 2.5], which is not further discussed here, since this paper is primarily interested in avoiding spatial aliasing.

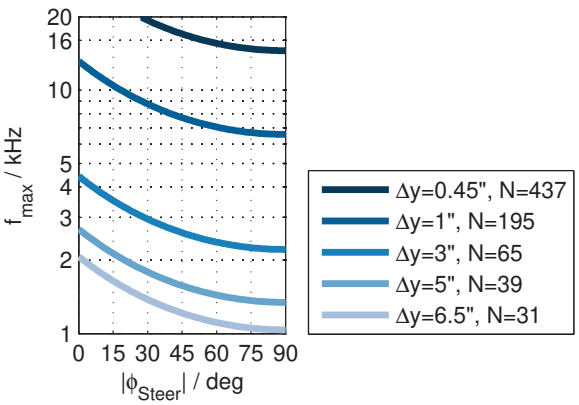

Fig. 4: Aliasing frequency over steering angle (33).

For typical source spacings in LSA designs the maximum allowed frequency $f_{\max}$ for grating lobe free beam steering over the steering angle ϕ_{Steer} is depicted in Fig. 4, assuming $q = 1$. The LSA length is always $L \approx 5\,\text{m}$. For the lowest audio frequencies typical larger electrodynamic loudspeakers are used and the range is approximately given as e.g. $400\,\text{Hz} < f_{\max} < 800\,\text{Hz}$ for $90° \geq \phi_{\text{Steer}} \geq 0°$ ($N = 13$, $\Delta y = 15$") and $500\,\text{Hz} < f_{\max} < 1000\,\text{Hz}$ for $90° \geq \phi_{\text{Steer}} \geq 0°$ ($N = 17$, $\Delta y = 12$"). The low frequency band is thus uncritical for grating lobe free beam steering. However large waveguides of about the same dimension are not capable of pure electronic beam steering for high audio frequencies

due to the comparably low $f_{\max}$ [2, 22]. Therefore such LSAs have to be curved geometrically in addition and delay-and-sum beamforming should there be avoided for the high frequencies. The mid-band of audio frequencies is very often driven by 5" or 6.5" speakers and an appropriate trade-off between the crossover lowpass cut-frequency and the allowed maximum steering angle has to be defined. The high-band of audio frequencies is still the most critical w.r.t. spatial aliasing and requires very small distances between drivers to avoid it. While this was not considered feasible when approaching LSA designs in the early 1990s for the first time, such techniques have been engineered nowadays. In the given example the 1"-piston would allow grating lobe free sound fields up to 10 kHz, when restricting $|\phi_{\text{Steer,max}}| < 20°$, while the 0.45"-design would allow endfire beams up to 15 kHz.

5. DISCUSSION OF WST #3:

The 3rd WST criterion was derived for an LSA with directly adjacent horns (with no gaps) that exhibit a specified wavefront curvature (WFC). By discussing the 1st (1) and 3rd (3) WST criterion separately in [5, 13], one may erroneously assume that they are not interrelated. However, both criteria interact and determine the quality of grating lobe avoidance and suppression, which is discussed in this section.

5.1. Line Piston with Wavefront Curvature

Since a line piston with wavefront curvature exhibits a specific postfilter characteristics $H_{\text{Post}}(k_y, \omega)$, the discussion remains consistent within the signal processing in Fig. 2 by interpreting the resulting spatio-temporal spectrum $D_{w,\text{S,H}}(k_y, \omega)$. This discussion – based on the product theorem – was already given in [12, 13], however the farfield radiation pattern of a physically arc-shaped, uniformly driven source is utilized, i.e. the Huygens principle is applied. We propose to use Rayleigh-Sommerfeld diffraction of a baffled, infinitesimal narrow slit of finite length that is 'illuminated' by a point source. The wavefront curvature can be controlled by the point source position $\mathbf{x}_{\text{PS}} = (-x_{\text{PS}}, 0, 0)^T$ behind the slit on y-axis, i.e. the distance x_{PS} in Fig. 1. With the line piston's length l and a desired wavefront curvature in terms of a wave length ratio $S = \alpha\,\lambda$, the geometric length and angle relations

$$x_{\text{PS}} = \frac{l^2}{8\,S} - \frac{S}{2} = \frac{l^2}{8\,\alpha\,\lambda} - \frac{\alpha\,\lambda}{2}, \tag{34}$$

$$r = \frac{l^2}{8\,S} + \frac{S}{2} = \frac{l^2}{8\,\alpha\,\lambda} + \frac{\alpha\,\lambda}{2}, \tag{35}$$

$$\tan\phi = \frac{\frac{l}{2}}{\frac{l^2}{8\,S} - \frac{S}{2}} = \frac{\frac{l}{2}}{\frac{l^2}{8\,\alpha\,\lambda} - \frac{\alpha\,\lambda}{2}} \tag{36}$$

are derived according to Fig. 1. We require the distance $x_{\text{PS}} > 0$, which is valid if $l^2/4 > (\alpha\,\lambda)^2$.

SFS of a virtual point source using a linear, finite length, continuous secondary source distribution that models the slit is employed. The diffracted sound field is synthesized with [23, (16,31)]

$$P(\mathbf{x}, \omega) = \int_{-l/2}^{+l/2} D_{\text{WFC}}(y_0, \omega)\, G_N(\mathbf{x}, \mathbf{x_0}, \omega)\, \mathrm{d}y_0, \tag{37}$$

using the slit $\mathbf{x_0} = (0, y_0, 0)^T$ on y-axis, $\mathbf{x} = (x > 0, y, 0)^T$ and the 3D Neumann Green's function $G_N(\mathbf{x}, \mathbf{x_0}, \omega) = 2\,G(\mathbf{x}, \mathbf{x_0}, \omega)$. Using (34), the Spectral Division Method driving function [23, (24)]

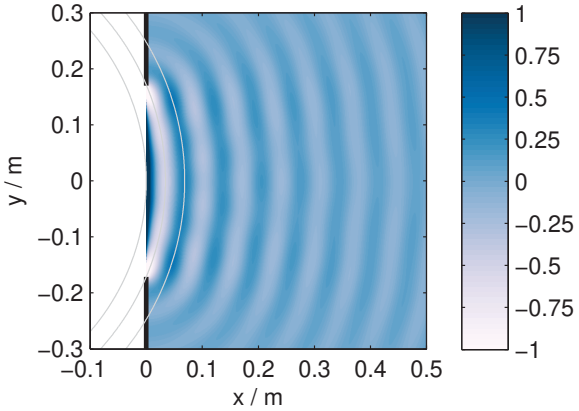

Fig. 5: Diffracted sound field $\Re\{P(\mathbf{x}, \omega)\}$ of a point source synthesized by a baffled line piston with $l = 0.343\,\text{m}$ for $f = 5\,\text{kHz}$ using a wavefront curvature $\alpha = 1/2$, $x_{\text{PS}} = 0.4116\,\text{m}$, $\vartheta = 22.62°$, $c = 343\,\text{m/s}$. Normalized to $\Re\left\{P(\mathbf{x} = (\lambda/2, 0, 0)^T, \omega)\right\} = -1/2$.

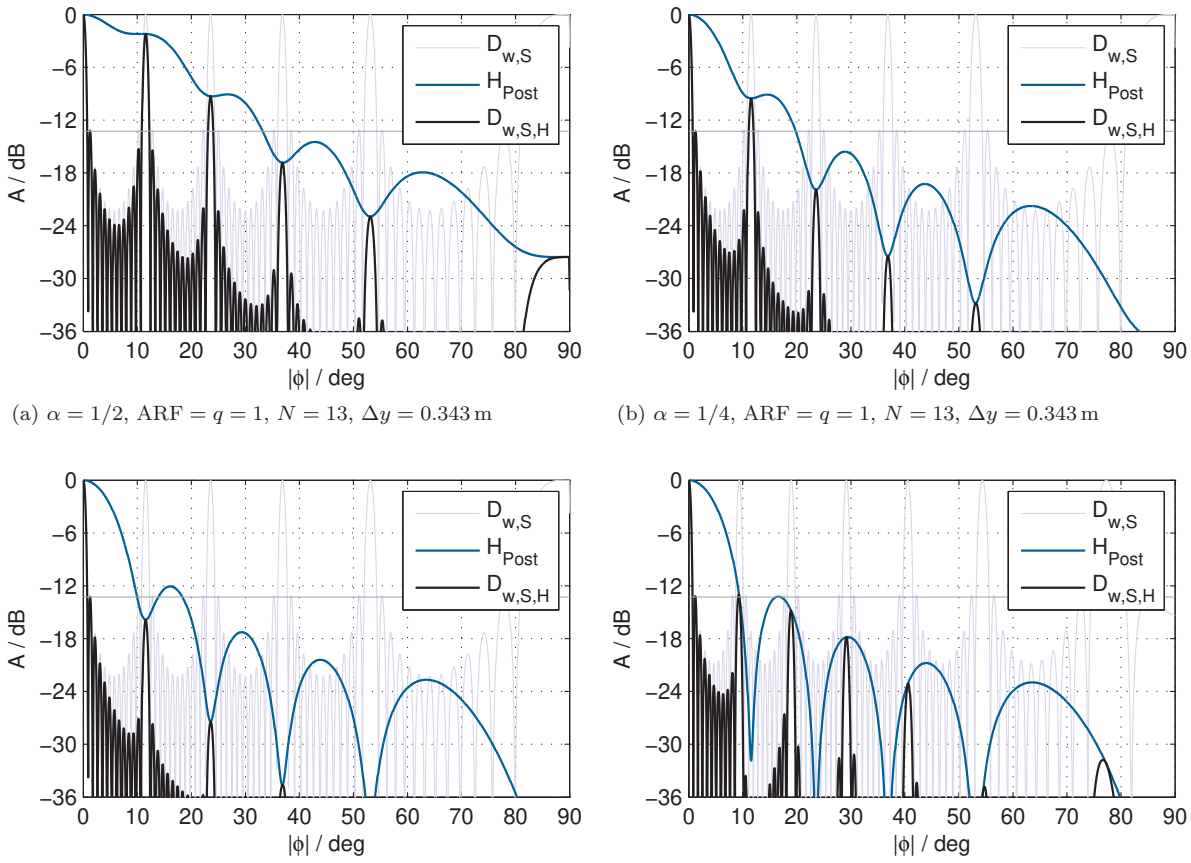

(a) $\alpha = 1/2$, ARF $= q = 1$, $N = 13$, $\Delta y = 0.343\,\mathrm{m}$

(b) $\alpha = 1/4$, ARF $= q = 1$, $N = 13$, $\Delta y = 0.343\,\mathrm{m}$

(c) $\alpha = 1/8$, ARF $= q = 1$, $N = 13$, $\Delta y = 0.343\,\mathrm{m}$

(d) $\alpha = 1/50$, ARF $= q = 0.812797$, $N = 11$, $\Delta y = 0.422\,\mathrm{m}$

Fig. 6: Uniformly driven LSA with line pistons that exhibit a specified wavefront curvature. The excitation function $D_{\mathrm{w,S}}(\phi)$ (12), the postfilter $H_{\mathrm{Post}}(\phi)$ (39) and the resulting LSA farfield radiation pattern $D_{\mathrm{w,S,H}}(\phi) = D_{\mathrm{w,S}}(\phi) \cdot H_{\mathrm{Post}}(\phi)$ for $f = 5\,\mathrm{kHz}$, $l = 0.343\,\mathrm{m}$, $c = 343\,\mathrm{m/s}$ are visualized.

reads

$$D_{\mathrm{WFC}}(y_0, \omega) = \frac{1}{4}\sqrt{\frac{x_{\mathrm{ref}}}{x_{\mathrm{ref}} + x_{\mathrm{PS}}}}\,\mathrm{j}\frac{\omega}{c}\,(-x_{\mathrm{PS}})\times \quad (38)$$
$$\frac{1}{\|\mathbf{x_0} - \mathbf{x}_{\mathrm{PS}}\|} \cdot H_1^{(2)}\left(\frac{\omega}{c}\,\|\mathbf{x_0} - \mathbf{x}_{\mathrm{PS}}\|\right),$$

denoting the Hankel function of second kind of order one as $H_1^{(2)}(\cdot)$ [16, §10.2]. In contrast to Wave Field Synthesis driving functions [23, 24], (38) is also valid for point sources close to the slit, when the reference point x_{ref} – at which the sound field is to be synthesized correctly in amplitude and phase – is chosen very large. This is in accordance for the quested farfield radiation pattern. Since the driving function is proportional to the normal source velocity, the spatial-temporal spectrum [19, Ch. 3.6]

$$H_{\mathrm{WFC}}(k_y, \omega) = \int_{-l/2}^{+l/2} D_{\mathrm{WFC}}(y_0, \omega)\,\mathrm{e}^{+\mathrm{j}\,k_y\,y_0}\,\mathrm{d}y_0, \quad (39)$$

normalized to unity gain at $k_y = 0$ for consistency, includes the farfield radiation pattern of the line piston with wavefront curvature. The integral is not

treatable for an analytic closed form solution and therefore numerical evaluation with a zero-padded FFT of the spatially discretized version of (38) is used. In Fig. 5 an example of the diffracted sound field for a wavefront curvature of $\alpha = 1/2$ is given. The shown circles exhibit a radius increment of $\lambda/2$. One circle intersects the line piston in the origin and the subsequent circle with radius increment of $\lambda/2$ intersects the line piston at its ends, which defines the sagitta S. In the following subsections the influence of the wavefront curvature w.r.t. grating lobe suppression is discussed for exemplarily chosen LSA setups and frequencies.

5.2. Single Waveguide LSA Element

For Fig. 6 different LSAs of about the same physical length $L = (N-1)\,\Delta y + l \approx 4.5\,\mathrm{m}$ are modeled with line pistons of the same length $l = 0.343\,\mathrm{m}$ that exhibit different wavefront curvatures and ARF. The specific postfilters and the resulting LSA farfield radiation patterns over radiation angle ϕ are depicted for $f = 5\,\mathrm{kHz}$.

The line piston with $\alpha = 1/2$ from Fig. 5 is used to model an ARF=1, N=13 LSA in Fig. 6a. The first grating lobes, with radiation angles $\approx \pm 10°$, are attenuated by $\approx 2\,\mathrm{dB}$ (cf. [12, Fig. 20]), the second by 9 dB. For Fig. 6b the wavefront curvature is decreased to $\alpha = 1/4$, the maximum grating lobe level is about $-10\,\mathrm{dB}$ relative to the main lobe level (cf. [12, Fig. 19], [5, p.919]). According to the 3rd WST criterion (3), $\alpha = 1/4$ is the maximum tolerated wavefront curvature, which however violates the 1st WST criterion (1) (min. 13.5 dB grating lobe suppression), even for ARF = 1.

A wavefront curvature of $\alpha = 1/8$ is depicted in Fig. 6c (cf. [12, Fig. 18]). The maximum grating lobe level does not exceed approx. $-16\,\mathrm{dB}$ for ARF = 1 and approx. $-11.5\,\mathrm{dB}$ for ARF = 0.82. Hence, this wavefront curvature violates the 1st WST criterion for ARF = 0.82. In compliance with a tolerated maximum grating lobe level of $-13.26\,\mathrm{dB}$ a wavefront curvature of $\alpha = 1/6$ is required, which however holds only for ARF $\approx$ 1. If ARF = 0.82 is allowed, thus fulfilling the 1st WST criterion, the curvature $\alpha > 1/50$ ensures the maximum allowed grating lobe level $-13.26\,\mathrm{dB}$, as shown in Fig. 6d. For curvatures $\alpha > 1/50$ the postfilter exhibits almost the same characteristics as the ideal line piston without wavefront curvature.

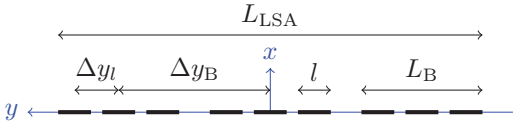

Fig. 7: Schematical sketch of an LSA built from $N_{\mathrm{B}} = 3$ boxes of physical height L_{B} spaced by Δy_{B}. Each box has $N_l = 3$ line pistons of height l spaced by Δy_l. The total physical length of the LSA is L_{LSA}. N_{B} and N_l are assumed to be odd-numbered.

5.3. Multiple Waveguide LSA Box

The discussion above is valid for a single waveguide that spans about the entire height of a single LSA cabinet. In practical designs an LSA cabinet is often built from multiple and smaller waveguides each coupled to an individual compression driver, cf. Fig. 7. Ideally the waveguides should be driven individually, since this improves the capability for electronic beam forming, cf. Sec. 4. However, it is still common practice to drive high frequencies uniformly, i.e. all compression drivers per LSA cabinet get the same signal. For a uniformly driven, straight LSAs this can be modeled with the product theorem for nested arrays, also referred to as subarrays, cf. eg. [18]. The spatio-temporal spectrum is then given as

$$D_{w,\mathrm{S,H}}(k_y,\omega) = \overbrace{\frac{1}{N_l}\frac{\sin(k_y\,\Delta y_l\,N_l/2)}{\sin(k_y\,\Delta y_l/2)}}^{D_{\mathrm{w,S,l}}(k_y,\omega)} \cdot H_{\mathrm{Post}}(k_y,\omega)\times \underbrace{\frac{1}{N_{\mathrm{B}}}\frac{\sin(k_y\,\Delta y_{\mathrm{B}}\,N_{\mathrm{B}}/2)}{\sin(k_y\,\Delta y_{\mathrm{B}}/2)}}_{D_{\mathrm{w,S,B}}(k_y,\omega)}, \tag{40}$$

for which the first product models the farfield radiation pattern of a single LSA cabinet build from N_l pistons, each featuring the spatial postfilter characteristics $H_{\mathrm{Post}}(k_y,\omega)$ (39). The subsequent product using (12) then models the complete farfield radiation pattern of the LSA built from N_{B} cabinets. From Fig. 7 the geometrical relations between the individual ARFs and physical lengths are derived to

$$q_{\mathrm{l}} = \frac{l}{\Delta y_l} \qquad L_{\mathrm{B}} = (N_l - 1)\,\Delta y_l + l, \tag{41}$$

$$q_{\mathrm{B}} = \frac{L_{\mathrm{B}}}{\Delta y_{\mathrm{B}}} \qquad L_{\mathrm{LSA}} = (N_{\mathrm{B}} - 1)\,\Delta y_{\mathrm{B}} + L_{\mathrm{B}}. \tag{42}$$

Due to the interaction of three spatial spectra, the discussion is slightly more complicated and for line pistons with wavefront curvature no closed form solution exists so far. We give some numerical examples of the farfield radiation pattern in Fig. 8 for an assumed highest operating frequency $f = 16\,\mathrm{kHz}$ for a 'multiple waveguides per cabinet'-LSA design. For Fig. 8a and Fig. 8b three rather large waveguides are used per LSA element and the wavefront curvature is varied. The chosen parameters closely match typical LSA designs, i.e. $q_l = 1$ and $\mathrm{ARF} = q_\mathrm{B} = 0.82$. For Fig. 8c and Fig. 8d the waveguides are smaller, thus fitting more of them per LSA element and the $\mathrm{ARF} = q_\mathrm{B}$ is varied, while $q_l = 1$.

For the chosen source spacing and frequency no LSA is grating lobe free, due to violating the 2nd WST criterion. The large wavefront curvature in Fig. 8a leads to grating lobes larger than $-12\,\mathrm{dB}$ for small radiation angles, which can be reduced when decreasing the curvature in Fig. 8b. When comparing Fig. 8b (large waveguides) and Fig. 8c (small waveguides) with otherwise same parameters, it is observed that the grating lobes at small angles ϕ are more attenuated for the latter LSA, due to the larger decay of $D_{\mathrm{w,S,l}}(k_y, \omega)$. It is worth realizing at this point, that grating lobes at small angles corrupt the intended sound field in a much larger spatial region than those radiated with large angles. This advantage, however comes with a comparably larger grating lobe level at $|\phi| \approx 30°$. Due to the almost perfect coincidence of the aliased-sinc grating lobe maxima of $D_{\mathrm{w,S,l}}(k_y, \omega)$ (1st maximum) and $D_{\mathrm{w,S,B}}(k_y, \omega)$ (11th maximum) the postfilter only determines the attenuation level, which yields over 30 dB in Fig. 8b and about 16 dB in Fig. 8c. The coincidence of common maxima from $D_{\mathrm{w,S,l}}(k_y, \omega)$ and $D_{\mathrm{w,S,B}}(k_y, \omega)$ can be controlled by

$$q_\mathrm{B} = \frac{q_l \cdot L_\mathrm{B}}{\sigma \cdot l} \qquad \sigma \geq N_l,\, \sigma \in \mathbb{N} \tag{43}$$

for which $\sigma = N_l$ generally models $q_\mathrm{B} = 1$ if $q_l = 1$. This is an ARF=1 LSA, for which the grating lobe suppression depends only on the spatial postfilter characteristics. The example in Fig. 8c closely matches $\sigma = N_l + 2 = 9 + 2 \rightarrow q_\mathrm{B} = 0.\overline{81}$. By increasing the ARF in Fig. 8d compared to Fig. 8c the grating lobes are generally more attenuated. Grating lobes at $\approx 30°$ differ significantly due to different interaction of the involved functions.

In comparison to Sec. 5.2 larger wavefront curvature (in the example $\alpha \leq 1/8$) is tolerated to fulfill the 1st WST criterion when using multiple smaller waveguides per LSA element. This is due to the additional spatial lowpass filter characteristic of $D_{\mathrm{w,S,l}}(k_y, \omega)$, which compensates the insufficient lowpass characteristic of a waveguide with large wavefront curvature.

Despite the comparably large grating lobe level at about 30°, the LSAs in Fig. 8c, Fig. 8d could be preferred, due to the smaller discretization step (leaving more frequency bandwidth uncorrupted from aliasing, improved capability for electronic beam forming) and due to the larger decay of grating lobe levels for small radiation angles (larger spatial region without spatial aliasing).

CONCLUSION

This paper presents an extended analysis to the first three Wavefront Sculpture Technology criteria for straight line source arrays, that deal with different approaches to avoid or reduce grating lobes. The correct ARF theorem for a circular piston array is furthermore given. For arrays with rather small source spacing the sampling theorem becomes important, when aiming at electronic beam forming and -steering. Meaningful radiation angles for steered arrays are given in terms of grating lobe avoidance. A line piston model for wavefront curvature is introduced and the subarray product theorem is applied to arrays which exhibit more than one waveguide per cabinet. In the latter case the allowed maximum wavefront curvature of a line piston is more relaxed.

6. REFERENCES

[1] Schultz, F.; Rettberg, T.; Spors, S. (2014): "On spatial-aliasing-free sound field reproduction using infinite line source arrays." In: *Proc. of the 136th Audio Eng. Soc. Conv., Berlin*, #9078.

[2] Schultz, F.; Rettberg, T.; Spors, S. (2014): "On spatial-aliasing-free sound field reproduction using finite length line source arrays." In: *Proc. of the 137th Audio Eng. Soc. Conv., Los Angeles*, #9098.

[3] Heil, C.; Urban, M. (1992): "Sound fields radiated by multiple sound sources arrays." In: *Proc. of 92nd Audio Eng. Soc. Conv., Vienna*, #3269.

[4] Urban, M.; Heil, C.; Baumann, P. (2001): "Wavefront Sculpture Technology." In: *Proc. of 111th Audio Eng. Soc. Conv., New York*, #5488.

[5] Urban, M.; Heil, C.; Baumann, P. (2003): "Wavefront Sculpture Technology." In: *J. Audio Eng. Soc.*, **51**(10):912–932.

[6] Start, E.W.; Valstar, V.G.; de Vries, D. (1995): "Application of spatial bandwidth reduction in Wave Field Synthesis." In: *Proc. of the 98th Audio Eng. Soc. Conv., Paris*, #3972.

[7] Start, E.W. (1997): *Direct Sound Enhancement by Wave Field Synthesis*. Ph.D. thesis, Delft University of Technology.

[8] Verheijen, E. (1997): *Sound Reproduction by Wave Field Synthesis*. Ph.D. thesis, Delft University of Technology.

[9] Ahrens, J.; Spors, S. (2010): "On the anti-aliasing loudspeaker for sound field synthesis employing linear and circular distributions of secondary sources." In: *Proc. of the 129th Audio Eng. Soc. Conv., San Francisco*, #8246.

[10] Van Trees, H.L. (2002): *Optimum Array Processing*. New York: Wiley.

[11] Balanis, C.A. (2005): *Antenna Theory - Analysis and Design*. Hoboken: Wiley, 3. ed.

[12] Ureda, M.S. (2001): "Line arrays: Theory and applications." In: *Proc. of 110th Audio Eng. Soc. Conv., Amsterdam*, #5304.

[13] Ureda, M.S. (2004): "Analysis of loudspeaker line arrays." In: *J. Audio Eng. Soc.*, **52**(5):467–495.

[14] Thompson, A. (2009): "Improved methods for controlling touring loudspeaker arrays." In: *Proc. of 127th Audio Eng. Soc. Conv., New York*, #7828.

[15] Ahrens, J.; Spors, S. (2010): "Sound field reproduction using planar and linear arrays of loudspeakers." In: *IEEE Trans. Audio Speech Language Process.*, **18**(8):2038–2050.

[16] Olver, F.W.J.; Lozier, D.W.; Boisvert, R.F.; Clark, C.W. (2010): *NIST Handbook of Mathematical Functions*. Cambridge University Press, 1. ed.

[17] Stenzel, H. (1929): "Über die Richtcharakteristik von in einer Ebene angeordneten Strahlern." In: *Elektrische Nachrichtentechnik*, **6**(5):165–181.

[18] Brockett, T.J.; Rahmat-Samii, Y. (2012): "Subarray design diagnostics for the suppression of undesirable grating lobes." In: *IEEE Trans. Antennas and Propagation*, **60**(3):1373–1380.

[19] Möser, M. (2009): *Engineering Acoustics, An Introduction to Noise Control*. Dordrecht, Berlin, Heidelberg, New York: Springer, 2. ed.

[20] Spors, S.; Rabenstein, R. (2006): "Spatial aliasing artifacts produced by linear and circular loudspeaker arrays used for wave field synthesis." In: *Proc. of the 120th Audio Eng. Soc. Conv., Paris*, #6711.

[21] Stenzel, H. (1927): "Über die Richtwirkung von Schallstrahlern." In: *Elektrische Nachrichtentechnik*, **4**(6):239–253.

[22] Meyer Sound Laboratories Inc. (2002): "DSP beam steering with modern line arrays." Tech. rep., `https://www.meyersound.com/pdf/support/papers/beam_steering.pdf`, last seen on 2014-10-17.

[23] Spors, S.; Ahrens, J. (2010): "Analysis and improvement of pre-equalization in 2.5-dimensional Wave Field Synthesis." In: *Proc. of the 128th Audio Eng. Soc. Conv., London*, #8121.

[24] Spors, S.; Rabenstein, R.; Ahrens, J. (2008): "The theory of Wave Field Synthesis revisited." In: *Proc. of the 124th Audio Eng. Soc. Conv., Amsterdam*, #7358.

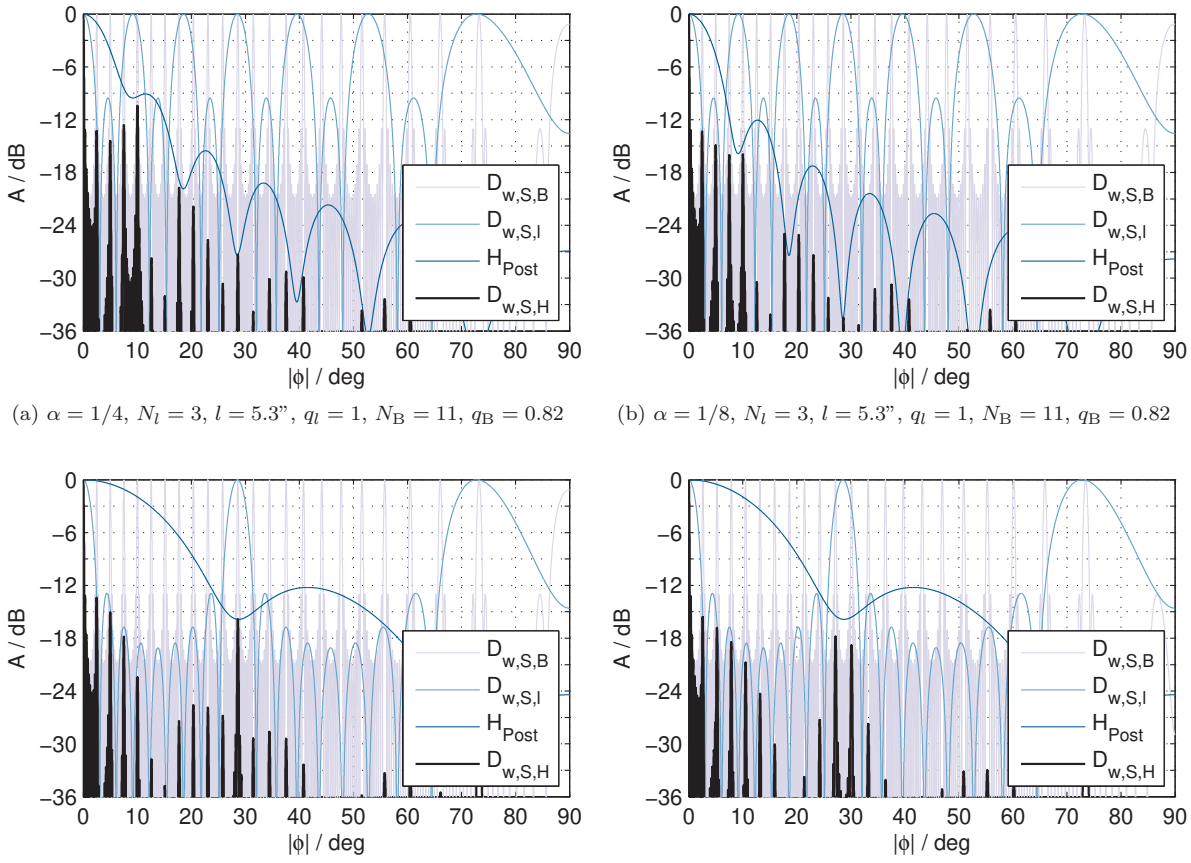

(a) $\alpha = 1/4$, $N_l = 3$, $l = 5.3$", $q_l = 1$, $N_\mathrm{B} = 11$, $q_\mathrm{B} = 0.82$

(b) $\alpha = 1/8$, $N_l = 3$, $l = 5.3$", $q_l = 1$, $N_\mathrm{B} = 11$, $q_\mathrm{B} = 0.82$

(c) $\alpha = 1/8$, $N_l = 9$, $l = (5.3/3)$", $q_l = 1$, $N_\mathrm{B} = 11$, $q_\mathrm{B} = 0.82$

(d) $\alpha = 1/8$, $N_l = 9$, $l = (5.3/3)$", $q_l = 1$, $N_\mathrm{B} = 11$, $q_\mathrm{B} = 0.86$

Fig. 8: Grating lobe levels over $|\phi|$ for uniformly driven LSAs with line pistons of specified wavefront curvature α using (40) with (38) and (39), $f = 16\,\mathrm{kHz}$, $c = 343\,\mathrm{m/s}$. Fig. a) and b) use 3x 5.3" waveguides per LSA cabinet, α is varied. Fig. c) and d) use 9x 1.76" waveguides per LSA cabinet, q_B is varied. q_l=1 for all cases.

Evaluation Strategies for the Optimization of Line Source Arrays

Florian Straube[1], Frank Schultz[2], Michael Makarski[3], Sascha Spors[2] and Stefan Weinzierl[1]

[1]*Audio Communication Group, TU Berlin, DE-10587, Berlin, Germany*

[2]*Institute of Communications Engineering, University of Rostock, DE-18119, Rostock, Germany*

[3]*Four Audio GmbH & Co. KG, DE-52134, Herzogenrath, Germany*

Correspondence should be addressed to Florian Straube (`florian.straube@tu-berlin.de`)

ABSTRACT

Line source arrays (LSAs) are used for large scale sound reinforcement, aiming at the synthesis of highly spatial aliasing-free sound fields for the whole audio bandwidth. Numerical optimization of the loudspeakers' driving functions can considerably improve the homogeneity of the intended sound field. In this paper we propose enhanced visualization techniques characterizing the array performance. This may lead to a more convenient interpretation of the LSA radiation behavior. By additionally recommended technical quality measures the LSA design and the optimization requirements might be improved. The approach is exemplarily discussed for fictitious LSA models. Based on a least-mean-square error optimization using a loudspeaker weight energy constraint, the driving functions are derived. It is shown by means of the visualizations and measures why this optimization scheme being common practice in sound field synthesis applications is inappropriate for the problem at hand and that spatial aliasing has a large impact on the synthesized sound fields. We recommend to incorporate the proposed quality measures as criteria for future optimization approaches.

1. INTRODUCTION

Optimized electronic control of curved line source arrays (LSAs) for improved sound reinforcement has gained interest in the last two decades. The calculation of appropriate driving signals, i.e. FIR filters for the individual LSA loudspeakers in order to generate a desired sound field by numerical optimization techniques was discussed in [1–7]. These approaches yield considerable improvements with respect to homogeneous audience coverage and/or avoidance of high side lobe energy compared to manually adjusted setups.

It is common practice to select control positions which the sound field is to be optimized at in the vertical LSA radiation plane (here the *xy*-plane), thus assuming that horizontal radiation is homogeneous. The control positions may include audience (target) and non-audience (avoid) zones, cf. [1, Fig. 17], [3, Fig. 1], [4, Fig. 2], [5, Fig. 1], [6, Fig. 4], [7, Fig. 3]. Typically the predicted sound field is either visualized as the sound pressure level (SPL) over the whole *xy*-plane for single frequencies or frequency bands (e. g. MAPP Online Pro [8], EASE Focus, [4, Fig. 3]) or given as a so called position index plot (also termed positional map), where the SPL spectra for certain evaluated positions (mainly the control positions) within the *xy*-plane are depicted [6, Fig. 5], [3, Fig. 2]. Recent software also include plots of the SPL distribution on 3D audience surfaces, e. g. EAW Resolution 2, EASE Focus 2.

In some papers the resulting LSA far-field radiation pattern is given as frequency dependent polar plots or isobar plots [1, 6]. To the authors' knowledge, this is not supported by any prediction software so far. Furthermore, a spectral deviation measure, as discussed in [6], is not yet incorporated into commercial software.

The resulting driving functions for the individual loudspeakers, typically realized with FIR-filters, are rarely documented except in [2]. Hence, a valid judgment of the approaches' feasibility in terms of the electrical load and load balancing is not possible.

In this contribution, we aim at an enhanced visual treatment of the data that may be helpful for an improved interpretation of the sound fields generated by LSAs.

This includes the SPL distribution over space for frequency bands (SPLxy), the frequency responses for all audience positions (FAP), the position index plot (PIP), the far-field radiation pattern (FRP) as an isobar plot and the driving function index plot (DFIP) as magnitude and group delay spectra and/ or impulse responses for the individual loudspeakers. Each visualization exhibits advantages and disadvantages for the interpretation of the occurring phenomena. Therefore, the different graphics should be presented and discussed in combination.

A complex-directivity point source model (CDPS) [9] of a curved LSA, commonly used for sound field prediction, is generated from ideally baffled pistons for our discussion. This modeling may not properly represent practical LSAs with respect to low frequencies and rearward radiation but it allows to design reproducible LSA setups with a convenient parametrization. Two models of LSA cabinets are used. They differ in the number of the individual drivers per cabinet in the mid and high frequency section. Thus, we follow [7] demonstrating improved optimization by increasing the driving granularity of the LSA in order to reduce spatial aliasing. LSA designs that are compliant to the initial Wavefront Sculpture Technology (WST) [10] or behave similarly feature rather large waveguides. Their capability of pure electronic beam steering without producing spatial aliasing is therefore limited for the highest audio frequencies [8]. These LSAs have to be adapted to the listener region by geometrical curving, additionally to the electronic control. Different spatial aliasing effects are investigated for the two LSA designs that can be conveniently discussed by means of the proposed visualization and measures.

The paper is organized as follows: In Sec. 2 the chosen LSA models and the venue under evaluation are given. The CDPS model and further mathematical fundamentals are shortly revisited in Sec. 3. The selected optimization algorithm solving the inverse problem is discussed in Sec. 4. The proposed visualizations and measures for the optimized LSAs are introduced in Sec. 5 and discussed in Sec. 6.

2. SETUP

A curved LSA setup is examined for a common concert venue following a practical example presented in [5, Ch. 6.1]: a multi-stand arena with audience and non-audience sections given within the *xy*-plane.

2.1. LSA Setup

The LSA setup and the geometry under discussion is schematically depicted in Fig. 1. A total number of

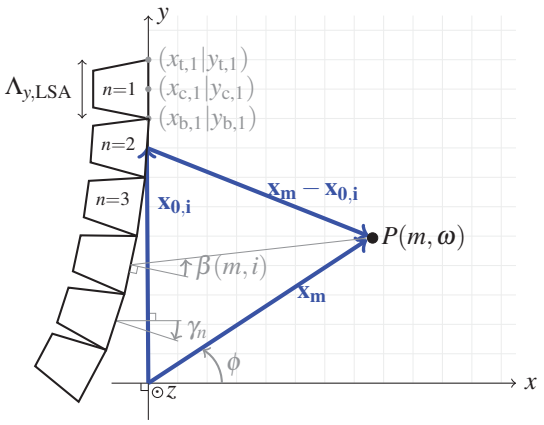

Fig. 1: Sketch of the LSA setup under discussion. A total of $N = 16$ LSA cabinets of the height $\Lambda_{y,\mathrm{LSA}} = 0.372\,\mathrm{m}$ is used. See Tab. 6 for exact positions.

$N = 16$ LSA cabinets with $n = 1,2,...,N$ is used. $\Lambda_{y,\mathrm{LSA}}$ denotes the front grille's height of a single LSA cabinet, chosen to $\Lambda_{y,\mathrm{LSA}} = 0.372\,\mathrm{m}$ resulting in an overall LSA length of ≈5.95 m. The front grille top and bottom coordinates $(x_\mathrm{t}, y_\mathrm{t})$ and $(x_\mathrm{b}, y_\mathrm{b})$ resp. of the individual cabinets are given as

$$\begin{pmatrix} x_{\mathrm{t},n} \\ y_{\mathrm{t},n} \end{pmatrix} = \begin{pmatrix} x_\mathrm{H} \\ y_\mathrm{H} \end{pmatrix} - \sum_{\mu=1}^{\mu=n-1} \Lambda_{y,\mathrm{LSA}} \begin{pmatrix} \sin\gamma_\mu \\ \cos\gamma_\mu \end{pmatrix}, \quad (1)$$

$$\begin{pmatrix} x_{\mathrm{b},n} \\ y_{\mathrm{b},n} \end{pmatrix} = \begin{pmatrix} x_\mathrm{H} \\ y_\mathrm{H} \end{pmatrix} - \sum_{\mu=1}^{\mu=n} \Lambda_{y,\mathrm{LSA}} \begin{pmatrix} \sin\gamma_\mu \\ \cos\gamma_\mu \end{pmatrix}, \quad (2)$$

using $x_\mathrm{H} = 0\,\mathrm{m}$ and $y_\mathrm{H} = 3\,\mathrm{m}$ as the initial front grille top position of the top LSA cabinet ($n = 1$) and the individual tilting angles γ_n. The tilting angles were set according to the intended audience coverage and are compliant to the 5th WST criterion [10, p. 929]. The arrays' physical opening angle amounts to about 41°. In Tab. 5 in the Appendix, the chosen tilting angles γ_n and the resulting front grille center positions $(x_{\mathrm{c},n}, y_{\mathrm{c},n})$ are listed.

The LSA is built from multi-way cabinets, each modeled with L_LF, L_MF, L_HF vertically stacked, individually controlled drivers for the low, mid and high frequency band (LF, MF, HF). With (1) and (2) the front grille center position of the i-th LSA driver is given as

$$\mathbf{x_{0,i}} = \begin{pmatrix} x_{0,i} \\ y_{0,i} \end{pmatrix} = \begin{pmatrix} x_{\mathrm{t},n} \\ y_{\mathrm{t},n} \end{pmatrix} + \frac{l-0.5}{L} \begin{pmatrix} x_{\mathrm{b},n} - x_{\mathrm{t},n} \\ y_{\mathrm{b},n} - y_{\mathrm{t},n} \end{pmatrix}, \quad (3)$$

using $l = 1,2,...,L$ and $i = (n-1)\cdot L + l$ for $L = \{L_{\mathrm{LF}}, L_{\mathrm{MF}}, L_{\mathrm{HF}}\}$ with respect to the different frequency bands. We have exemplarily chosen two LSA cabinet designs

$$\mathrm{LSA}_1 = \begin{cases} L_{\mathrm{LF}} = 1 \\ L_{\mathrm{MF}} = 2 \\ L_{\mathrm{HF}} = 1 \end{cases} \quad \mathrm{LSA}_2 = \begin{cases} L_{\mathrm{LF}} = 1 \\ L_{\mathrm{MF}} = 4 \\ L_{\mathrm{HF}} = 10 \end{cases},$$

deploying the circular piston model (8) for LF and MF and the line piston model (9) for HF as well as ideal crossover filters (brick wall) with the frequencies $f_{\mathrm{LF,MF}} = 400\,\mathrm{Hz}$ and $f_{\mathrm{MF,HF}} = 1.5\,\mathrm{kHz}$. The Active Radiating Factor (ARF) [10, Ch. 3.2] is used to specify the piston dimensions – i.e. the circular piston radius R and the line piston length Λ_y – related to the fixed distance between adjacent piston centers (discretization)

$$\Delta y = \frac{\Lambda_{y,\mathrm{LSA}}}{L}. \tag{4}$$

The ARF of a line piston reads [11, (21)], [10, Sec. 3.2]

$$\mathrm{ARF}_{\mathrm{line}} = \alpha = \frac{\Lambda_y}{\Delta y} \qquad 0 \le \alpha \le 1, \tag{5}$$

and the ARF for a circular piston can be written as [11, (26,27)]

$$\mathrm{ARF}_{\mathrm{circ}} = \frac{\pi}{4}\alpha^2 = \frac{\pi}{4}\left(\frac{2R}{\Delta y}\right)^2 \qquad 0 \le \alpha \le 1. \tag{6}$$

Note that $\mathrm{ARF}_{\mathrm{circ}}$ is in fact a ratio of surface areas ($\mathrm{ARF}_{\mathrm{circ}} \neq \alpha$), whereas a ratio of line lengths is defined for the line piston ($\mathrm{ARF}_{\mathrm{line}} = \alpha$). We use $\alpha = 0.82$ for both the line and the circular piston, consequently fulfilling the first WST criterion for line pistons (cf. [10, p. 917], [11]). The piston dimensions $\{\Lambda_y, 2R\}$ and the piston center distances Δy for the two LSA cabinets are listed in Tab. 1. Table 2 indicates the assumed loudspeaker sensitivities and the expected aliasing frequencies for straight arrays that may differ slightly from these of curved arrays. The LSA_1 models a typical WST-compliant array of the first generation, whereas the LSA_2 model with a larger number of individual pistons in the MF and HF band is comparable with some recent array designs.

L	Δy/cm	Δy/in	$\{\Lambda_y, 2R\}$/cm	$\{\Lambda_y, 2R\}$/in
1	37.2	14.65	30.5	12
2	18.6	7.32	15.25	6
4	9.3	3.66	7.63	3
10	3.72	1.46	3.05	1.2

Table 1: Relation between the number L of employed pistons per LSA cabinet, the discretization Δy (distance between adjacent pistons centers) and the piston dimensions: diameter $2R$ or length Λ_y for $\alpha = 0.82$.

Freq	L	f_{alias}/Hz	$\{\Lambda_y, 2R\}$/in	$\mathrm{dB}_{\mathrm{SPL@1W,1m}}$
$\mathrm{LF}_{1,2}$	1	461	12 (circ)	96
MF_1	2	922	6 (circ)	94
MF_2	4	1844	3 (circ)	86
HF_1	1	461	12 (line)	112
HF_2	10	4610	1.2 (line)	112

Table 2: Piston dimensions $\{\Lambda_y, 2R\}$ and assumed sensitivities $\mathrm{dB}_{\mathrm{SPL@1W,1m}}$ for LSA_1 and LSA_2 (separately for the different frequency bands and with L drivers per cabinet). The aliasing frequency f_{alias} refers to the spatial sampling condition $\Delta y \le \frac{c}{2f}$ for straight arrays.

2.2. Venue Geometry

A multi-stand arena with audience and non-audience sections, i.e. zones to be covered and zones to be avoided, is modeled by a two dimensional slice representation. The xy-plane only is considered for vertical radiation, cf. Fig. 2. This is a common approach for optimiza-

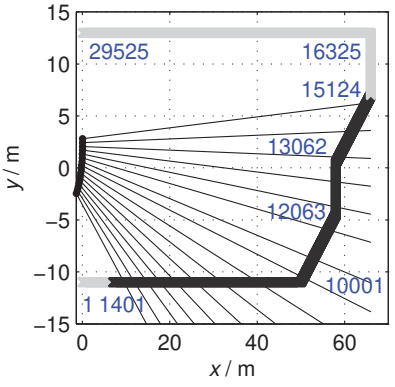

Fig. 2: Venue slice within the xy-plane with audience (black) as well as non-audience/ avoid (gray) zones and selected index numbers from M receiver positions.

tion schemes, cf. [1–7,12]. $M = 29\,525$ receiver positions with $m = 1,2,...,M$ are taken into account. This corresponds to a distance of 0.005 m between the receiver positions ensuring a discretization which approximately equals one fourth of the wave length at 17.2 kHz. The receiver positions are composed of M_a audience positions from the set $\mathscr{M}_\mathrm{a}$ and M_na non-audience positions from the set $\mathscr{M}_\mathrm{na}$ which $M = M_\mathrm{a} + M_\mathrm{na}$ holds for. They are characterized by the position vectors $\mathbf{x_m} = (x_m, y_m, 0)^\mathrm{T}$ and are numbered counterclockwise starting from the position under the LSA that is the closest one to the LSA (index 1, cf. Fig. 2). The venue slice coordinates are documented in Tab. 6 in the Appendix.

Note that the terms *bright zone* and *dark zone* used in the field of multi-zone sound field synthesis (MZSFS) [13–18] correspond to the audience zone and the non-audience zone used in the field of sound reinforcement.

3. CDPS MODEL

The sound field prediction is based on the complex-directivity point source model of baffled piston far-field radiation patterns. Using the $\mathrm{e}^{+\mathrm{j}\omega t}$ time convention it reads [19, (5)], [1, (3-5)], [20, Sec. 1.1], [9, (11)]

$$P(m,\omega) = \sum_{i=1}^{i=LN} D(i,\omega) \times \underbrace{H_\mathrm{post}(\beta(m,i),\omega) \cdot \frac{\mathrm{e}^{-\mathrm{j}\frac{\omega}{c}|\mathbf{x_m}-\mathbf{x_{0,i}}|}}{4\pi|\mathbf{x_m}-\mathbf{x_{0,i}}|} \cdot \frac{\Lambda_{y,\mathrm{LSA}}}{L}}_{G(m,i,\omega)}. \tag{7}$$

Air is assumed to be homogeneous and dissipation-less with a constant speed of sound $c = 343\,\mathrm{m/s}$. $P(m,\omega)$ denotes the sound pressure spectrum at the receiver position $\mathbf{x_m}$ with $[P(m,\omega)] = 1\,\mathrm{Pa/Hz}$. The complex driving function spectrum $D(i,\omega)$ with $[D(i,\omega)] = 1\,\mathrm{Pa/Hz}$ of the i-th source is directly proportional to the source's velocity spectrum. Terming the acoustic transfer function (ATF) from the i-th source to the receiver positions, $G(m,i,\omega)$ is composed of the free-field 3D Green's function $\frac{\mathrm{e}^{-\mathrm{j}\frac{\omega}{c}|\mathbf{x_m}-\mathbf{x_{0,i}}|}}{4\pi|\mathbf{x_m}-\mathbf{x_{0,i}}|}$ (i.e. the ideal point source), a specific far-field radiation pattern $H_\mathrm{post}(\beta(m,i),\omega)$ and the distance $\Delta y = \Lambda_{y,\mathrm{LSA}}/L$ between adjacent piston centers (discretization) for L sources per LSA cabinet. The index *post* refers to the spatial lowpass postfilter characteristics of the speakers within the spatial sampling model, cf. [21]. In the remainder the notation of the dependence $\beta(m,i)$ is omitted.

The far-field radiation pattern of the baffled circular piston with a constant surface velocity is [22, (26.42)]

$$H_\mathrm{post,circ}(\beta,\omega) = \frac{2J_1\left(\frac{\omega}{c}R\sin\beta\right)}{\frac{\omega}{c}R\sin\beta}, \tag{8}$$

denoting the cylindrical Bessel function of 1st kind of 1st order as $J_1(\cdot)$ [23, (10.2.2)]. The line piston models an ideal waveguide for the HF band and its far-field radiation pattern can be written as [22, (26.44)]

$$H_\mathrm{post,line}(\beta,\omega) = \frac{\sin\left(\frac{\omega}{c}\frac{\Lambda_y}{2}\sin\beta\right)}{\frac{\omega}{c}\frac{\Lambda_y}{2}\sin\beta}. \tag{9}$$

Note that these patterns exhibit main lobe unity gain in order to control the energy radiated by the pistons via the assumed sensitivities.

This modeling was also approached in [4, 19]. The model certainly has some drawbacks, such as (i) the infinite, straight baffle assumption, (ii) the constant diaphragm's velocity assumption and (iii) no valid rearward and low-frequency prediction. BEM-based models and measured LSA cabinet data [7, 20] provide results that closer match the reality. However, since we are mainly interested in different visualization methods and measures, the baffled piston model is sufficiently precise, especially for demonstrating spatial aliasing phenomena for high audio frequencies. Note that (7) correctly synthesizes the Fresnel (chaotic) and collective Fraunhofer region [24, Fig. 16] of the whole array if the respective receiver position is located in the far-field of the individual pistons [9, 11]. This does not impose any practical limitations as the audience is typically located in some meters distance from individual LSA cabinets.

4. OPTIMIZATION

For the application of optimization algorithms, (7) is transformed to matrix notation accounting for all receiver positions M for a single frequency (cf. [5, (1)], [4, (1)])

$$\mathbf{p}(\omega) = \mathbf{G}(\omega)\,\mathbf{d}(\omega) \tag{10}$$

with $\mathbf{p}(\omega)$ denoting the $(M \times 1)$ vector of sound pressure spectra at all considered positions $\mathbf{x_m}$, $\mathbf{G}(\omega)$ denoting the $(M \times LN)$ ATF matrix and $\mathbf{d}(\omega)$ denoting the $(LN \times 1)$ vector of the complex driving weights per angular frequency ω at all source positions $\mathbf{x_{0,i}}$. Then, for a desired sound field at the evaluation positions $\mathbf{x_m}$,

$$\mathbf{p}_\mathrm{des}(\omega) = \mathbf{G}(\omega)\,\mathbf{d}(\omega) \tag{11}$$

has to be solved for the loudspeaker driving weights $\mathbf{d}(\omega)$. Since $M > LN$, i.e. the number of evaluation positions is larger than the number of individual sources, an ill-posed inverse problem must be analyzed [25–27]. In this paper, we use a least-mean-square (LMS) optimization method with Tikhonov regularization imposing an energy constraint on the loudspeaker weights [28]. This is often used for numerical sound field synthesis applications. The optimization is performed separately for each frequency.

The desired sound field $\mathbf{p}_{\text{des}}(\omega)$ in principle could be set arbitrarily. However, the used array geometry restricts the choice to physically realizable sound fields. Typically a desired level decay over the audience zone and a level offset for the avoid zone can be defined in practical realizations [3]. We have chosen

$$P_{\text{des,3 dB}}(m,\omega) \propto \frac{\mathrm{e}^{-\mathrm{j}\frac{\omega}{c}|\mathbf{x_m}-\mathbf{x_S}|}}{\sqrt{|\mathbf{x_m}-\mathbf{x_S}|}} \tag{12}$$

as the target function for the optimization. We thus aim at a desired sound field that complies with a sound field generated by a virtual line monopole at the position $\mathbf{x_S}$ deploying the large argument-approximation of the 2D Green's function and simultaneously ignoring the temporal lowpass characteristics and the frequency independent $\pi/4$-phase shift [29, (26)]. The source position is chosen to

$$\mathbf{x_S} = \frac{1}{2}\left[\begin{pmatrix} x_{\text{t},1} \\ y_{\text{t},1} \end{pmatrix} + \begin{pmatrix} x_{\text{b},16} \\ y_{\text{b},16} \end{pmatrix}\right] = \begin{pmatrix} -0.7537\,\text{m} \\ 0.1938\,\text{m} \end{pmatrix}, \tag{13}$$

ensuring that the origin of the virtual line source is located behind the LSA. A target sound pressure level of 100 dB_{SPL} at the first receiver position (index 1401) within the audience zone was chosen. For the avoid zone we require a level decrease of 20 dB compared to the audience zone using a smooth dB-transition between audience and non-audience zones.

In [28] the LMS optimization with Tikhonov regularization of the loudspeakers' driving functions is termed loudspeaker weight energy (LWE) according to the considered constraint. In order to solve (11) w.r.t. the loudspeaker weights, the objective function to be minimized reads

$$\begin{aligned} &\min_{\mathbf{d}(\omega)} \|\mathbf{G}(\omega)\mathbf{d}(\omega) - \mathbf{p}_{\text{des}}(\omega)\|_2^2 \\ &\text{subject to:} \quad \|\mathbf{d}(\omega)\|_2^2 \leq D_{\text{max}}^2 \end{aligned} \tag{14}$$

denoting the squared Euclidean norm $\|\cdot\|_2^2$ [23, (3.2.13)] and the constraint D_{max}^2 as the limit for the summed squares of the driving functions' absolute values (cf. [28, (1)]). The solution is well known as

$$\mathbf{d}(\omega,\lambda_{\text{reg}}) = \left[\mathbf{G}(\omega)^{\text{H}}\mathbf{G}(\omega) + \lambda_{\text{reg}}\mathbf{I}_{LN}\right]^{-1}\mathbf{G}(\omega)^{\text{H}}\mathbf{p}_{\text{des}}(\omega), \tag{15}$$

with the regularization parameter λ_{reg}. Taking D_{max}^2 into account, λ_{reg} can be found by means of singular value analysis and using the Newton's method, cf. [28, Sec. II. B/C]. The Hermitian, i.e. the conjugate transpose, is denoted by $^{\text{H}}$ and $\mathbf{I}_{LN}$ is the $(LN \times LN)$ identity matrix. Note that this approach does not allow for the limitation of the maximum tolerated electric power of the individual sources. Therefore, the resulting loads of the individual drivers must be carefully monitored. This is one significant drawback of the LWE algorithm. Other approaches were discussed in literature that are presumably better suited for LSA optimization [1, 3, 5].

5. EVALUATION

In this section the proposed visualizations and measures are introduced by means of optimization examples for the two fictitious LSAs. The optimizations were performed for a logarithmically spaced frequency vector with $f_{\text{start}} = 200\,\text{Hz}$, $f_{\text{stop}} = 20\,\text{kHz}$ and $1/36$ octave resolution. In Fig. 11 in the Appendix the optimization parameters are depicted.

5.1. Graphical Representation

The position index plots (PIPs) and the far-field radiation patterns (FRPs) over frequency as well as an overlay of all frequency responses for the audience positions (FAP) are depicted in Fig. 3. Using the indexing of Fig. 2 the PIP shows the resulting SPL spectra at all control positions $\mathbf{x_m}$. The frequency response within the audience zone should ideally be as linear as possible following the desired level decay resulting from the different distances to the virtual line source (12). In the avoid zone the desired SPL reduction should ideally be met. The widespread method of optimizing sound fields for selected positions in a venue slice bears the risk of neglecting the sound field that was excluded from optimization, i.e. positions that are not part of PIP. It is thus important to offer further visualizations. The FRP represents the polar patterns for radiating angles $|\phi| \leq 90^\circ$ as an isobar plot over all evaluated frequencies. It conveniently indicates strong side lobes (from windowing, i.e. because of the finite length of the LSA) and grating lobes (from spatial aliasing, i.e. because of the distance between adjacent drivers) that should be avoided to obtain a homogeneous audience coverage as well as low

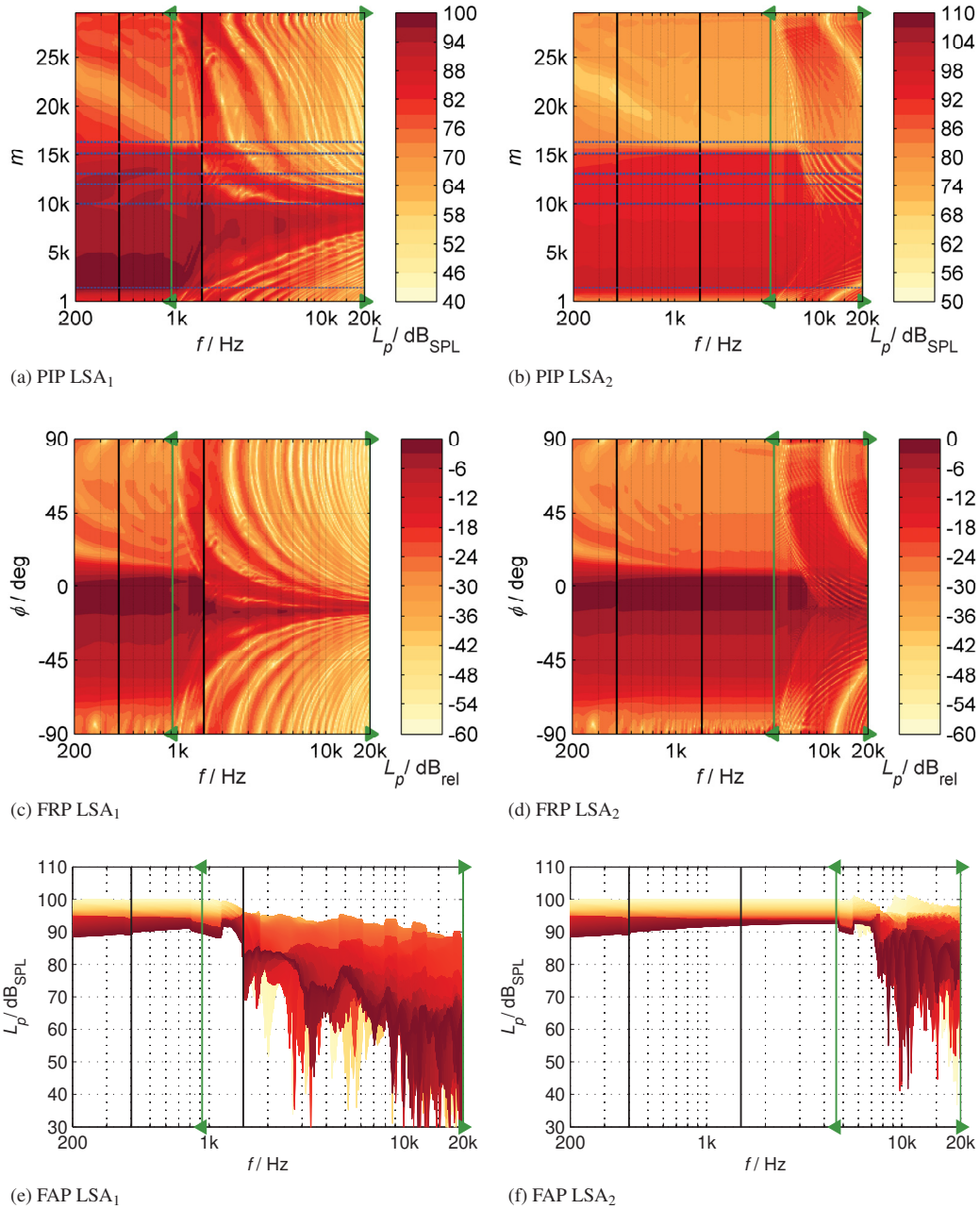

(a) PIP LSA$_1$

(b) PIP LSA$_2$

(c) FRP LSA$_1$

(d) FRP LSA$_2$

(e) FAP LSA$_1$

(f) FAP LSA$_2$

Fig. 3: Position index plot (PIP), far-field radiation pattern (FRP) and frequency responses for all audience positions (FAP) for the LSA$_1$ (left) and the LSA$_2$ (right). In the FAP the color transition from yellow to red corresponds to the transition of the positions close to the LSA to the positions far from the LSA. The crossover frequencies (black) and the spatial aliasing frequencies of straight arrays (green with arrows) according to Tab. 2 are charted for orientation.

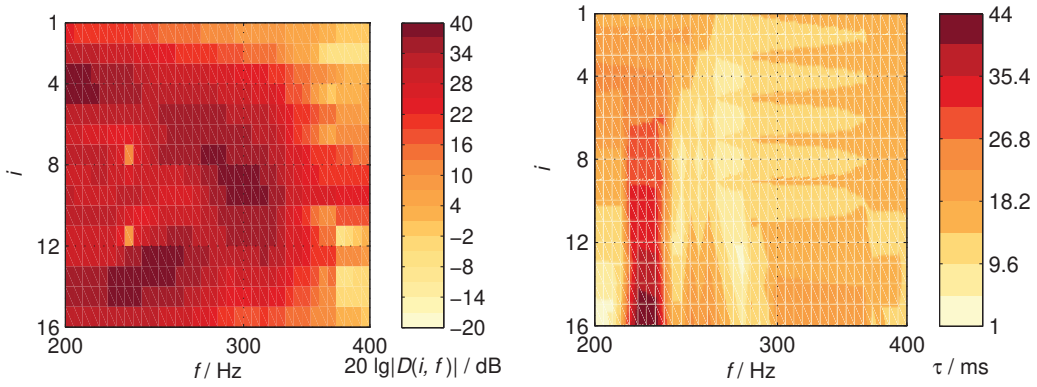

(a) DFIP (magnitudes) for LF

(b) DFIP (delays) for LF

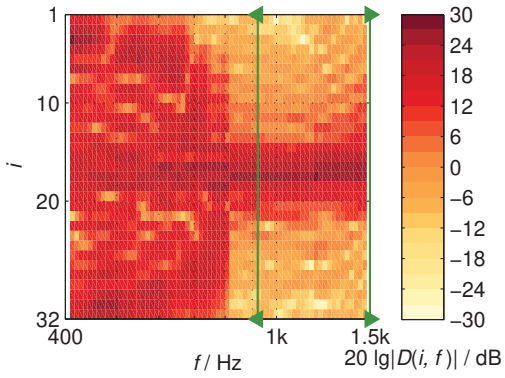

(c) DFIP (magnitudes) for MF

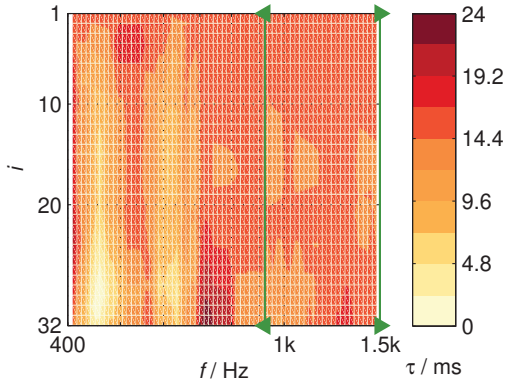

(d) DFIP (delays) for MF

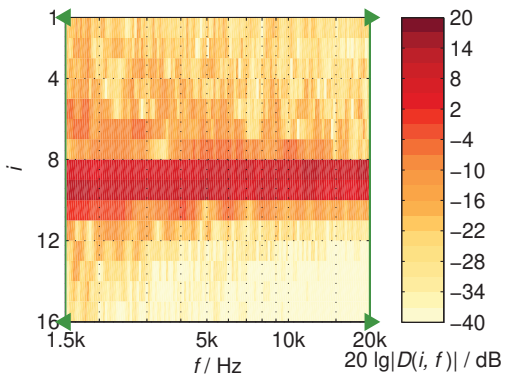

(e) DFIP (magnitudes) for HF

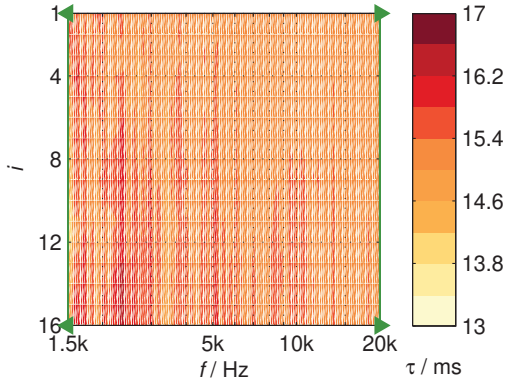

(f) DFIP (delays) for HF

Fig. 4: Driving Function Index Plots (DFIPs) over frequency f and source number i for the LWE-optimized LSA_1. Magnitudes and delays are visualized separately for the low (LF), mid (MF) and high (HF) frequency range. The spatial aliasing frequencies of straight arrays (green with arrows) according to Tab. 2 are charted for orientation.

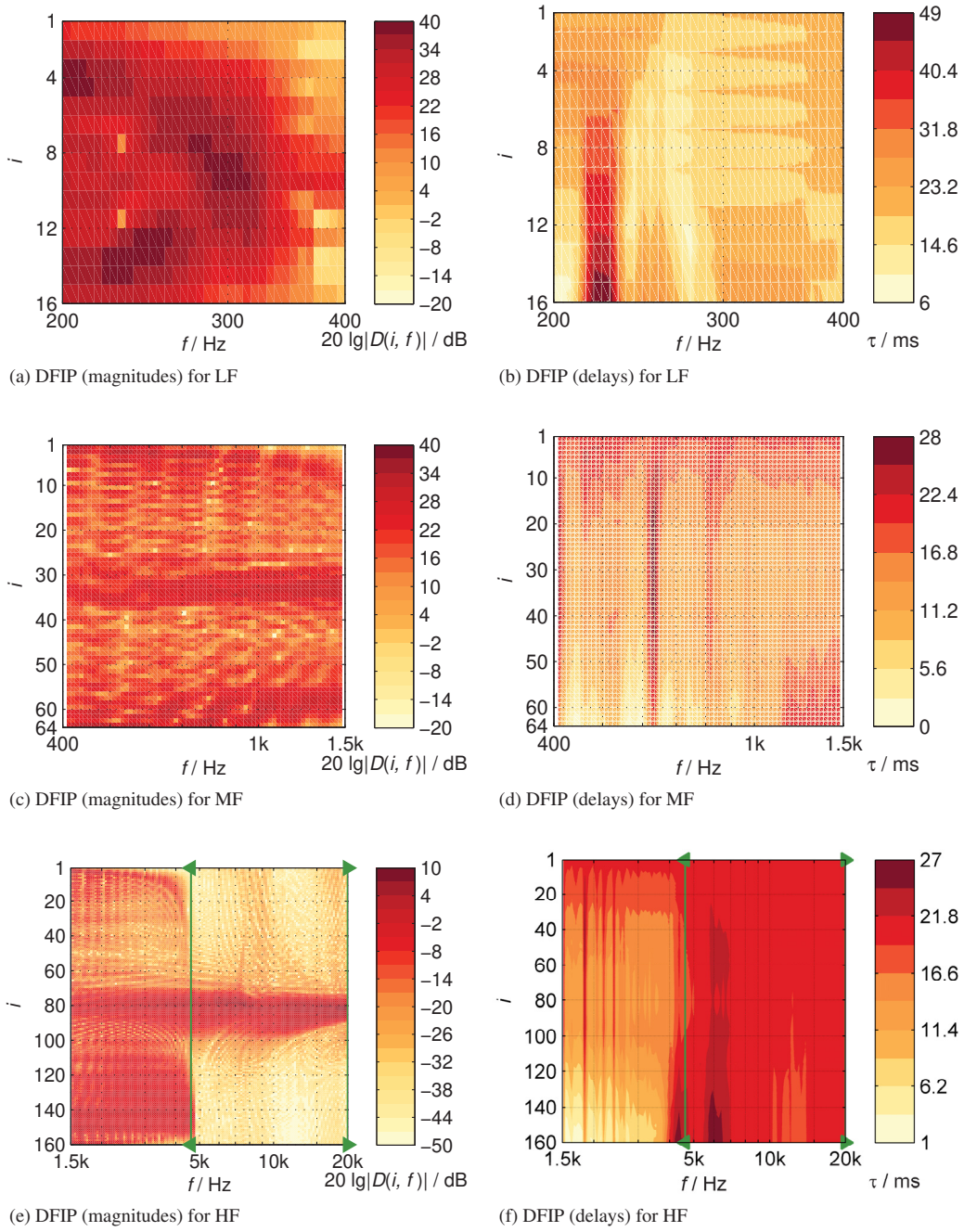

(a) DFIP (magnitudes) for LF

(b) DFIP (delays) for LF

(c) DFIP (magnitudes) for MF

(d) DFIP (delays) for MF

(e) DFIP (magnitudes) for HF

(f) DFIP (delays) for HF

Fig. 5: Driving Function Index Plots (DFIPs) over frequency f and source number i for the LWE-optimized LSA_2. Magnitudes and delays are visualized separately for the low (LF), mid (MF) and high (HF) frequency range. The spatial aliasing frequencies of straight arrays (green with arrows) according to Tab. 2 are charted for orientation.

short name	item	variable	parameters
PIP	position index plot	sound pressure level L_p	frequency f, position index m
FRP	far-field radiation pattern	sound pressure level L_p	frequency f, vertical angle ϕ
FAP	frequency responses of all audience positions	sound pressure level L_p	frequency f
SPLxy	sound pressure levels in the xy-plane	sound pressure level L_p	coordinates x, y
DFIP	driving function index plot	magnitudes and phases (as delay τ) of the driving functions $D(i,\omega)$	frequency f, driver index i

Table 3: Overview of the proposed visualizations.

SPLs within the avoid zones. This cannot necessarily be seen in the PIP. Illustrating the SPLs for the evaluated *xy*-plane and specified frequencies or frequency bands is another common approach to evaluate the radiation characteristics. For specified frequencies this can be viewed in the SPLxy plots (Fig. 9 and Fig. 10 in the Appendix) for both LSAs under discussion. While giving a fast overview of the coverage and the side and the grating lobes at those frequencies, the obtained SPL spectra for the intended listener and avoid positions are not easily accessible. Hence, all four visualizations (PIP, FRP, FAP, SPLxy) should be provided in combination for convenient interpretation.

The driving function index plots (DFIP) are depicted individually for the LF, MF and HF band in Fig. 4 for the LSA_1 and in Fig. 5 for the LSA_2. They represent the magnitudes and group delays over frequency that have to be applied to the individual sources i in order to obtain the optimized sound field. On the one hand the load and the load balancing of the drivers can be evaluated by the magnitude plot, on the other hand the required FIR filter length can be estimated by the delay plot. An overview of the proposed visualizations can be found in Tab. 3.

5.2. Technical Quality Measures

In sound field synthesis applications either the frequency dependent absolute error of (14) or the position and frequency dependent relative error

$$\varepsilon_{\mathrm{abs}}(\omega) = \|\mathbf{G}(\omega)\mathbf{d}(\omega) - \mathbf{p}_{\mathrm{des}}(\omega)\|_2^2, \qquad (16)$$

$$\varepsilon_{\mathrm{rel}}(m,\omega) = \left|\frac{P_{\mathrm{des}}(m,\omega) - P(m,\omega)}{P_{\mathrm{des}}(m,\omega)}\right|^2, \qquad (17)$$

resp. are typically evaluated to rate the obtained sound field's technical quality. We propose two further measures using the magnitudes of the sound pressure that might deliver additional insights. The first frequency dependent measure relates the obtained average levels of the audience zone and the non-audience zone

$$L_{p,\mathrm{a,na}}(\omega) = 10\log_{10}\left(\frac{\frac{1}{M_{\mathrm{a}}}\|\mathbf{p}_{m\in\mathscr{M}_{\mathrm{a}}}(\omega)\|_2^2}{\frac{1}{M_{\mathrm{na}}}\|\mathbf{p}_{m\in\mathscr{M}_{\mathrm{na}}}(\omega)\|_2^2}\right), \qquad (18)$$

that is depicted in Fig. 6a and Fig. 6b for the two LWE-optimized LSAs. This measure corresponds to the acoustic contrast [13, (16)], [15, (2)], [16, (2)] established in MZSFS. It allows for a direct judgment of the energy steering but might be misleading if the audience coverage is insufficient due to spatial aliasing.

Furthermore, we recommend to deploy the frequency dependent distribution measure

$$L_{p,\mathrm{des,opt},q}(\omega) = \underset{m}{\mathscr{Q}_q}\left[10\log_{10}\left(\frac{|P_{\mathrm{des}}(m,\omega)|^2}{|P(m,\omega)|^2}\right)\right] \qquad (19)$$

using the operator $\underset{m}{\mathscr{Q}_q}[\cdot]$ to calculate the $q = \{0.05, 0.25, 0.5, 0.75, 0.95\}$ quantiles of the level difference between the desired and the obtained sound field over all receiver positions $\mathbf{x_m}$ in this particular case. This can be viewed in Fig. 6c and Fig. 6d. When the obtained sound field $|\mathbf{p}(\omega)|$ conforms very well to the desired one $|\mathbf{p}_{\mathrm{des}}(\omega)|$, the measure should provide a median (i.e. the 0.5-quantile) near 0 dB and very little spread in the other quantiles. In contrast to the errors in (16) and (17), $L_{p,\mathrm{des,opt},q}(\omega)$ additionally provides the spread of the deviations and disregards the effect of phase differences between the desired and the obtained sound field.

To receive further impressions of the required power and load balancing (LB) necessary for producing the sound fields, the following source related distribution measures may be useful. They are in line with the con-

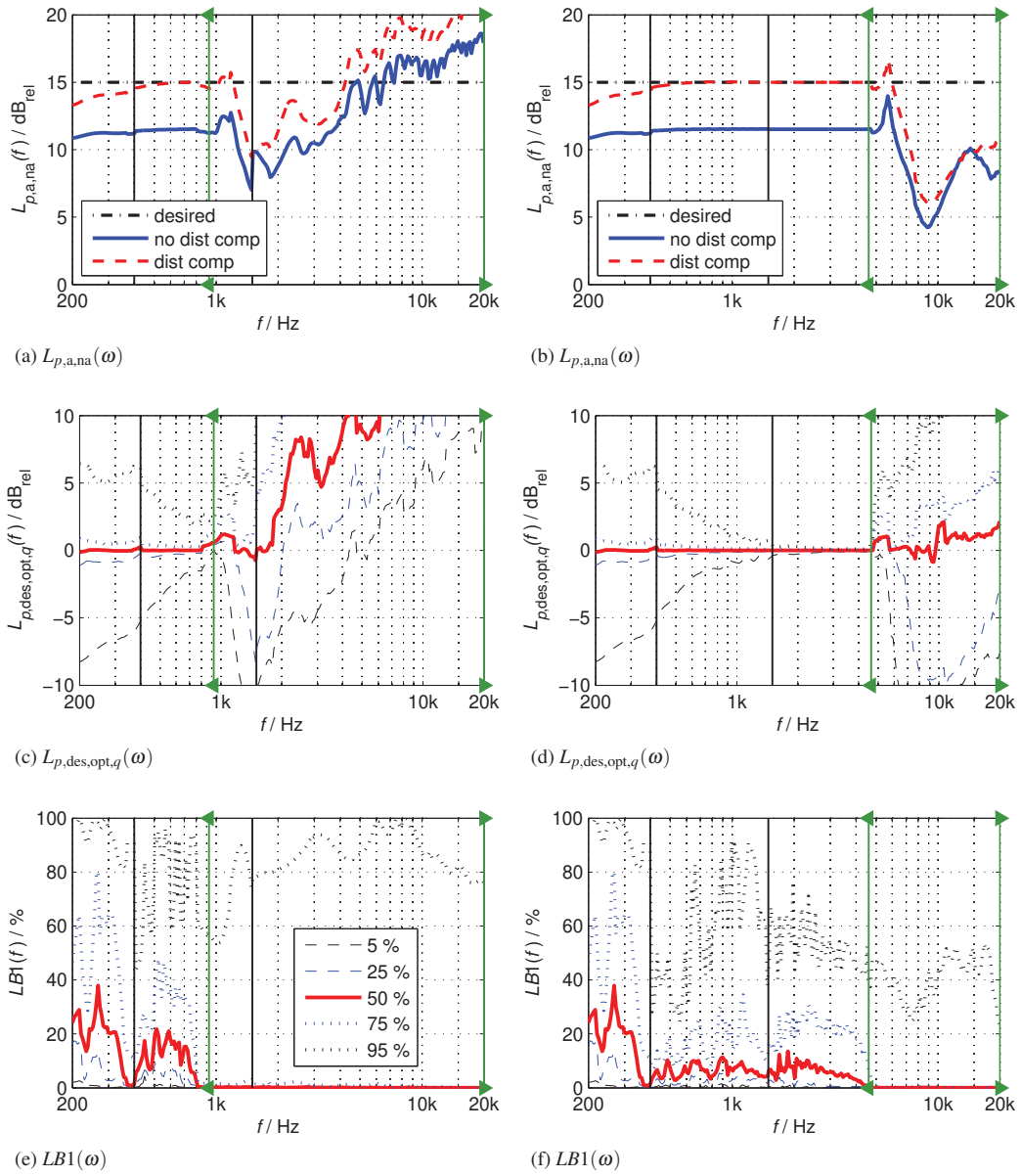

(a) $L_{p,\mathrm{a,na}}(\omega)$ (b) $L_{p,\mathrm{a,na}}(\omega)$

(c) $L_{p,\mathrm{des,opt},q}(\omega)$ (d) $L_{p,\mathrm{des,opt},q}(\omega)$

(e) $LB1(\omega)$ (f) $LB1(\omega)$

Fig. 6: Evaluation plots for the LSA_1 (left) and the LSA_2 (right), top: relation of the obtained average levels of the audience and the non-audience zone $L_{p,\mathrm{a,na}}(\omega)$, eq. (18) – the desired relation, the relation without distance compensation, and with distance compensation, i.e. compensation of the level decay, mid: frequency dependent distribution measure $L_{p,\mathrm{des,opt},q}(\omega)$, eq. (19), bottom: frequency dependent load balancing $LB1(\omega)$ of the drivers, eq. (20). Note that the legend in (e) is valid for all depicted distribution measures. The crossover frequencies (black) and the spatial aliasing frequencies of straight arrays (green with arrows) according to Tab. 2 are charted for orientation.

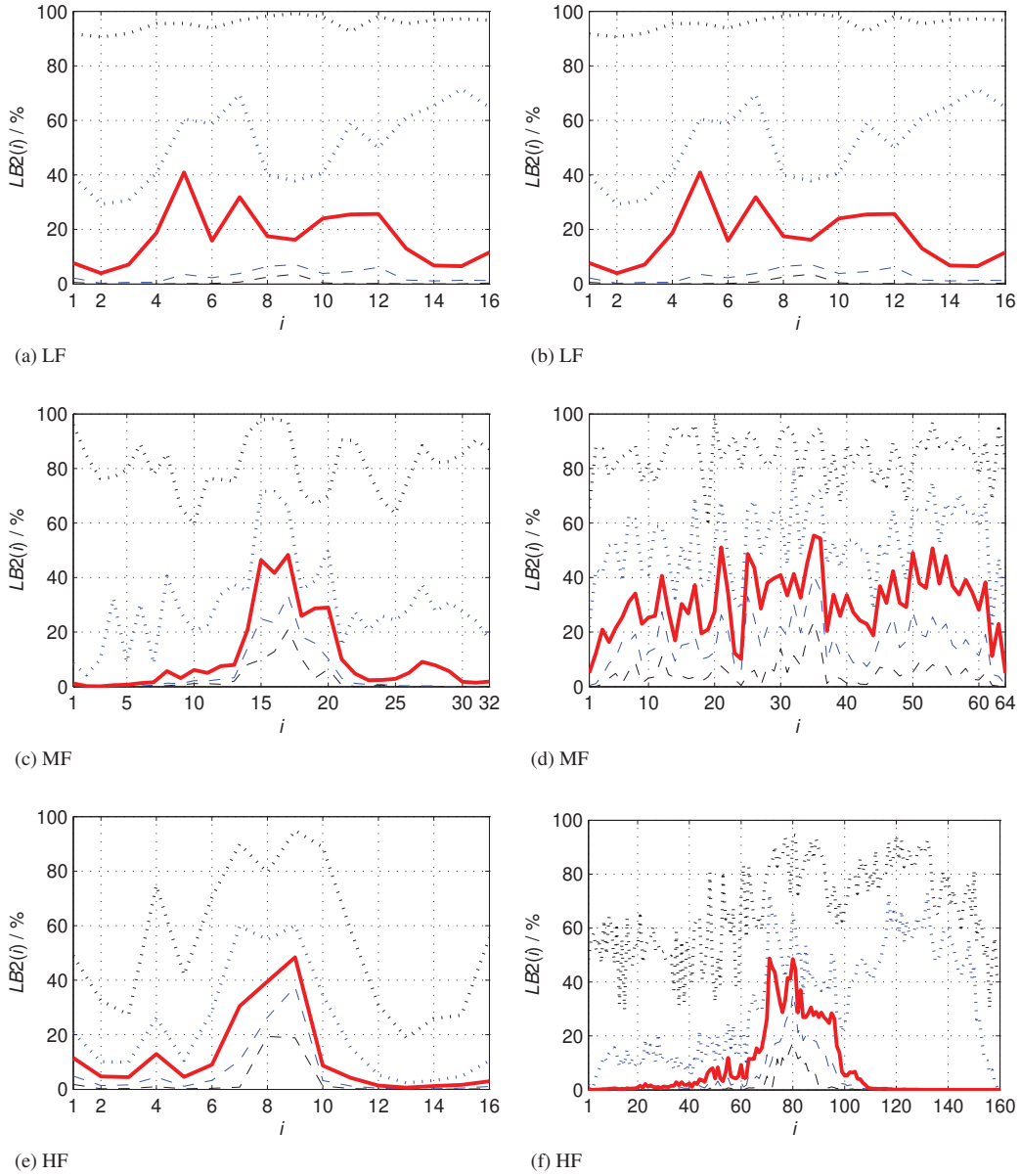

Fig. 7: Evaluation plots for the LSA_1 (left) and the LSA_2 (right): source dependent load balancing $LB2(i)$, eq. (21), visualized separately for the low (LF), mid (MF) and high (HF) frequency range. Consider the legend in Fig. 6e that is valid for all depicted distribution measures.

trol effort [15, (3)], [16, (3)] in MZSFS and they quantitatively specify whether the individual sources are rather evenly or unevenly controlled. It could be possible that only few individual drivers are highly loaded whereas others are almost powered off. This should be avoided in practice due to loudspeaker and amplifier design and

symbol	item
$\varepsilon_{\mathrm{abs}}(\omega)$	frequency dependent absolute error
$\varepsilon_{\mathrm{rel}}(m,\omega)$	position and frequency dependent relative error
$L_{p,\mathrm{a,na}}(\omega)$	relation of the obtained average sound pressure levels of the audience and the non-audience zone
$L_{p,\mathrm{des,opt},q}(\omega)$	frequency dependent distribution measure of the level difference between the desired and the obtained sound field
$LB1(\omega)$	frequency dependent distribution measure of the drivers' load balancing with respect to the driver
$LB2(i)$	driver dependent distribution measure of the drivers' load balancing with respect to the frequency

Table 4: Overview of the proposed technical quality measures.

especially economical reasons. The first frequency dependent measure

$$LB1(\omega) = \frac{\underset{i}{\mathscr{Q}_q}\left[|D(i,\omega)|^2\right]}{\max\limits_{i}\left[|D(i,\omega)|^2\right]} \tag{20}$$

involves the calculation of the quantiles of the squared driving function weights with respect to all drivers i in relation to the maximum squared driving function weight for the respective frequency. Note that the squared driving function weights are proportional to the squared root mean square (RMS) voltage and are thereby proportional to the electrical power when assuming a real impedance. $LB1(\omega)$ is depicted in Fig. 6e and Fig. 6f.

Similarly, the outcome of the second proposed – source related – measure $LB2(i)$ are the quantiles with respect to the angular frequency ω in relation to the maximum squared driving function weight for the respective driver. Its equation is

$$LB2(i) = \frac{\underset{\omega}{\mathscr{Q}_q}\left[|D(i,\omega)|^2\right]}{\max\limits_{\omega}\left[|D(i,\omega)|^2\right]}. \tag{21}$$

This is visualized for the LF, MF and HF band of the two LWE-optimized LSAs in Fig. 7. In Tab. 4 an overview of the proposed technical quality measures is given.

6. DISCUSSION

The proposed visualizations and technical quality measures are discussed separately for the two LWE-optimized fictitious LSAs in this section.

6.1. Position Index Plots

As depicted in Fig. 3a and Fig. 3b the PIPs show acceptable optimization success with respect to the lowest frequencies for both considered LSAs. The LSA_2 provides a homogeneous sound field within the audience zone up to the spatial aliasing frequency of the HF band, whereas the LSA_1 produces aliasing within the MF and HF band since both exceed the allowed aliasing-free bandwidth. Due to insufficient audience coverage and severe corruption by spatial aliasing, the HF band of the LSA_1 synthesized sound field is unsuitable for sound reinforcement. Although WST-compliant the LSA_1 is not accessible for electronic control of the phase/ group delay in the HF band. Hence, only the magnitudes of the driving functions should be optimized, which is presumably approached in [6] to obtain satisfying results. Note that the WST criteria were derived for uniformly driven LSAs [10]. Only in this case large waveguides are appropriate post-filters to avoid or reduce spatial aliasing [11]. Both arrays exhibit an acceptable SPL reduction within the non-audience zones up to the spatial aliasing frequency.

6.2. Far-Field Radiation Patterns

The observations from the former sections can be confirmed by analyzing the FRPs in Fig. 3c and Fig. 3d. Moreover, they reveal a beam width of little larger than 45° for frequencies which the optimization performs at as intended. The beam width thus approximately matches the physical opening angle of the LSA spiral. For audience positions close to the LSA less power is required to produce the desired SPL. This can be traced back to the decreased level in the FRP at about $-60°$. The HF band of the LSA_1 exhibits a polar pattern that is similar to a uniformly driven, rectangular windowed LSA. This indicates that the optimization algorithm is not able to find a meaningful configuration other than

that with least occurring spatial aliasing. A very narrow main lobe accompanied by side and grating lobes for frequencies larger than 1 kHz is obtained. The LSA_2 exhibits a more homogeneous polar pattern up to the spatial aliasing frequency in the HF band. At about 4 kHz aliasing artifacts begin to enter the LSA_2's visible region (i.e. $\pm 90^\circ$). With increasing frequency those artifacts spread over a larger radiation angle range until finally entering the beam that is responsible for sound reinforcement of the audience zone. Hence, the sound field is severely corrupted within the audience and non-audience zones. The resulting frequency response coloration due to spatial aliasing plays a major role for the perceived sound quality, cf. [30, Fig. 5.10].

6.3. Sound Pressure Levels in the *xy*-plane

On the basis of the SPLxy plots in Fig. 9 and Fig. 10 analogue findings can be made as discussed above by means of the PIPs and FRPs. Especially the radiation behavior at very low and high frequencies with little optimization success due to the LSA characteristics should be taken into account (the LSA is too short for LF, the discretization Δy is too large for the highest frequencies). Referring to the LSA_2 Fig. 10e and Fig. 10f particularly give a vivid impression of the aliasing artifacts that corrupt the intended beam.

6.4. Driving Function Index Plots

In the DFIP plots (Fig. 4 for the LSA_1 and Fig. 5 for the LSA_2) the magnitude and group delay spectra for the individual LSA sources are shown for the LF, MF and HF band. A magnitude of 0 dB corresponds to the nominal driver sensitivity. This allows an estimation of the required power for the individual drivers. It leads to feasible results for the LF and HF band but not for the MF band with respect to the typical rated power load capacities of electrodynamic loudspeakers. Thus, the LSA modeling and the derived results must be seen as didactic design studies. As a general trend it can be stated that the LWE constraint causes an energy concentration in the middle of the LSA for the MF and HF band, whereas a more balanced load can be observed for the LF band. There are obvious differences in the MF band for $f < 800\,\mathrm{Hz}$ comparing the LSA_1 and the LSA_2. The DFIP of the LSA_1's HF band confirms the almost uniformly driven LSA only using the drivers in the middle of the array. Additionally, the delay does not change considerably above 5 kHz. Due to the high driving granularity of the LSA_2 the HF sources $i > 100$ are controlled in order to obtain the desired sound field for the very first audience positions. This works satisfactorily up to the spatial aliasing frequency. Regarding the 'system latency' due to the required FIR filters which is determined by the highest occurring group delays of the MF and HF band, the optimizations yield results which could be just used for live sound applications.

6.5. Sound Field Related Quality Measures

The measure $L_{p,\mathrm{a,na}}(\omega)$ (18) visualized in Fig. 6a and Fig. 6b reassures the preceding statements made with the help of the PIPs, FRPs and SPLxy. For the LF and MF band the averaged level difference is about 12 dB for the non-distance compensated case, i.e. the values are affected by the level decay due to the distance increase. Mainly differing from the first type in an offset and a drop for the lowest frequencies the respective level difference of the distance compensated version amounts to ca. 15 dB. This corresponds to the desired level difference of 20 dB reduced by the impact of the smooth transition between the audience and the non-audience zones. Beyond the spatial aliasing frequency $L_{p,\mathrm{a,na}}(\omega)$ strongly decreases after a peak for the LSA_1's MF and HF band at ca. 1.2 kHz and for the LSA_2's HF band at ca. 6 kHz. This measure misleadingly suggests a desirable high and increasing selectivity between the audience and non-audience zones in the LSA_1's HF band which is caused by the insufficient audience coverage.

By means of the distribution measure $L_{p,\mathrm{des,opt},q}(\omega)$ (19) that is depicted in Fig. 6c and Fig. 6d the general trends already stated above can be conveniently reviewed. A median near 0 dB and very little spread in the other quantiles are almost perfectly achieved from 1.5 kHz to 5 kHz for the LSA_2 indicating that a high LSA driving granularity leads to very good optimization results if the LSA length is much larger than the radiated wave length. Above the spatial aliasing frequency the spread increases exhibiting a non-symmetrical behavior. It can be noticed for the LSA_1 that a very high and unusable deviation and a spread arise in the HF band. For both LSAs the spread decreases with increasing frequency in the LF and MF band due to the varying 'wave length/ LSA length'-ratio. $L_{p,\mathrm{des,opt},q}(\omega)$ of the LSA_1's MF band evidently indicates by the increased spread the occurrence of spatial aliasing starting at about 1 kHz.

6.6. Source Related Quality Measures

The load balancing measure $LB1(\omega)$ in (20) that can be viewed in Fig. 6e and Fig. 6f shows that the individual sources are rather unevenly controlled, which can also be seen in the DFIPs. Only very few drivers provide

the largest amount of the total energy in the HF band of the LSA_1. Interestingly, the median and the interquartile range (IQR) tend to become very small for frequencies above the spatial aliasing frequency, except some IQR-outliers in the HF band of the LSA_1. However, the large 0.95-quantile reveals that single drivers are loaded with very much power. Here the LSA_1 performs worse in the MF and HF band than the LSA_2.

A quantitative specification of the power distribution over the frequencies for each individual source can be pointed out by the $LB2(i)$ in (21) and is visualized in Fig. 7. As already observed the LF band is quite balanced, whereas the energy is concentrated in rather few sources referring to the HF band. In contrast to the LSA_1's MF band, the LSA_2's MF band exhibits a very balanced loading over the sources with respect to the individual frequencies.

7. CONCLUSION

By means of exemplarily performed optimizations of two modeled line source arrays several data visualizations are recollected and several technical measures are proposed in this paper. These are deployed in order to evaluate and interpret the technical quality of sound reinforcement. It is discussed that a full, in-depth and convenient interpretation of the observed phenomena is only possible when considering all the different graphical representation approaches in combination. This also prevents misinterpretation. The suggested technical measures may help to quantify the achieved optimization in terms of the sound field's and the driving functions' characteristics. The performed simulations unveil the common acoustic problems of spatial aliasing for high frequencies and insufficient beam forming capability for low frequencies. Spatial aliasing can be reduced by increasing the number of individually controlled drivers and decreasing the discretization step between them. Low frequency beam forming can be enhanced by using larger arrays. Since the performed evaluation is primarily intended as a design study introducing the strategies, it should be noted that other optimization algorithms may perform better, especially for the usage of line arrays with large waveguides. It is planned to incorporate the proposed technical quality measures as criteria for future optimization approaches. When using measured loudspeaker data it may be reasonable to include a further distribution measure for the required power and load balancing that relates the actual driving functions and the rated power. Analogue to the PIP magnitude data of the sound pressure, the corresponding phases should also be considered in the future in order to identify significant phase shifts that may affect the quality of auditory perception.

8. REFERENCES

[1] van Beuningen, G.W.J.; Start, E.W. (2000): "Optimizing directivity properties of DSP controlled loudspeaker arrays." In: *Proc. of the Inst. of Acoustics: Reproduced Sound*, **22**(6):17–37.

[2] Thompson, A. (2008): "Real world line array optimisation." In: *Proc. of the Institute of Acoustics*, **30**(6).

[3] Thompson, A. (2009): "Improved methods for controlling touring loudspeaker arrays." In: *Proc. of the 127th Audio Eng. Soc. Conv., New York*, #7828.

[4] Terrell, M.; Sandler, M. (2010): "Optimising the controls of a homogenous loudspeaker array." In: *Proc. of the 129th Audio Eng. Soc. Conv., San Francisco*, #8159.

[5] Thompson, A.; Baird, J.; Webb, B. (2011): "Numerically optimised touring loudspeaker arrays - Practical applications." In: *Proc. of the 131st Audio Eng. Soc. Conv., New York*, #8511.

[6] Feistel, S.; Sempf, M.; Köhler, K.; Schmalle, H. (2013): "Adapting loudspeaker array radiation to the venue using numerical optimization of FIR filters." In: *Proc. of the 135th Audio Eng. Soc. Conv., New York*, #8937.

[7] Thompson, A.; Luzarraga, J. (2013): "Drive granularity for straight and curved loudspeaker arrays." In: *Proc. of the Inst. of Acoustics*, **35**(2):210–218.

[8] Meyer Sound Laboratories Inc. (2002): "DSP beam steering with modern line arrays." Tech. rep., `https://www.meyersound.com/pdf/support/papers/beam_steering.pdf`, last seen on 2014-10-17.

[9] Feistel, S.; Thompson, A.; Ahnert, W. (2009): "Methods and limitations of line source simulation." In: *J. Audio Eng. Soc.*, **57**(6):379–402.

[10] Urban, M.; Heil, C.; Bauman, P. (2003): "Wavefront Sculpture Technology." In: *J. Audio Eng. Soc.*, **51**(10):912–932.

[11] Schultz, F.; Straube, F.; Spors, S. (2015): "Discussion of the Wavefront Sculpture Technology criteria for straight line arrays." In: *Proc. of the 138th Audio Eng. Soc. Conv., Warsaw*, #9323.

[12] Thompson, A. (2006): "Line array splay angle optimisation." In: *Proc. of the Inst. of Acoustics*, **28**(8):135–148.

[13] Choi, J.W.; Kim, Y.H. (2002): "Generation of an acoustically bright zone with an illuminated region using multiple sources." In: *J. Acoust. Soc. Am.*, **111**(4):1695–1700.

[14] Elliott, S.J.; Cheer, J.; Murfet, H.; Holland, K.R. (2010): "Minimally radiating sources for personal audio." In: *J. Acoust. Soc. Am.*, **128**(4):1721–1728.

[15] Coleman, P.; Jackson, P.J.B.; Olik, M.; Møller, M.; Olsen, M.; Pedersen, J.A. (2014): "Acoustic contrast, planarity and robustness of sound zone methods using a circular loudspeaker array." In: *J. Acoust. Soc. Am.*, **135**(4):1929–1940.

[16] Coleman, P.; Jackson, P.J.B.; Olik, M.; Pedersen, J.A. (2014): "Personal audio with a planar bright zone." In: *J. Acoust. Soc. Am.*, **136**(4):1725–1735.

[17] Bai, M.R.; Wen, J.C.; Hsu, H.; Hua, Y.H.; Hsieh, Y.H. (2014): "Investigation on the reproduction performance versus acoustic contrast control in sound field synthesis." In: *J. Acoust. Soc. Am.*, **136**(4):1591–1600.

[18] Cai, Y.; Wu, M.; Yang, J. (2014): "Sound reproduction in personal audio systems using the least-squares approach with acoustic contrast control constraint." In: *J. Acoust. Soc. Am.*, **135**(2):734–741.

[19] Meyer, D.G. (1984): "Computer simulation of loudspeaker directivity." In: *J. Audio Eng. Soc.*, **32**(5):294–315.

[20] Meyer, P.; Schwenke, R. (2003): "Comparison of the directional point source model and BEM model for arrayed loudspeakers." In: *Proc. of the Institute of Acoustics*, **25**(4).

[21] Schultz, F.; Rettberg, T.; Spors, S. (2014): "On spatial-aliasing-free sound field reproduction using finite length line source arrays." In: *Proc. of the 137th Audio Eng. Soc. Conv., Los Angeles*, #9098.

[22] Skudrzyk, E. (1971): *The Foundations of Acoustics*. New York: Springer.

[23] Olver, F.W.J.; Lozier, D.W.; Boisvert, R.F.; Clark, C.W. (2010): *NIST Handbook of Mathematical Functions*. Cambridge University Press, 1. ed.

[24] Heil, C.; Urban, M. (1992): "Sound fields radiated by multiple sound sources arrays." In: *Proc. of 92nd Audio Eng. Soc. Conv., Vienna*, #3269.

[25] Deschamps, G.A.; Cabayan, H.S. (1972): "Antenna synthesis and solution of inverse problems by regularization methods." In: *IEEE Trans. on Antennas and Propagation*, **20**(3):268–274.

[26] Nelson, P.A. (2001): "A review of some inverse problems in acoustics." In: *J. Acoust. and Vibr.*, **6**(3):118–134.

[27] Kim, Y.; Nelson, P. (2004): "Optimal regularisation for acoustic source reconstruction by inverse methods." In: *J. of Snd. Vibr.*, **275**(3):463–487.

[28] Betlehem, T.; Withers, C. (2012): "Sound field reproduction with energy constraint on loudspeaker weights." In: *IEEE Trans. on Audio, Speech, and Language Processing*, **20**(8):2388–2392.

[29] Ahrens, J.; Spors, S. (2010): "Sound field reproduction using planar and linear arrays of loudspeakers." In: *IEEE Trans. Audio Speech Language Process.*, **18**(8):2038–2050.

[30] Wierstorf, H. (2014): *Perceptual assessment of sound field synthesis*. Ph.D. thesis, TU Berlin.

[31] Malyshev, A.N. (2003): "A unified theory of conditioning for linear least squares and Tikhonov regularization methods." In: *SIAM J. Matrix Anal. Appl.*, **24**(4):1186–1196.

9. APPENDIX

LSA cabinet	γ_n / deg	$x_{c,n}$ / m	$y_{c,n}$ / m
1	-3	0.0097	2.8143
2	-1	0.0227	2.4425
3	1	0.0227	2.0706
4	3	0.0097	1.6989
5	5	-0.0162	1.3278
6	7	-0.0551	0.9579
7	10	-0.1101	0.5901
8	12	-0.1810	0.2250
9	15	-0.2678	-0.1366
10	18	-0.3735	-0.4931
11	21	-0.4976	-0.8437
12	24	-0.6399	-1.1872
13	27	-0.8000	-1.5229
14	30	-0.9774	-1.8497
15	34	-1.1744	-2.1650
16	38	-1.3930	-2.4657

Table 5: Front grille center positions and tilting angles of the LSA cabinets for the geometry used in Fig. 1.

m	x_m / m	y_m / m
1	0	-11
1401	7	-11
10001	50	-11
12063	58.0017	-4.4986
13062	58.0017	0.4964
15124	66.0035	6.9978
16325	66.0035	13.0028
29525	0.0035	13.0028

Table 6: Selected venue slice coordinates according to Fig. 2.

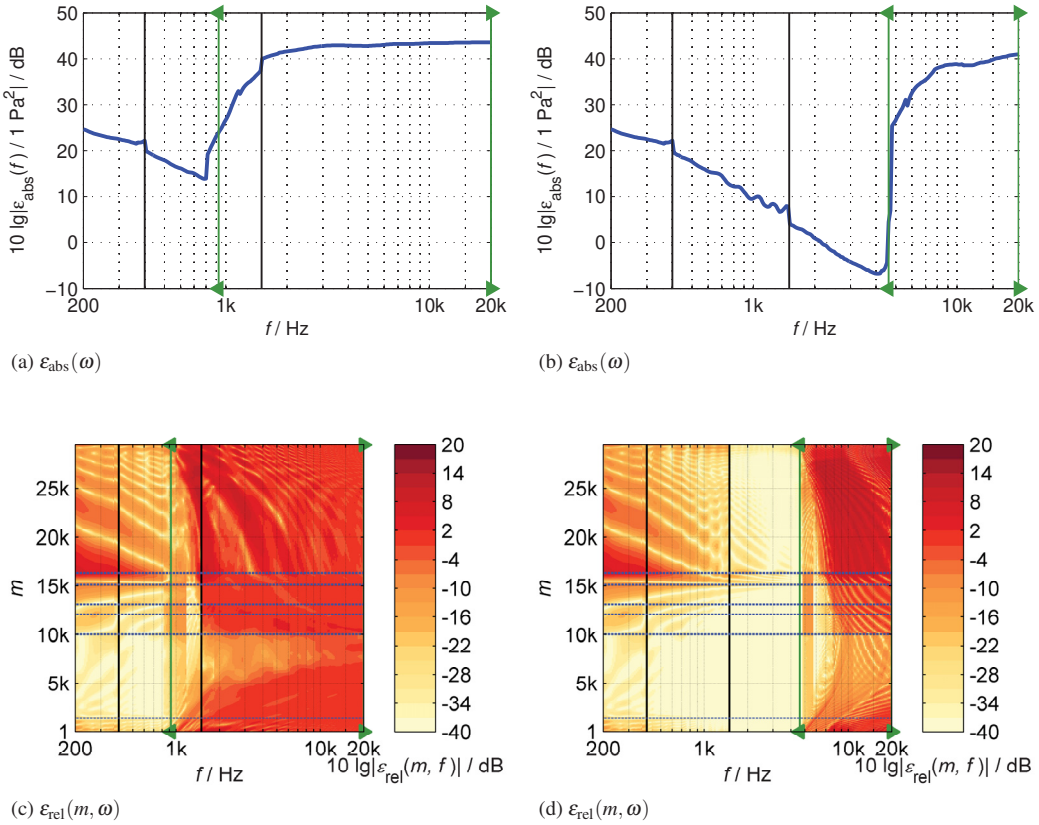

(a) $\varepsilon_{\mathrm{abs}}(\omega)$ (b) $\varepsilon_{\mathrm{abs}}(\omega)$

(c) $\varepsilon_{\mathrm{rel}}(m,\omega)$ (d) $\varepsilon_{\mathrm{rel}}(m,\omega)$

Fig. 8: Evaluation plots for the LSA_1 (left) and the LSA_2 (right), top: frequency dependent absolute error $\varepsilon_{\mathrm{abs}}(\omega)$, eq. (16), bottom: position and frequency dependent relative error $\varepsilon_{\mathrm{rel}}(m,\omega)$, eq. (17). The crossover frequencies (black) and the spatial aliasing frequencies of straight arrays (green with arrows) according to Tab. 2 are charted for orientation.

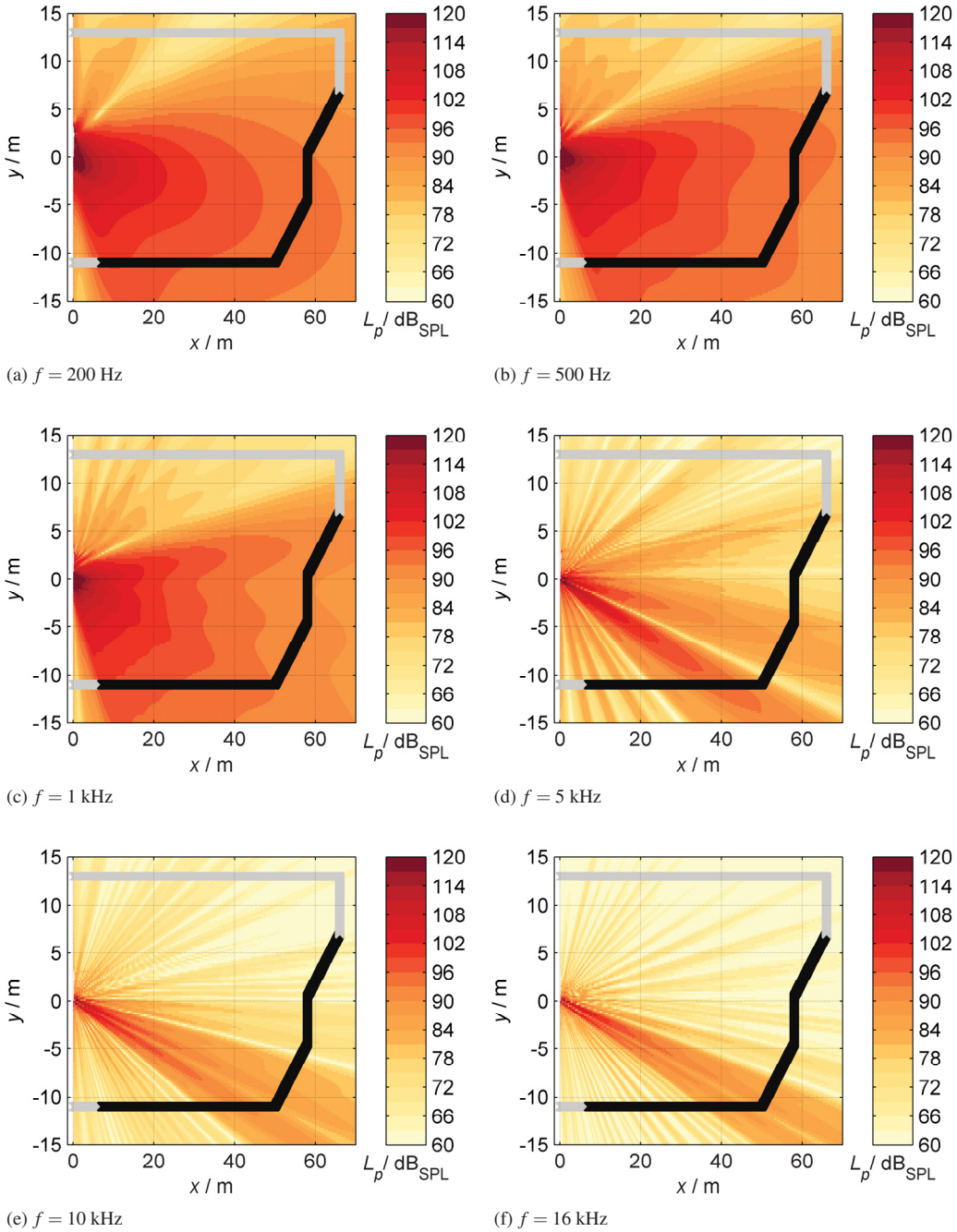

(a) $f = 200$ Hz (b) $f = 500$ Hz

(c) $f = 1$ kHz (d) $f = 5$ kHz

(e) $f = 10$ kHz (f) $f = 16$ kHz

Fig. 9: Sound pressure levels in the *xy*-plane (SPLxy) for the LWE-optimized LSA_1. Optimized for the position index plot points.

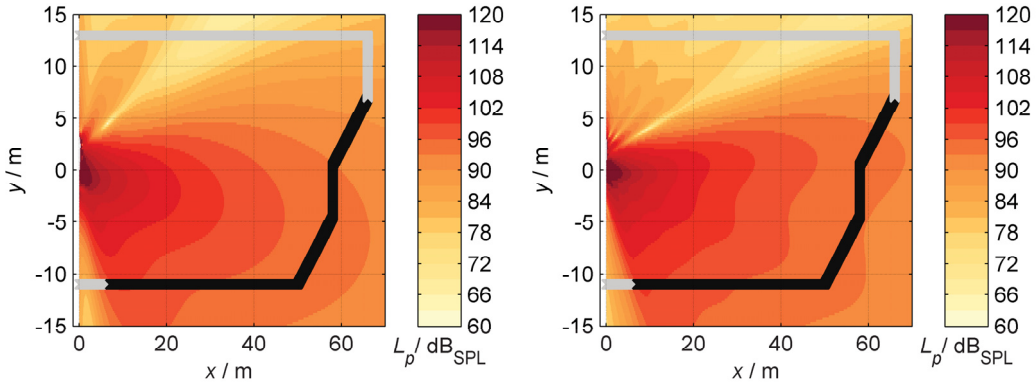

(a) $f = 200$ Hz (b) $f = 500$ Hz

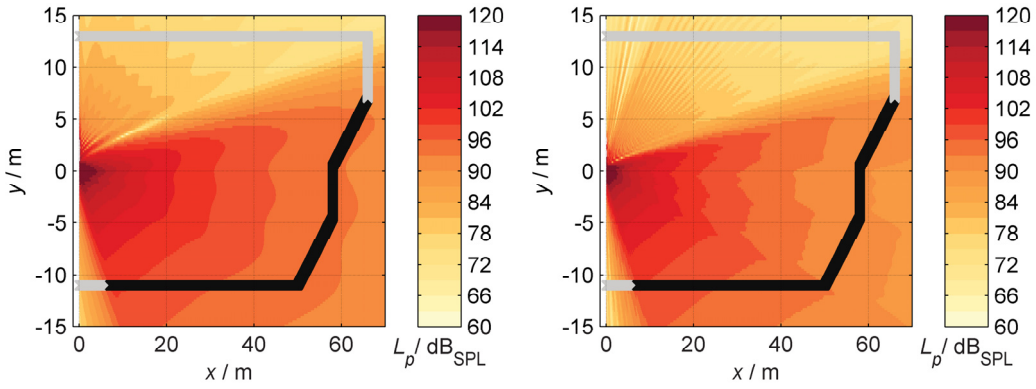

(c) $f = 1$ kHz (d) $f = 5$ kHz

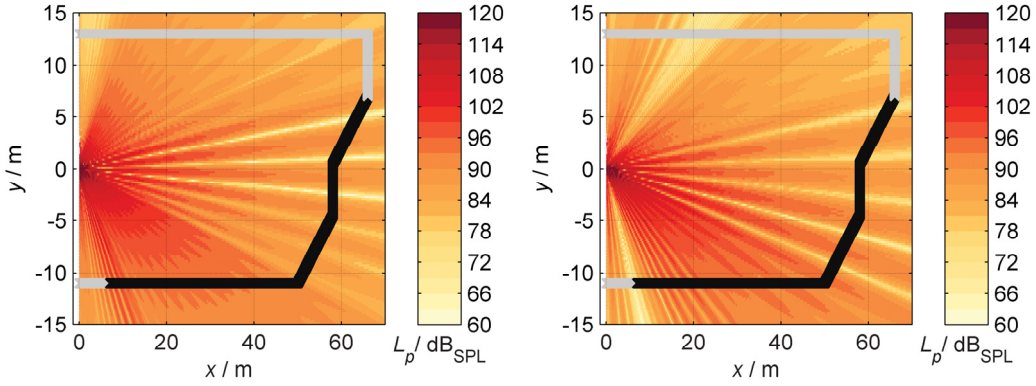

(e) $f = 10$ kHz (f) $f = 16$ kHz

Fig. 10: Sound pressure levels in the *xy*-plane (SPLxy) for the LWE-optimized LSA_2. Optimized for the position index plot points.

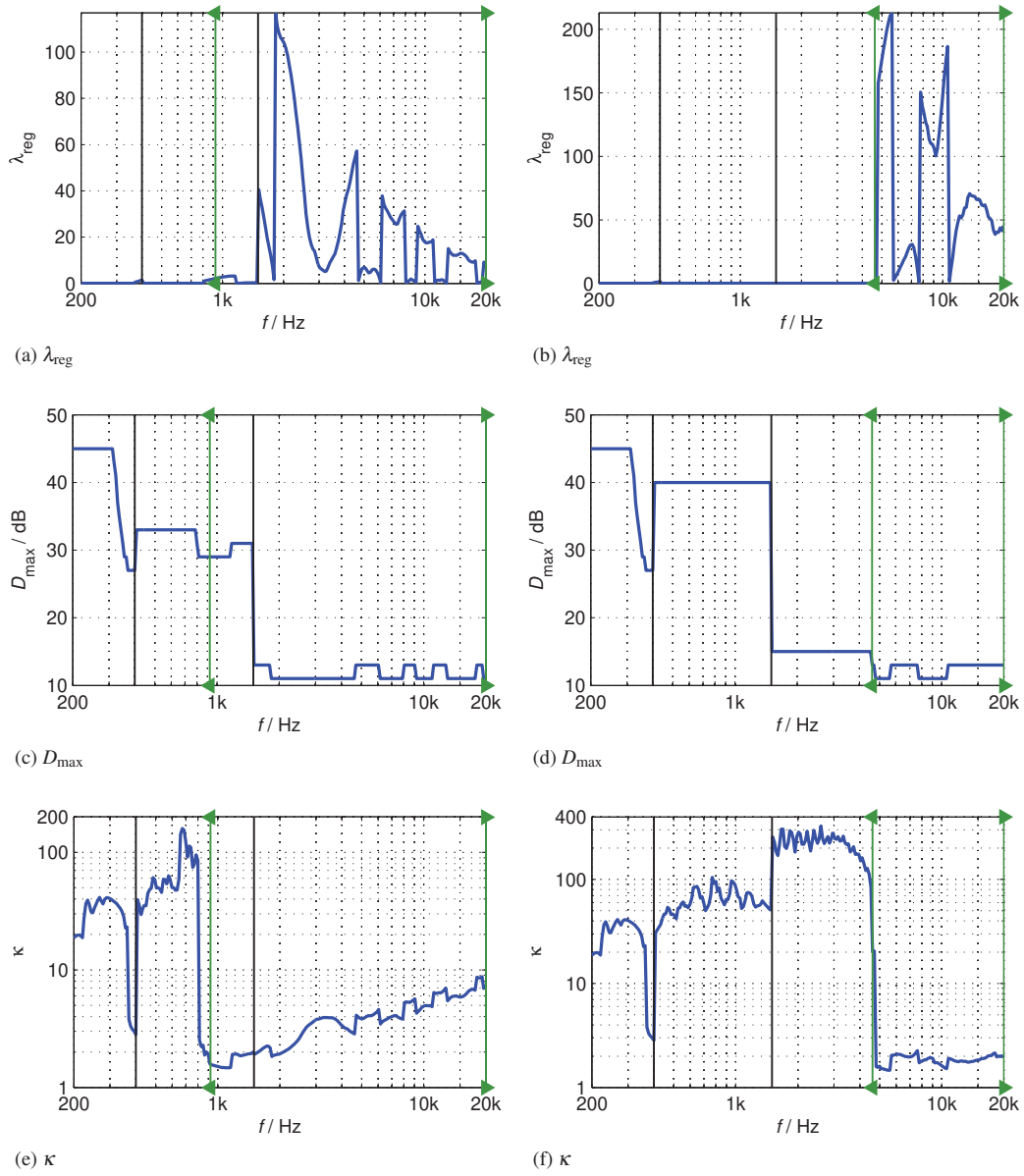

(a) λ_{reg} (b) λ_{reg}

(c) D_{max} (d) D_{max}

(e) κ (f) κ

Fig. 11: Optimization parameters for the LSA_1 (left) and the LSA_2 (right), top: regularization parameter λ_{reg}, mid: D_{max}, bottom: condition number κ for the Tikhonov regularized solution, cf. [26], [31, (3.1b)]. The crossover frequencies (black) and the spatial aliasing frequencies of straight arrays (green with arrows) according to Tab. 2 are charted for orientation.

Optimized Driving Functions for Curved Line Source Arrays Using Modeled and Measured Loudspeaker Data

Florian Straube[1], Frank Schultz[2], Michael Makarski[3], Stefan Weinzierl[1]

[1] *Audio Communication Group, TU Berlin, 10587, Berlin, Germany, E-mail: florian.straube@tu-berlin.de*

[2] *Institute of Communications Engineering, University of Rostock, 18119, Rostock, Germany*

[3] *Four Audio GmbH & Co. KG, 52134, Herzogenrath, Germany*

Introduction

Line Source Arrays (LSAs) are used for large-scale sound reinforcement aiming at the synthesis of homogenous wavefronts for the whole audio bandwidth. The deployed loudspeaker cabinets are generally rigged with different tilt angles in order to ensure the coverage of the audience zones and to avoid or reduce undesirable radiation that may be directed at the ceiling, reflective walls or residential areas. By choosing (numerically) optimized driving functions for the individual loudspeakers the homogeneity of the intended wavefront can be further improved [1–7]. This contribution presents an evaluation of driving functions optimized using a goal attainment multiobjective optimization approach as well as a comparison of the synthesized sound fields for modeled and measured loudspeaker data. The complex-directivity point source (CDPS) model-based calculations include far-field radiation patterns of baffled line and circular pistons and the actual loudspeaker data originate from vertical directivity measurements. The analyses are performed for a typical concert venue employing curved LSA setups.

It will be shown with the help of position index plots (PIPs), far-field radiation patterns (FRPs) and driving function index plots (only amplitudes, $\mathrm{DFIP_a}$s) that the model-based multiobjective optimizations provide superior results compared to those obtained via common regularized least-mean-square error optimization approaches. The results are similar for modeled and measured loudspeaker data. In the latter case, however, the quality of the approach critically depends on the spatial resolution of the measured directivity and the correct identification of the spatial aliasing behavior. It is therefore concluded that modeled LSA data are more beneficial than measured directivities for the design and evaluation of appropriate LSA optimization strategies and that this multiobjective optimization approach needs to be extended by additional constraints or the results need to be post-processed for realizable and feasible FIR filters.

LSA setup

A curved LSA setup with a total of $N = 22$ LSA cabinets with $n = 1, 2, ..., N$ is deployed. The front grille's height $\Lambda_{y,\mathrm{LSA}}$ of a single LSA cabinet is set to 0.258 m resulting in an overall LSA length of ca. 5.68 m. γ_n denotes the individual tilt angles and $\mathbf{x_{0,i}}$ denotes the front grille center position of the i-th LSA driver. Detailed information on the geometric configuration can be seen in Fig. 1 and

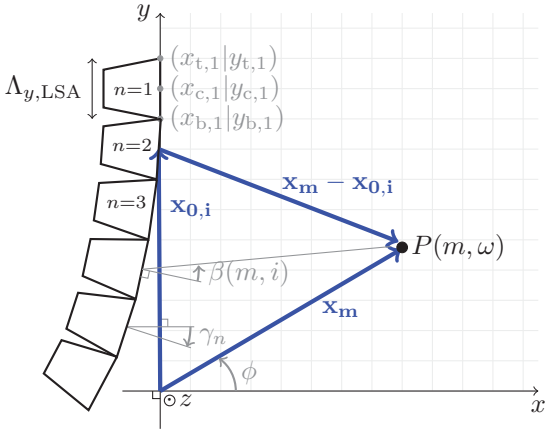

Figure 1: Sketch of the LSA setup under discussion. A total of $N = 22$ LSA cabinets of the height $\Lambda_{y,\mathrm{LSA}} = 0.258\,\mathrm{m}$ is used.

can be found in [8, 9].

Built from two-way cabinets in this paper, the exemplarily chosen LSA consists of $L_{\mathrm{LF}} = 1$ and $L_{\mathrm{HF}} = 1$ vertically stacked, individually controlled drivers per cabinet for the low and the high frequency band (LF, HF). Different loudspeaker sensitivities are assumed in order to obtain realistic sound pressure values, $S_{\mathrm{dB,LF}} = 92$ dB and $S_{\mathrm{dB,HF}} = 112$ dB for vertical radiation in this case. The relation of the pistons' dimensions to the fixed distance between adjacent piston centers which is also known as Active Radiating Factor (ARF) [10, Ch. 3.2], [11] amounts to approximately 0.79. On the one hand, the circular piston model [12, (26.42)] is deployed for LF, the line piston model [12, (26.44)] is deployed for HF and on the other hand measured loudspeaker directivity data are incorporated. For the frequency band crossover, fourth-order Linkwitz-Riley (LR4) filters with a transition frequency $f_{\mathrm{LF,HF}} = 1000$ Hz are used.

Venue Geometry

Following a practical example presented in [5, Sec. 6.1], a multi-stand arena with audience and non-audience sections, i.e. zones to be covered and zones to be avoided, is modeled by a two dimensional slice representation. Only the xy-plane is considered for vertical radiation, cf. Fig. 2. This is a common approach for optimization schemes as the horizontal radiation is assumed to be convenient anyway, cf. [1–7, 13]. $M = 29\,525$ receiver positions with $m = 1, 2, ..., M$ are taken into account. This

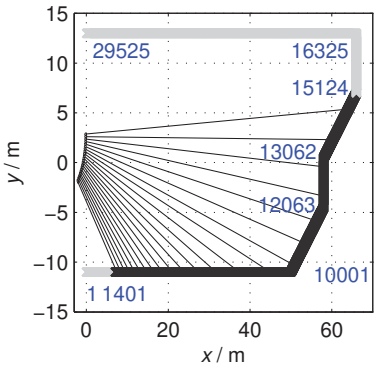

Figure 2: Venue slice within the xy-plane with audience (black) as well as non-audience/avoid (gray) zones and selected index numbers (change of audience/avoid zone and/or polygonal line's segment angle) from M receiver positions.

corresponds to a distance of 0.005 m between the receiver positions ensuring a discretization which approximately equals one fourth of the wavelength at 17.2 kHz.

Calculation Model

Modeling multi-way cabinets the total sound pressure is composed of the sound pressures of the different frequency bands, e.g.

$$P(m,\omega) = P_{\mathrm{LF}}(m,\omega) + P_{\mathrm{HF}}(m,\omega). \tag{1}$$

Since the calculations are performed separately for each frequency band with a subsequent summation, the frequency band indices (LF, HF) are omitted for generalization in the following. The sound field prediction is based on a complex-directivity point source model of baffled piston far-field radiation patterns. Its fundamental equation [14, (11)], [15, Sec. 1.1] reads

$$P(m,\omega) = \sum_{i=1}^{L\,N} G(m,i,\omega)\, D(i,\omega). \tag{2}$$

$P(m,\omega)$ denotes the sound pressure spectrum at the receiver position $\mathbf{x_m}$ with $[P(m,\omega)] = 1\,\mathrm{Pa/Hz}$. $G(m,i,\omega)$ terms the acoustic transfer function (ATF) from the i-th source to the receiver points. The complex driving function spectrum $D(i,\omega)$ with $[D(i,\omega)] = 1\,\mathrm{Pa/Hz}$ of the i-th source is directly proportional to the source's velocity spectrum.

(2) is modified including a loudspeaker sensitivity standardization in order to obtain realistic absolute sound pressure levels (SPLs). Therefore $G(m,i,\omega)$ is considered as a scaled ATF

$$G(m,i,\omega) = H_{\mathrm{post}}(\beta(m,i),\omega)\, \frac{\mathrm{e}^{-\mathrm{j}\,\frac{\omega}{c}\,\|\mathbf{x_m}-\mathbf{x_{0,i}}\|_2}}{\left(\frac{\|\mathbf{x_m}-\mathbf{x_{0,i}}\|_2}{\mathrm{m}}\right)} \times \tag{3}$$
$$\left(\frac{p_0}{\mathrm{Pa}}\right)\, 10^{\frac{1}{20}\left(\frac{S_{\mathrm{dB}}(i,\omega)}{\mathrm{dB_{SPL}\,\frac{m}{W}}}\right)}$$

being composed of a specific far-field radiation pattern $H_{\mathrm{post}}(\beta(m,i),\omega)$, the $4\,\pi$-discarded free-field 3D Green's function $\frac{\mathrm{e}^{-\mathrm{j}\,\frac{\omega}{c}\,\|\mathbf{x_m}-\mathbf{x_{0,i}}\|_2}}{\|\mathbf{x_m}-\mathbf{x_{0,i}}\|_2}$ (i.e. the ideal point source), the reference sound pressure p_0 that commonly amounts to $2\times10^{-5}\,\mathrm{Pa}$ in air and the loudspeaker sensitivity $S_{\mathrm{dB}}(i,\omega)$ specifying the SPL in 1 m distance for an electrical input power of 1 W. The sensitivity is assumed to be constant for all drivers and all frequencies per frequency band, i.e. $S_{\mathrm{dB}}(i,\omega) = S_{\mathrm{dB}}$.

Consisting of the signal input spectrum $D_{\mathrm{in}}(i,\omega)$ with $[D_{\mathrm{in}}(i,\omega)] = 1\,\mathrm{Pa/Hz}$, the complex optimized filter $D_{\mathrm{opt}}(i,\omega)$ with $[D_{\mathrm{opt}}(i,\omega)] = 1$ and the complex frequency band crossover as well as high-/lowpass filter $D_{\mathrm{xo}}(\omega)$ with $[D_{\mathrm{xo}}(\omega)] = 1$, thus

$$D(i,\omega) = D_{\mathrm{in}}(i,\omega)\, D_{\mathrm{opt}}(i,\omega)\, D_{\mathrm{xo}}(\omega), \tag{4}$$

an upper limit for the driving function's absolute value can be given as

$$D_{\mathrm{max,dB}}(\omega) \geq \max_i\{D_{\mathrm{in,dB}}(i,\omega)\} + \max_i\{D_{\mathrm{opt,dB}}(i,\omega)\} + D_{\mathrm{xo,dB}}(\omega) \; + D_{\mathrm{hr,dB}}(\omega). \tag{5}$$

This is directly related to the source's maximum electric input power. While the absolute value of the crossover filter usually does not exceed 0 dB, the provided (amplifier) headroom $D_{\mathrm{hr,dB}}(\omega)$ is typically set to e.g. 3 dB.

In line with this modeling, air absorption is neglected, a constant velocity of sound ($c = 343$ m/s) and for the modeled sources infinite, straight baffles and a constant surface velocity are assumed.

Multiobjective Optimization

For the application of optimization algorithms, (2) is rewritten in matrix notation, accounting for all receiver positions M for a single frequency

$$\mathbf{p}(\omega) = \mathbf{G}(\omega)\, \mathbf{d}(\omega) \tag{6}$$

with $\mathbf{p}(\omega)$ denoting the $(M\times1)$ vector of sound pressure spectra at all considered positions $\mathbf{x_m}$, $\mathbf{G}(\omega)$ denoting the $(M\times L\,N)$ (scaled) ATF matrix and $\mathbf{d}(\omega)$ denoting the $(L\,N\times1)$ vector of the complex driving weights at all source positions $\mathbf{x_{0,i}}$ per angular frequency ω. Then, for a desired sound field $\mathbf{p}_{\mathrm{des}}(\omega)$ at the evaluation positions $\mathbf{x_m}$ (6) is solved for the weights $\mathbf{d}(\omega)$. In this case, ca. 3 dB attenuation per distance doubling is requested and a goal attainment multiobjective optimization approach [16] is used. This method is presumably also applied in [5, 6]. Its equation is (cf. [16, (1)] for the general formula)

$$\begin{aligned} &\min_{\zeta,\mathbf{d}(\omega)} \zeta \\ \text{such that:}\quad &\mathbf{F}[\mathbf{d}(\omega)] - \mathbf{w}\,\zeta \leq \mathbf{F}^*[\mathbf{d}(\omega)] \\ \text{subject to:}\quad &|D_{\mathrm{opt}}(i,\omega)| \leq D_{\mathrm{opt,max}}(\omega) \quad \forall i \\ &|D_{\mathrm{opt}}(i,\omega)| \geq D_{\mathrm{opt,min}}(\omega) \quad \forall i \end{aligned} \tag{7}$$

with the vector of objective functions

$$\mathbf{F}[\mathbf{d}(\omega)] = \begin{pmatrix} F_1[\mathbf{d}(\omega)] \\ F_2[\mathbf{d}(\omega)] \end{pmatrix} = \begin{pmatrix} \epsilon_{\mathrm{abs}}(\omega) \\ L_{p,\mathrm{a,na}}(\omega) \end{pmatrix} \tag{8}$$

that shall incorporate the frequency dependent absolute error $\epsilon_{\mathrm{abs}}(\omega)$ (see [9, (16)]) and a frequency dependent measure $L_{p,\mathrm{a,na}}(\omega)$ (see [9, (18)]) that relates

the obtained average levels of the audience zone and the non-audience zone. The latter is established as acoustic contrast in multi-zone sound field synthesis [17, (16)], [18, (2)]. In addition, (7) comprises a set of design goals $\mathbf{F}^*[\mathbf{d}(\omega)]$ for the objective functions and a weighting vector $\mathbf{w}$ with $\mathbf{w} = (w_1, w_2)^{\mathrm{T}}$ to determine a balance between the different objectives. Note that $\max_{\omega}\{|D_{\mathrm{opt}}(i,\omega)|\}$ provides quantitative information on the common trade-off between the increase of the sound field's homogeneity and the decrease of the maximum SPL output.

Discussion

In Fig. 3 the PIPs, i.e. the SPL spectra at all control positions $\mathbf{x_m}$, the FRPs, i.e. the polar patterns for radiating angles $|\phi| \leq 90°$ as an isobar plot over all evaluated frequencies, and the $\mathrm{DFIP_a}$s, i.e. the magnitudes over frequency that have to be applied to the individual sources, can be seen. For the chosen LSA setup with modeled as well as measured loudspeaker data, the optimizations are performed separately for each frequency of a logarithmically spaced frequency vector with $f_{\mathrm{start}} = 200$ Hz, $f_{\mathrm{stop}} = 20$ kHz and 1/36th octave resolution. The aliasing frequency f_{alias} referring to the spatial sampling condition $\Delta y \leq \frac{c}{2f}$ for straight arrays is ca. 664.73 Hz.

The PIPs show that the desired sound field is quite sufficiently obtained for LF and for some extent also for HF. Due to the single LF piston (vertically) per cabinet and the large waveguide, (complex) optimized filters are not very meaningful to be applied for high frequencies for this LSA design. For frequencies below roughly 2 kHz mostly the non-audience positions are just scarcely fed and a homogenous audience coverage is provided. Above this frequency the sound field is severely corrupted by spatial aliasing and the sound is also radiated into the regions that are to be avoided. In the FRPs, this is also visible on the basis of the grating lobes for the high frequencies. Mainly the sources in the middle of the LSAs are loaded for frequencies larger than f_{alias}, whereas the drivers' loads are quite balanced below this value, cf. Fig. 3e, Fig. 3f. Note that the DFIP phases as group delays are not depicted here.

Conclusion

The model-based multiobjective optimizations provide superior results compared to those obtained via common regularized least-mean-square error optimization approaches (cf. [9]) as the distinct drivers' loads can be controlled individually. Using the CDPS model for both modeled and measured loudspeaker data, the results are very similar for the LF as well as the HF range, remarkable differences can be observed only for HF. These mainly involve the correct identification of the spatial aliasing behavior since the spatial resolution of the measured loudspeaker directivity may not be sufficient and because of the specific waveguide characteristics. For the design and evaluation of appropriate LSA optimization strategies it may be therefore favorable to focus on modeled loudspeaker data, whereas the measured loudspeaker data do not necessarily have to be utilized before the drive computation of practical LSA setups. It is also recommendable to limit the bandwidth of numerical optimizations, depending on the array length and the spatial aliasing frequency. The calculated driving functions could be further improved by frequency smoothing in order to allow only small changes between nearby frequencies. A technically or psychoacoustically-motivated constraint for the DFIP phases as group delays (e.g. linear phases) should be added for realizable and feasible FIR filters. An alternative approach may be using an amplitude shading, bearing on the LSA and receiver geometry and being numerically refined.

References

[1] van Beuningen, G.W.J.; Start, E.W. (2000): "Optimizing directivity properties of DSP controlled loudspeaker arrays." In: *Proc. of the Inst. of Acoustics: Reproduced Sound*, **22**(6):17–37.

[2] Thompson, A. (2008): "Real world line array optimisation." In: *Proc. of the Institute of Acoustics*, **30**(6).

[3] Thompson, A. (2009): "Improved methods for controlling touring loudspeaker arrays." In: *Proc. of the 127th Audio Eng. Soc. Conv., New York*, #7828.

[4] Terrell, M.; Sandler, M. (2010): "Optimising the controls of a homogenous loudspeaker array." In: *Proc. of the 129th Audio Eng. Soc. Conv., San Francisco*, #8159.

[5] Thompson, A.; Baird, J.; Webb, B. (2011): "Numerically optimised touring loudspeaker arrays - Practical applications." In: *Proc. of the 131st Audio Eng. Soc. Conv., New York*, #8511.

[6] Feistel, S.; Sempf, M.; Köhler, K.; Schmalle, H. (2013): "Adapting loudspeaker array radiation to the venue using numerical optimization of FIR filters." In: *Proc. of the 135th Audio Eng. Soc. Conv., New York*, #8937.

[7] Thompson, A.; Luzarraga, J. (2013): "Drive granularity for straight and curved loudspeaker arrays." In: *Proc. of the Inst. of Acoustics*, **35**(2):210–218.

[8] Straube, F.; Schultz, F.; Weinzierl, S. (2015): "On the effect of spatial discretization of curved Line Source Arrays." In: *Fortschritte der Akustik: Tagungsband d. 41. DAGA, Nuremberg*, 459–462.

[9] Straube, F.; Schultz, F.; Makarski, M.; Spors, S.; Weinzierl, S. (2015): "Evaluation strategies for the optimization of Line Source Arrays." In: *Proc. of the 59th Audio Eng. Soc. Int. Conf. on Sound Reinforcement, Montreal.*

[10] Urban, M.; Heil, C.; Bauman, P. (2003): "Wavefront Sculpture Technology." In: *J. Audio Eng. Soc.*, **51**(10):912–932.

[11] Schultz, F.; Straube, F.; Spors, S. (2015): "Discussion of the Wavefront Sculpture Technology criteria for straight line arrays." In: *Proc. of the 138th Audio Eng. Soc. Conv., Warsaw*, #9323.

[12] Skudrzyk, E. (1971): *The Foundations of Acoustics.* New York: Springer.

[13] Thompson, A. (2006): "Line array splay angle optimisation." In: *Proc. of the Inst. of Acoustics*, **28**(8):135–148.

[14] Feistel, S.; Thompson, A.; Ahnert, W. (2009): "Methods and limitations of line source simulation." In: *J. Audio Eng. Soc.*, **57**(6):379–402.

[15] Meyer, P.; Schwenke, R. (2003): "Comparison of the directional point source model and BEM model for arrayed loudspeakers." In: *Proc. of the Institute of Acoustics*, **25**(4).

[16] Gembicki, F.W.; Haimes, Y.Y. (1975): "Approach to performance and sensitivity multiobjective optimization: The goal attainment method." In: *IEEE Trans. on Automatic Control*, **20**(6):769–771.

[17] Choi, J.W.; Kim, Y.H. (2002): "Generation of an acoustically bright zone with an illuminated region using multiple sources." In: *J. Acoust. Soc. Am.*, **111**(4):1695–1700.

[18] Coleman, P.; Jackson, P.J.B.; Olik, M.; Møller, M.; Olsen, M.; Pedersen, J.A. (2014): "Acoustic contrast, planarity and robustness of sound zone methods using a circular loudspeaker array." In: *J. Acoust. Soc. Am.*, **135**(4):1929–1940.

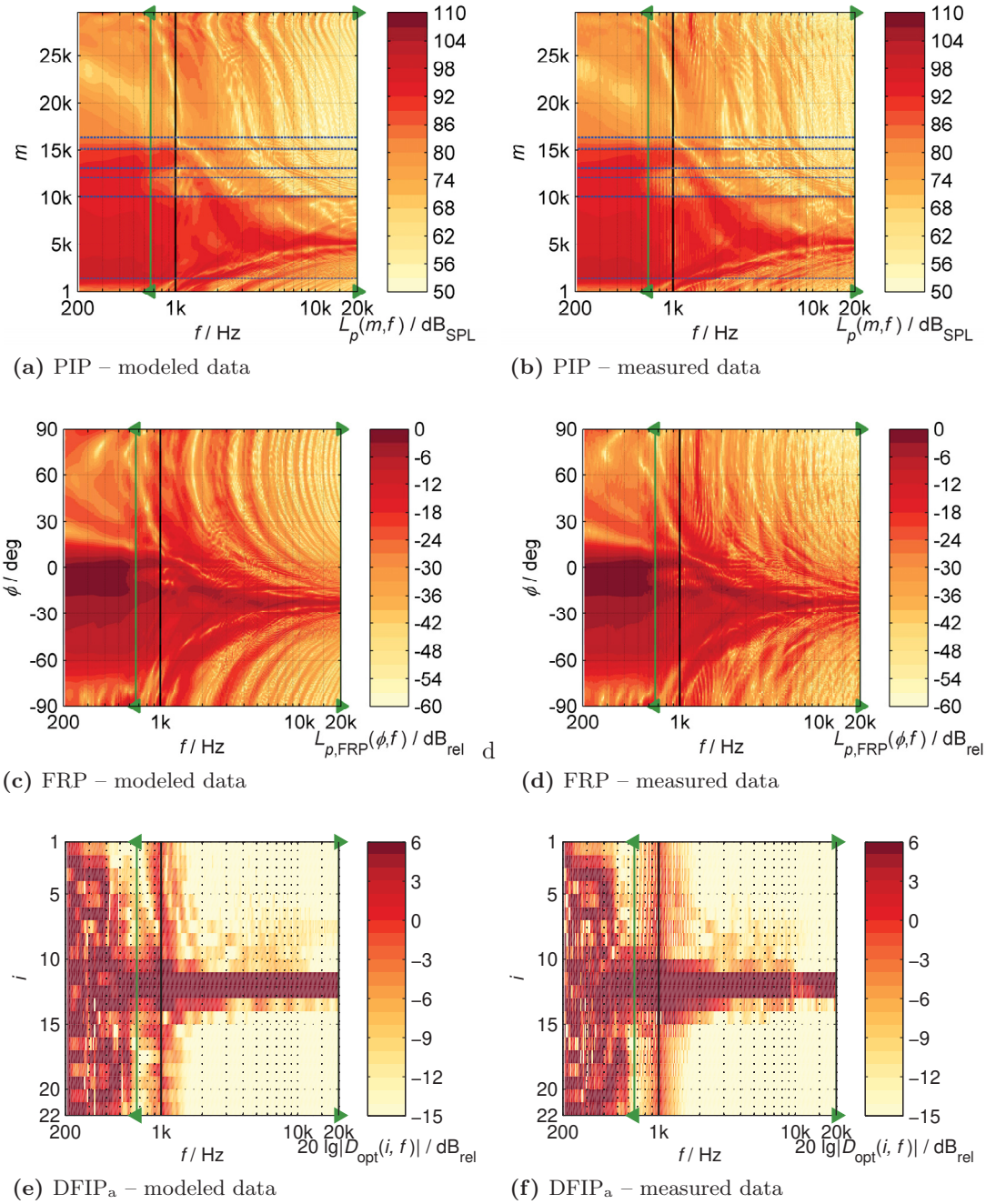

(a) PIP – modeled data **(b)** PIP – measured data

(c) FRP – modeled data **(d)** FRP – measured data

(e) DFIP$_a$ – modeled data **(f)** DFIP$_a$ – measured data

Figure 3: Position index plots (PIPs, first row), far-field radiation patterns (FRPs, second row) and driving function index plots (DFIP$_a$s, only amplitudes) for an optimized drive of the exemplarily chosen LSA design. The optimizations with $\mathbf{F}^*[\mathbf{d}(\omega)] = (10^{-6}, 15\,\mathrm{dB})^\mathrm{T}$, $\mathbf{w} = (1, -1/0.3)^\mathrm{T}$ and $D_{\mathrm{opt,max,dB}}(\omega) = 6\,\mathrm{dB}$, $D_{\mathrm{opt,min,dB}}(\omega) = -15\,\mathrm{dB}$ for all drivers are based on modeled (left) and measured loudspeaker directivity data (right). The crossover frequency $f_{\mathrm{LF,HF}}$ (black) and the spatial aliasing frequency f_{alias} of an equivalent straight array (green with arrows) are charted for orientation.

Adjungierten-basierte Schallfeldsynthese und Beschallung

Mathias Lemke[1], Florian Straube[2], Jörn Sesterhenn[1], Stefan Weinzierl[2]
[1] *Institut für Strömungsmechanik und Technische Akustik, TU Berlin, 10623, Berlin, E-mail: mlemke@tnt.tu-berlin.de*
[2] *Audio Communication Group, TU Berlin, 10587, Berlin*

Einleitung

Das Bestimmen einer geeigneten geometrischen Anordnung sowie einer geeigneten elektronischen Ansteuerung für Line Source Arrays (LSAs), die heutzutage typischerweise für Großbeschallungsaufgaben eingesetzt werden, ist im mathematischen Sinne ein schlecht gestelltes, inverses Problem. In der Praxis werden die benötigten Filterkoeffizienten entweder manuell durch erfahrene Benutzer in einem zeitaufwendigen Prozess oder durch numerische Optimierungsverfahren im Frequenzbereich bestimmt [1–4]. Die verwendeten Algorithmen und ihre Parametrisierung sind kaum öffentlich zugänglich dokumentiert und typischerweise herstellerabhängig.

Der in diesem Beitrag verwendete adjungierten-basierte Ansatz ist eine alternative Herangehensweise. Abhängig von einer Zielfunktion - definiert durch ein Zielschallfeld - erlaubt die Methode die Optimierung von Quellen in Zeit und Raum. Das Verfahren beruht auf den adjungierten Euler-Gleichungen. Sowohl die optimalen Positionen der Schallquellen als auch die optimalen Treiberfunktionen zum Generieren eines gewünschten Schallfeldes können bestimmt werden. Zudem lassen sich mit der adjungierten-basierten Methode Grundströmungen berücksichtigen. Auch für nicht-glatte Quellenanordnungen lassen sich Lösungen finden. An den Grenzen des untersuchten Gebietes können verschiedene Randbedingungen behandelt werden.

In diesem Beitrag werden die Grundlagen der adjungierten-basierten Methode zum Generieren von Schallfeldern sowie ein Beispiel zur Validierung vorgestellt.

Adjungierten-Methode

In der Strömungsmechanik hat sich der Einsatz von adjungierten Verfahren als erfolgreicher Lösungsweg zur Bestimmung von einer Vielzahl von Modellparametern herausgestellt [5]. Eine Übertragung auf die Akustik ist naheliegend, da die üblicherweise verwendeten adjungierten kompressiblen Euler- bzw. Navier-Stokes-Gleichungen [6, 7] die Akustik, sowohl für eine ruhende Umgebung als auch eine Grundströmung, beinhalten. Im Gegensatz zu den im Beschallungsbereich typischen Verfahren im Frequenzbereich, die auf einer Integraldarstellung der homogenen Wellengleichung für diskrete Quellenverteilungen beruhen, handelt es sich hier um eine allgemeinere Darstellung der Wellenausbreitung im Zeitbereich.

Adjungierte allgemein

Es wird, angelehnt an die Beschreibung in [5], ein System betrachtet, welches die zeitliche Schallausbreitung in einem endlichen Volumen beschreibt:

$$Aq = f. \tag{1}$$

Dabei definiert A die beschreibende Systemgleichung, q den Systemzustand und f die Quellen im System. Gesucht ist eine optimale Ansteuerung der Quellen f, um einen gewünschten Systemzustand (q_{ziel}) unter den beschreibenden Gleichungen A zu erzeugen. Das Optimum leitet sich aus einem integralen Maß J (Zielfunktional) mit

$$J = g^{\mathrm{T}} q \tag{2}$$

ab, welches als Produkt von Systemzustand q und einem noch zu bestimmenden Gewicht g definiert ist. Die Sensitivität der Quellen f auf das Zielfunktional lässt sich mit Hilfe der adjungierten Gleichung

$$A^{\mathrm{T}} q^* = g, \tag{3}$$

mit q^* als adjungierter Variable einfach berechnen, da

$$J = g^{\mathrm{T}} q = (A^{\mathrm{T}} q^*)^{\mathrm{T}} u = {v^*}^{\mathrm{T}} A q = {q^*}^{\mathrm{T}} f \tag{4}$$

gilt. Die adjungierte Variable enthält demnach Informationen, welchen Einfluss die Aktuatoren f auf das Zielfunktional J haben bzw. wie f zu ändern ist. Der Adjungierten-Ansatz kann daher direkt zu einer Lösung für die optimale Anregung bei der Schallfeldgenerierung führen.

Die numerisch diskrete Variante von (3) kann auf unterschiedliche Weise hergeleitet werden. Im *diskreten* Ansatz wird die beschreibende Differentialgleichung zunächst diskretisiert. Der resultierende Operator wird dann transponiert und zur Lösung der adjungierten Gleichung verwendet. Im *kontinuierlichen* Ansatz werden die beschreibenden Gleichungen zunächst linearisiert und dann zur analytischen Herleitung der adjungierten Gleichungen genutzt. Diese werden im Anschluss diskretisiert und zur Lösung verwendet. Wir folgen hier dem kontinuierlichen Ansatz.

Adjungierte zur Schallfeldsynthese

Entsprechend der angestrebten Anwendung, der Schallfeldsynthese im Zeitbereich, wird das Zielfunktional J in Raum und Zeit $\mathrm{d}\Omega = \mathrm{d}x_i \mathrm{d}t$ definiert:

$$J = \frac{1}{2} \iint \left(q - q_{\text{ziel}}\right)^2 \mathrm{d}\Omega. \tag{5}$$

Die Größe q enthält alle zur Systembeschreibung notwendigen Variablen mit $q = [\varrho, u_j, p]$. Dabei bezeichnet ϱ die Dichte, u_j die Geschwindigkeit in Richtung x_j und p den Druck, der hier allein ausgewertet werden soll, also

$$J = \frac{1}{2} \iint (p - p_{\text{ziel}})^2 \, \mathrm{d}\Omega. \tag{6}$$

Im Sinne der Schallfelderzeugung ist ein Minimum von J optimal, wobei p_{ziel} noch geeignet zu definieren ist.

Das Minimum soll unter einer Nebenbedingung erreicht werden, der Gültigkeit der Euler-Gleichungen. Es wird dazu das folgende System eingeführt, analog zu (1):

$$N(q)\, q = f \tag{7}$$

mit N als beschreibenden Operator für die Euler-Gleichungen:

$$\partial_t (\varrho) + \partial_{x_i} (\varrho u_i) = f_\varrho \tag{8}$$

$$\partial_t (u_j) + u_i \partial_{x_i} (u_j) + \frac{1}{\varrho} \partial_{x_j} (p) = f_{u_j} \tag{9}$$

$$\partial_t \left(\frac{p}{\gamma - 1} \right) + \partial_{x_i} \left(\frac{u_i p \gamma}{\gamma - 1} \right) - u_i \partial_{x_i} (p) = f_p. \tag{10}$$

Die Terme $f = [f_\varrho, f_{u_j}, f_p]$ auf der rechten Seite der Gleichungen repräsentieren Quellen für Masse, Impuls und Energie. Über sie lässt sich die Lösung des Systems beeinflussen. Durch optimale Anpassung von f soll eine Lösung der Euler-Gleichungen bestimmt werden, die möglichst gut mit dem Optimierungsziel p_{ziel} übereinstimmt.

Die Quellen f lassen sich als Schallquellen beziehungsweise Lautsprecher interpretieren. Reine Monopolquellen lassen sich allein durch Energiequellen f_p beschreiben. Direktivitäten lassen sich über die Impulsterme f_{u_j} miteinbeziehen. Eine Optimierung von f entspricht damit einer Optimierung der Ausgangssignale der Lautsprecher.

Um den zuvor beschriebenen Adjungierten-Ansatz zur Optimierung von f anwenden zu können, ist es notwendig das beschreibende System und das Zielfunktional zu linearisieren. Es ergeben sich

$$N_{\text{lin}} \delta q = \delta f \tag{11}$$

und

$$\delta J = \iint \underbrace{(p - p_{\text{ziel}})}_{=g} \delta p \mathrm{d}\Omega, \tag{12}$$

mit dem nun definierten Gewicht $g = (p - p_{\text{ziel}})$. Die Kombination von linearisiertem System und Zielfunktional in Lagrange-Art liefert

$$\delta J = g^{\mathrm{T}} \delta q - {q^*}^{\mathrm{T}} \underbrace{(N_{\text{lin}} \delta q - \delta f)}_{=0} \tag{13}$$

$$= {q^*}^{\mathrm{T}} \delta f + \delta q^{\mathrm{T}} \left(g - N_{\text{lin}}^{\mathrm{T}} q^* \right). \tag{14}$$

Die adjungierte Gleichung $N^* = N_{\text{lin}}^T$ ergibt sich aus der Forderung

$$g - N_{\text{lin}}^{\mathrm{T}} q^* = 0, \tag{15}$$

mit $q^* = [\varrho^*, u_j^*, p^*]$, analog zu (3). Zur detaillierten Herleitung der adjungierten Euler-Gleichungen wird auf [8, S. 19] verwiesen. Die Änderung des Zielfunktionals ist gegeben als

$$\delta J = {q^*}^{\mathrm{T}} \delta f. \tag{16}$$

Die Lösung der adjungierten Gleichung lässt sich als Gradient für die Quellterme f interpretieren

$$\nabla_f J = q^*. \tag{17}$$

Iteratives Vorgehen

Er wird verwendet, um eine initiale Quellenverteilung f^0 in Raum und Zeit optimal anzupassen. Zunächst werden die Euler-Gleichungen mit f^0 vorwärts in der Zeit gelöst. Im Anschluss werden die adjungierten Gleichungen rückwärts in der Zeit unter Verwendung der direkten Lösung und der Gewichtungsfunktion g gelöst. Basierend auf der adjungierten Lösung wird der Gradient $\nabla_f J$ bestimmt und zum Aktualisieren der Quellenverteilung f^n verwendet:

$$f^{n+1} = f^n + \alpha \nabla_f J, \tag{18}$$

wobei α eine geeignete Schrittweite und n die Iterationsnummer beschreibt. Der Gradient wird für das gesamte Rechengebiet und die gesamte Simulationszeit bestimmt, aber nur dort ausgewertet wo erwünscht, etwa an vorgegebenen Lautsprecher- beziehungsweise Quellenpositionen. Das Prozedere wird mit dem aktuellen f^n wiederholt, bis Konvergenz im Zielfunktional erreicht ist, siehe Abb. 1 zur Übersicht.

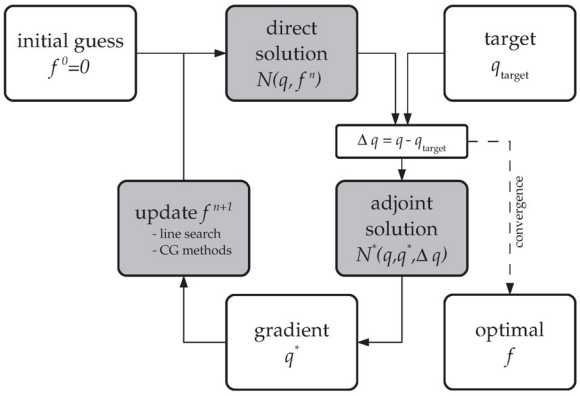

Abbildung 1: Adjungierten-basierte Methode zum Finden einer optimalen Ansteuerung f. Rechenzeitaufwendige Schritte sind grau markiert.

Validierung

Zur Validierung, ob die adjungierten-basierte Methode grundsätzlich zum Finden einer geeigneten Ansteuerung von LSA-Lautsprechern eingesetzt werden kann, werden für ein zwei-dimensionales Setup mit zwei Quellen optimale Anregungssignale gesucht. Die Quellen werden dazu als Lautsprecher interpretiert. Zwischen den Lautsprechern wird ein Abstand von 0.1 m angesetzt und es werden Monopol-Abstrahleigenschaften angenommen. Es wird ein Gebiet von 1 m x 1 m betrachtet, siehe Abb. 2.

Mit Hilfe des Complex-Directivity-Point-Source-(CDPS)-Modells, das üblicherweise für die Schallfeldprädiktion von LSAs verwendet wird [9, Gl. (5)], [1,

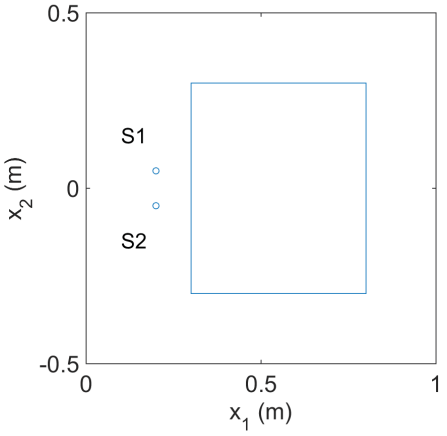

Abbildung 2: Validierungs-Setup: Das Gebiet, in dem das Zielfunktional ausgewertet werden soll, ist durch das Rechteck markiert. Die Lautsprecher S1 und S2 sind durch Punkte gekennzeichnet.

Gl. (3-5)], [10, Abs. 1.1], [11, Gl. (11)], [12, Gl. (2)], wird im Frequenzbereich für eine festgelegte elektronische Ansteuerung der Lautsprecher zunächst das Zielschallfeld p_{ziel} berechnet und in den Zeitraum transformiert. Beide Lautsprecher werden mit einem Sinussignal von 2 kHz mit einem Phasenversatz von zwei Samples angesteuert.

Ziel ist es, mit der adjungierten-basierten Methode die gewählte Ansteuerung allein auf Grundlage des berechneten Schallfelds wiederzufinden. Das Zielschallfeld wird für einen ausgewählten Zeitpunkt in Abb. 3 dargestellt.

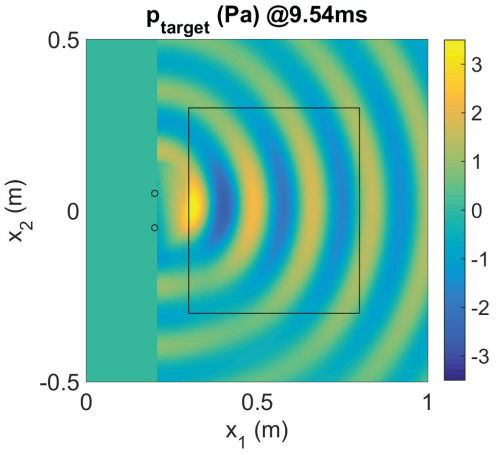

Abbildung 3: Zielschallfeld in der x_1x_2-Ebene für einen ausgewählten Zeitpunkt.

In der Folge wird die adjungierte Lösung berechnet. Die Berechnung erfolgt rückwärts in der Zeit. Die adjungierte Lösung p^* wird in Abb. 4 für den schon zuvor betrachteten Zeitpunkt dargestellt. Die adjungierte Lösung enthält Informationen über die optimale Ansteuerung und Positionierung der Quellen.

Über die betragsweise Summation der Sensitivitäten lassen sich diejenigen Positionen bestimmen, welche einen möglichst großen Einfluss auf das Zielfunktional

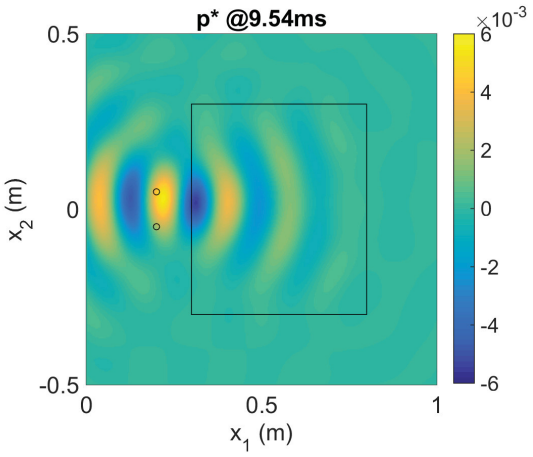

Abbildung 4: Adjungierte Lösung p^* in der x_1x_2-Ebene für einen ausgewählten Zeitpunkt.

haben:

$$\hat{q} = \sum_{t_{n=0}}^{t_{n=\text{end}}} |q^*|, \tag{19}$$

siehe [13]. Für den Fall von $f = 0$ erlaubt $\hat{q}$, komponentenweise ausgewertet, eine optimale Anordnung der Quellen. Das Ergebnis für $\hat{p}$ ist in Abb. 5 dargestellt.

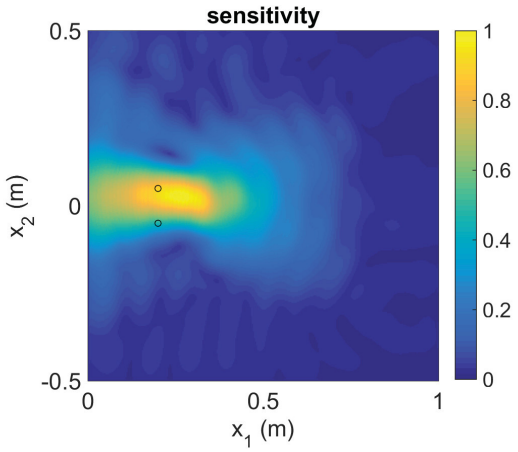

Abbildung 5: Sensitivität $\hat{p}$. Die Verteilung erlaubt Rückschlüsse auf die optimalen Lautsprecherpositionen.

Da in diesem Validierungsbeispiel die Orte der Quellen bekannt sind, wird die adjungierte Lösung lediglich an den Lautsprecherpositionen ausgewertet. In Abb. 6 ist erkennbar, dass zwei Sinussignale mit einer Frequenz von 2 kHz gefunden werden. Diese weisen das vorher festgelegte Amplitudenverhältnis von 2 zu 1 auf. Das Anregungssignal für Lautsprecher 1 ist, wie eingestellt, um 2 Abtastwerte gegenüber dem von Lautsprecher 2 verzögert.

Bis auf die genaue Amplitude konnte das gesuchte Ansteuerungssignal durch einmalige Berechnung der Adjungierten bestimmt werden. Für komplexere Setups ist ein iteratives Vorgehen notwendig, siehe Abb. 1. Im Fall einer multi-frequenten Anregung und für das Einbeziehen spezifischer Lautsprechereigenschaften wäre anschließend eine Entfaltung im Frequenzbereich notwen-

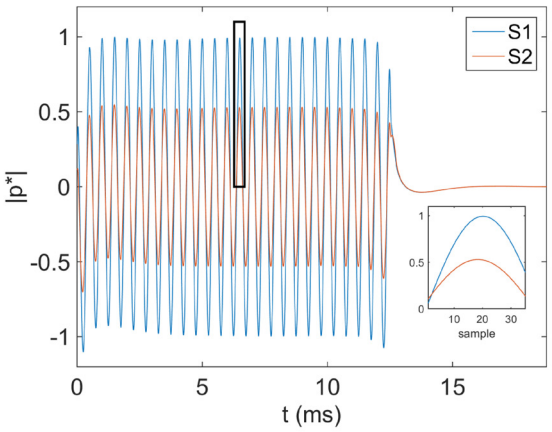

Abbildung 6: Normierte adjungierte Sensitivität $|p^*|$ für f_p an den vorgegeben Quellenpositionen.

dig, siehe Abb. 7.

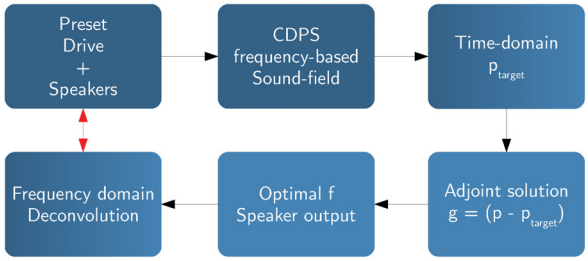

Abbildung 7: Arbeitsablauf zum Validieren beziehungsweise Bestimmen optimaler Treiberfunktionen mit der vorgeschlagenen Methode.

Zusammenfassung

In diesem Beitrag wurde das Adjungierten-Verfahren als alternative Methode im Zeitbereich zum Finden einer geeigneten Ansteuerung von Line-Array-Lautsprechern präsentiert. Ein grundlegendes zwei-dimensionales Validierungsbeispiel diente dazu, die prinzipielle Eignung des Verfahrens für das Bestimmen der Ansteuerung zu demonstrieren. Es bietet ebenfalls Informationen über eine passende Lautsprecheranordnung. Die Lösung der adjungierten-basierten Methode ist unabhängig von der Anzahl der Lautsprecher und ihrer Anordnung.

Mit dem vorgestellten Ansatz kann prinzipiell eine Grundströmung berücksichtigt werden, um z. B. den Einfluss von Wind auf eine Beschallungssituation zu beschreiben. An den Grenzen des untersuchten Gebietes können verschiedene Randbedingungen berücksichtigt werden.

Literatur

[1] van Beuningen, G.W.J.; Start, E.W. (2000): "Optimizing directivity properties of DSP controlled loudspeaker arrays." In: *Proc. of the Inst. of Acoustics: Reproduced Sound*, **22**(6):17–37.

[2] Thompson, A. (2009): "Improved methods for controlling touring loudspeaker arrays." In: *Proc. of the 127th Audio Eng. Soc. Conv., New York*, #7828.

[3] Thompson, A.; Baird, J.; Webb, B. (2011): "Numerically optimised touring loudspeaker arrays - Practical applications." In: *Proc. of the 131st Audio Eng. Soc. Conv., New York*, #8511.

[4] Feistel, S.; Sempf, M.; Köhler, K.; Schmalle, H. (2013): "Adapting loudspeaker array radiation to the venue using numerical optimization of FIR filters." In: *Proc. of the 135th Audio Eng. Soc. Conv., New York*, #8937.

[5] Giles, M.; Pierce, N. (2000): "An introduction to the adjoint approach to design." In: *Flow, Turbulence and Combustion*, **65**:393–415.

[6] Lemke, M.; Reiss, J.; Sesterhenn, J. (2014): "Adjoint based optimisation of reactive compressible flows." In: *Combustion and Flame*, **161**(10):2552–2564.

[7] Lemke, M.; Sesterhenn, J. (2016): "Adjoint-based pressure determination from PIV data in compressible flows – validation and assessment based on synthetic data." In: *European Journal of Mechanics - B Fluids*, **58**:29–38.

[8] Lemke, M. (2015): *Adjoint based data assimilation in compressible flows with application to pressure determination from PIV data*. Ph.D. thesis, Technische Universität Berlin.

[9] Meyer, D.G. (1984): "Computer simulation of loudspeaker directivity." In: *J. Audio Eng. Soc.*, **32**(5):294–315.

[10] Meyer, P.; Schwenke, R. (2003): "Comparison of the directional point source model and BEM model for arrayed loudspeakers." In: *Proc. of the Institute of Acoustics*, **25**(4).

[11] Feistel, S.; Thompson, A.; Ahnert, W. (2009): "Methods and limitations of line source simulation." In: *J. Audio Eng. Soc.*, **57**(6):379–402.

[12] Straube, F.; Schultz, F.; Bonillo, D.A.; Weinzierl, S. (2017): "An analytical approach for optimizing the curving of Line Source Arrays." In: *Proc. of the 142nd Audio Eng. Soc. Conv., Berlin*, submitted and accepted.

[13] Lemke, M.; Westphal, C.; Reiss, J.; Sesterhenn, J. (2015): "Adjoint based data assimilation of sound sources." In: *Fortschritte der Akustik: Tagungsband d. 41. DAGA, Nürnberg*, 635–638.

Zur Optimierung der Krümmung von Line Source Arrays

Florian Straube, David Albanés Bonillo, Frank Schultz, Stefan Weinzierl
Audio Communication Group, TU Berlin, 10587, Berlin, Germany, E-mail: florian.straube@tu-berlin.de

Einleitung

Für Großbeschallungsanwendungen (z. B. bei Open-Air-Veranstaltungen, in Arenen und Stadien) werden typischerweise Line Source Arrays (LSAs) eingesetzt, mit den Zielen homogene Schallfelder für den gesamten wahrnehmbaren Frequenzbereich zu generieren und möglichst hohe Schalldruckpegel zu erreichen. Die verwendeten Lautsprecherboxen werden zueinander angewinkelt und/oder geeignet elektronisch angesteuert, um wie beabsichtigt die Zuhörerbereiche zu beschallen und die Abstrahlung in Richtung Decken, reflektierenden Wänden und bewohnten Gebieten zu vermeiden.

In diesem Beitrag wird der analytische Ansatz Polygonal Audience Line Curving (PALC) vorgestellt. Dieser wird verwendet, um abhängig von der Geometrie des Veranstaltungsortes und von der gewünschten Abstrahlung geeignete Neigungswinkel für die Lautsprecherboxen zu finden. PALC kann entweder separat oder im Voraus einer Optimierung der Filterfunktionen der einzelnen Lautsprecher angewandt werden. Mit der Methode können unterschiedliche Zielstellungen verfolgt werden, z. B. eine unveränderliche Interaktion zwischen benachbarten Boxen im Zuhörerbereich sowie mit der zusätzlichen Berücksichtigung entfernungsabhängiger Amplitudenabnahme. Akustische Simulationen, die auf dem Complex-Directivity-Point-Source (CDPS)-Modell basieren, liefern die Daten für die Evaluation. PALC wird für ein jeweils uniform angesteuertes LSA für einen exemplarisch ausgewählten Veranstaltungsort mit anderen typischen LSA-Curving-Verfahren (Straight, Arc, J und Progressive) verglichen. Die Vorteile des präsentierten Ansatzes bezüglich der Schallfeld-Homogenität und der zielorientierten Abstrahlung werden mit Hilfe technischer Qualitätsmaße gezeigt.

Evaluations-Setup

Das LSA-Setup und die betrachtete Geometrie sind in Abb. 1 dargestellt. Es werden insgesamt $N = 16$ LSA-Boxen mit $n = 1, 2, ..., N$ verwendet. Die Länge $\Lambda_{y,\mathrm{LSA}}$ einer LSA-Box beträgt 0.372 m, so dass sich eine Gesamtlänge des Arrays von ca. 5.96 m ergibt. γ_n bezeichnet jeweils den Neigungswinkel der n-ten Box und der Ortsvektor $\mathbf{x_{0,i}}$ charakterisiert die Position des i-ten LSA-Lautsprechers bezogen auf das entsprechende Frontgitter einer Box. Detaillierte Informationen zur geometrischen Konfiguration sind in [1] zu finden.

Die einzelnen LSA-Boxen sind in diesem Beitrag als Drei-Wege-System ausgeführt, wobei pro Kabinett $L_{\mathrm{LF}} = 1$, $L_{\mathrm{MF}} = 4$ und $L_{\mathrm{HF}} = 10$ vertikal übereinander angeordnete und individuell ansteuerbare Treiber für den tiefen (LF), den mittleren (MF) und den hohen Frequenzweg (HF) zur Verfügung stehen. Es handelt sich dabei um

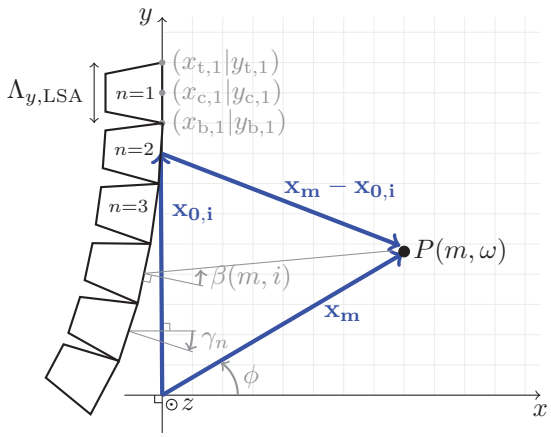

Abbildung 1: Schematische Darstellung des betrachteten LSA-Setups. Es werden insgesamt $N = 16$ LSA-Boxen der Länge $\Lambda_{y,\mathrm{LSA}} = 0.372\,\mathrm{m}$ verwendet.

Treiber der Größe 12 Zoll für LF, 3 Zoll für MF und 1.2 Zoll für HF. Für die verschiedenen Lautsprecher werden frequenzunabhängige Empfindlichkeiten (1 W / 1 m) angenommen, um auf plausible Schalldruckwerte schließen zu können. Diese betragen $S_{\mathrm{dB,LF}} = 96$ dB, $S_{\mathrm{dB,MF}} = 88$ dB und $S_{\mathrm{dB,HF}} = 112$ dB für die vertikale Abstrahlung. Das Verhältnis der Treibergrößen zum festen Abstand zwischen den Mittelpunkten der Treiber, welches unter dem Begriff Active Radiating Factor (ARF) [2, Sec. 3.2], [3] bekannt ist, beträgt ungefähr 0.82. Für LF und MF wird das Modell einer Kolbenmembran und für HF das Modell einer Zeilenmembran genutzt. Linkwitz-Riley-Filter 4. Ordnung mit den Übernahmefrequenzen $f_{\mathrm{LF,MF}} = 400$ Hz und $f_{\mathrm{MF,HF}} = 1500$ Hz werden als Frequenzweichenfilter für die verschiedenen Frequenzwege eingesetzt.

Eine komplex aufgebaute Arena mit Stehplatzflächen sowie Rängen und Tribünen [4, Sec. 6.1] wird durch eine zweidimensionale Venue Slice modelliert. Der Zuhörerbereich besteht aus 4 Sektionen mit unterschiedlichen Neigungswinkeln. In diesem Beitrag werden Near-Fills, Side-Fills und verzögerte Arrays, die in praktischen Realisierungen üblich sind, nicht berücksichtigt. Typischerweise wird lediglich die vertikale Abstrahlungsebene, hier xy-Ebene, betrachtet, vgl. Abb. 2. Das ist ein konventioneller Ansatz für Optimierungsmethoden der Treiberfunktionen, da davon ausgegangen wird, dass die horizontale Abstrahlung bereits geeignet ist [4–8]. Insgesamt werden $M = 297$ Empfängerpositionen für den exemplarisch ausgewählten Veranstaltungsort berücksichtigt. Das entspricht einem Abstand von 0.5 m zwischen den Kontrollpositionen. Diese Positionen werden durch die Ortsvektoren $\mathbf{x_m} = (x_m, y_m, 0)^{\mathrm{T}}$ beschrieben und gegen den Uhrzeigersinn nummeriert, begin-

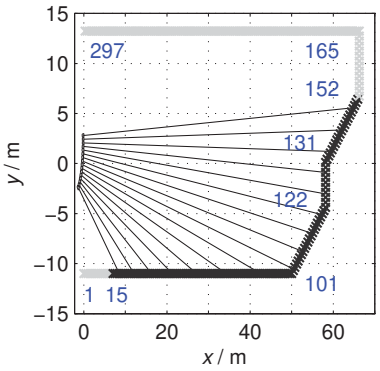

Abbildung 2: Venue Slice in der xy-Ebene mit Zuhörer- (schwarz) sowie Nicht-Zuhörerpositionen (grau) und ausgewählten Indizes der M Empfänger-Positionen, die entweder einen Wechsel zwischen Zuhörer- und Nicht-Zuhörerbereich und/oder eine Änderung des Neigungswinkels der Polygonzug-Sektion der Kontrollpositionen spezifizieren.

nend von der Position unterhalb des LSAs, die sich am nächsten zum LSA befindet (Index 1, vgl. Abb. 2).

Es ist zu erwähnen, dass die Begriffe *Bright Zone* und *Dark Zone*, die in der Mehrzonen-Schallfeldsynthese (MZSFS) [9,10] gebräuchlich sind, den Zuhörerbereichen bzw. Nicht-Zuhörerbereichen bei Großbeschallungsproblemen entsprechen.

Berechnungsmodell

Der Gesamtschalldruck setzt sich aus den Wirkungen der einzelnen Frequenzwege zusammen, d. h.

$$P(m,\omega) = P_{\mathrm{LF}}(m,\omega) + P_{\mathrm{MF}}(m,\omega) + P_{\mathrm{HF}}(m,\omega). \quad (1)$$

Im Folgenden werden die Indizes LF, MF und HF der Frequenzwege zur Verallgemeinerung vernachlässigt. Die Schallfeldberechnung basiert auf dem Complex-Directivity-Point-Source (CDPS)-Modell mit idealen Fernfeld-Direktivitäten von Lautsprechern. Dessen Grundgleichung [11, Gl. (5)], [5, Gl. (3-5)], [12, Sec. 1.1], [13, Gl. (11)] lautet

$$P(m,\omega) = \sum_{i=1}^{L\,N} G(m,i,\omega)\, D(i,\omega). \quad (2)$$

$P(m,\omega)$ bezeichnet das Frequenzspektrum des Schalldrucks an den Empfängerpositionen. $G(m,i,\omega)$ steht für die akustische Transferfunktion (ATF) von der i-ten Quelle zur m-ten Empfängerposition. Das komplexe Treiberfunktionsspektrum $D(i,\omega)$ der i-ten Quelle ist direkt proportional zum Schnellespektrum der Quelle. Die Schallfelder werden für uniform angesteuerte Lautsprecher und für einen logarithmisch verteilten Frequenzvektor mit $f_{\mathrm{start}} = 200\,\mathrm{Hz}$, $f_{\mathrm{stop}} = 20\,\mathrm{kHz}$ und einer 1/36-Oktavauflösung prädiziert.

Polygonal Audience Line Curving

Polygonal Audience Line Curving (PALC) ist ein analytischer Ansatz, um abhängig von der Geometrie eines Veranstaltungsortes und abhängig vom gewünschten Schallfeld die Neigungswinkel γ_n der einzelnen LSA-Boxen zu

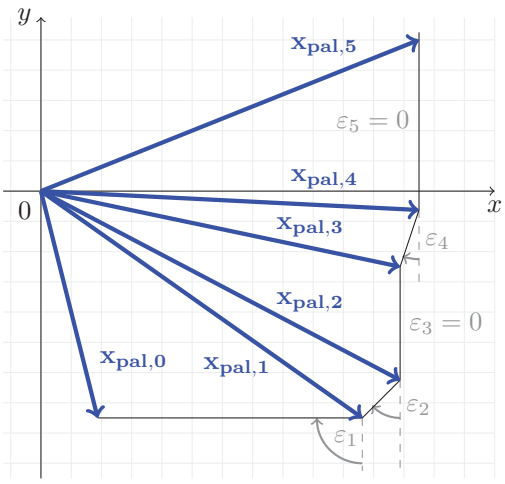

Abbildung 3: Polygonal Audience Line (PAL) mit K Sektionen (in diesem Fall: $K = 5$). Die Anfangsposition der k-ten Sektion des Polygonzuges wird durch den Vektor $\mathbf{x_{pal,k-1}}$ beschrieben und die Endposition ist durch den Vektor $\mathbf{x_{pal,k}}$ gegeben. ε_k bezeichnet den Neigungswinkel der k-ten Sektion des Polygonzuges.

berechnen. Aus der vertikalen Abstrahlungsebene werden dafür die Zuhörerpositionen heraus extrahiert. Diese Anordnung kann geometrisch als Polygonzug interpretiert werden. Abb. 3 zeigt einen exemplarischen Zuhörer-Polygonzug, der sich an dem in diesem Paper betrachteten Veranstaltungsort orientiert.

Die Neigungswinkel der einzelnen Boxen werden iterativ von der obersten zur untersten Box als auch von der obersten zur untersten Sektion des Polygonzugs berechnet. Eine ausführliche Beschreibung des Algorithmus ist in [14] zu finden. Dieser Ansatz kann mit unterschiedlichen Zielen verwendet werden. Die Intention von PALC1 besteht darin, dass die Interaktion der einzelnen LSA-Boxen auf dem Zuhörer-Polygonzug möglichst konstant ist, d. h., dass sich der abgestrahlte Schall der Einzelquellen unter einem konstanten Winkel ψ im Fernfeld der Einzelquellen auf dem Polygonzug überschneidet. Mathematisch lässt sich das als

$$\psi_1 = \psi_2 = \psi_3 = ... = \mathrm{const.} \quad (3)$$

ausdrücken. PALC1 ist ähnlich zu einem Arc-Array, allerdings bezieht sich das Ziel nicht auf das Array selbst, also konstante Neigungswinkel zwischen allen Boxen, sondern auf die Form der Empfängergeometrie.

Beim Fall PALC2 werden zudem die Abstände zwischen den Quellen und den Mittelpunkten der betreffenden beschallten Abschnitte des Polygonzuges miteinbezogen. Das Ziel besteht darin, das Produkt aus dem (Fernfeld-) Winkel ψ und diesem Abstand d zwischen Quelle und Mittelpunkt konstant zu halten, also

$$\psi_1\, d_1 = \psi_2\, d_2 = ... = \mathrm{const.} \quad (4)$$

Diese Forderung resultiert aus der Intention, dass alle Längen der von den unterschiedlichen Lautsprechern beschallten Polygonzug-Abschnitte gleich groß sein sollen. Gl. (4) enthält die Vereinfachung von $\tan(\psi)$ zu ψ für kleine ψ sowie die Annahme, dass alle Neigungswinkel

ε_k der Polygonzug-Sektionen und alle Neigungswinkel γ_n der Array-Boxen entweder gleich groß oder klein gegenüber 0 sind.

Diskussion

Die Evaluation erfolgt auf Grundlage von Schallfeldern, die mit dem CDPS-Modell generiert werden. PALC1 und PALC2 werden mit den LSA-Krümmungen Straight, Arc, J und Progressive [15] verglichen. Eine Auswahl von Evaluationskriterien, die in [1] vorgeschlagen wurden, dienen zur Bewertung der unterschiedlichen Curving-Methoden. Die Position Index Plots (PIPs) zeigen die resultierenden SPL-Spektren für alle Empfängerpositionen, also die Schalldruckpegel in Abhängigkeit von der Frequenz f und dem Ortsindex m. In den Abb. 4a, 4b, 4c und 4d ist für die Fälle Arc, Progressive, PALC1 sowie PALC2 zu erkennen, dass wie gewünscht nur wenig Energie in die Nicht-Zuhörerbereiche abgestrahlt wird. Die vom Arc- und vom PALC1-Array generierten Schallfelder sind im Zuhörerbereich sehr ähnlich. Quantitative Schlussfolgerungen lassen sich allerdings nicht aus den PIP-Visualisierungen ziehen.

Daher beruht die quantitative Evaluation auf zwei technischen Maßen: Das frequenzabhängige Verhältnis $L_{p,\mathrm{a,na}}(\omega)$ der mittleren Schalldruckpegel im Zuhörer und im Nicht-Zuhörerbereich [1, Gl. (18)], das in der MZSFS als akustischer Kontrast bekannt ist [9, 10], wird genutzt. Zusätzlich wird das Homogenitätsmaß $H1(\omega)$ verwendet [14, Gl. (37)], das die Standardabweichung der abstandskompensierten Schalldruckpegel an allen Zuhörerpositionen angibt. In Abb. 4e wird deutlich, dass der Wert des akustischen Kontrasts für alle Methoden prinzipiell mit zunehmender Frequenz ansteigt. Bei ca. 8.5 kHz fallen die Werte aufgrund des einsetzenden räumlichen Aliasings stark ab. PALC1 und PALC2 liefern abhängig von der Frequenz bis zu (1...1.5) dB größere $L_{p,\mathrm{a,na}}(\omega)$-Werte als J, Arc und Progressive. Das gerade Array weist die besten Werte auf, was jedoch darin begründet ist, dass dieses Array aufgrund der für alle Konfigurationen gewählten gleichen Gesamtlänge nicht alle Zuhörer-Positionen direkt beschallt, sondern die ersten und die letzten Zuhörer-Positionen nicht direkt erreicht.

Dieses Verhalten spiegelt sich ebenfalls in den Homogenitätswerten wider, siehe Abb. 4f. $H1(\omega)$ des geraden Arrays liegt für alle Frequenzen oberhalb der anderen Werte. Das progressive Curving liefert, wie es für eine Vielzahl von Venues als robuste Anfangslösung bekannt ist, sehr gute Ergebnisse. Es hat neben PALC2 die geringste Standardabweichung. Das Arc- und das J-Array erlauben keine Anpassung an die komplexe Form des gewählten Veranstaltungsortes und der PALC1-Ansatz scheint entgegen der Erwartung bezogen auf die Homogenität keine sinnvollen Neigungswinkel zu produzieren.

Zusammenfassung

Um verschiedene Veranstaltungsorte mit Line-Arrays zu beschallen, bedarf es jeweils einer Anpassung des Curvings des Arrays, wenn nicht allein durch elektronisches Beamsteering das gewünschte Schallfeld generiert werden kann bzw. soll. Der analytische Ansatz PALC zum Finden geeigneter Neigungswinkel für LSA-Boxen wird in diesem Beitrag mit Standard-LSA-Curving-Verfahren verglichen. PALC basiert auf der Geometrie der Empfängerpositionen und der beabsichtigten Abdeckung. Er ist den Standard-Methoden überlegen, weil er eine flexible Anpassung an die konkrete Geometrie des Veranstaltungsortes erlaubt. Die Berechnung lässt sich effizient implementieren.

PALC soll um verschiedene Ziele erweitert werden und die möglichen Lösungen für die Neigungswinkel sollen auf eine diskrete Sammlung von Winkelwerten reduziert werden, wie es für praktische Realisierungen erforderlich ist. Ein geplanter Vergleich mit in der Praxis gängigen numerischen Methoden soll Aufschluss über Effizienz, Genauigkeit und Relevanz des entwickelten Verfahrens geben. Es wird beabsichtigt, PALC als Vorstufe für die Optimierung der elektronischen Ansteuerung von Line-Arrays zu verwenden.

Literatur

[1] Straube, F.; Schultz, F.; Makarski, M.; Spors, S.; Weinzierl, S. (2015b): "Evaluation strategies for the optimization of Line Source Arrays." In: *Proc. of the 59th Audio Eng. Soc. Int. Conf. on Sound Reinforcement, Montreal*.

[2] Urban, M.; Heil, C.; Bauman, P. (2003): "Wavefront Sculpture Technology." In: *J. Audio Eng. Soc.*, **51**(10):912–932.

[3] Schultz, F.; Straube, F.; Spors, S. (2015): "Discussion of the Wavefront Sculpture Technology criteria for straight line arrays." In: *Proc. of the 138th Audio Eng. Soc. Conv., Warsaw*, #9323.

[4] Thompson, A.; Baird, J.; Webb, B. (2011): "Numerically optimised touring loudspeaker arrays - Practical applications." In: *Proc. of the 131st Audio Eng. Soc. Conv., New York*, #8511.

[5] van Beuningen, G.W.J.; Start, E.W. (2000): "Optimizing directivity properties of DSP controlled loudspeaker arrays." In: *Proc. of the Inst. of Acoustics: Reproduced Sound*, **22**(6):17–37.

[6] Thompson, A. (2006): "Line array splay angle optimisation." In: *Proc. of the Inst. of Acoustics*, **28**(8):135–148.

[7] Thompson, A. (2009): "Improved methods for controlling touring loudspeaker arrays." In: *Proc. of the 127th Audio Eng. Soc. Conv., New York*, #7828.

[8] Feistel, S.; Sempf, M.; Köhler, K.; Schmalle, H. (2013): "Adapting loudspeaker array radiation to the venue using numerical optimization of FIR filters." In: *Proc. of the 135th Audio Eng. Soc. Conv., New York*, #8937.

[9] Choi, J.W.; Kim, Y.H. (2002): "Generation of an acoustically bright zone with an illuminated region using multiple sources." In: *J. Acoust. Soc. Am.*, **111**(4):1695–1700.

[10] Coleman, P.; Jackson, P.J.B.; Olik, M.; Pedersen, J.A. (2014): "Personal audio with a planar bright zone." In: *J. Acoust. Soc. Am.*, **136**(4):1725–1735.

[11] Meyer, D.G. (1984): "Computer simulation of loudspeaker directivity." In: *J. Audio Eng. Soc.*, **32**(5):294–315.

[12] Meyer, P.; Schwenke, R. (2003): "Comparison of the directional point source model and BEM model for arrayed loudspeakers." In: *Proc. of the Inst. of Acoustics*, **25**(4).

[13] Feistel, S.; Thompson, A.; Ahnert, W. (2009): "Methods and limitations of line source simulation." In: *J. Audio Eng. Soc.*, **57**(6):379–402.

[14] Straube, F.; Schultz, F.; Bonillo, D.A.; Weinzierl, S. (2017): "An analytical approach for optimizing the curving of Line Source Arrays." In: *Proc. of the 142nd Audio Eng. Soc. Conv., Berlin*, submitted and accepted.

[15] Ureda, M.S. (2004): "Analysis of loudspeaker line arrays." In: *J. Audio Eng. Soc.*, **52**(5):467–495.

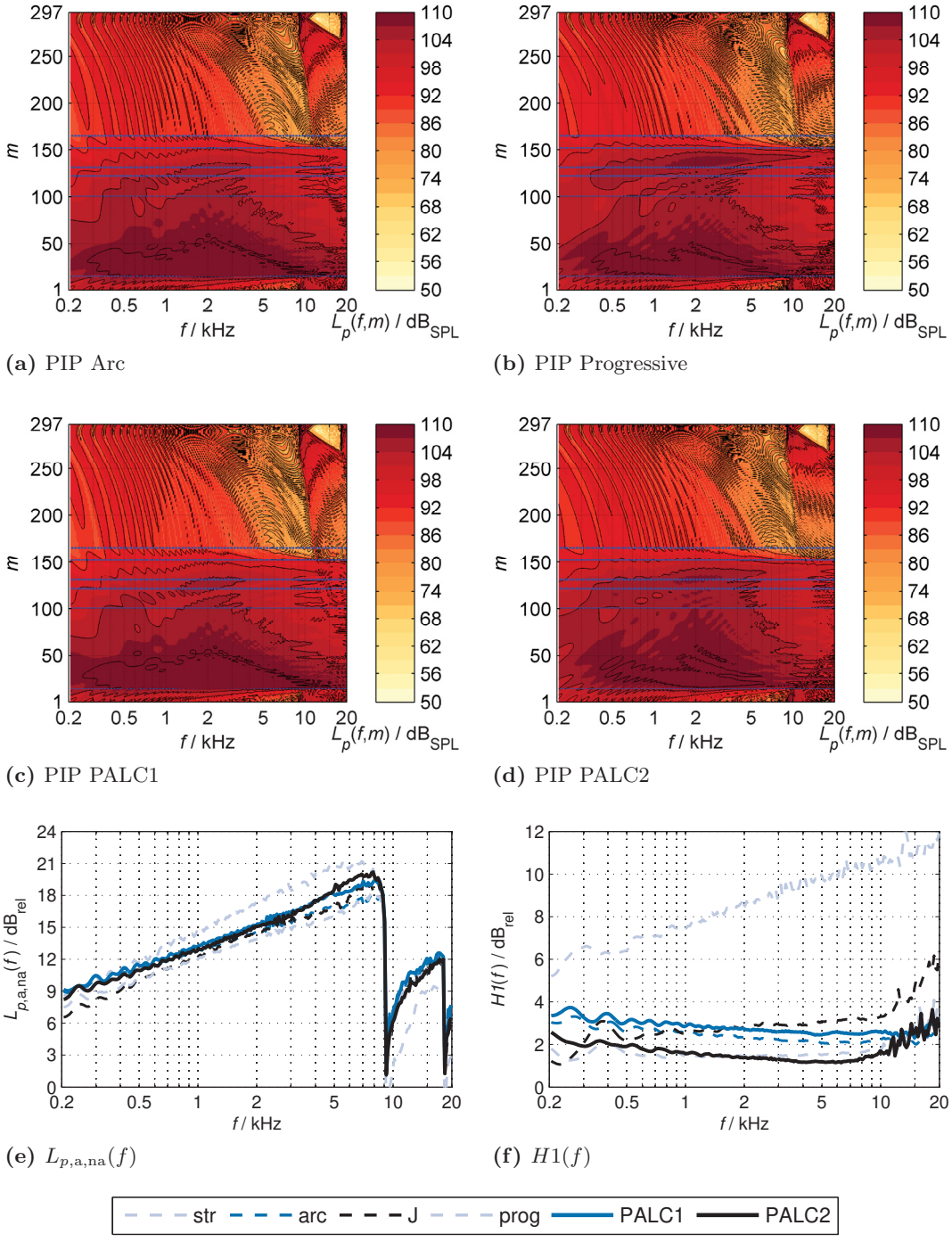

(a) PIP Arc

(b) PIP Progressive

(c) PIP PALC1

(d) PIP PALC2

(e) $L_{p,\mathrm{a,na}}(f)$

(f) $H1(f)$

Abbildung 4: Technische Qualitätsmaße für alle untersuchten Curving-Methoden und Position Index Plots (PIPs) für die Fälle Arc, Progressive, PALC1 und PALC2.

Audio Engineering Society

Convention Paper 9699

Presented at the 142nd Convention
2017 May 20–23, Berlin, Germany

An Analytical Approach for Optimizing the Curving of Line Source Arrays

Florian Straube, Frank Schultz, David Albanés Bonillo, and Stefan Weinzierl

Audio Communication Group, TU Berlin, DE-10587 Berlin, Germany

Correspondence should be addressed to Florian Straube (florian.straube@tu-berlin.de)

ABSTRACT

Line source arrays (LSAs) are used for large-scale sound reinforcement aiming at the synthesis of homogeneous sound fields for the whole audio bandwidth. The deployed loudspeaker cabinets are rigged with different tilt angles and/or electronically controlled in order to provide the intended coverage of the audience zones and to avoid radiation towards the ceiling, reflective walls or residential areas. This contribution introduces the analytical polygonal audience line curving (PALC) approach for finding appropriate LSA cabinet tilt angles with respect to the geometry of the receiver area and the intended coverage. PALC can be previously applied to a numerical optimization of the loudspeakers' driving functions. The method can be used with different objectives, such as a constant interaction between adjacent cabinets with respect to the receiver geometry or by additionally considering amplitude attenuation over distance. PALC is compared with typical standard LSA curving schemes. The advantages of the presented approach regarding sound field homogeneity and target-oriented radiation will be shown with the help of technical quality measures.

1 Introduction

For the optimization of the curving and the electronic control of line source arrays (LSAs) for improved sound reinforcement there is no standard procedure. Both a pure geometric and a pure electronic wavefront shaping as well as combinations thereof are realized. Even state-of-the-art line array systems such as the Martin Audio MLA and the EAW Anya with extensive beam steering capabilities differ fundamentally [1]. Since they comprise several individually controllable, small drivers, beam steering is feasible up to high audio frequencies. While the cabinets of the first array system are curved in addition to the beam steering, the cabinets of the latter are rigged as a straight line.

Recent, mostly proprietary, software such as Martin Audio Display, EAW Resolution 2, d&b ArrayCalc and AFMG's FIRmaker offer (numerical) optimization schemes but the algorithms and the parametrization are rarely publicly documented. In the literature, the calculation of appropriate driving signals, i.e. FIR filters for the individual LSA loudspeakers in order to generate a desired sound field by numerical optimization techniques was discussed in [2–8]. These approaches yield considerable improvements with respect to homogeneous audience coverage and/or avoidance of high side lobe energy compared to manually adjusted setups. In [4,6,9] also the LSA cabinet tilt angles are determined by numerical optimization methods.

As the process for mixed geometric-electronic opti-

mizations typically starts with the curving, this paper is only focused on finding optimal tilt angles. These could be taken as a pre-processing stage for the optimization of the loudspeakers' driving functions, i.e. for the calculation of the FIR filter coefficients, or could also be applied for uniformly driven line arrays without further computation.

In this paper, we aim at introducing the analytical polygonal audience line curving (PALC) approach for finding appropriate LSA cabinet tilt angles with respect to the geometry of the receiver area and the intended coverage. The method can be used with different objectives, such as a constant interaction between adjacent cabinets with respect to the receiver geometry or by additionally considering amplitude attenuation over distance, i.e. sound pressure level (SPL) loss over distance. PALC is evaluated in comparison with typical standard LSA curving schemes (straight, arc, J, progressive, numerically optimized). Acoustic simulations based on the complex-directivity point source (CDPS) model [2, 10–12] including far-field radiation patterns of baffled line and circular pistons provide the data for an evaluation of the introduced approach. One uniformly driven LSA model is analyzed for two concert venues.

The paper is organized as follows. In Sec. 2 the chosen LSA model and the selected concert venues are presented. Mathematical fundamentals – among them especially the adjusted CDPS model – are shortly revisited in Sec. 3. In Sec. 4 the PALC algorithm is described. The evaluation criteria and the results for the different LSA curving schemes are shown in Sec. 5 and discussed in Sec. 6.

2 Setup

An LSA setup is examined for two concert venues following practical examples presented in [6, Sec. 6.1] and in [13, Sec. 4.2.2] with audience and non-audience sections given within the *xy*-plane. While the first location is a typical multi-stand arena, the second one resembles a common open-air amphitheater geometry.

2.1 LSA setup

The LSA setup and the geometry under discussion are schematically depicted in Fig. 1. A total of $N = 16$ LSA cabinets with $n = 1, 2, \ldots, N$ is deployed. The front grille's height $\Lambda_{y,\mathrm{LSA}}$ of a single LSA cabinet is

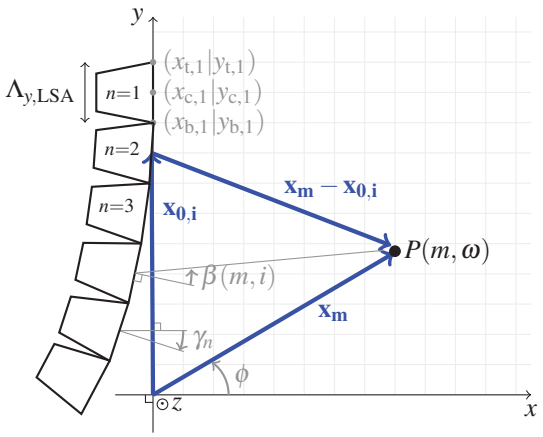

Fig. 1: Sketch of the LSA setup under discussion. A total of $N = 16$ LSA cabinets of the height $\Lambda_{y,\mathrm{LSA}} = 0.372\,\mathrm{m}$ is used. See Tab. 3 and Tab. 4 for the used tilt angles γ_n.

set to 0.372 m resulting in an overall LSA length of ca. 5.96 m. γ_n denotes the individual tilt angles and $\mathbf{x_{0,i}}$ denotes the front grille center position of the *i*-th LSA driver. Detailed information on the geometric configuration can be found in [14, 15].

Built from three-way cabinets in this paper, the exemplarily chosen LSA consists of $L_{\mathrm{LF}} = 1$, $L_{\mathrm{MF}} = 4$ and $L_{\mathrm{HF}} = 10$ vertically stacked, individually controlled drivers per cabinet for the low, the mid and the high frequency band (LF, MF, HF). Thus, 12 inch, 3 inch and 1.2 inch speakers are used for LF, MF and HF, respectively. Different frequency independent loudspeaker sensitivities are assumed in order to obtain realistic sound pressure values, $S_{\mathrm{dB,LF}} = 96$ dB, $S_{\mathrm{dB,MF}} = 88$ dB and $S_{\mathrm{dB,HF}} = 112$ dB for vertical radiation in this case. The relation of the pistons' dimensions to the fixed distance between adjacent piston centers which is also known as Active Radiating Factor (ARF) [16, Sec. 3.2], [17] amounts to approximately 0.82. For LF and MF the circular piston model is deployed, while for HF the line piston model is used. For the frequency band crossover, fourth-order Linkwitz-Riley filters with the transition frequencies $f_{\mathrm{LF,MF}} = 400$ Hz and $f_{\mathrm{MF,HF}} = 1500$ Hz are applied.

2.2 Venue Geometry

A multi-stand arena [6, Sec. 6.1] and an open-air amphitheater [13, Sec. 4.2.2] with audience and non-audience sections, i.e. zones to be covered and zones

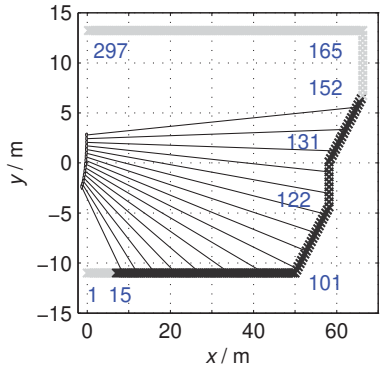

(a) Venue 1: multi-stand arena

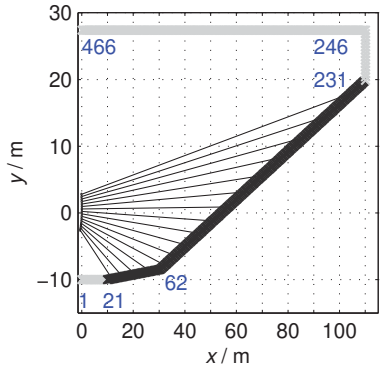

(b) Venue 2: amphitheater

Fig. 2: Venue slices within the *xy*-plane with audience (black) as well as non-audience/avoid (gray) zones and selected index numbers (change of audience/avoid zone and/or polygonal line's segment angle) from M receiver positions.

to be avoided, are modeled by two dimensional slice representations. The multi-stand arena slice representation consists of four audience lines with different tilt angles and typifies a rather complex source-receiver configuration. Venue 2 resembles the Waldbuehne in Berlin and is composed of two audience lines with different tilt angles for the sake of simplicity. It conforms to an extreme long-throw application. In this paper, near-fills, side-fills and delayed arrays that are routine in practical realizations are not considered. Only the *xy*-plane is considered for vertical radiation, cf. Fig. 2. This is a common approach for optimization schemes of the loudspeakers' driving functions as the horizontal radiation is assumed to be convenient anyway, cf. [2–9]. $M_{\mathrm{v1}} = 297$ for venue 1 and $M_{\mathrm{v2}} = 466$ for venue 2 receiver positions of which $m = 1, 2, ..., M$ are taken into account. This corresponds to a distance of 0.5 m between the receiver positions. The receiver positions are composed of M_{a} audience positions from the set $\mathscr{M}_{\mathrm{a}}$ and M_{na} non-audience positions from the set $\mathscr{M}_{\mathrm{na}}$ with $M = M_{\mathrm{a}} + M_{\mathrm{na}}$. They are characterized by the position vectors $\mathbf{x_m} = (x_m, y_m, 0)^{\mathrm{T}}$ and are numbered counterclockwise starting from the position under the LSA that is closest to the LSA (index 1, cf. Fig. 2). The venue slice coordinates are documented in Tab. 1 for venue 1 and in Tab. 2 for venue 2 in the Appendix.

Note that the terms *bright zone* and *dark zone* used in the field of multi-zone sound field synthesis (MZSFS) [18–21] correspond to the audience zone and the non-audience zone used in the field of sound reinforcement.

3 Calculation Model

Modeling multi-way cabinets the total sound pressure is composed of the sound pressures of the different frequency bands, i.e.

$$P(m,\omega) = P_{\mathrm{LF}}(m,\omega) + P_{\mathrm{MF}}(m,\omega) + P_{\mathrm{HF}}(m,\omega). \quad (1)$$

Since the calculations are performed separately for each frequency band with a subsequent summation, the frequency band indices (LF, MF, HF) are omitted for generalization in the following. The sound field prediction is based on a complex-directivity point source (CDPS) model of baffled piston far-field radiation patterns. Its fundamental equation [11, Eq. (5)], [2, Eq. (3-5)], [12, Sec. 1.1], [10, Eq. (11)] reads

$$P(m,\omega) = \sum_{i=1}^{LN} G(m,i,\omega)\, D(i,\omega). \quad (2)$$

$P(m,\omega)$ denotes the sound pressure spectrum at the receiver position $\mathbf{x_m}$ with $[P(m,\omega)] = 1\,\mathrm{Pa/Hz}$. $G(m,i,\omega)$ terms the acoustic transfer function (ATF) from the i-th source to the m-th receiver position. The complex driving function spectrum $D(i,\omega)$ with $[D(i,\omega)] = 1\,\mathrm{Pa/Hz}$ of the i-th source is directly proportional to the source's velocity spectrum.

Eq. (2) is modified including a loudspeaker sensitivity standardization in order to obtain realistic absolute SPLs. Therefore $G(m,i,\omega)$ is considered as a scaled

ATF

$$G(m,i,\omega) = H_{\text{post}}(\beta(m,i),\omega) \cdot \frac{\mathrm{e}^{-\mathrm{j}\frac{\omega}{c}|\mathbf{x_m}-\mathbf{x_{0,i}}|}}{\left(\frac{|\mathbf{x_m}-\mathbf{x_{0,i}}|}{\mathrm{m}}\right)} \cdot \ldots$$
$$\left(\frac{p_0}{\mathrm{Pa}}\right) \cdot 10^{\frac{1}{20}\left(\frac{S_{\text{dB}}(i,\omega)}{\frac{\text{dB}_{\text{SPL}}\,\text{m}}{\text{W}}}\right)} \tag{3}$$

being composed of a specific far-field radiation pattern $H_{\text{post}}(\beta(m,i),\omega)$, the 4π-discarded free-field 3D Green's function $\frac{\mathrm{e}^{-\mathrm{j}\frac{\omega}{c}|\mathbf{x_m}-\mathbf{x_{0,i}}|}}{|\mathbf{x_m}-\mathbf{x_{0,i}}|}$ (i.e. the ideal point source), the reference sound pressure p_0 that commonly amounts to $2\cdot10^{-5}$ Pa in air and the loudspeaker sensitivity $S_{\text{dB}}(i,\omega)$ specifying the SPL in 1 m distance for an electrical input power of 1 W. The sensitivity is assumed to be constant for all drivers and all frequencies per frequency band, i.e. $S_{\text{dB}}(i,\omega) = S_{\text{dB}}$. The driving function $D(i,\omega)$ consists of the signal input spectrum $D_{\text{in}}(i,\omega)$ with $[D_{\text{in}}(i,\omega)] = 1$ Pa/Hz, the complex optimized filter $D_{\text{opt}}(i,\omega)$ with $[D_{\text{opt}}(i,\omega)] = 1$ and the complex frequency band crossover as well as high-/lowpass filter $D_{\text{xo}}(\omega)$ with $[D_{\text{xo}}(\omega)] = 1$, thus

$$D(i,\omega) = D_{\text{in}}(i,\omega)\,D_{\text{opt}}(i,\omega)\,D_{\text{xo}}(\omega). \tag{4}$$

As this paper is exclusively focused on the curving of the LSA cabinets, only uniformly driven sources are considered, i.e.

$$D_{\text{opt}}(i,\omega) = 1 \qquad \forall i \text{ and } \forall\omega. \tag{5}$$

The far-field radiation pattern of the baffled circular piston with a constant surface velocity is [22, Eq. (26.42)]

$$H_{\text{post,circ}}(\beta,\omega) = \frac{2J_1\left(\frac{\omega}{c}R\sin\beta\right)}{\frac{\omega}{c}R\sin\beta}, \tag{6}$$

denoting the cylindrical Bessel function of 1st kind of 1st order as $J_1(\cdot)$ [23, Eq. (10.2.2)]. The line piston models an ideal waveguide for the HF band and its far-field radiation pattern can be written as [22, Eq. (26.44)]

$$H_{\text{post,line}}(\beta,\omega) = \frac{\sin\left(\frac{\omega}{c}\frac{\Lambda_y}{2}\sin\beta\right)}{\frac{\omega}{c}\frac{\Lambda_y}{2}\sin\beta}. \tag{7}$$

Note that these patterns exhibit main lobe unity gain (i.e. 0 dB for $\beta = 0$) in order to control the energy radiated by the pistons via the assumed sensitivities.

In line with this modeling, air absorption is neglected, a constant velocity of sound ($c = 343$ m/s) and for the modeled sources infinite, straight baffles and a constant surface velocity are assumed. The sound field predictions are performed for a logarithmically spaced frequency vector with $f_{\text{start}} = 200$ Hz, $f_{\text{stop}} = 20$ kHz and $1/36$ octave resolution.

4 Curving Optimization

Since it is a common approach to restrict the optimization schemes for the LSA driving functions to the vertical plane, it may also be advantageous to seek appropriate tilt angles of the LSA cabinets based on the venue slice representation. In [4, 6, 9] this is executed by a numerical multi-objective optimization method that is used for determining the electronic drive as well.

In this contribution a purely analytical approach for finding practical LSA cabinet tilt angles with respect to the geometry of the receiver area and the intended coverage is presented: the polygonal audience line curving (PALC). PALC was originally developed to be applied beforehand to a numerical optimization of the loudspeakers' driving functions. The method can be used with different objectives, such as a constant interaction between adjacent cabinets with respect to the receiver geometry or by additionally considering SPL loss over distance.

4.1 Polygonal Audience Line

The positions of the audience zones in the vertical radiation plane can be mathematically interpreted as polygonal line. Fig. 3 represents an exemplary polygonal audience line (pal) that is similar to venue 1 with K sections $[k = 0,1,2,\ldots,K]$ with the tilt angles ε_k. The k-th line section is specified by the vectors $\mathbf{x_{pal,k-1}}$ for the start position and $\mathbf{x_{pal,k}}$ for the stop position. These line sections are covered by N LSA cabinets with $n = 1,2,\ldots,N$. The polygonal audience line is therefore divided into N segments that represent the main radiation area of the LSA cabinets. Γ_n denotes the length of the n-th segment with the distance $\Gamma_{n,1}$ from the top to the center position and $\Gamma_{n,2}$ from the center to the bottom position of the segment, i.e. $\Gamma_n = \Gamma_{n,1} + \Gamma_{n,2}$. From

$$\Gamma = \sum_{n=1}^{n=N} \Gamma_n \tag{8}$$

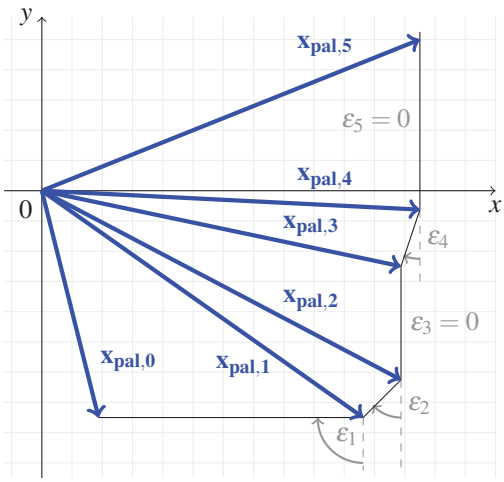

Fig. 3: Polygonal audience line (pal) with K sections (in this case: $K = 5$). The start position of the k-th line section is specified by the vector $\mathbf{x}_{\mathbf{pal},\mathbf{k-1}}$ and the stop position is given by the vector $\mathbf{x}_{\mathbf{pal},\mathbf{k}}$. ε_k denotes the tilt angle of the k-th line section.

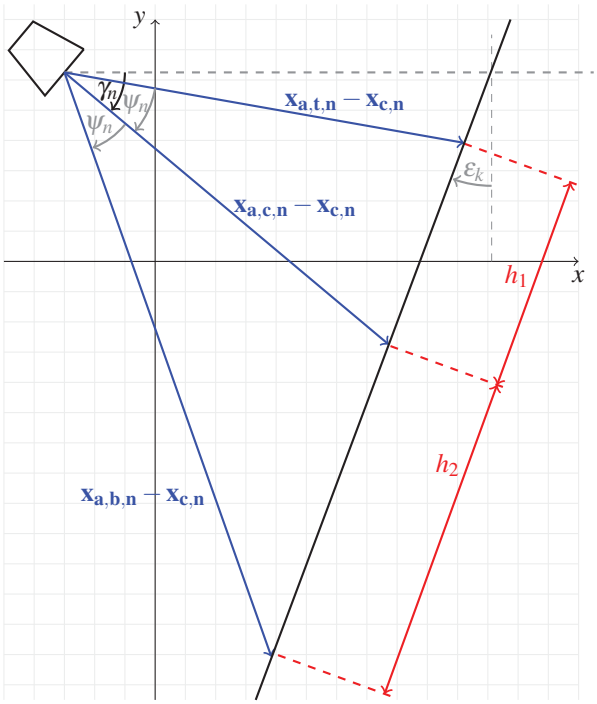

Fig. 4: Sketch of one section of the polygonal audience line with the n-th segment including only one section. The line section is not changed.

the total length of the covered audience line sections can be concluded. The different audience zones are indexed from the lowest to the highest audience positions. In order to calculate the position and the tilt angle γ_n of each LSA cabinet, it is necessary to start with the uppermost cabinet and compute iteratively from top to bottom.

4.2 PALC Algorithm

Starting with $n = 1$ and $k = K$, i.e. the topmost LSA cabinet and the topmost audience positions, n is iteratively increased and k is decreased. See Fig. 4 for detailed geometric information. Note that only discrete values can be typically set for the tilt angles of practical LSAs. The algorithm can be easily adapted concerning this matter.

I) Compute the tilt angle γ_n of the n-th LSA cabinet from the slope

$$\tan(-\gamma_n + \psi_n) = \frac{y_{\mathrm{a,t},n} - y_{\mathrm{c},n}}{x_{\mathrm{a,t},n} - x_{\mathrm{c},n}} \tag{9}$$

and the vector $\mathbf{x}_{\mathbf{c},\mathbf{n}}$ of the n-th LSA cabinet center position

$$\mathbf{x}_{\mathbf{c},\mathbf{n}} = \begin{pmatrix} x_{\mathrm{c},n} \\ y_{\mathrm{c},n} \end{pmatrix} = \begin{pmatrix} x_{\mathrm{t},n} \\ y_{\mathrm{t},n} \end{pmatrix} - \frac{\Lambda_{y,\mathrm{LSA}}}{2} \begin{pmatrix} \sin\gamma_n \\ \cos\gamma_n \end{pmatrix}. \tag{10}$$

The initial values are set to

$$\begin{pmatrix} x_{\mathrm{t},1} \\ y_{\mathrm{t},1} \end{pmatrix} = \begin{pmatrix} x_{\mathrm{H}} \\ y_{\mathrm{H}} \end{pmatrix} \tag{11}$$

and

$$\mathbf{x}_{\mathbf{a},\mathbf{t},\mathbf{1}} = \mathbf{x}_{\mathbf{pal},\mathbf{K}} \tag{12}$$

with the mounting positions x_{H} and y_{H} of the topmost LSA cabinet and the vector of the top position of the K-th audience section.

II) Calculate the center position vector $\mathbf{x}_{\mathbf{c},\mathbf{n}}$ of every LSA cabinet with eq. (10), i.e. for $n = 1, 2, ..., N$.

III) Compute the length of h_1 with

$$h_1 = |\mathbf{x}_{\mathbf{a},\mathbf{t},\mathbf{n}} - \mathbf{x}_{\mathbf{c},\mathbf{n}}| \frac{\sin\psi_n}{\cos(\varepsilon_k - \gamma_n)}. \tag{13}$$

We have to consider two cases: for case (i) equation

$$h_1 \leq |\mathbf{x}_{\mathbf{a},\mathbf{t},\mathbf{n}} - \mathbf{x}_{\mathbf{pal},\mathbf{k-1}}| \tag{14}$$

holds, i.e. the section of the polygonal audience line is not changed. The center position vector of the current segment can be calculated with

$$\mathbf{x_{a,c,n}} = \mathbf{x_{a,t,n}} + h_1 \begin{pmatrix} \cos\varepsilon_k \\ \sin\varepsilon_k \end{pmatrix} \tag{15}$$

and hence the segment's upper partial length is

$$\Gamma_{n,1} = h_1. \tag{16}$$

If for case (ii) equation

$$h_1 > |\mathbf{x_{a,t,n}} - \mathbf{x_{pal,k-1}}| \tag{17}$$

holds, i.e. the section of the polygonal audience line is changed, the segment angle $\tilde{\psi}_n$ has to be calculated with

$$\frac{|\mathbf{x_{a,t,n}} - \mathbf{x_{pal,k-1}}|}{|\mathbf{x_{a,t,n}} - \mathbf{x_{c,n}}|} = \frac{\sin(\psi_n - \tilde{\psi}_n)}{\cos(\varepsilon_k - \gamma_n + \tilde{\psi}_n)}. \tag{18}$$

The length $\tilde{h}_1$ of the segment is thus

$$\tilde{h}_1 = |\mathbf{x_{pal,k-1}} - \mathbf{x_{c,n}}| \frac{\sin\tilde{\psi}_n}{\cos(\varepsilon_{k-1} - \gamma_n)} \tag{19}$$

and the center position of the current segment can be written as

$$\mathbf{x_{a,c,n}} = \mathbf{x_{pal,k-1}} + \tilde{h}_1 \begin{pmatrix} \cos\varepsilon_{k-1} \\ \sin\varepsilon_{k-1} \end{pmatrix} \tag{20}$$

and hence

$$\Gamma_{n,1} = |\mathbf{x_{a,t,n}} - \mathbf{x_{pal,k-1}}| + \tilde{h}_1 \tag{21}$$

is the segment's upper partial length.

IV) Update k: k is not changed if the section of the polygonal audience line was not changed (step III, case (i)). k has to be decreased by 1 if the section of the polygonal audience line was changed (step III, case (ii)).

V) Calculate the length of h_2 with

$$h_2 = |\mathbf{x_{a,c,n}} - \mathbf{x_{c,n}}| \frac{\sin\psi_n}{\cos(\varepsilon_k - \gamma_n - \psi_n)}. \tag{22}$$

We again have to consider two cases: for case (i) equation

$$h_2 > |\mathbf{x_{a,c,n}} - \mathbf{x_{pal,k-1}}| \tag{23}$$

holds, i.e. the section of the polygonal audience line is changed. The segment angle $\tilde{\psi}_n$ then has to be calculated with

$$\frac{|\mathbf{x_{a,c,n}} - \mathbf{x_{pal,k-1}}|}{|\mathbf{x_{a,c,n}} - \mathbf{x_{c,n}}|} = \frac{\sin\tilde{\psi}_n}{\cos(\varepsilon_k - \gamma_n - \tilde{\psi}_n)}. \tag{24}$$

Therefore the length $\tilde{h}_2$ of the segment is

$$\tilde{h}_2 = |\mathbf{x_{pal,k-1}} - \mathbf{x_{c,n}}| \frac{\sin(\psi_n - \tilde{\psi}_n)}{\cos(\varepsilon_{k-1} - \gamma_n - \psi_n)} \tag{25}$$

and the bottom position vector of the current segment can be written as

$$\mathbf{x_{a,b,n}} = \mathbf{x_{pal,k-1}} + \tilde{h}_2 \begin{pmatrix} \cos\varepsilon_{k-1} \\ \sin\varepsilon_{k-1} \end{pmatrix}. \tag{26}$$

Hence the segment's lower partial length is

$$\Gamma_{n,2} = |\mathbf{x_{a,c,n}} - \mathbf{x_{pal,k-1}}| + \tilde{h}_2. \tag{27}$$

If for case (ii) equation

$$h_2 \leq |\mathbf{x_{a,c,n}} - \mathbf{x_{pal,k-1}}| \tag{28}$$

is valid, i.e. the section of the polygonal audience line is not changed, the bottom position vector of the current segment can be calculated with

$$\mathbf{x_{a,b,n}} = \mathbf{x_{a,c,n}} + h_2 \begin{pmatrix} \cos\varepsilon_k \\ \sin\varepsilon_k \end{pmatrix} \tag{29}$$

and eventually

$$\Gamma_{n,2} = h_2. \tag{30}$$

is the segment's lower partial length.

VI) Update k: k is not changed if the section of the polygonal audience line was not changed (step V, case (ii)). k has to be decreased by 1 if the section of the polygonal audience line was changed (step V, case (i)).

The steps I) - VI) have to be repeated until $n = N$ and $k = 0$.

5 Evaluation

Acoustic simulations based on the CDPS model including far-field radiation patterns of baffled line and circular pistons provide the data for an evaluation of the introduced approach. The evaluation is performed for two conditions and in comparison with typical standard LSA curving schemes such as straight, arc, J and

progressive [24] as well as two numerically optimized versions resulting from the Martin Audio *Display* prediction and optimization software [4, 9].

PALC1 incorporates the goal of an invariant interaction between adjacent cabinets with respect to the receiver geometry in order that the radiated sound of the different sources overlap at a constant coverage angle ψ in the far-field of the individual sources. This constraint simply reads

$$\psi_1 = \psi_2 = \psi_3 = ... = \text{const.} \tag{31}$$

PALC1 is similar to an arc array but the goal does not refer to the array itself, i.e. constant splay angles between all cabinets, but it refers to the shape of the receiver geometry. The distances of the different positions from the sources and the desired sound field are considered in PALC2. It demands a constant product of the coverage angle ψ and the distance from the source to the receiver positions, i.e.

$$\begin{aligned}&\psi_1 \cdot |\mathbf{x_{a,c,1}} - \mathbf{x_{c,1}}| \\ &\quad = \psi_2 \cdot |\mathbf{x_{a,c,2}} - \mathbf{x_{c,2}}| = ... = \text{const.},\end{aligned} \tag{32}$$

cf. Fig. 4. This results from an approximation of

$$\begin{aligned}&\tan\psi_1 \cdot |\mathbf{x_{a,c,1}} - \mathbf{x_{c,1}}| \\ &\quad = \tan\psi_2 \cdot |\mathbf{x_{a,c,2}} - \mathbf{x_{c,2}}| = ... = \text{const.}\end{aligned} \tag{33}$$

for small ψ_n. Eq. (33) arises from a simplification of attaining a constant length Γ_n for all n segments. The PALC2 constraint should not be confused with the Wavefront Sculpture Technology criterion #4 [16, p. 929].

For the evaluation cases MA1 and MA2, the tilt angles were extracted from the commercially available prediction and optimization software Martin Audio *Display* (version 2.1.10) which provides suitable tilt angles and also – if desired – the electronic control by means of a numerical multi-objective optimization scheme [4, 6, 9]. The weighting parameters for target and leakage each are set to 1 for MA1 and are set to 10 and 4 for MA 2 allowing a SPL attenuation of 10 dB from the first to the last audience position. Note that the optimization parameters target and leakage are quantitatively specified as the absolute error (34) and the acoustic contrast (36) in our case.

A reasonable selection of the evaluation criteria that were suggested in [15] is utilized to assess the quality of the different curving approaches. The position index plots (PIPs) show the resulting SPL spectra at all receiver positions $\mathbf{x_m}$, i.e. the sound pressure levels depending on the frequency f and the position index m. They are depicted in Fig. 5 for PALC1, PALC2, MA1 and MA2 for venue 1 and in Fig. 6 for venue 2. Also known as positional map, the PIPs were used in [3, 4, 6, 7, 9] as well.

The quantitative evaluation is based on three technical quality measures. The frequency dependent absolute amplitude error [15, Eq. (16)]

$$\varepsilon_{\text{abs}}(\omega) = \|\mathbf{p}_{m\in\mathscr{M}_\text{a}}(\omega) - \mathbf{p}_{\text{des},m\in\mathscr{M}_\text{a}}(\omega)\|_2^2 \tag{34}$$

between the obtained and the desired sound field in the audience zone is additionally smoothed in third-octave bands. The desired sound field $\mathbf{p}_{\text{des}}(\omega)$ could in principle be set arbitrarily. However, the used array geometry restricts the choice to physically realizable wave fronts. Typically a desired level decay over the audience zone and a level offset for the avoid zone can be defined in practical realizations [4]. We have chosen

$$P_{\text{des,3 dB}}(m,\omega) \propto \frac{\mathrm{e}^{-\mathrm{j}\frac{\omega}{c}|\mathbf{x_m}-\mathbf{x_S}|}}{\sqrt{|\mathbf{x_m}-\mathbf{x_S}|}} \tag{35}$$

as the basis for the comparison. This desired sound field complies with a sound field generated by a virtual line source at the position $\mathbf{x_S}$ deploying the large argument-approximation of the 2D Green's function and ignoring the temporal lowpass characteristics as well as the frequency independent $\frac{\pi}{4}$-phase shift [25, Eq. (26)]. The source position $\mathbf{x_S}$ is thus chosen ensuring that the origin of the virtual line source is located behind the LSA in every case. A target sound pressure level of 100 dB_SPL at the first receiver position within the audience zone is expected.

Moreover, the frequency dependent relation of the obtained average SPLs of the audience and the non-audience zone

$$L_{p,\text{a,na}}(\omega) = 10\log_{10}\left(\frac{\frac{1}{M_\text{a}}\|\mathbf{p}_{m\in\mathscr{M}_\text{a}}(\omega)\|_2^2}{\frac{1}{M_\text{na}}\|\mathbf{p}_{m\in\mathscr{M}_\text{na}}(\omega)\|_2^2}\right) \tag{36}$$

[15, Eq. (18)] is evaluated. This measure is depicted in Fig. 5e and Fig. 6e and corresponds to the acoustic contrast [18, Eq. (16)], [19, Eq. (2)], [20, Eq. (2)] established in MZSFS. Quantifying the homogeneity of the generated sound field, the frequency dependent standard deviation of the distance compensated SPLs

of all audience positions

$$H1(\omega) = \underset{m\in\mathscr{M}_\mathrm{a}}{\sigma}\left[20\log_{10}\left(\frac{|P(m,\omega)|}{p_0}\sqrt{\frac{|\mathbf{x_m}-\mathbf{x_S}|}{|\mathbf{x_{min(m)}}-\mathbf{x_S}|}}\right)\right], \quad (37)$$

cf. [7, e.g. Fig. 6, Fig. 8], is analyzed. It is visualized in Fig. 5f and Fig. 6f.

6 Discussion

The PIPs for venue 1 (Fig. 2a) shown in Fig. 5 reveal that only little energy is radiated into the non-audience zones compared to the audience zones for all of the algorithmic curving schemes. This intended behavior is confirmed by $L_{p,\mathrm{a,na}}(\omega)$ (36) in Fig. 5e for the optimized curvings as well as for the standard curving schemes (straight, arc, J and progressive) that were manually adjusted to the receiver geometry. It can be seen in the PIPs and by means of $L_{p,\mathrm{a,na}}(\omega)$ that the relation of the energy radiated into the audience and the non-audience zones is very similar for all tilt angle sets and increases with increasing frequency. The latter results from the radiation characteristics of the sources: the radiation is more directed, the higher the frequency.

$L_{p,\mathrm{a,na}}(\omega)$ features acceptable values larger than 12 dB for frequencies above 1 kHz and below ca. 8.5 kHz. For frequencies above ca. 8.5 kHz spatial aliasing effects are visible leading to more energy in the non-audience zones and significantly reduced acoustic contrast values. The grating lobes which are causal for that appear at rather high frequencies compared to conventional LSA designs due to the small distances between the HF sources. Choosing equal weights for target and leakage, the final angle of the numerically optimized MA1 is rather small. Therefore, the first audience rows are hardly reinforced as it can be deduced from the MA1 PIP. Increasing the target weight in relation to the leakage weight, the final angle of MA2 approximately corresponds to those of the other curving methods. Comparing MA1 and MA2, the effect of the reduced focus on leakage can be clearly observed by means of $L_{p,\mathrm{a,na}}(\omega)$ for frequencies above ca. 700 Hz.

Significant performance differences can be found with the help of the homogeneity measure $H1(\omega)$ (37). The straight array does not cover the whole audience zone so that there are large deviations considering the front, the middle and the back audience positions. For the front positions, MA1 shows a similar performance due to the small final angle. The arc and J array suffer from limited adjustment capabilities to the given receiver geometry. PALC2 and MA2 provide the best homogeneity values with MA2 being more homogeneous than PALC2 for frequencies below ca. 2 kHz. For frequencies above ca. 2 kHz, $H1(\omega)$ of PALC2 is smaller than the one of MA2 for up to (1...1.5) dB. The PIP of MA2, however, reveals some coverage gaps for the middle positions around $m \approx 110$ due to some large splay angles. An invariant interaction between adjacent cabinets which was intended with PALC1 does not seem to be practical considering homogeneity. As expected, the progressive curving yields solid results without paying attention to the specific composition of the receiver geometry.

For venue 2 (Fig. 2b) resembling a typical open-air amphitheater the results are very similar to those for venue 1. Only the expected difference of the acoustic contrast $L_{p,\mathrm{a,na}}(\omega)$ between MA1 and MA2 is not observable for venue 2. Note that the absolute error $\varepsilon_{\mathrm{abs}}(\omega)$ (34) is not visualized as it provides no meaningful results for the uniformly driven LSAs.

7 Conclusion

A purely analytical approach for finding appropriate LSA cabinet tilt angles was presented in this paper. The polygonal audience line curving (PALC) is based on the geometry of the receiver area and the intended coverage. Its target condition can be freely chosen, also including source-receiver distances and SPL loss over distance. This algorithm is faster and more efficient than numerical methods and can be extended so that it only seeks from a discrete set of tilt angle values as it is required for practical realizations. It was compared with typical standard LSA curving schemes. We conclude that the PALC is superior to them due to its flexible adaptability with respect to the receiver geometry.

Since identical specifications for the presented analytical and the evaluated numerical optimization approach cannot be completely ensured, a final comparative statement regarding accuracy does not seem to be advisable. These specifications especially comprise the exact conversion from the selectable goal parameters to the desired sound field as well as the considered frequency ranges, possibly also with emphases, of the

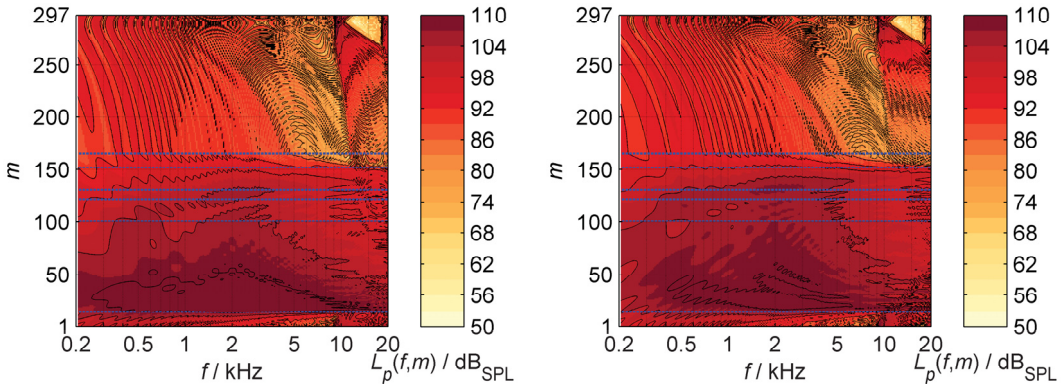

(a) PIP PALC1

(b) PIP PALC2

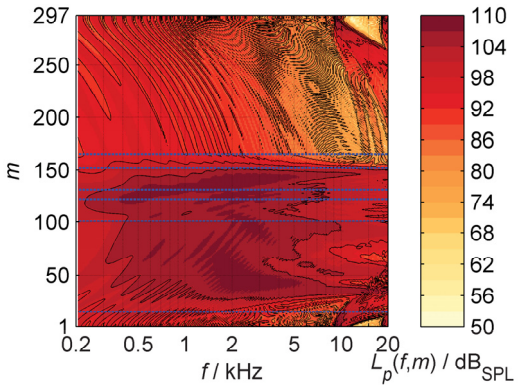

(c) PIP MA1

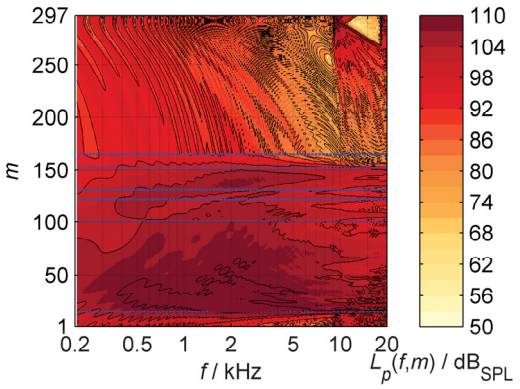

(d) PIP MA2

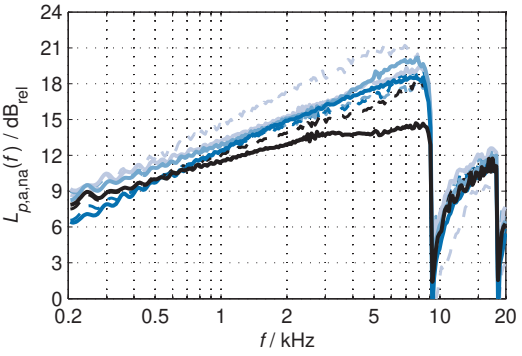

(e) $L_{p,\mathrm{a,na}}(f)$

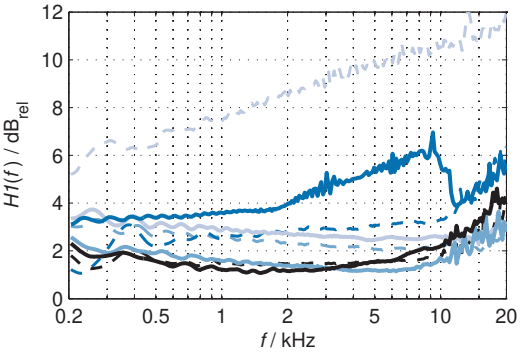

(f) $H1(f)$

Fig. 5: Technical quality measures for all analyzed curvings and position index plots (PIPs) for PALC1, PALC2, MA1 and MA2 for venue 1 from Fig. 2a.

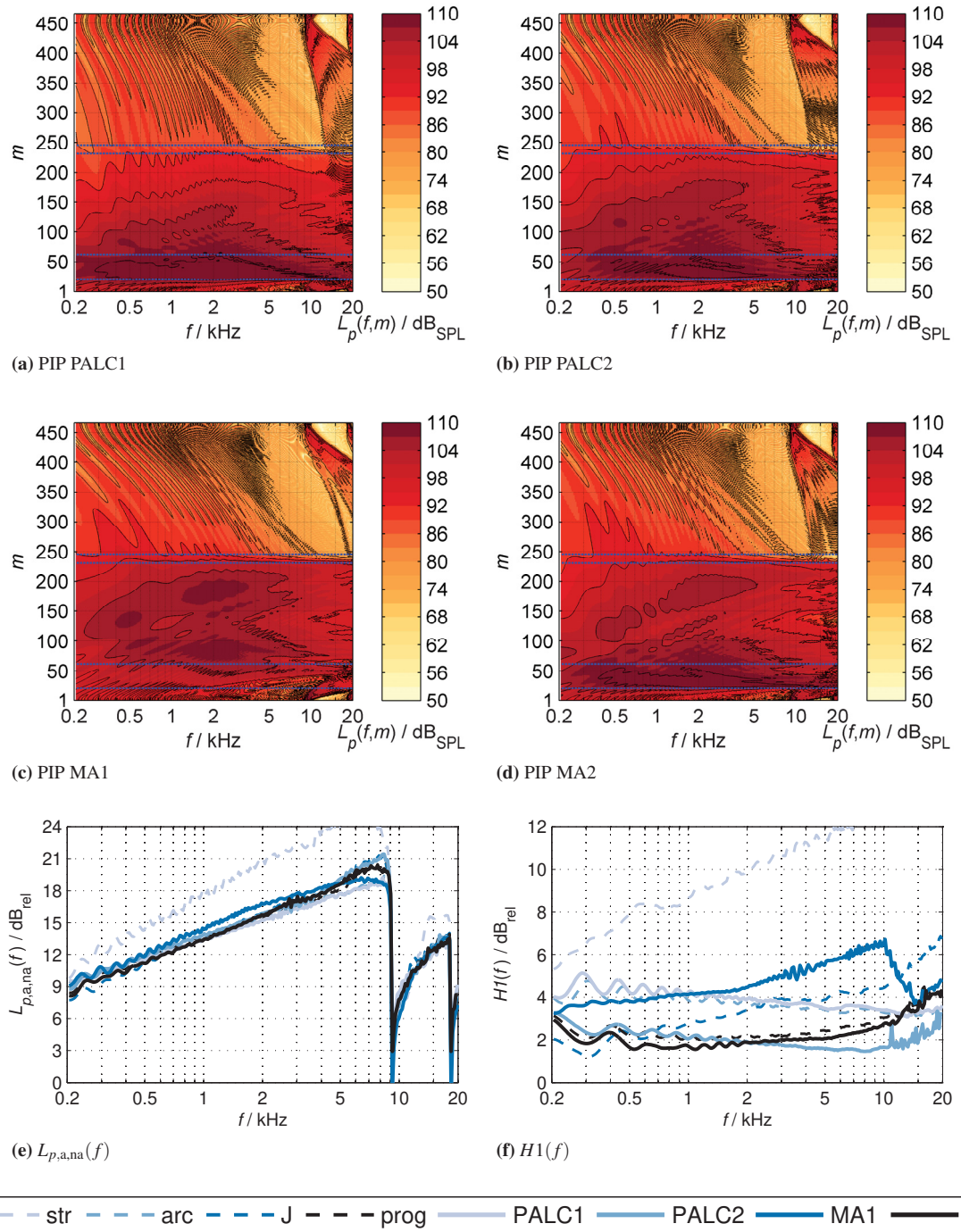

(a) PIP PALC1

(b) PIP PALC2

(c) PIP MA1

(d) PIP MA2

(e) $L_{p,\mathrm{a,na}}(f)$

(f) $H1(f)$

Fig. 6: Technical quality measures for all analyzed curvings and position index plots (PIPs) for PALC1, PALC2, MA1 and MA2 for venue 2 from Fig. 2b.

numerical algorithm and the fact that this numerical algorithm is based on proprietary, not extractable loudspeaker directivity data. The effort and the computing time of the numerical approach are however significantly higher than for the analytical approach.

References

[1] Scheirman, D. (2015): "Large-scale loudspeaker arrays: Past, present and future (part two – electroacoustic considerations)." In: *Proc. of the 59th Audio Eng. Soc. Int. Conf. on Sound Reinforcement, Montreal*.

[2] van Beuningen, G.W.J.; Start, E.W. (2000): "Optimizing directivity properties of DSP controlled loudspeaker arrays." In: *Proc. of the Inst. of Acoustics: Reproduced Sound*, **22**(6):17–37.

[3] Thompson, A. (2008): "Real world line array optimisation." In: *Proc. of the Inst. of Acoustics*, **30**(6).

[4] Thompson, A. (2009): "Improved methods for controlling touring loudspeaker arrays." In: *Proc. of the 127th Audio Eng. Soc. Conv., New York*, #7828.

[5] Terrell, M.; Sandler, M. (2010): "Optimising the controls of a homogenous loudspeaker array." In: *Proc. of the 129th Audio Eng. Soc. Conv., San Francisco*, #8159.

[6] Thompson, A.; Baird, J.; Webb, B. (2011): "Numerically optimised touring loudspeaker arrays - Practical applications." In: *Proc. of the 131st Audio Eng. Soc. Conv., New York*, #8511.

[7] Feistel, S.; Sempf, M.; Köhler, K.; Schmalle, H. (2013): "Adapting loudspeaker array radiation to the venue using numerical optimization of FIR filters." In: *Proc. of the 135th Audio Eng. Soc. Conv., New York*, #8937.

[8] Thompson, A.; Luzarraga, J. (2013): "Drive granularity for straight and curved loudspeaker arrays." In: *Proc. of the Inst. of Acoustics*, **35**(2):210–218.

[9] Thompson, A. (2006): "Line array splay angle optimisation." In: *Proc. of the Inst. of Acoustics*, **28**(8):135–148.

[10] Feistel, S.; Thompson, A.; Ahnert, W. (2009): "Methods and limitations of line source simulation." In: *J. Audio Eng. Soc.*, **57**(6):379–402.

[11] Meyer, D.G. (1984): "Computer simulation of loudspeaker directivity." In: *J. Audio Eng. Soc.*, **32**(5):294–315.

[12] Meyer, P.; Schwenke, R. (2003): "Comparison of the directional point source model and BEM model for arrayed loudspeakers." In: *Proc. of the Inst. of Acoustics*, **25**(4).

[13] Schultz, F. (2016): *Sound Field Synthesis for Line Source Array Applications in Large-Scale Sound Reinforcement*. Ph.D. thesis, University of Rostock.

[14] Straube, F.; Schultz, F.; Weinzierl, S. (2015a): "On the effect of spatial discretization of curved Line Source Arrays." In: *Fortschritte der Akustik: Tagungsband d. 41. DAGA, Nuernberg*, 459–462.

[15] Straube, F.; Schultz, F.; Makarski, M.; Spors, S.; Weinzierl, S. (2015b): "Evaluation strategies for the optimization of Line Source Arrays." In: *Proc. of the 59th Audio Eng. Soc. Int. Conf. on Sound Reinforcement, Montreal*.

[16] Urban, M.; Heil, C.; Bauman, P. (2003): "Wavefront Sculpture Technology." In: *J. Audio Eng. Soc.*, **51**(10):912–932.

[17] Schultz, F.; Straube, F.; Spors, S. (2015): "Discussion of the Wavefront Sculpture Technology criteria for straight line arrays." In: *Proc. of the 138th Audio Eng. Soc. Conv., Warsaw*, #9323.

[18] Choi, J.W.; Kim, Y.H. (2002): "Generation of an acoustically bright zone with an illuminated region using multiple sources." In: *J. Acoust. Soc. Am.*, **111**(4):1695–1700.

[19] Coleman, P.; Jackson, P.J.B.; Olik, M.; Møller, M.; Olsen, M.; Pedersen, J.A. (2014): "Acoustic contrast, planarity and robustness of sound zone methods using a circular loudspeaker array." In: *J. Acoust. Soc. Am.*, **135**(4):1929–1940.

[20] Coleman, P.; Jackson, P.J.B.; Olik, M.; Pedersen, J.A. (2014): "Personal audio with a planar bright zone." In: *J. Acoust. Soc. Am.*, **136**(4):1725–1735.

[21] Bai, M.R.; Wen, J.C.; Hsu, H.; Hua, Y.H.; Hsieh, Y.H. (2014): "Investigation on the reproduction performance versus acoustic contrast control in sound field synthesis." In: *J. Acoust. Soc. Am.*, **136**(4):1591–1600.

[22] Skudrzyk, E. (1971): *The Foundations of Acoustics*. New York: Springer.

[23] Olver, F.W.J.; Lozier, D.W.; Boisvert, R.F.; Clark, C.W. (2010): *NIST Handbook of Mathematical Functions*. Cambridge University Press, 1. ed.

[24] Ureda, M.S. (2004): "Analysis of loudspeaker line arrays." In: *J. Audio Eng. Soc.*, **52**(5):467–495.

[25] Ahrens, J.; Spors, S. (2010): "Sound field reproduction using planar and linear arrays of loudspeakers." In: *IEEE Trans. on Audio Speech Language Process.*, **18**(8):2038–2050.

8 Appendix

m	x_m / m	y_m / m
1	0	-11
15	7	-11
101	50	-11
122	58.1492	-4.3788
131	58.1492	0.1212
152	66.2984	6.7424
165	66.2984	13.2424
297	0.2984	13.2424

Table 1: Selected venue slice coordinates according to venue 1 from Fig. 2a.

m	x_m / m	y_m / m
1	0	-10
21	10	-10
62	30.4426	-8.4668
231	110.0423	19.8906
246	110.0423	27.3906
466	0.0423	27.3906

Table 2: Selected venue slice coordinates according to venue 2 from Fig. 2b.

LSA cabinet	γ_n / deg arc	γ_n / deg J	γ_n / deg prog	γ_n / deg PALC1	γ_n / deg PALC2	γ_n / deg MA1	γ_n / deg MA2
1	-2	-1	-2	-1.53	-2.45	-3	-3
2	1	-1	-1.62	1.84	-0.85	-2.5	-2.5
3	4	-1	-0.85	5.2	0.82	-2	-0.5
4	7	-1	0.3	8.55	2.54	-1	0
5	10	-1	1.83	11.88	4.29	0	4
6	13	-1	3.75	15.19	6.04	1	6
7	16	-1	6.05	18.39	7.83	2	10
8	19	4	8.73	21.48	9.69	3	10.5
9	22	9	11.8	24.45	11.62	4	14.5
10	25	14	15.25	27.31	13.75	5	16.5
11	28	19	19.1	30.05	16.3	7	18.5
12	31	24	23.32	32.67	19.43	9	22.5
13	34	29	27.92	35.18	23.27	11	26.5
14	37	34	32.9	37.57	28.01	12	30.5
15	40	39	38.27	39.84	33.83	18	38
16	43	44	44	42	40.95	25.5	45.5

Table 3: Tilt angles of the LSA cabinets for the geometry used in Fig. 1 and for venue 1 from Fig. 2a for the different curvings (arc, J, progressive, PALC1, PALC2, MA1 and MA2). Every cabinet of the straight array is tilted by 7 deg.

LSA cabinet	γ_n / deg arc	γ_n / deg J	γ_n / deg prog	γ_n / deg PALC1	γ_n / deg PALC2	γ_n / deg MA1	γ_n / deg MA2
1	-7.14	-7	-7.1	-7.14	-8.24	-9.3	-8.8
2	-4.54	-7	-6.78	-4.03	-7.24	-8.8	-8.3
3	-1.94	-7	-6.13	-0.98	-6.12	-8.3	-7.8
4	0.66	-7	-5.15	2.01	-4.89	-7.8	-7.3
5	3.26	-7	-3.85	4.94	-3.51	-7.3	-5.3
6	5.86	-7	-2.23	7.81	-1.99	-6.8	-4.8
7	8.46	-7	-0.28	10.63	-0.29	-6.3	0.2
8	11.06	-7	2	13.39	1.6	-5.8	3.2
9	13.66	-2.13	4.6	16.09	3.71	-5.3	6.2
10	16.26	2.75	7.53	18.69	6.06	-3.3	9.2
11	18.86	7.63	10.78	21.18	8.68	-1.3	12.2
12	21.46	12.5	14.35	23.56	11.6	0.7	15.2
13	24.06	17.38	18.25	25.83	14.98	2.7	20.2
14	26.66	22.25	22.48	27.97	19.1	4.7	23.2
15	29.26	27.13	27.03	30	24.25	6.7	27.2
16	31.86	32	31.9	31.91	30.68	14.2	30.2

Table 4: Tilt angles of the LSA cabinets for the geometry used in Fig. 1 and for venue 2 from Fig. 2b for the different curvings (arc, J, progressive, PALC1, PALC2, MA1 and MA2). Every cabinet of the straight array is tilted by -4 deg.

Audio Engineering Society

Conference Paper

Presented at the Conference on
Sound Reinforcement
2017 August 30 – September 2, Struer, Denmark

Adjoint-Based Time Domain Sound Reinforcement

Mathias Lemke[1], Florian Straube[2], Frank Schultz[2], Jörn Sesterhenn[1], and Stefan Weinzierl[2]

[1]*Computational Fluid Dynamics, TU Berlin, DE-10623 Berlin, Germany*
[2]*Audio Communication Group, TU Berlin, DE-10587 Berlin, Germany*

Correspondence should be addressed to Mathias Lemke (mlemke@tnt.tu-berlin.de)

ABSTRACT

Line Source Arrays (LSAs) are used for sound reinforcement aiming at the synthesis of homogeneous sound fields for the whole audio bandwidth. The deployed loudspeaker cabinets are rigged with different tilt angles and/or electronically controlled. The determination of the optimal geometric arrangement and electronic drive is an ill-posed inverse problem. In this contribution an adjoint-based approach is introduced. By defining a target sound field within an objective function the method allows the optimization of acoustic sources. It is based on the Euler equations and the corresponding adjoint which are solved by means of computational aeroacoustic (CAA) techniques. In this way, both optimal driving functions and optimal positions of sources for the synthesis of a desired sound field can be determined. The adjoint approach allows the consideration of a base flow, such as the influence of wind. We will present the fundamentals and features of the method together with two validation examples. It is shown, that the method is suitable to identify predetermined driving functions and that it provides reasonable driving functions when considering a base flow.

1 Introduction

For the optimization of the curving and the electronic control of line source arrays (LSAs) for improved sound reinforcement there is no standard procedure nowadays. Both a pure geometric and a pure electronic wavefront shaping as well as combinations thereof are realized [1]. In [2–4] numerical optimization schemes are applied for finding LSA cabinet tilt angles. An analytical approach for determining the LSA splay angles with respect to the receiver geometry and the intended coverage is introduced in [5].

The calculation of appropriate driving signals, i.e. finite impulse response (FIR) filters for individual LSA loudspeakers, is usually based on frequency domain approaches [3, 4, 6–10] such as the numerical multi-objective goal attainment method [11] or genetic algorithms [12]. While the first scheme allows the calculation of ideal loudspeaker driving functions at selected control positions, i.e. commonly audience and non-audience positions, they are typically computed separately for each frequency. Depending on the optimization goals and the complexity of the receiver geometry, this results in non-smooth frequency responses and requires adequate windowing for obtaining feasible FIR filters from the ideal driving functions. Genetic algorithms suffer from a reduced solution space as they are based on predetermined sets of parameters. However, they provide less complex solutions and are computationally efficient. Recent, mostly proprietary

software such as Martin Audio Display, EAW Resolution, d&b ArrayCalc and AFMG FIRmaker offer (numerical) optimization schemes but the algorithms and the parametrization are rarely publicly documented. None of the methods is able to consider a base flow, e.g. the influence of wind.

In this paper, we aim at introducing an adjoint-based approach for application in sound reinforcement. It is a time domain method based on the Euler equations and the corresponding adjoint which are solved by means of computational aeroacoustic (CAA) techniques. It provides solutions for both the positions of the loudspeakers and their individual driving functions. Since it allows the consideration of base flows, it could be particularly valuable in the case of open air events under windy conditions.

In fluid mechanics, the use of adjoint-based methods has proven to be an effective approach for determining various model parameters [13]. Utilizing these methods for acoustic problems is convenient as the adjoint compressible Euler equations and Navier-Stokes equations [14, 15] also capture acoustics, both for a stationary environment and a base flow.

The paper is organized as follows: In Sec. 2 the adjoint-based method is introduced in general and tailored for the application in wavefront shaping. In Sec. 3 a validation by means of two simplified configurations is presented in order to verify that the approach is applicable for sound reinforcement problems. In Sec. 4 a summary is given.

2 Adjoint-Based Method

In contrast to frequency domain approaches, which are common in sound reinforcement and are based on an integral representation of the homogeneous wave equation for discrete source distributions [6, 16–18], the adjoint-based method makes use of a more general representation of the wave propagation in the time domain.

2.1 Adjoint Equations

Adjoint equations can be defined in a continuous or discrete manner. For the sake of simplicity they are introduced in discrete version as in [13]. A matrix-vector notation is used. The vector space is the full solution in space and time. This section is based on [19].

Adjoint equations arise by a so called objective function J, which is defined by the product between a geometric weight g and a system state q.

$$J = g^{\mathrm{T}} q, \qquad g, q \in \mathbb{R}^n \tag{1}$$

The system state q corresponds to the solution of the governing system

$$Aq = f, \qquad A \in \mathbb{R}^{n\times n}, \;\; f \in \mathbb{R}^n \tag{2}$$

with A as governing operator and f as source terms on the right hand side. In terms of an optimization of J by means of f, the equation has to be solved for every different f. In order to reduce the computational effort, the adjoint equation can be used

$$A^{\mathrm{T}} q^* = g, \tag{3}$$

with the adjoint variable q^*. By

$$J = g^{\mathrm{T}} q = \left(A^{\mathrm{T}} q^*\right)^{\mathrm{T}} q = q^{*\mathrm{T}} A q = q^{*\mathrm{T}} f \tag{4}$$

an expression is found, which enables the computation of J without the need to solve the system for every discrete f. After solving the adjoint equation, the objective can be determined by a simple and computationally cheap scalar product. Thus, the adjoint approach enables an efficient computation of gradients for J with respect to f.

2.2 Adjoint Sound Field Synthesis

According to the intended application – the sound field synthesis in time domain – the objective function J is defined in space and time with $\mathrm{d}\Omega = \mathrm{d}x_i \mathrm{d}t$:

$$J = \frac{1}{2} \iint \left(q - q_{\text{target}}\right)^2 \mathrm{d}\Omega. \tag{5}$$

The variable $q = [\rho, u_j, p]$ comprises all quantities which are necessary for a state description of the governing system, defined by the Euler equations. The variable q_{target} denotes a desired system state, ρ the density, u_j the velocity in the direction x_j and p the pressure, which is used solely for evaluation of the objective

$$J = \frac{1}{2} \iint \left(p - p_{\text{target}}\right)^2 \sigma \, \mathrm{d}\Omega. \tag{6}$$

The additional weight $\sigma(x_i, t)$ defines where and when the objective is evaluated. In practice, the objective

function is supplemented by a regularization term, which is omitted here for the sake of clarity. With a suitably defined p_{target} a minimum of J is optimal.

The minimum is to be achieved under the constraint that the Euler equations E are valid. Similar to (2), the following system is introduced:

$$E(q)\,q = f \tag{7}$$

abbreviating

$$\begin{aligned} \partial_t \begin{pmatrix} \rho \\ \rho u_j \\ \frac{p}{\gamma-1} \end{pmatrix} &+ \partial_{x_i} \begin{pmatrix} \rho u_i \\ \rho u_i u_j + p\delta_{ij} \\ \frac{u_i p \gamma}{\gamma-1} \end{pmatrix} \\ &- u_i \partial_{x_i} \begin{pmatrix} 0 \\ 0 \\ p \end{pmatrix} = \begin{pmatrix} f_\rho \\ f_{\rho u_j} \\ f_p \end{pmatrix}. \end{aligned} \tag{8}$$

with γ as heat capacity ratio. The summation convention applies. See [14] for details on the formulation.

The terms $f = [f_\rho, f_{\rho u_j}, f_p]$ on the right side of the equations characterize sources for mass, momentum and energy. They enable a control of the system state respectively the solution of the equations. The general goal is to obtain a solution of the Euler equations, which matches q_{target} respectively p_{target} in an optimal sense, by adapting f.

The sources f can be interpreted as sound sources or loudspeakers. Pure monopole sources can be described solely by energy sources f_p. Using the momentum terms $f_{\rho u_j}$, it is possible to consider loudspeaker directivities. Thus, an optimization of f corresponds to an optimization of the loudspeakers' output signals.

In order to use the adjoint approach for optimizing f, it is necessary to linearize the objective function (6) and the governing system (8). This results in

$$\delta J = \iint \underbrace{\left(p - p_{\text{target}}\right)\sigma}_{=g} \delta p \mathrm{d}\Omega, \tag{9}$$

and

$$E_{\text{lin}}\delta q = \delta f \tag{10}$$

with the now defined weight $g = (p - p_{\text{target}})\sigma$. Combining the linearized system and the objective in a Lagrangian manner leads to

$$\begin{aligned} \delta J &= g^{\mathrm{T}}\delta q - q^{*\mathrm{T}} \underbrace{\left(E_{\text{lin}}\delta q - \delta f\right)}_{=0} \\ &= q^{*\mathrm{T}}\delta f + \delta q^{\mathrm{T}}\left(g - E_{\text{lin}}^{\mathrm{T}} q^*\right). \end{aligned} \tag{11}$$

For the sake of simplicity the integrals are not shown. The adjoint equation $E^* = E_{\text{lin}}^{\mathrm{T}}$ results from

$$g - E_{\text{lin}}^{\mathrm{T}} q^* = 0, \tag{12}$$

with $q^* = [\rho^*, u_j^*, p^*]$, similar to (3). See [19, p. 19] for a detailed derivation of the adjoint Euler equations, which are given by

$$\partial_t q^* = \tilde{A}\left[-(B^i)^{\mathrm{T}}\partial_{x_i} q^* - \partial_{x_i}(C^i)^{\mathrm{T}} q^* + \tilde{C}^i \partial_{x_i} c - g\right] \tag{13}$$

with $\tilde{A} = \left(A^{\mathrm{T}}\right)^{-1}$ and $\tilde{C}^i$ as resorting

$$q_\alpha^* \delta C_{\alpha\beta}^i \partial_{x_i} c_\beta = q_\alpha^* \delta q_\kappa \frac{\partial C_{\alpha\beta}^i}{\partial q_\kappa} \partial_{x_i} c_\beta \tag{14}$$

abbreviated as $\delta q_\kappa \tilde{C}_{\kappa\beta}^i \partial_{x_i} c_\beta$. The matrices A, B^i and C^i result from linearization of the Euler equations (8) and are given in the appendix.

The change of the objective function reads

$$\delta J = q^{*\mathrm{T}}\delta f. \tag{15}$$

The solution of the adjoint equation can be interpreted as gradient of J with respect to the source terms f

$$\nabla_f J = q^*. \tag{16}$$

Initial and boundary conditions of the adjoint Euler equations as well as the derivation of the adjoint compressible Navier-Stokes equations are discussed in [19].

2.3 Iterative Process

Using the gradient, an initial source distribution f^0 is optimally adjusted. First, the Euler equations are solved forward in time with $f^0 = 0$. Subsequently, the adjoint equations are calculated backwards in time deploying the direct solution and the weight g. Based on the adjoint solution, the gradient $\nabla_f J$ is determined and used to update the source distribution f^n:

$$f^{n+1} = f^n + \alpha \nabla_f J, \tag{17}$$

with α denoting an appropriate step size and n the iteration number. The gradient is calculated for the whole computational domain and the entire simulation time but is only evaluated at desired loudspeaker positions. While convergence is not accomplished in the objective function, the process is repeated with the current f^n.

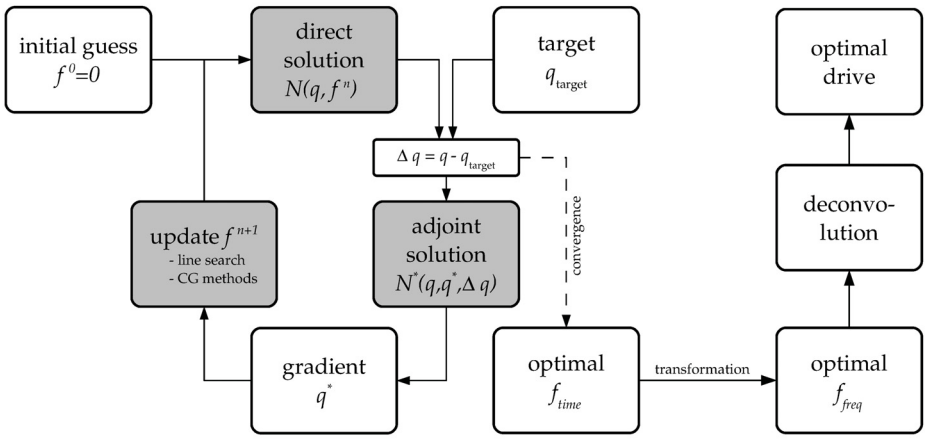

Fig. 1: Iterative procedure for the determination of an optimal f and subsequent conversion to optimal loudspeaker drives. Computationally intensive steps are marked in gray. Details are given in the text.

The resulting optimal f is deconvolved with the considered primitive input signal and the loudspeaker properties resulting in an optimal driving for every considered loudspeaker. See Fig. 1 for an overview of the procedure.

The proposed technique optimizes towards local extrema. Detecting global optima is not ensured. The computational costs of the adjoint-based approach are independent of the number of loudspeakers and their arrangement. They only depend on the size of the computational domain and the considered frequency range. The computational problem is fully parallelizable.

3 Validation

In order to prove that the proposed adjoint-based method is able to determine practical driving functions of LSA loudspeakers, a two-dimensional setup is considered. An optimal drive of three sources in a curved arrangement is sought. Monopole characteristics and a distance of 0.1 m between the loudspeakers are assumed. An area of 1 m x 1 m is considered, cf. Fig. 2 for details.

Based on the complex-directivity point source (CDPS) model, which is commonly used for the sound field prediction of LSAs [17, Eq. (5)], a sound field is calculated using predetermined driving functions. Each loudspeaker is driven by a sine with 2 kHz. These signals feature an amplitude ratio of 4 : 2 : 1 and a phase shift of two samples each for a sampling frequency

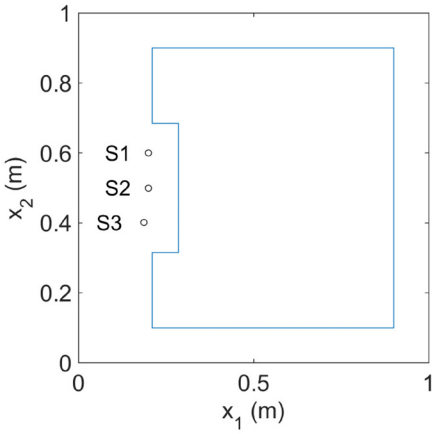

Fig. 2: Validation setup: The integral objective J is evaluated in the outlined (blue) region. The loudspeaker positions S are indicated by small circles.

$f_s = 160\,\text{kHz}$. Note that this sampling frequency was chosen as it corresponds to the discrete time step of the numerical computation of the Euler and the corresponding adjoint equations. It can be reduced if required. The resulting field is transformed into the time domain defining p_{target}. Finding the predefined driving functions by means of the adjoint-based method only using the predetermined sound field is the goal of the validation.

Two configurations are analyzed: one without base flow

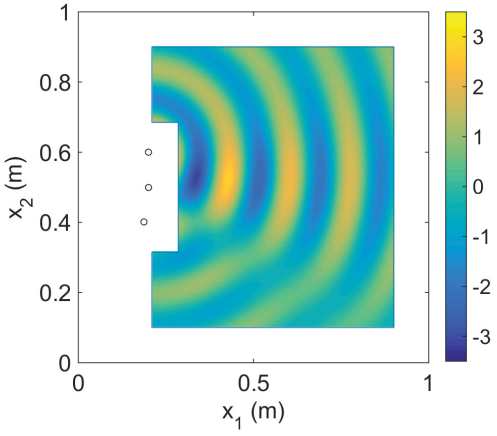

Fig. 3: Configuration 1: Target sound field (alternating component of p) in Pa for a selected time step ($t = 9.38\,\mathrm{ms}$).

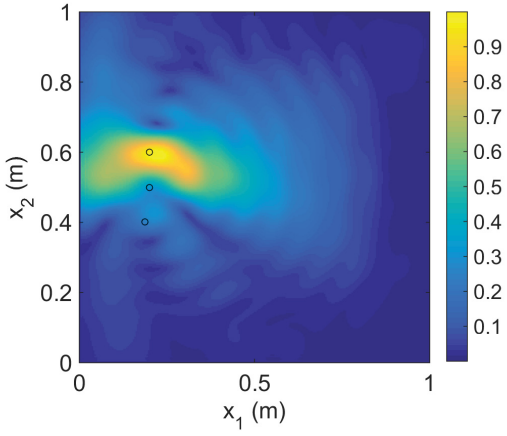

Fig. 4: Configuration 1: Normalized adjoint sensitivity $|p^*|$ within the first iteration with $f = 0$.

and one including a base flow characterizing the influence of wind. In both cases the computational domain is discretized by an equidistant grid with 256×256 points. A fourth-order finite difference stencil is used. For the discretization in time a standard fourth-order Runge-Kutta is applied. Non-reflecting conditions are used for all boundaries. For the adjoint computation, the same discretization is used. The gradient evaluation (17) is modified by a quadratic line-search. Due to the assumed monopole characteristics the optimization is restricted to f_p.

3.1 Configuration 1: No Base Flow

In Fig. 3 the target sound field is depicted for a selected time step. The adjoint solution is computed backwards in time. Several time steps of p^* of the first iteration with $f = 0$ are visualized in Fig. 10. The solution contains information on the optimal positioning of the sources. By the point and component wise summation of the absolute adjoint sensitivities over all computed time steps

$$\hat{q} = \sum_{t_n=0}^{t_{n=\mathrm{end}}} |q^*|, \tag{18}$$

the positions featuring maximum impact on the objective function can be identified by the maxima of $\hat{q}$. These correspond to the most likely source positions. Thus, the first adjoint solution allows for an optimal geometric arrangement of the sources, cf. Fig. 4.

Since the positions of the sources are known in this case, the adjoint solution is only evaluated at the prescribed loudspeaker locations. Thirty iterations have been performed. The objective function has converged and is reduced by nearly three orders of magnitude, see Fig. 5

In Fig. 6 the resulting optimal f_p is shown. Three sine signals with a frequency of 2 kHz can be identified. They exhibit the selected amplitude ratio of $4 : 2 : 1$. As defined, the excitation signals of the loudspeakers are delayed by 2 samples each. Thus, for this configuration the desired driving functions were successfully determined.

In the case of a multi-frequency input and for the consideration of specific loudspeaker characteristics, a deconvolution of f or suitable parts of it in the frequency domain would be necessary, see Fig. 1.

3.2 Configuration 2: With Base Flow

Within this configuration an additional, simple base flow is considered by means of corresponding initial and boundary conditions, see Fig. 7. All other parameters remain unaltered from the previous configuration. Also the same p_{target}, based on the CDPS calculation without base flow, is used.

Again 30 iterations of the adjoint framework were performed. The objective function has converged and is reduced by two orders of magnitude. As the target sound field is not fully attainable due to the presence

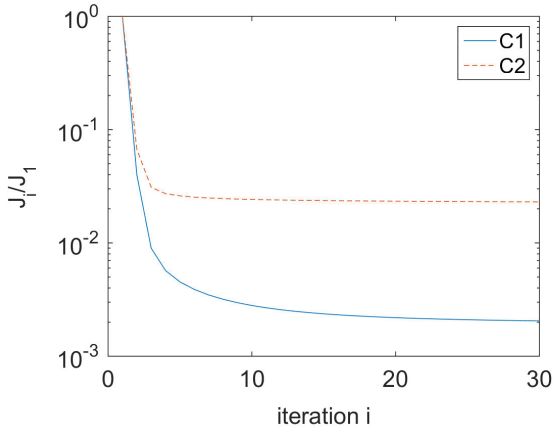

Fig. 5: Configuration 1 & 2: Progress of the objective function for configuration 1 (C1) and 2 (C2) normalized to the corresponding initial value J_1.

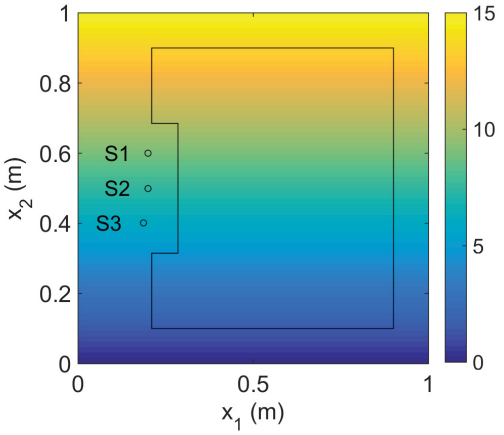

Fig. 7: Configuration 2: Linear base flow $u_1(x_2)$ in m/s. The loudspeaker positions S are unchanged and indicated by small circles.

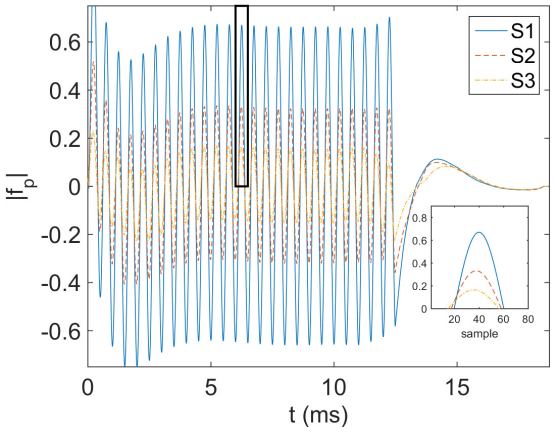

Fig. 6: Configuration 1: Resulting normalized optimal forcing f_p for the prescribed source positions S.

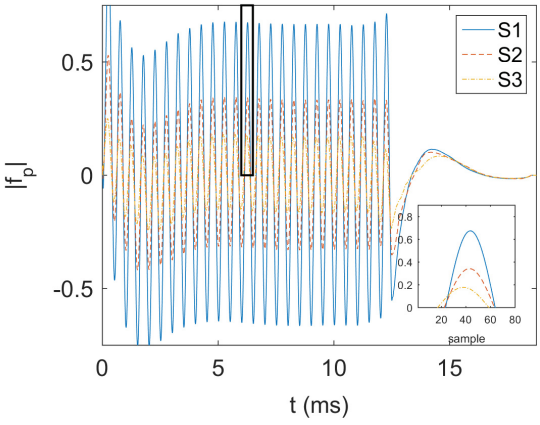

Fig. 8: Configuration 2: Resulting normalized optimal forcing f_p for the prescribed source positions S.

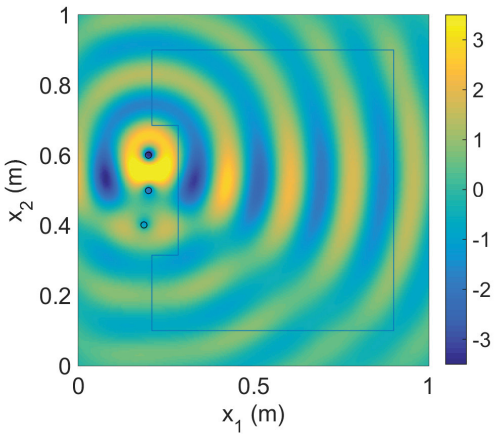

Fig. 9: Configuration 2: Resulting sound field (alternating component of p) after 30 iterations in Pa for a selected time step ($t = 9.38\,\text{ms}$), analogous to Fig. 3.

of the base flow, the worse performance of J does not come unexpected. The resulting optimal forcing f_p for all considered loudspeaker positions is shown in Fig. 8.

Because of the missing option to validate the approach by means of a CDPS calculation with base flow, the resulting sound field for the same time step as in Fig. 3 is shown in Fig. 9. It corresponds to the desired one in its characteristic properties. Again, an optimum excitation f_p is found and, thus, optimal driving functions are determined.

4 Summary

An adjoint-based method for finding practical driving functions for line source arrays was introduced. The approach also provides information on an appropriate loudspeaker positioning. By means of a two-dimensional setup it has been successfully validated that the method is able to determine optimal driving functions, also considering a base flow, e.g. for characterizing the influence of wind on an sound reinforcement setting.

Future work incorporates an efficient implementation of the adjoint-based approach for acoustic problems and for practical sound reinforcement setups as well as an adequate adaptation framework for the adjoint-based solutions.

References

[1] Scheirman, D. (2015): "Large-scale loudspeaker arrays: Past, present and future (part two – electroacoustic considerations)." In: *Proc. of the 59th Audio Eng. Soc. Int. Conf. on Sound Reinforcement, Montreal*.

[2] Thompson, A. (2006): "Line array splay angle optimisation." In: *Proc. of the Inst. of Acoustics*, **28**(8):135–148.

[3] Thompson, A. (2009): "Improved methods for controlling touring loudspeaker arrays." In: *Proc. of the 127th Audio Eng. Soc. Conv., New York*, #7828.

[4] Thompson, A.; Baird, J.; Webb, B. (2011): "Numerically optimised touring loudspeaker arrays - Practical applications." In: *Proc. of the 131st Audio Eng. Soc. Conv., New York*, #8511.

[5] Straube, F.; Schultz, F.; Bonillo, D.A.; Weinzierl, S. (2017): "An analytical approach for optimizing the curving of Line Source Arrays." In: *Proc. of the 142nd Audio Eng. Soc. Conv., Berlin*, #9699.

[6] van Beuningen, G.W.J.; Start, E.W. (2000): "Optimizing directivity properties of DSP controlled loudspeaker arrays." In: *Proc. of the Inst. of Acoustics: Reproduced Sound*, **22**(6):17–37.

[7] Thompson, A. (2008): "Real world line array optimisation." In: *Proc. of the Institute of Acoustics*, **30**(6).

[8] Terrell, M.; Sandler, M. (2010): "Optimising the controls of a homogenous loudspeaker array." In: *Proc. of the 129th Audio Eng. Soc. Conv., San Francisco*, #8159.

[9] Feistel, S.; Sempf, M.; Köhler, K.; Schmalle, H. (2013): "Adapting loudspeaker array radiation to the venue using numerical optimization of FIR filters." In: *Proc. of the 135th Audio Eng. Soc. Conv., New York*, #8937.

[10] Thompson, A.; Luzarraga, J. (2013): "Drive granularity for straight and curved loudspeaker arrays." In: *Proc. of the Inst. of Acoustics*, **35**(2):210–218.

[11] Gembicki, F.W.; Haimes, Y.Y. (1975): "Approach to performance and sensitivity multiobjective optimization: The goal attainment method." In: *IEEE Trans. on Automatic Control*, **20**(6):769–771.

[12] Goldberg, D.E. (1989): *Genetic Algorithms in Search, Optimization, and Machine Learning*. Boston, MA: Addison-Wesley Publishing Company Inc., 1. ed.

[13] Giles, M.; Pierce, N. (2000): "An introduction to the adjoint approach to design." In: *Flow, Turbulence and Combustion*, **65**:393–415.

[14] Lemke, M.; Reiss, J.; Sesterhenn, J. (2014): "Adjoint based optimisation of reactive compressible flows." In: *Combustion and Flame*, **161**(10):2552–2564.

[15] Lemke, M.; Sesterhenn, J. (2016): "Adjoint-based pressure determination from PIV data in compressible flows – validation and assessment based on synthetic data." In: *European Journal of Mechanics - B Fluids*, **58**:29–38.

[16] Feistel, S.; Thompson, A.; Ahnert, W. (2009): "Methods and limitations of line source simulation." In: *J. Audio Eng. Soc.*, **57**(6):379–402.

[17] Meyer, D.G. (1984): "Computer simulation of loudspeaker directivity." In: *J. Audio Eng. Soc.*, **32**(5):294–315.

[18] Meyer, P.; Schwenke, R. (2003): "Comparison of the directional point source model and BEM model for arrayed loudspeakers." In: *Proc. of the Institute of Acoustics*, **25**(4).

[19] Lemke, M. (2015): *Adjoint based data assimilation in compressible flows with application to pressure determination from PIV data*. Ph.D. thesis, TU Berlin.

5 Appendix

Linearization of the governing Euler equations (8) with respect to the components of q around a given base state q_0 with $q = q_0 + \delta q$ results in

$$\partial_t A\delta q + \partial_{x_i} B^i \delta q + C^i \partial_{x_i} \delta q + \delta C^i \partial_{x_i} c = \delta f. \quad (19)$$

The summation convention applies. For the sake of completeness the resulting matrices are stated below for three dimensions. The two-dimensional matrices can be easily derived.

$$A = \begin{bmatrix} 1 & 0 & 0 & 0 & 0 \\ u_1 & \rho & 0 & 0 & 0 \\ u_2 & 0 & \rho & 0 & 0 \\ u_3 & 0 & 0 & \rho & 0 \\ 0 & 0 & 0 & 0 & \frac{1}{\gamma-1} \end{bmatrix} \quad (20)$$

$$B^1 = \begin{bmatrix} u_1 & \rho & 0 & 0 & 0 \\ u_1^2 & 2\rho u_1 & 0 & 0 & 1 \\ u_1 u_2 & \rho u_2 & \rho u_1 & 0 & 0 \\ u_1 u_3 & \rho u_3 & 0 & \rho u_1 & 0 \\ 0 & \frac{\gamma p}{\gamma-1} & 0 & 0 & \frac{\gamma u_1}{\gamma-1} \end{bmatrix} \quad (21)$$

$$B^2 = \begin{bmatrix} u_2 & 0 & \rho & 0 & 0 \\ u_1 u_2 & \rho u_2 & \rho u_1 & 0 & 0 \\ u_2^2 & 0 & 2\rho u_2 & 0 & 1 \\ u_2 u_3 & 0 & \rho u_3 & \rho u_2 & 0 \\ 0 & 0 & \frac{\gamma p}{\gamma-1} & 0 & \frac{\gamma u_2}{\gamma-1} \end{bmatrix} \quad (22)$$

$$B^3 = \begin{bmatrix} u_3 & 0 & 0 & \rho & 0 \\ u_1 u_3 & \rho u_3 & 0 & \rho u_1 & 0 \\ u_2 u_3 & 0 & \rho u_3 & \rho u_2 & 0 \\ u_3^2 & 0 & 0 & 2\rho u_3 & 1 \\ 0 & 0 & 0 & \frac{\gamma p}{\gamma-1} & \frac{\gamma u_3}{\gamma-1} \end{bmatrix} \quad (23)$$

$$C^i = \begin{bmatrix} 0 & 0 & 0 & 0 & 0 \\ 0 & 0 & 0 & 0 & 0 \\ 0 & 0 & 0 & 0 & 0 \\ 0 & 0 & 0 & 0 & 0 \\ 0 & 0 & 0 & 0 & -u_i \end{bmatrix} \quad (24)$$

$$\delta C^i = \begin{bmatrix} 0 & 0 & 0 & 0 & 0 \\ 0 & 0 & 0 & 0 & 0 \\ 0 & 0 & 0 & 0 & 0 \\ 0 & 0 & 0 & 0 & 0 \\ 0 & 0 & 0 & 0 & -\delta u_i \end{bmatrix} \quad (25)$$

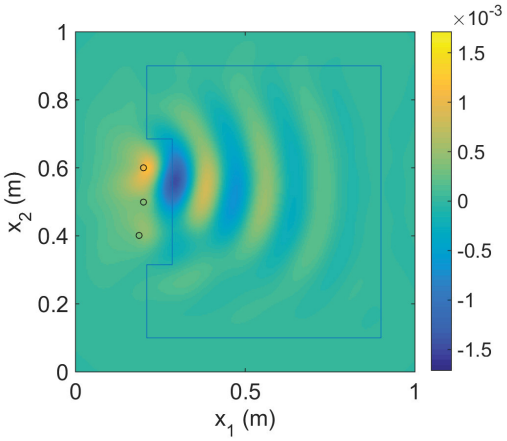

(a) $t = 12.5$ ms

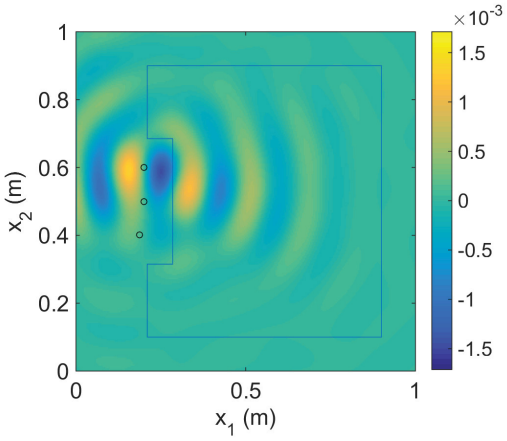

(b) $t = 9.38$ ms

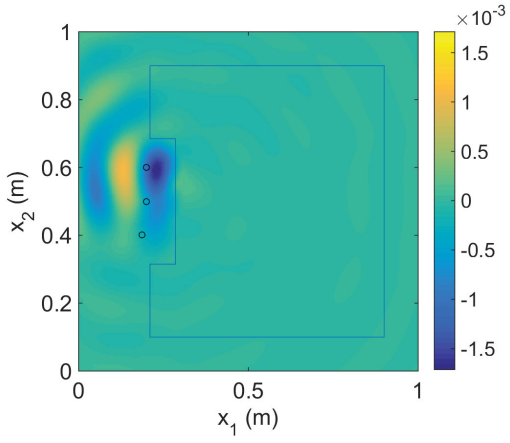

(c) $t = 0.31$ ms

Fig. 10: Configuration 1: Adjoint solution p^* for selected time steps within the first iteration ($f = 0$).

F. Straube, F. Schultz, D. A. Bonillo, and S. Weinzierl,
"An Analytical Approach for Optimizing the Curving of Line Source Arrays,"
J. Audio Eng. Soc., vol. 66, no. 1/2, pp. 4–20, (2018 January/February.).
DOI: https://doi.org/10.17743/jaes.2017.0043

An Analytical Approach for Optimizing the Curving of Line Source Arrays

FLORIAN STRAUBE, *AES Associate Member*, **FRANK SCHULTZ,** *AES Associate Member*,
(florian.straube@tu-berlin.de) (frank.schultz@tu-berlin.de)

DAVID ALBANÉS BONILLO, AND STEFAN WEINZIERL
(davidalbanes@gmail.com) (stefan.weinzierl@tu-berlin.de)

Audio Communication Group, TU Berlin, DE-10587 Berlin, Germany

Line source arrays (LSAs) are used for large-scale sound reinforcement aiming at the synthesis of homogeneous sound fields for the whole audio bandwidth. The deployed loudspeaker cabinets are rigged with different tilt angles and/or are electronically controlled in order to provide the intended coverage of the audience zones and to avoid radiation towards the ceiling, reflective walls or residential areas. This contribution introduces the analytical polygonal audience line curving (PALC) approach for finding appropriate LSA cabinet tilt angles with respect to the geometry of the receiver area and the intended coverage. PALC can be applied in advance of a numerical optimization of the loudspeakers' driving functions. The method can be used with different objectives, such as a constant interaction between adjacent cabinets with respect to the receiver geometry or by additionally considering amplitude attenuation over distance. PALC is compared with typical standard LSA curving schemes. The advantages of the presented approach regarding sound field homogeneity and target-oriented radiation are evaluated based on technical quality measures.

0 INTRODUCTION

For the optimization of the curving and the electronic control of line source arrays (LSAs) for advanced sound reinforcement there is no standard procedure. In practice, both a pure geometric and a pure electronic wavefront shaping as well as combinations thereof are realized. Even state-of-the-art line array systems with extensive beam steering capabilities differ significantly [1]. Since they comprise several individually controllable, small drivers, beam steering is feasible up to high audio frequencies. While the cabinets of some array systems are curved in addition to the beam steering, the cabinets of other systems are rigged as a straight line.

Recent, mostly proprietary software such as Martin Audio Display [2], EAW Resolution 2 [3], d&b ArrayCalc [4], and AFMG FIRmaker [5] offer (numerical) optimization schemes but the algorithms and the parametrization are rarely publicly documented. In the literature the calculation of appropriate driving signals, i.e., finite impulse response (FIR) filters for the individual LSA loudspeakers in order to generate a desired sound field by numerical optimization techniques, was discussed in [6–12]. These approaches yield considerable improvements with respect to homogeneous audience coverage and/or avoidance of high side lobe energy compared to manually adjusted setups. In [8, 10, 13] also the LSA cabinet tilt angles are determined by numerical optimization methods. The established Wavefront Sculpture Technology (WST) criteria for LSAs [14, p. 929] also comprise a geometrical criterion for audience coverage considering the splay angles between LSA cabinets and the source-to-receiver distances.

As the process for combined geometric-electronic optimization typically starts with the curving, this article is only focused on finding optimal tilt angles. These could be taken as a pre-processing stage for the optimization of the loudspeakers' driving functions, i.e., for the calculation of the FIR filter coefficients, or could also be applied for uniformly driven line arrays without further computation.

In this article we aim at introducing the analytical polygonal audience line curving (PALC) approach for finding appropriate LSA cabinet tilt angles with respect to the geometry of the receiver area and the intended coverage. The method can be used with different objectives, such as a constant interaction between adjacent cabinets with respect to the receiver geometry or by additionally considering amplitude attenuation over distance, i.e., sound pressure level (SPL) loss over distance. PALC is evaluated in comparison with typical standard LSA curving schemes (straight, arc, J, progressive, numerically optimized). Acoustic simulations based on the complex-directivity point source (CDPS) model [6, 15–17] including far-field radiation patterns

Table 1. List of abbreviations.

ARF	active radiating factor
ATF	acoustic transfer function
BEM	boundary element method
CDPS	complex-directivity point source
FIR	finite impulse response
HF	high frequency
LF	low frequency
LSA	line source array
MA	Martin Audio
MF	mid frequency
MZSFS	multi-zone sound field synthesis
PAL	polygonal audience line
PALC	polygonal audience line curving
PIP	position index plot
prog	progressive array
SPL	sound pressure level
str	straight array
WST	Wavefront Sculpture Technology

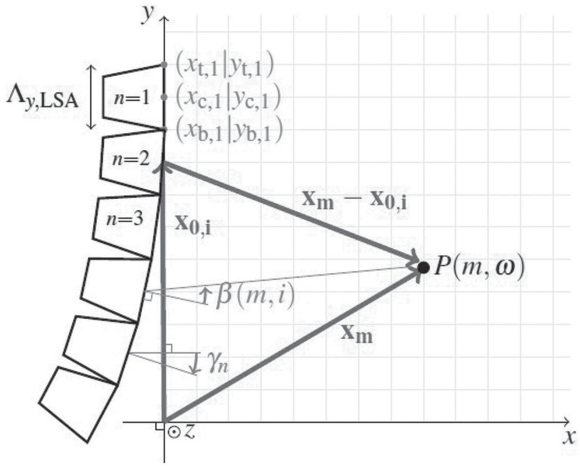

Fig. 1. Sketch of the LSA setup under discussion. A total of $N = 16$ LSA cabinets of the height $\Lambda_{y,\mathrm{LSA}} = 0.372$ m is used. See Table 11 and Table 12 for the deployed tilt angles γ_n.

of baffled line and circular pistons provide the basis for an evaluation of the introduced approach. One uniformly driven LSA model is analyzed for two concert venues.

The article is organized as follows. In Sec. 1 the chosen LSA model and the selected concert venues are presented. Mathematical fundamentals—among them especially the adjusted CDPS model—are shortly revisited in Sec. 2. In Sec. 3 the established WST approach is considered and the PALC algorithm is described. The evaluation criteria and the results for the different LSA curving schemes are shown in Sec. 4 and are discussed in Sec. 5. In Table 1 frequently used abbreviations of this article and in the Appendix in Table 2, Table 3, Table 4, Table 5 as well as in Table 6 frequently used mathematical variables of this article are arranged with regard to their application and formalism.

1 SIMULATION SETUP

An LSA setup is examined for two concert venues following practical examples presented in [10, Sec. 6.1] and in [18, Sec. 4.2.2] with audience and non-audience sections given within the vertical LSA radiation plane, i.e., the *xy*-plane in this case. While the first location is a typical multi-stand arena, the second one resembles a common open-air amphitheater geometry.

1.1 Line Source Array Setup

The LSA setup and the geometry under discussion are schematically depicted in Fig. 1 for calculating the sound pressure $P(m, \omega)$ at the m-th receiver position characterized by the vector $\mathbf{x_m}$ at the angular frequency ω. A total of $N = 16$ LSA cabinets with $n = 1, 2, ..., N$ is deployed. The front grille's height $\Lambda_{y,\mathrm{LSA}}$ of a single LSA cabinet is set to 0.372 m resulting in an overall LSA length of ca. 5.96 m. γ_n denotes the individual tilt angle of the n-th LSA cabinet and $\mathbf{x_{0,i}}$ denotes the vector of the front grille center position of the i-th LSA driver. The vectors $\mathbf{x_{t,n}}$, $\mathbf{x_{c,n}}$ and $\mathbf{x_{b,n}}$ define the top, center, and bottom position of the n-th LSA cabinet, respectively. With the radiation angle $\beta(m, i)$, the source-receiver configuration is specified for the i-th source and the m-th receiver position. Detailed information on the geometric setup can be found in [19, 20].

Built from three-way cabinets in this article, the exemplarily chosen LSA consists of $V_{\mathrm{LF}} = 1$, $V_{\mathrm{MF}} = 4$ and $V_{\mathrm{HF}} = 10$ vertically stacked, individually controlled drivers per cabinet for the low, the mid, and the high frequency band (LF, MF, HF). 12-inch, 3-inch, and 1.2-inch speakers are used for LF, MF, and HF, respectively. Thus, the LSA consists of a total of VN sources with $i = 1, 2, ..., VN$ for each frequency band.

Different frequency independent loudspeaker sensitivities are assumed in order to obtain realistic sound pressure values, $S_{\mathrm{LF}} = 96$ dB, $S_{\mathrm{MF}} = 88$ dB and $S_{\mathrm{HF}} = 112$ dB for vertical radiation in this case. The relation of the pistons' dimensions to the fixed distance between adjacent piston centers that is also known as Active Radiating Factor (ARF) [14, Sec. 3.2], [21] amounts to approximately 0.82. For LF and MF the circular piston model is deployed, while for HF the line piston model is used. For the frequency band crossover, fourth-order Linkwitz-Riley filters with the transition frequencies $f_{\mathrm{LF,\ MF}} = 400$ Hz and $f_{\mathrm{MF,\ HF}} = 1500$ Hz are applied.

1.2 Venue Geometry

A multi-stand arena [10, Sec. 6.1] and an open-air amphitheater [18, Sec. 4.2.2] with audience and non-audience sections, i.e., zones to be covered and zones to be avoided, are modeled by two dimensional slice representations. The multi-stand arena slice representation consists of four audience lines with different tilt angles and typifies a rather complex source-receiver configuration. Venue 2 resembles the Waldbuehne in Berlin and is composed of two audience lines with different tilt angles for the sake of simplicity. It conforms to an extreme long-throw application. In this article near-fills, side-fills and delayed arrays— that are

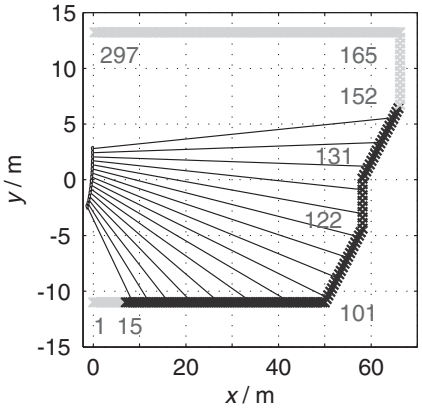

(a) Venue 1: multi-stand arena

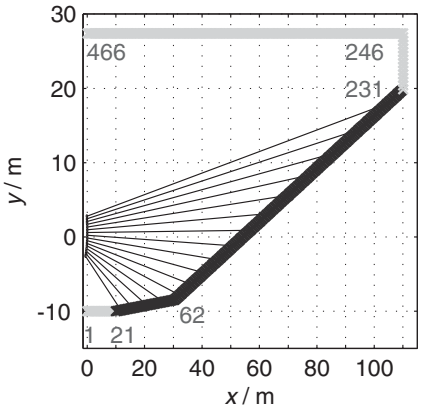

(b) Venue 2: amphitheater

Fig. 2. Venue slices within the *xy*-plane with audience (black) and non-audience/avoid (gray) zones and selected index numbers (change of audience/avoid zone and/or polygonal line's section angle) from M receiver positions.

routine in practical realizations—are not considered. Only the *xy*-plane is considered for vertical radiation, cf., Fig. 2. This is a common approach for optimization schemes of the loudspeakers' driving functions as the horizontal radiation is assumed to be convenient anyway, cf., [6–13].

The number of receiver positions taken into account is $M_{\mathrm{v1}} = 297$ for venue 1 and $M_{\mathrm{v2}} = 466$ for venue 2. They each comprise the receiver positions m with $m = 1, 2, ..., M$. This corresponds to a distance of 0.5 m between the receiver positions. The receiver positions are composed of M_{a} audience positions from the set $\mathcal{M}_{\mathrm{a}}$ and M_{na} non-audience positions from the set $\mathcal{M}_{\mathrm{na}}$ with $M = M_{\mathrm{a}} + M_{\mathrm{na}}$. They are characterized by the position vectors $\mathbf{x_m} = (x_m, y_m, 0)^{\mathrm{T}}$ and are numbered counterclockwise starting from the position under the LSA that is closest to the LSA (index 1, cf., Fig. 2). The venue slice coordinates are documented in Table 7 for venue 1 and in Table 8 for venue 2 in the Appendix.

Note that the terms *bright zone* and *dark zone* used in the field of multi-zone sound field synthesis (MZSFS) [22–24] correspond to the audience zone and the non-audience zone used in the field of sound reinforcement.

2 CALCULATION MODEL

The calculation model presented in this section is used for sound field prediction and for the evaluation of the different curving schemes. However, please note that the introduced analytical approach for finding LSA cabinet tilt angles (PALC) does not depend on a specific sound field prediction model.

Modeling multi-way cabinets, the total sound pressure at the receiver position m at the angular frequency ω is composed of the complex sound pressures, i.e., magnitudes and phases, of the different frequency bands as

$$P(m, \omega) = P_{\mathrm{LF}}(m, \omega) + P_{\mathrm{MF}}(m, \omega) + P_{\mathrm{HF}}(m, \omega). \quad (1)$$

Since the calculations are performed separately for each frequency band with a subsequent summation, the frequency band indices (LF, MF, HF) are omitted for generalization in the article. The sound field prediction is based on a complex-directivity point source (CDPS) model of baffled piston far-field radiation patterns. Its fundamental equation [16, Eq. (5)], [6, Eqs. (3–5)], [17, Sec. 1.1], [15, Eq. (11)] reads

$$P(m, \omega) = \sum_{i=1}^{i=V\,N} G(m, i, \omega)\, D(i, \omega) \quad (2)$$

considering the sources i with a total of N LSA cabinets each equipped with V loudspeakers in a specified frequency band.

$P(m, \omega)$ denotes the sound pressure at the receiver position $\mathbf{x_m}$ at the angular frequency ω. $G(m, i, \omega)$ terms the acoustic transfer function (ATF) from the i-th source to the m-th receiver position. The complex driving function $D(i, \omega)$ of the i-th source at the angular frequency ω is directly proportional to the source's velocity spectrum. Utilizing Eq. (2) for the sound field prediction, the calculated sound fields result from the superposition of the impact of each individual source i. The impact of each source is characterized by the source-receiver propagation characteristics—described by the ATF $G(m, i, \omega)$—and by the signal characteristics, i.e., the signal input as well as the electronic filters affecting the input of each source—described by the driving function $D(i, \omega)$.

Eq. (2) is modified including a loudspeaker sensitivity standardization in order to obtain absolute SPLs. Therefore $G(m, i, \omega)$ is considered as a scaled ATF for unit transformation

$$G(m, i, \omega) = p_0\, 10^{\frac{S(i,\omega)}{20}}\, R(\beta(m, i), \omega) \frac{\mathrm{e}^{-\mathrm{j}\,\frac{\omega}{c}\,|\mathbf{x_m} - \mathbf{x_{0,i}}|}}{|\mathbf{x_m} - \mathbf{x_{0,i}}|} \quad (3)$$

with the distance $|\mathbf{x_m} - \mathbf{x_{0,i}}|$ in meter, the reference sound pressure p_0 in Pascal and the sensitivity $S(i, \omega)$ in $\mathrm{dB_{SPL}}$ at 1 meter per Watt. The scaled ATF is composed of a specific far-field radiation pattern $R(\beta(m, i), \omega)$ for the radiation angle $\beta(m, i)$ at the angular frequency ω, the ideal point source wave propagation $\frac{\mathrm{e}^{-\mathrm{j}\,\frac{\omega}{c}\,|\mathbf{x_m} - \mathbf{x_{0,i}}|}}{|\mathbf{x_m} - \mathbf{x_{0,i}}|}$ with the velocity of sound c, the reference sound pressure p_0 that commonly amounts to $2 \cdot 10^{-5}$ Pa in air and the loudspeaker sensitivity $S(i, \omega)$ specifying the SPL in 1 m distance for 1 W electrical

input power. For all drivers and all frequencies per frequency band, the sensitivity is assumed to be constant, i.e., $S(i, \omega) = \text{const.}$

The complex driving function $D(i, \omega)$ of the i-th source at the angular frequency ω consists of the signal input $D_{\text{in}}(i, \omega)$, the complex optimized filter $D_{\text{opt}}(i, \omega)$ and the complex frequency band crossover as well as high-/lowpass filter $D_{\text{xo}}(\omega)$, thus

$$D(i, \omega) = D_{\text{in}}(i, \omega)\, D_{\text{opt}}(i, \omega)\, D_{\text{xo}}(\omega). \tag{4}$$

Gain and delay are mathematically considered as the amplitude and phase of these complex functions. As this article is exclusively focused on the curving of the LSA cabinets, only uniformly driven sources are considered, i.e.,

$$D_{\text{opt}}(i, \omega) = 1 \qquad \forall i \text{ and } \forall \omega. \tag{5}$$

The far-field radiation pattern of the baffled circular piston with radius Θ with a constant surface velocity is the normalized so-called jinc function [25, Eq. (26.42)]

$$R_{\text{c}}(\beta, \omega) = \frac{2\, J_1\left(\frac{\omega}{c}\Theta \sin\beta\right)}{\frac{\omega}{c}\Theta \sin\beta}, \tag{6}$$

denoting the cylindrical Bessel function of first kind of first order as $J_1(\,\cdot\,)$ [26, Eq. (10.2.2)]. The line piston models an ideal waveguide of height Λ_y for the HF band and its sinc-function far-field radiation pattern can be written as [25, Eq. (26.44)]

$$R_{\text{l}}(\beta, \omega) = \frac{\sin\left(\frac{\omega}{c}\frac{\Lambda_y}{2}\sin\beta\right)}{\frac{\omega}{c}\frac{\Lambda_y}{2}\sin\beta}. \tag{7}$$

Note that these patterns exhibit main lobe unity gain (i.e., 0 dB for $\beta = 0$) in order to control the energy radiated by the pistons via the assumed sensitivities.

Accounting for all receiver positions M for a single angular frequency ω, Eq. (2) is rewritten in matrix notation,

$$\mathbf{p}(\omega) = \mathbf{G}(\omega)\, \mathbf{d}(\omega) \tag{8}$$

with $\mathbf{p}(\omega)$ denoting the $(M \times 1)$ vector of sound pressures for all considered receiver positions $\mathbf{x_m}$, $\mathbf{G}(\omega)$ denoting the $(M \times VN)$ scaled ATF matrix for all sources i and for all receiver positions m and $\mathbf{d}(\omega)$ denoting the $(VN \times 1)$ vector of the complex driving functions for all sources i per angular frequency ω.

In line with this modeling, air absorption is neglected, a constant velocity of sound ($c = 343$ m/s) and for the modeled sources infinite, straight baffles and a constant piston's surface velocity are assumed. The sound field predictions are performed for a logarithmically spaced frequency vector with $f_{\text{start}} = 200$ Hz, $f_{\text{stop}} = 20$ kHz and 1/36 octave resolution.

3 CURVING OPTIMIZATION

Since it is a common approach to restrict the optimization schemes for the LSA driving functions to the vertical plane, it may also be advantageous to seek appropriate tilt angles of the LSA cabinets based on the venue slices from Sec. 1.2. In [8, 10, 13] this is executed by a numerical multi-objective optimization method that is used for determining the electronic drive as well. From [14, p. 929] the Wavefront Sculpture Technology (WST) criteria for LSAs are known. The practical consequences of criterion number four for determining the tilt angles are revisited in Sec. 3.1.

In Sec. 3.2 and Sec. 3.3 of this contribution, a purely analytical approach for finding practical LSA cabinet tilt angles with respect to the geometry of the receiver area and the intended coverage is presented: the polygonal audience line curving (PALC). PALC was originally developed to be applied beforehand to a numerical optimization of the loudspeakers' driving functions. The method can be used with different objectives, such as a constant interaction between adjacent cabinets with respect to the receiver geometry or by additionally considering SPL loss over distance.

3.1 Wavefront Sculpture Technology Approach

In [14, 27, 28], several criteria based on the Fresnel approach and analytical derivations of the diffraction theory are denoted as Wavefront Sculpture Technology. WST consists of five criteria how to create a homogeneous wavefront based on geometric LSA shaping. These criteria include the spatial sampling condition specifying the maximum allowed distance between adjacent sources and the Active Radiating Factor (ARF) theorem specifying the maximum relation of the pistons' dimensions to the fixed distance between the acoustic centers of adjacent sources. A further criterion defines the maximum allowed wavefront curvature at the waveguide's exit for high frequency radiation. These criteria are aimed for minimized grating lobe radiation that generally enables homogeneous wavefront shaping. The remaining criteria define the maximum allowed splay angle between adjacent LSA cabinets and an optimal array curvature to provide a homogeneous and frequency independent SPL loss over the audience using an appropriate wavefront shape, cf., [21, 29, 30].

Considering the splay angles, criterion number four states that the product of the splay angle α_n, i.e., the difference of the tilt angles of the $(n + 1)$-th and the n-th LSA cabinet, and the distance Δ_n from the center of the respective boxes to the receivers should be constant for an SPL attenuation of 3 dB per distance doubling.

Three different LSA curvatures derived from WST number four are introduced in [31]: the constant curvature, the J-shape curvature, and the progressive curvature as visualized in Fig. 3. The progressive curvature corresponds to the SPL attenuation of 3 dB per distance doubling directly resulting from WST number four. For an SPL attenuation of 6 dB per distance doubling the constant curvature with $\alpha_n = \text{const.}$ is recommended. If a constant sound pressure level over the audience zone is demanded, the J-shape curvature with $\alpha_n \cdot \Delta_n^2 = \text{const.}$ is used.

3.2 Polygonal Audience Line

The positions of the audience zones in the vertical radiation plane can be mathematically interpreted as polygonal line with the total length Γ_0. Fig. 4 represents an exemplary

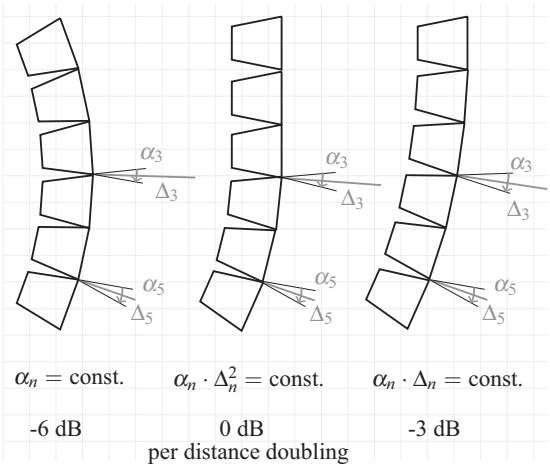

Fig. 3. Constant curvature, J-shape curvature, and progressive curvature according to WST for obtaining the denoted target SPL characteristics per distance doubling. The prerequisites for the splay angles α_n and the distances Δ_n to the receivers are denoted.

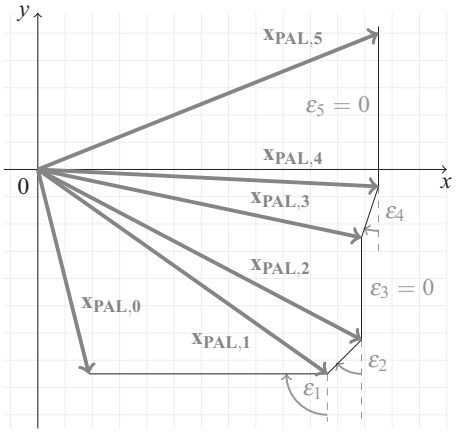

Fig. 4. Polygonal audience line (PAL) with K sections (in this case: $K = 5$). The start position of the k-th line section is specified by the vector $\mathbf{x_{PAL,k-1}}$ and the stop position is given by the vector $\mathbf{x_{PAL,k}}$. ε_k denotes the tilt angle of the k-th line section.

polygonal audience line (PAL) that is similar to venue 1 with K sections [$k = 0, 1, 2, ..., K$] with the tilt angles ε_k. The k-th line section is specified by the vectors $\mathbf{x_{PAL,k-1}}$ for the start position and $\mathbf{x_{PAL,k}}$ for the stop position. With these vectors, the total PAL length is

$$\Gamma_0 = \sum_{k=1}^{k=K} |\mathbf{x_{PAL,k}} - \mathbf{x_{PAL,k-1}}|. \tag{9}$$

The K PAL sections are covered by N LSA cabinets with $n = 1, 2, ..., N$. The polygonal audience line is therefore divided into N segments that represent the main radiation area of the LSA cabinets. Γ_n denotes the length of the n-th segment with the distance $\Gamma_{n,1}$ from the top to the center

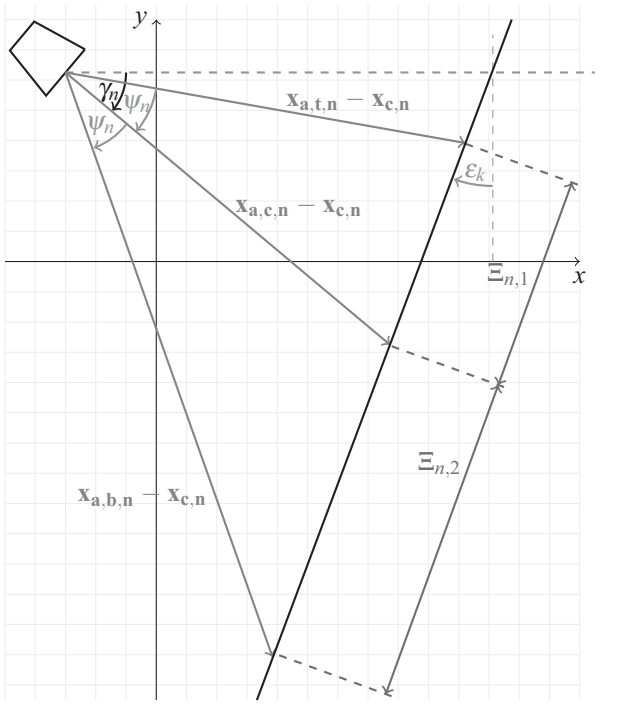

Fig. 5. Sketch of one section of the polygonal audience line with the n-th segment including only one section. The line section is not changed.

position and $\Gamma_{n,2}$ from the center to the bottom position of the segment, i.e., $\Gamma_n = \Gamma_{n,1} + \Gamma_{n,2}$. From

$$\Gamma = \sum_{n=1}^{n=N} \Gamma_n \tag{10}$$

the total length Γ of the covered audience line sections can be concluded. The different audience zones are indexed from the lowest to the highest audience positions. In order to calculate the position and the tilt angle γ_n of each LSA cabinet, it is necessary to start with the uppermost cabinet and compute iteratively from top to bottom.

3.3 PALC Algorithm

Starting with $n = 1$ and $k = K$, i.e., the topmost LSA cabinet and the topmost audience positions, n is iteratively increased and k is decreased. See Fig. 5 for detailed geometric information. Either the coverage angles ψ_n of all LSA cabinets are specified resulting in N required LSA cabinets that may differ from the intended original number of cabinets or the number N of LSA cabinets is fixed. The latter means that the angles ψ_n are found iteratively depending on the length Γ of the polygonal audience line and starting from the initial coverage angles ψ_{init} for all LSA boxes. Note that only discrete values can be typically set for the tilt angles of practical LSAs. By rounding the tilt angles γ_n in Eq. (11) after each calculation, the algorithm can be easily adapted concerning this matter. The algorithm is designed as follows:

I) Compute the tilt angle γ_n of the n-th LSA cabinet from the slope

$$\tan(-\gamma_n + \psi_n) = \frac{y_{\mathrm{a,t},n} - y_{\mathrm{c},n}}{x_{\mathrm{a,t},n} - x_{\mathrm{c},n}} \tag{11}$$

with the vector $\mathbf{x_{a,t,n}} = (x_{\mathrm{a,t},n},\, y_{\mathrm{a,t},n})^{\mathrm{T}}$ of the top position of the n-th polygonal audience line segment. The vector $\mathbf{x_{c,n}}$ of the n-th LSA cabinet center position is given as

$$\mathbf{x_{c,n}} = \begin{pmatrix} x_{\mathrm{c},n} \\ y_{\mathrm{c},n} \end{pmatrix} = \begin{pmatrix} x_{\mathrm{t},n} \\ y_{\mathrm{t},n} \end{pmatrix} - \frac{\Lambda_{y,\mathrm{LSA}}}{2} \begin{pmatrix} \sin\gamma_n \\ \cos\gamma_n \end{pmatrix} \tag{12}$$

with the height $\Lambda_{y,\mathrm{LSA}}$ of a single LSA cabinet and the vector $\mathbf{x_{t,n}} = (x_{\mathrm{t},n},\, y_{\mathrm{t},n})^{\mathrm{T}}$ of the n-th LSA cabinet top position. The initial values are set to

$$\begin{pmatrix} x_{\mathrm{t},1} \\ y_{\mathrm{t},1} \end{pmatrix} = \begin{pmatrix} x_{\mathrm{H}} \\ y_{\mathrm{H}} \end{pmatrix} \tag{13}$$

and

$$\mathbf{x_{a,t,1}} = \mathbf{x_{PAL,K}}. \tag{14}$$

x_{H} and y_{H} are the coordinates of the top position of the uppermost LSA cabinet and the vector $\mathbf{x_{PAL,K}}$ points at the top position of the K-th polygonal audience line section.

II) Calculate the center position vector $\mathbf{x_{c,n}}$ of every LSA cabinet with Eq. (12), i.e., for $n = 1, 2, ..., N$.

III) Compute the required distance $\Xi_{n,1}$ from the top to the center position of the n-th polygonal audience line segment with

$$\Xi_{n,1} = |\mathbf{x_{a,t,n}} - \mathbf{x_{c,n}}| \frac{\sin\psi_n}{\cos(\varepsilon_k - \gamma_n)}. \tag{15}$$

including the n-th coverage angle ψ_n and the tilt angle ε_k of the k-th polygonal audience line section.

We have to consider two cases: for case (i) equation

$$\Xi_{n,1} \le |\mathbf{x_{a,t,n}} - \mathbf{x_{PAL,k-1}}| \tag{16}$$

holds, i.e., the calculated distance $\Xi_{n,1}$ is equal or smaller than the distance from the start position of the k-th polygonal audience line section to the top position of the n-th polygonal audience line segment, so that the section of the polygonal audience line is not changed. The center position vector of the current polygonal audience line segment can be calculated with

$$\mathbf{x_{a,c,n}} = \mathbf{x_{a,t,n}} + \Xi_{n,1} \begin{pmatrix} \cos\varepsilon_k \\ \sin\varepsilon_k \end{pmatrix} \tag{17}$$

and hence the segment's upper partial length $\Gamma_{n,1}$ is

$$\Gamma_{n,1} = \Xi_{n,1}. \tag{18}$$

If for case (ii) equation

$$\Xi_{n,1} > |\mathbf{x_{a,t,n}} - \mathbf{x_{PAL,k-1}}| \tag{19}$$

holds, i.e., the calculated distance $\Xi_{n,1}$ is greater than the distance from the start position of the k-th polygonal audience line section to the top position of the n-th polygonal audience line segment, so that the section of the polygonal audience line is changed. The n-th partial segment angle $\tilde{\psi}_n$ has to be calculated with

$$\frac{|\mathbf{x_{a,t,n}} - \mathbf{x_{PAL,k-1}}|}{|\mathbf{x_{a,t,n}} - \mathbf{x_{c,n}}|} = \frac{\sin(\psi_n - \tilde{\psi}_n)}{\cos(\varepsilon_k - \gamma_n + \tilde{\psi}_n)}. \tag{20}$$

The partial distance $\tilde{\Xi}_{n,1}$ from the top to the center position of the n-th polygonal audience line segment is thus

$$\tilde{\Xi}_{n,1} = |\mathbf{x_{PAL,k-1}} - \mathbf{x_{c,n}}| \frac{\sin\tilde{\psi}_n}{\cos(\varepsilon_{k-1} - \gamma_n)} \tag{21}$$

and the center position vector of the current polygonal audience line segment can be written as

$$\mathbf{x_{a,c,n}} = \mathbf{x_{PAL,k-1}} + \tilde{\Xi}_{n,1} \begin{pmatrix} \cos\varepsilon_{k-1} \\ \sin\varepsilon_{k-1} \end{pmatrix} \tag{22}$$

and hence

$$\Gamma_{n,1} = |\mathbf{x_{a,t,n}} - \mathbf{x_{PAL,k-1}}| + \tilde{\Xi}_{n,1} \tag{23}$$

is the segment's upper partial length.

IV) Update k: k is not changed if the section of the polygonal audience line was not changed (step III, case (i)). k has to be decreased by 1 if the section of the polygonal audience line was changed (step III, case (ii)).

V) Calculate the required distance $\Xi_{n,2}$ from the center to the bottom position of the n-th polygonal audience line segment with

$$\Xi_{n,2} = |\mathbf{x_{a,c,n}} - \mathbf{x_{c,n}}| \frac{\sin\psi_n}{\cos(\varepsilon_k - \gamma_n - \psi_n)} \tag{24}$$

including the n-th coverage angle ψ_n and the tilt angle ε_k of the k-th polygonal audience line section.

We again have to consider two cases: for case (i) equation

$$\Xi_{n,2} > |\mathbf{x_{a,c,n}} - \mathbf{x_{PAL,k-1}}| \tag{25}$$

holds, i.e., the calculated distance $\Xi_{n,2}$ is greater than the distance from the start position of the k-th polygonal audience line section to the center position of the n-th polygonal audience line segment, so that the section of the polygonal audience line is changed. The n-th partial segment angle $\tilde{\psi}_n$ then has to be calculated with

$$\frac{|\mathbf{x_{a,c,n}} - \mathbf{x_{PAL,k-1}}|}{|\mathbf{x_{a,c,n}} - \mathbf{x_{c,n}}|} = \frac{\sin\tilde{\psi}_n}{\cos(\varepsilon_k - \gamma_n - \tilde{\psi}_n)}. \tag{26}$$

Therefore, the partial distance $\tilde{\Xi}_{n,2}$ from the center to the bottom position of the n-th polygonal audience line segment is

$$\tilde{\Xi}_{n,2} = |\mathbf{x_{PAL,k-1}} - \mathbf{x_{c,n}}| \frac{\sin(\psi_n - \tilde{\psi}_n)}{\cos(\varepsilon_{k-1} - \gamma_n - \psi_n)} \tag{27}$$

and the bottom position vector of the current polygonal audience line segment can be written as

$$\mathbf{x_{a,b,n}} = \mathbf{x_{PAL,k-1}} + \tilde{\Xi}_{n,2} \begin{pmatrix} \cos\varepsilon_{k-1} \\ \sin\varepsilon_{k-1} \end{pmatrix}. \tag{28}$$

Hence the segment's lower partial length is

$$\Gamma_{n,2} = |\mathbf{x_{a,c,n}} - \mathbf{x_{PAL,k-1}}| + \tilde{\Xi}_{n,2}. \tag{29}$$

If for case (ii) equation

$$\Xi_{n,2} \le |\mathbf{x_{a,c,n}} - \mathbf{x_{PAL,k-1}}| \tag{30}$$

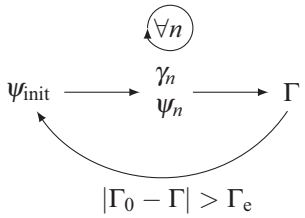

Fig. 6. Overview of the iterative PALC process with the initial coverage angle ψ_{init}, the n-th coverage angle ψ_n, the tilt angle γ_n of the n-th LSA cabinet, the total polygonal audience line length Γ_0, the total length of the covered polygonal audience line sections Γ and the termination condition Γ_e.

is valid, i.e., the calculated distance $\Xi_{n,2}$ is equal or smaller than the distance from the start position of the k-th polygonal audience line section to the center position of the n-th polygonal audience line segment, so that the section of the polygonal audience line is not changed, the bottom position vector of the current polygonal audience line segment can be calculated with

$$\mathbf{x_{a,b,n}} = \mathbf{x_{a,c,n}} + \Xi_{n,2}\begin{pmatrix}\cos\varepsilon_k\\ \sin\varepsilon_k\end{pmatrix} \tag{31}$$

and eventually

$$\Gamma_{n,2} = \Xi_{n,2}. \tag{32}$$

is the segment's lower partial length.

VI) Update k: k is not changed if the section of the polygonal audience line was not changed (step V, case (ii)). k has to be decreased by 1 if the section of the polygonal audience line was changed (step V, case (i)).

The steps I) – VI) have to be repeated until $n = N$ and $k = 0$. If the number N of LSA cabinets is fixed and the coverage angles ψ_n are to be determined, the values of the total polygonal audience line length Γ_0 and of the total length of the covered polygonal audience line sections Γ are compared after each complete iteration. All ψ_n are decreased if the total length of the covered polygonal audience line sections Γ is greater than the total polygonal audience line length Γ_0, and all ψ_n are increased if Γ is smaller than Γ_0. This termination condition is denoted as Γ_e. In Fig. 6, the iteration process is visualized.

4 EVALUATION

Acoustic simulations based on the CDPS model including far-field radiation patterns of baffled line and circular pistons provide the data for an evaluation of the introduced approach. The evaluation is performed for two conditions and in comparison with typical standard LSA curving schemes such as straight, arc, J, and progressive [30] as well as two numerically optimized versions resulting from the Martin Audio Display prediction and optimization software [8, 13]. Note that we deliberately distinguish between the WST curvatures from Sec. 3.1 and the specifications in [30]. The nomenclature from the latter is used for the curvings in this article.

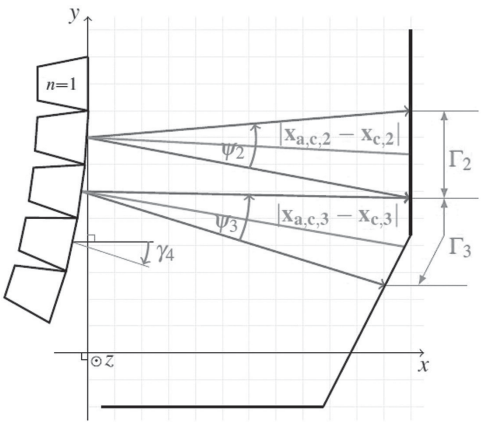

Fig. 7. Sketch of the LSA setup following the PALC1 and PALC2 approach. It is exemplarily shown for the second and the third LSA box. γ_n denotes the tilt angle of the n-th LSA cabinet, ψ_n denotes the n-th coverage angle, $|\mathbf{x_{a,c,n}} - \mathbf{x_{c,n}}|$ denotes the distance from the center positions of the n-th polygonal audience line segment and of the n-th LSA cabinet and Γ_n denotes the length of the n-th polygonal audience line segment.

PALC1 incorporates the goal of an invariant interaction between adjacent cabinets with respect to the receiver geometry in order that the radiated sound of the different sources overlap at a constant coverage angle ψ in the far-field of the individual sources. This constraint simply reads

$$\text{PALC1:} \qquad \psi_1 = \psi_2 = \psi_3 = ... = \text{const.} \tag{33}$$

PALC1 is similar to an arc array but the goal does not refer to the array itself, i.e., constant splay angles between all cabinets, but it refers to the shape of the receiver geometry.

The distances of the different positions from the sources and the desired sound field are considered in PALC2. It demands a constant product of the coverage angle ψ and the distance from the source to the receiver positions, i.e., the distance from the center positions of the n-th polygonal audience line segment and of the n-th LSA cabinet,

$$\begin{aligned}\text{PALC2:} \qquad & \psi_1 \cdot |\mathbf{x_{a,c,1}} - \mathbf{x_{c,1}}| \\ & = \psi_2 \cdot |\mathbf{x_{a,c,2}} - \mathbf{x_{c,2}}| = \ldots = \text{const.},\end{aligned} \tag{34}$$

cf., Fig. 5. This results from an approximation of

$$\begin{aligned}&\tan\psi_1 \cdot |\mathbf{x_{a,c,1}} - \mathbf{x_{c,1}}| \\ &\quad = \tan\psi_2 \cdot |\mathbf{x_{a,c,2}} - \mathbf{x_{c,2}}| = \ldots = \text{const.}\end{aligned} \tag{35}$$

for small ψ_n. Eq. (35) arises from a simplification of attaining a constant length Γ_n for all n polygonal audience line segments. In Fig. 7 the geometric variables being relevant for PALC1 and PALC2 are exemplarily shown for the second and the third LSA box. The PALC2 constraint should not be confused with the Wavefront Sculpture Technology criterion number four, cf., Sec. 3.1, Table 9, and Table 10.

For the evaluation cases MA1 and MA2, the tilt angles were extracted from the commercially available prediction and optimization software Martin Audio Display (version 2.1.10) that provides suitable tilt angles and also—if desired—the electronic control by means of a numerical multi-objective optimization scheme [8, 10, 13]. The

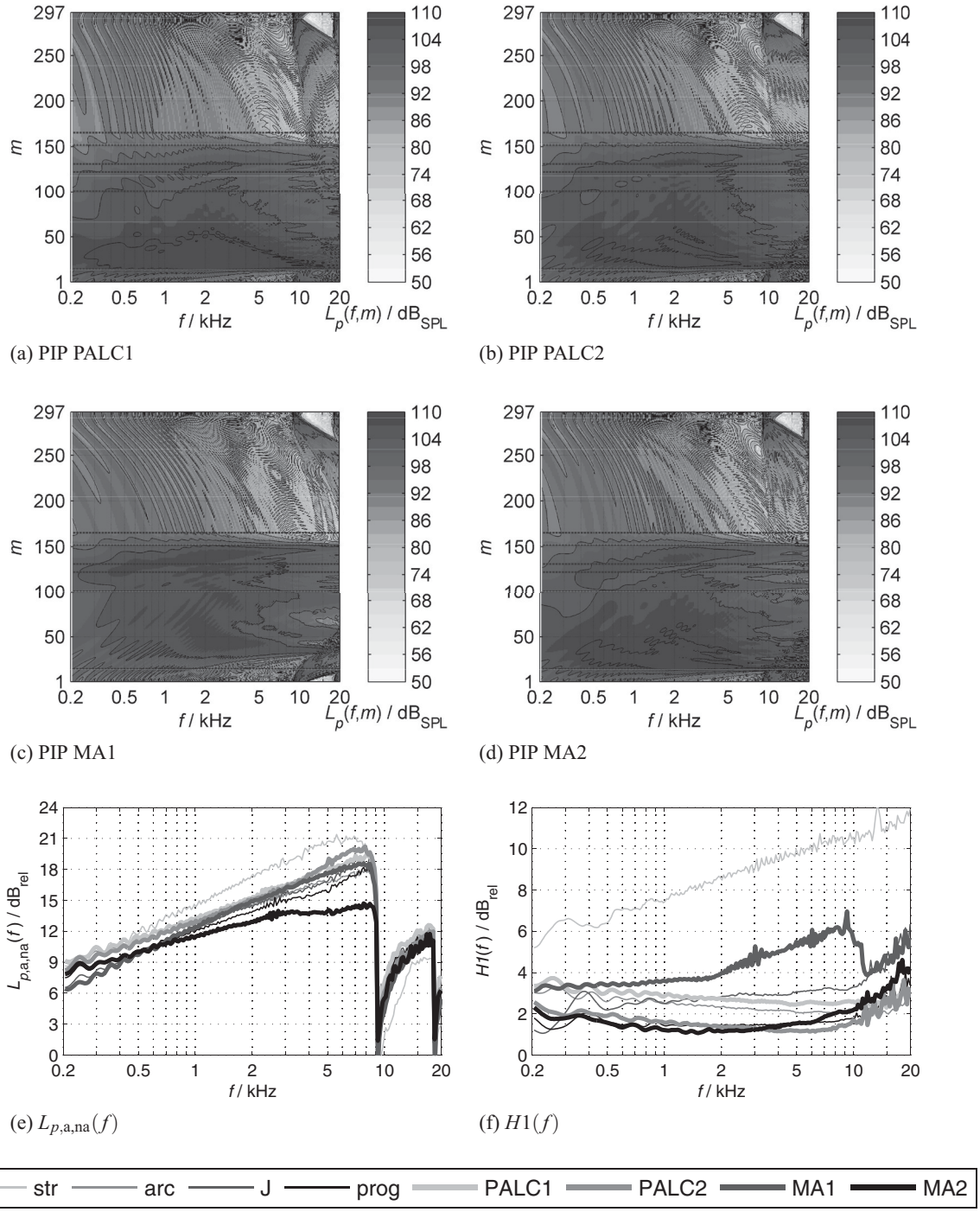

Fig. 8. Position index plots (PIPs) depending on the frequency f and the position index m for PALC1, PALC2, MA1 and MA2, the acoustic contrast $L_{p,\mathrm{a,na}}(f)$ and the homogeneity measure $H1(f)$ depending on the frequency f for all analyzed curvings for venue 1 from Fig. 2a. The dashed horizontal lines in the PIPs refer to the selected index numbers in Fig. 2a which represent changes of the audience/avoid zone and/or of the polygonal line's section angle.

weighting parameters for target and leakage each are set to 1 for MA1 and are set to 10 and 4 for MA 2 allowing a SPL attenuation of 10 dB from the first to the last audience position. Note that the optimization parameters target and leakage are quantitatively specified as the absolute error Eq. (36) and the acoustic contrast Eq. (39) in our case.

A reasonable selection of the evaluation criteria that were suggested in [20] is utilized to assess the quality of the different curving approaches. The position index plots (PIPs) show the resulting SPL spectra at all receiver positions $\mathbf{x_m}$, i.e., the sound pressure levels $L_p(\omega, m)$ depending on the angular frequency ω and the position index m. They are depicted in Fig. 8 for PALC1, PALC2, MA1, and MA2 for venue 1 and in Fig. 9 for venue 2. Also known as positional map, the PIPs were used in [7, 8, 10, 11, 13] as well. The "ideal" PIP depends on the application. In general, it is

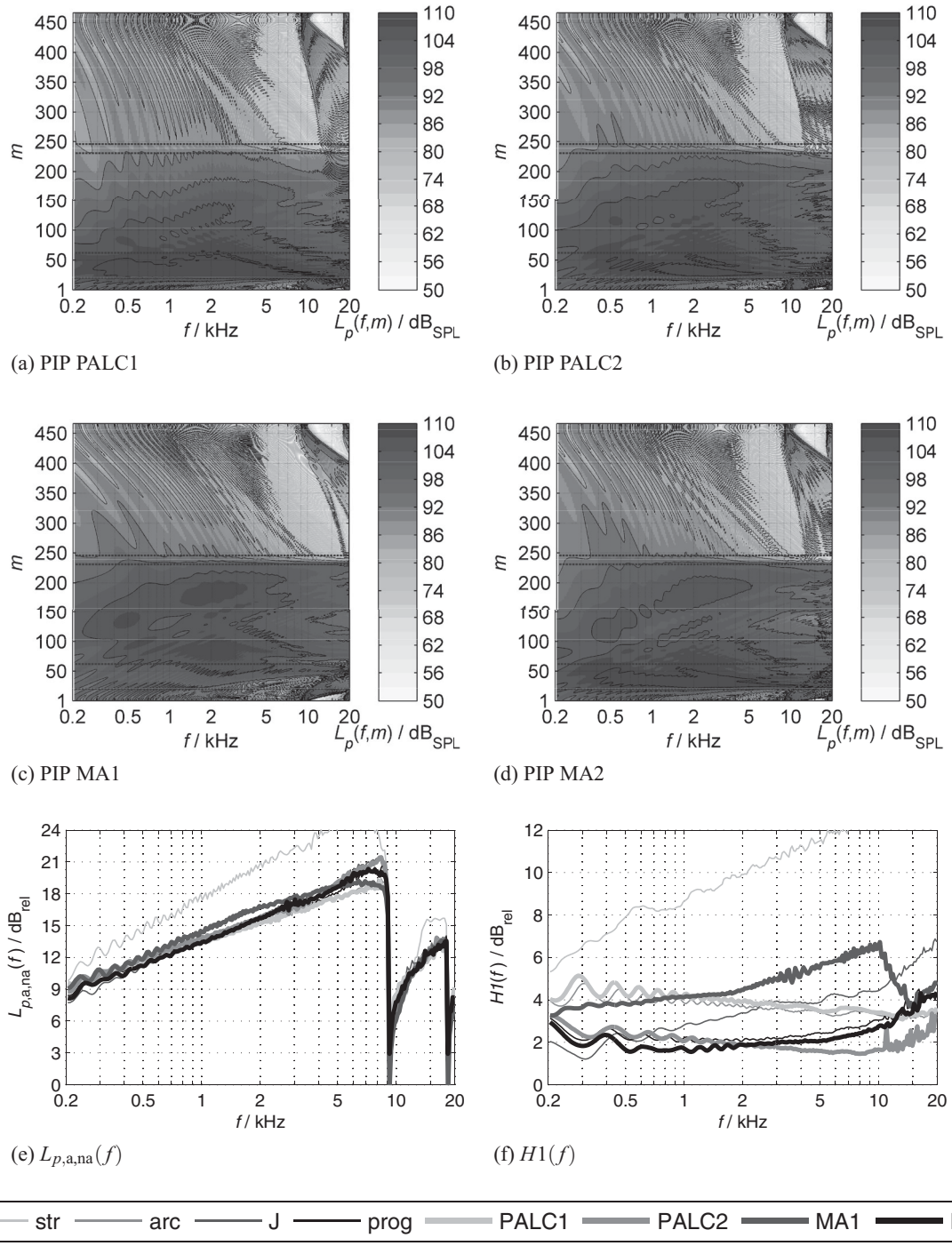

Fig. 9. Position index plots (PIPs) depending on the frequency f and the position index m for PALC1, PALC2, MA1 and MA2, the acoustic contrast $L_{p,\mathrm{a,na}}(f)$ and the homogeneity measure $H1(f)$ depending on the frequency f for all analyzed curvings for venue 2 from Fig. 2b. The dashed horizontal lines in the PIPs refer to the selected index numbers in Fig. 2b which represent changes of the audience/avoid zone and/or of the polygonal line's section angle.

desired that only little energy is radiated into the non-audience zones compared to the audience zones, i.e., for the position indices m that belong to the non-audience zones, low SPLs are expected all frequencies f. For the receiver positions m that belong to the audience zones, maximum SPLs, a predefined SPL or a constant SPL at all frequencies may be desired.

The quantitative evaluation is based on three technical quality measures. Denoting the squared Euclidean norm $\|\cdot\|_2^2$ [26, Eq. (3.2.13)], the frequency dependent absolute amplitude error [20, Eq. (16)]

$$E(\omega) = \left\| \underset{m\in\mathcal{M}_\mathrm{a}}{\mathbf{p}(\omega)} - \underset{m\in\mathcal{M}_\mathrm{a}}{\mathbf{p}_\mathrm{des}(\omega)} \right\|_2^2 \tag{36}$$

between the obtained sound field $\mathbf{p}(\omega)$ and the desired sound field $\mathbf{p}_\mathrm{des}(\omega)$ in the audience zone, i.e., $m \in \mathcal{M}_\mathrm{a}$, is additionally smoothed in third-octave bands. The desired

sound field $\mathbf{p}_{\mathrm{des}}(\omega)$ could in principle be set arbitrarily. However, the used array geometry restricts the choice to physically realizable wave fronts. Typically a desired level decay over the audience zone and a level offset for the avoid zone can be defined in practical realizations [8].

We have chosen

$$P_{\mathrm{des}}(m, \omega) \propto \frac{\mathrm{e}^{-\mathrm{j}\frac{\omega}{c}|\mathbf{x_m}-\mathbf{x_S}|}}{\sqrt{|\mathbf{x_m}-\mathbf{x_S}|}} \tag{37}$$

at the receiver position m and the angular frequency ω as the basis for the comparison. This desired sound field complies with a sound field generated by a virtual line source at the position $\mathbf{x_S}$ deploying the large argument-approximation of the 2D Green's function, i.e., for high frequencies and/or in the far-field [32, Eq. (26)]. The source position $\mathbf{x_S}$ is individually calculated for each LSA configuration depending on the top position vector $\mathbf{x_{t,1}}$ of the first (topmost) LSA cabinet and the bottom position vector $\mathbf{x_{b,16}}$ of the last (bottommost) LSA cabinet, i.e.,

$$\mathbf{x_S} = \frac{1}{2}\left[\begin{pmatrix} x_{\mathrm{t},1} \\ y_{\mathrm{t},1} \end{pmatrix} + \begin{pmatrix} x_{\mathrm{b},16} \\ y_{\mathrm{b},16} \end{pmatrix}\right]. \tag{38}$$

A target sound pressure level of 100 $\mathrm{dB_{SPL}}$ at the first receiver position within the audience zone is expected.

Alternatively, we could have also chosen other desired sound fields, such as constant SPLs or maximum SPLs at all receiver positions m or a 6 dB SPL loss per distance doubling. Since this article is focused on modeled loudspeaker data, we selected an ideal 3 dB SPL loss per distance doubling which is provided by an infinite, continuous line source and can be unambiguously expressed by Eq. (37). Using measured loudspeaker data, other target sound fields may be more advantageous, such as sound fields that are directly based on the sound fields generated by uniformly driven LSAs.

Moreover, the frequency dependent relation of the obtained average SPLs of the audience and the non-audience zone

$$L_{p,\mathrm{a,na}}(\omega) = 10\ \log_{10}\left(\frac{\frac{1}{M_{\mathrm{a}}}\left\|\mathbf{p}(\omega)_{m\in\mathcal{M}_{\mathrm{a}}}\right\|_2^2}{\frac{1}{M_{\mathrm{na}}}\left\|\mathbf{p}(\omega)_{m\in\mathcal{M}_{\mathrm{na}}}\right\|_2^2}\right) \tag{39}$$

[20, Eq. (18)] is evaluated, i.e., considering the sound pressures for the receiver positions of the set of the audience positions in the numerator and of the set of the non-audience positions in the denominator. This measure is depicted in Fig. 8e and Fig. 9e and corresponds to the acoustic contrast [22, Eq. (16)], [23, Eq. (2)] established in MZSFS. Quantifying the homogeneity of the generated sound field based on the magnitudes, neglecting the phases in this case, the frequency dependent standard deviation of the distance compensated SPLs of all audience positions

$$H1(\omega) = \underset{m\in\mathcal{M}_{\mathrm{a}}}{\sigma}\left[20\ \log_{10}\left(\frac{|P(m,\omega)|}{p_0}\sqrt{\frac{|\mathbf{x_m}-\mathbf{x_S}|}{|\mathbf{x_{min(m)}}-\mathbf{x_S}|}}\right)\right], \tag{40}$$

cf., [11, e.g. Fig. 6, Fig. 8], is analyzed. σ denotes the standard deviation and $\mathbf{x_{min(m)}}$ is the vector for the first audience position in this case. Note that the root term results from the distance compensation referring to the desired 3 dB SPL loss per distance doubling of a virtual line source. The homogeneity measure is visualized in Fig. 8f and Fig. 9f.

5 DISCUSSION

For two concert venues, the proposed algorithm for optimizing the tilt angles of line array cabinets was evaluated with respect to different quality measures. The position index plots (PIPs) for venue 1 (Fig. 2a) shown in Fig. 8 reveal that only little energy is radiated into the non-audience zones compared to the audience zones for all of the algorithmic curving schemes. Note that the dashed horizontal lines in the PIPs refer to the selected index numbers in Fig. 2 which represent changes of the audience/avoid zone and/or of the polygonal line's section angle. For both venues, the audience zone is located between the second uppermost and the bottommost dashed horizontal line.

The intended behavior is confirmed by $L_{p,\mathrm{a,na}}(\omega)$ from Eq. (39) in Fig. 8e for the optimized curvings as well as for the standard curving schemes (straight, arc, J, and progressive) that were manually adjusted to the receiver geometry. It can be seen in the PIPs and by means of $L_{p,\mathrm{a,na}}(\omega)$ that the relation of the energy radiated into the audience and the non-audience zones is very similar for all tilt angle sets and increases with increasing frequency. The latter results from the radiation characteristics of the sources: the radiation is more directed, the higher the frequency.

$L_{\ p,\mathrm{a,na}}(\omega)$ features acceptable values larger than 12 dB for frequencies above 1 kHz and below ca. 8.5 kHz. For frequencies above ca. 8.5 kHz spatial aliasing effects are visible leading to more energy in the non-audience zones and significantly reduced acoustic contrast values. The grating lobes that are causal for that appear at rather high frequencies compared to conventional LSA designs due to the small distances between the HF sources. Choosing equal weights for target and leakage, the final angle of the numerically optimized MA1 is rather small. Therefore, the first audience rows are hardly reinforced as it can be deduced from the MA1 PIP. Increasing the target weight in relation to the leakage weight, the final angle of MA2 approximately corresponds to those of the other curving methods. Comparing MA1 and MA2, the effect of the reduced focus on leakage can be clearly observed by means of $L_{p,\mathrm{a,na}}(\omega)$ for frequencies above ca. 700 Hz.

Significant performance differences can be found with the help of the homogeneity measure $H1(\omega)$ from Eq. (40). The straight array does not cover the whole audience zone so that there are large deviations considering the front, the middle, and the back audience positions. For the front positions, MA1 shows a similar performance due to the small final angle. The arc and J array suffer from limited adjustment capabilities to the given receiver geometry. PALC2 and MA2 provide the best homogeneity values with MA2

being more homogeneous than PALC2 for frequencies below ca. 2 kHz. For frequencies above ca. 2 kHz, $H1(\omega)$ of PALC2 is smaller than the one of MA2 for up to (1...1.5) dB. The PIP of MA2, however, reveals some coverage gaps for the middle positions around $m \approx 110$ due to some large splay angles. An invariant interaction between adjacent cabinets that was intended with PALC1 does not seem to be practical considering homogeneity. As expected, the progressive curving yields solid results without paying attention to the specific composition of the receiver geometry.

For venue 2 (Fig. 2b) resembling a typical open-air amphitheater, the results are very similar to those for venue 1. Only the expected difference of the acoustic contrast $L_{p,\mathrm{a,na}}(\omega)$ between MA1 and MA2 is not observable for venue 2. Note that the absolute error $E(\omega)$ from Eq. (36) is not visualized as it provides no meaningful results for the uniformly driven LSAs.

The tilt angles calculated with the PALC2 approach were compared with the established WST criterion number four for venue 1 and venue 2. It can be found in Table 9 and Table 10 in the Appendix that PALC2 provides results that are in accordance with the demand for a constant product of the splay angles and the respective source-to-receiver distances. The absolute values of the products are constant depending on the polygonal audience line section that the involved LSA cabinets are pointing at.

Using the PALC approach, it is assumed that all deployed LSA cabinets have similar radiation patterns. Frequency dependent behavior and individual characteristics of the LSA radiation are not considered. All audio frequencies are treated equally, there is no preference for selected frequencies or frequency bands. This enables a low-computational and straight-forward calculation without the need of numerical algorithms requiring high computational effort, but this may reduce the achievable accuracy. However, PALC completely incorporates the present receiver geometry. In addition, the comparison of the PALC2 results and the respective WST criterion reveals that the assumptions do not turn away from the assumptions made for the established WST approach.

The evaluation is not based on measurements in this article but only on simulations. Therefore, the results may differ from measured and perceived sound fields of practical LSAs. Since typical trial-and-error-approaches by sound engineers, i.e., manual adjustment of the LSA cabinet tilt angles, follow similar principles as PALC and due to the PALC tilt angles being in accordance with WST, similar results can be expected for measurements. The precision of the sound field prediction may be improved by incorporating data from balloon measurements that also include the influence of adjacent cabinets or by using boundary element method (BEM) data [17]. Measured loudspeaker data can be included as far-field radiation patterns $R(\beta, \omega)$ in the deployed CDPS calculation model. Comparing the sound fields generated with modeled and these measured loudspeaker data, we concluded that the design and development of optimization algorithms can be performed independent of the data [33]. Future verifications based on hands-on measurements are, however, essential.

6 CONCLUSION

Sound reinforcement in different venues requires adapted curving of line source arrays (LSAs). A purely analytical approach for finding appropriate LSA cabinet tilt angles was presented in this article. The polygonal audience line curving (PALC) is based on the geometry of the receiver area and the intended coverage. In comparison with typical standard LSA curving schemes, we conclude that the PALC is superior due to its flexible adaptability with respect to the receiver geometry.

This algorithm is faster than numerical methods. Since identical specifications for the presented analytical and the evaluated numerical optimization approach cannot be completely ensured, a final comparative statement regarding accuracy does not seem to be advisable. These specifications especially comprise the exact conversion from the selectable goal parameters to the desired sound field as well as the considered frequency ranges, possibly also weighted, of the numerical algorithms used as a reference and the fact that these are based on proprietary, not extractable loudspeaker directivity data. The effort and the computing time of the numerical approach are however significantly higher than for the analytical approach.

The PALC algorithm can be easily extended so that it only seeks from a discrete set of tilt angle values as it is required for practical realizations. It can be easily used in combination with subsequent electronic wavefront shaping. Since the LSA setup is restricted to fundamentals in this article, neglecting several aspects such as changes and uncertainties of the source configuration and of the frequency-dependent behavior, different LSA setups and their characteristics along with several curving optimization schemes should be discussed in the future. Also the human perception of phase effects in sound fields generated by LSAs should be examined. By listening tests, it may be possible to find quality criteria for phase position index plots (PIPs) analogue to the magnitude PIPs.

7 REFERENCES

[1] D. Scheirman, "Large-Scale Loudspeaker Arrays: Past, Present and Future (Part Two—Electroacoustic Considerations)," presented at the *AES 59th International Conference: Sound Reinforcement Engineering and Technology* (2015 July), conference paper 1-3.

[2] Martin Audio Ltd., "User Guide. Display 2.2, version 3.2," Tech. rep., https://martin-audio.com/downloads/software/Display-2.2-User-Guide-v3.2.pdf, last seen on 2017-08-21 (2017).

[3] Eastern Acoustic Works Inc., "EAW Resolution 2. Help File," Tech. rep., http://eaw.com/docs/3_Manuals/EAW last seen on 2017-08-21 (2017).

[4] d&b Audiotechnik GmbH, "ArrayCalc Simulation Software V8. ArrayProcessing Feature, Technical White Paper," Tech. rep., http://www.dbaudio.com/en/support/downloads/category/download/4195.html, last seen on 2017-08-21 (2017).

[5] AFMG Technologies GmbH, "AFMG FIRmaker. AFMG White Paper," Tech. rep., http://www.afmg-support.eu/SoftwareDownloadBase/FIRmaker/FIRmaker_White_Paper.pdf, last seen on 2017-08-21 (2017).

[6] G. W. van Beuningen and E. W. Start, "Optimizing Directivity Properties of DSP Controlled Loudspeaker Arrays," *Proc. of the Inst. of Acoustics: Reproduced Sound*, vol. 22, no. 6, pp. 17–37 (2000).

[7] A. Thompson, "Real World Line Array Optimisation," *Proc. of the Inst. of Acoustics*, vol. 30, no. 6 (2008).

[8] A. Thompson, "Improved Methods for Controlling Touring Loudspeaker Arrays," presented at the *127th Convention of the Audio Engineering Society* (2009 Oct.), convention paper 7828.

[9] M. Terrell and M. Sandler, "Optimising the Controls of a Homogenous Loudspeaker Array," presented at the *129th Convention of the Audio Engineering Society* (2010 Nov.) convention paper 8159.

[10] A. Thompson, J. Baird, and B. Webb, "Numerically Optimised Touring Loudspeaker Arrays - Practical Applications," presented at the *131st Convention of the Audio Engineering Society* (2011 Oct.), convention paper 8511.

[11] S. Feistel, M. Sempf, K. Köhler, and H. Schmalle, "Adapting Loudspeaker Array Radiation to the Venue Using Numerical Optimization of FIR Filters," presented at the *135th Convention of the Audio Engineering Society* (2013 Oct.), convention paper 8937.

[12] A. Thompson and J. Luzarraga, "Drive Granularity for Straight and Curved Loudspeaker Arrays," *Proc. of the Inst. of Acoustics*, vol. 35, no. 2, pp. 210–218 (2013).

[13] A. Thompson, "Line Array Splay Angle Optimisation," *Proc. of the Inst. of Acoustics*, vol. 28, no. 8, pp. 135–148 (2006).

[14] M. Urban, C. Heil, and P. Bauman, "Wavefront Sculpture Technology," *J. Audio Eng. Soc.*, vol. 51, pp. 912–932 (2003 Oct.).

[15] S. Feistel, A. Thompson and W. Ahnert, "Methods and Limitations of Line Source Simulation," *J. Audio Eng. Soc.*, vol. 57, pp. 379–402 (2009 Jun.).

[16] D. G. Meyer, "Computer Simulation of Loudspeaker Directivity," *J. Audio Eng. Soc.*, vol. 32, pp. 294–315 (1984 May).

[17] P. Meyer and R. Schwenke, "Comparison of the Directional Point Source Model and BEM Model for Arrayed Loudspeakers," *Proc. of the Inst. of Acoustics*, vol. 25, no. 4 (2003).

[18] F. Schultz, *Sound Field Synthesis for Line Source Array Applications in Large-Scale Sound Reinforcement*, Ph.D. thesis, University of Rostock (2016).

[19] F. Straube, F. Schultz, and S. Weinzierl, "On the Effect of Spatial Discretization of Curved Line Source Arrays," Fortschritte der Akustik: Tagungsband d. 41. DAGA, Nuremberg, pp. 459–462 (2015).

[20] F. Straube, F. Schultz, M. Makarski, S. Spors, and S. Weinzierl, "Evaluation Strategies for the Optimization of Line Source Arrays," presented at the *AES 59th International Conference: Sound Reinforcement Engineering and Technology* (2015 July), conference paper 2-1.

[21] F. Schultz, F. Straube, and S. Spors, "Discussion of the Wavefront Sculpture Technology Criteria for Straight Line Arrays," presented at the *138th Convention of the Audio Engineering Society* (2015 May), convention paper 9323.

[22] J.-W. Choi and Y.-H. Kim, "Generation of an Acoustically Bright Zone with an Illuminated Region Using Multiple Sources," *J. Acoust. Soc. Am.*, vol. 111, no. 4, pp. 1695–1700 (2002 Apr.), doi:https://doi.org/10.1121/1.1456926.

[23] P. Coleman, P. J. Jackson, M. Olik, M. Møller, M. Olsen, and J. A. Pedersen, "Acoustic Contrast, Planarity and Robustness of Sound Zone Methods Using a Circular Loudspeaker Array," *J. Acoust. Soc. Am.*, vol. 135, no. 4, pp. 1929–1940 (2014 Apr.), doi:https://doi.org/10.1121/1.4866442.

[24] M. R. Bai, J.-C. Wen, H. Hsu, Y.-H. Hua, and Y.-H. Hsieh, "Investigation on the Reproduction Performance versus Acoustic Contrast Control in Sound Field Synthesis," *J. Acoust. Soc. Am.*, vol. 136, no. 4, pp. 1591–1600 (2014 Oct.), doi:https://doi.org/10.1121/1.4894693.

[25] E. Skudrzyk, *The Foundations of Acoustics* (Springer, New York, 1971).

[26] F. W. J. Olver, D. W. Lozier, R. F. Boisvert, and C. W. Clark, *NIST Handbook of Mathematical Functions, 1st ed.* (Cambridge University Press, Cambridge, 2010).

[27] C. Heil and M. Urban, "Sound Fields Radiated by Multiple Sound Sources Arrays," presented at the *92nd Convention of the Audio Engineering Society* (1992 Mar.), convention paper 3269.

[28] M. Urban, C. Heil, and P. Bauman, "Wavefront Sculpture Technology," presented at the *111th Convention of the Audio Engineering Society* (2001 Nov.), convention paper 5488.

[29] M. S. Ureda, "Line Arrays: Theory and Applications," presented at the *110th Convention of the Audio Engineering Society* (2001 May), convention paper 5304.

[30] M. S. Ureda, "Analysis of Loudspeaker Line Arrays," *J. Audio Eng. Soc.*, vol. 52, pp. 467–495 (2004 May).

[31] L'Acoustics, "Training Module Variable Curvature Line Source" (2016).

[32] J. Ahrens and S. Spors, "Sound Field Reproduction Using Planar and Linear Arrays of Loudspeakers," *IEEE Trans. on Audio Speech Language Process.*, vol. 18, no. 8, pp. 2038–2050 (2010 Nov.).

[33] F. Straube, F. Schultz, M. Makarski, and S. Weinzierl, "Optimized Driving Functions for Curved Line Source Arrays Using Modeled and Measured Loudspeaker Data," *Fortschritte der Akustik: Tagungsband d. 42. DAGA, Aachen*, pp. 1136–1139 (2016).

APPENDIX

Table 2. List of variables—sound field prediction and evaluation

c	velocity of sound
$D(i, \omega)$	complex driving function of the i-th source at the angular frequency ω
$\mathbf{d}(\omega)$	$(VN \times 1)$ vector of the complex driving functions for all sources i per angular frequency ω
$D_{\text{in}}(i, \omega)$	(complex) signal input of the i-th source at the angular frequency ω
$D_{\text{opt}}(i, \omega)$	complex optimized filter of the i-th source at the angular frequency ω
$D_{\text{xo}}(\omega)$	complex frequency band crossover at the angular frequency ω
$E(\omega)$	frequency dependent absolute error between the obtained and the desired sound field in the audience zone
f	frequency
$f_{\text{LF, MF}}$	low/mid crossover frequency
$f_{\text{MF, HF}}$	mid/high crossover frequency
f_{start}	start frequency for the calculations
f_{stop}	stop frequency for the calculations
$G(m, i, \omega)$	scaled ATF from the i-th source to the m-th receiver position at the angular frequency ω
$\mathbf{G}(\omega)$	$(M \times VN)$ scaled ATF matrix for all sources i and for all receiver positions m at the angular frequency ω
$H1(\omega)$	frequency dependent standard deviation of the distance compensated SPLs of all audience positions
j	imaginary unit, $\text{j}^2 = -1$
$L_p(\omega, m)$	frequency and position index dependent SPL
$L_{p,\text{a,na}}(\omega)$	frequency dependent relation of the obtained average SPLs of the audience and the non-audience zone
$P(m, \omega)$	sound pressure at the m-th receiver position at the angular frequency ω
$P_{\text{des}}(m, \omega)$	desired sound pressure at the m-th receiver position at the angular frequency ω
$\mathbf{p}(\omega)$	$(M \times 1)$ vector of sound pressures at all receiver positions m at the angular frequency ω
$\mathbf{p}_{\text{des}}(\omega)$	$(M \times 1)$ vector of desired sound pressures at all receiver positions m at the angular frequency ω
p_0	reference sound pressure, $p_0 = 2 \cdot 10^{-5}$ Pa
$R(\beta, \omega)$	specific far-field radiation pattern for the radiation angle β at the angular frequency ω
$S(i, \omega)$	i-th loudspeaker sensitivity specifying the SPL in 1 m distance for 1 W electrical input power at the angular frequency ω
σ	standard deviation
ω	angular frequency

Table 3. List of variables—LSA setup and venue characteristics

i	index of the LSA loudspeakers, with $i = 1, 2, ..., VN$
K	number of sections of the PAL
k	index of the PAL section, with $k = 0, 1, 2, ..., K$
M	number of receiver positions in the vertical radiation plane, with $M = M_{\text{a}} + M_{\text{na}}$
M_{a}	number of audience positions in the vertical radiation plane
$\mathcal{M}_{\text{a}}$	set of audience positions in the vertical radiation plane
M_{na}	number of non-audience positions in the vertical radiation plane
$\mathcal{M}_{\text{na}}$	set of non-audience positions in the vertical radiation plane
M_{v1}	number of receiver positions in the vertical radiation plane of venue 1
M_{v2}	number of receiver positions in the vertical radiation plane of venue 2
m	index of the receiver positions, with $m = 1, 2, ..., M$
N	number of individual LSA cabinets and therefore also number of PAL segments
n	index of the LSA cabinet, with $n = 1, 2, ..., N$
V	number of vertically stacked loudspeakers per LSA cabinet (different for each frequency band)

Table 4. List of variables—lengths

Γ	total length of the covered PAL sections
Γ_0	total length of the PAL
Γ_e	tolerated difference of the total PAL length and the total length of the covered PAL sections
Γ_n	length of the n-th PAL segment, with $\Gamma_n = \Gamma_{n,1} + \Gamma_{n,2}$
$\Gamma_{n,1}$	distance from the top to the center position of the n-th PAL segment, i.e., the segment's upper partial length
$\Gamma_{n,2}$	distance from the center to the bottom position of the n-th PAL segment, i.e., the segment's lower partial length
Δ_n	distance from the center of the $(n + 1)$-th and the n-th LSA cabinet to the receiver positions (for WST)
Θ	radius of a baffled circular piston
Λ_y	height of a line piston
$\Lambda_{y,\mathrm{LSA}}$	front grille's height of a single LSA cabinet
$\Xi_{n,1}$	required distance from the top to the center position of the n-th PAL segment
$\Xi_{n,2}$	required distance from the center to the bottom position of the n-th PAL segment
$\tilde{\Xi}_{n,1}$	partial distance from the top to the center position of the n-th PAL segment
$\tilde{\Xi}_{n,2}$	partial distance from the center to the bottom position of the n-th PAL segment

Table 5. List of variables—vectors and room coordinates

x	room coordinate
$\mathbf{x}$	two-dimensional vector with $\mathbf{x} = (x, y)^{\mathrm{T}}$
$\mathbf{x_{0,i}}$	vector of the i-th LSA source's front grille center position
$\mathbf{x_{a,b,n}}$	vector of the bottom position of the n-th PAL segment
$\mathbf{x_{a,c,n}}$	vector of the center position of the n-th PAL segment
$\mathbf{x_{a,t,n}}$	vector of the top position of the n-th PAL segment
$\mathbf{x_{b,n}}$	vector of the bottom position of the n-th LSA cabinet
$\mathbf{x_{c,n}}$	vector of the (front grille) center position of the n-th LSA cabinet
x_{H}	x-coordinate of the top position of the uppermost LSA cabinet
$\mathbf{x_m}$	vector of the m-th receiver position
$\mathbf{x_{PAL,k}}$	vector of the stop position of the k-th PAL section
$\mathbf{x_{PAL,k-1}}$	vector of the start position of the k-th PAL section
$\mathbf{x_S}$	vector of the source position of the virtual line source
$\mathbf{x_{t,n}}$	vector of the top position of the n-th LSA cabinet
y	room coordinate
y_{H}	y-coordinate of the top position of the uppermost LSA cabinet
z	room coordinate

Table 6. List of variables—angles

α_n	splay angle between the $(n + 1)$-th and the n-th LSA cabinet
$\beta(m, i)$	radiation angle for the m-th receiver position from the i-th source
γ_n	tilt angle of the n-th LSA cabinet
ε_k	tilt angle of the k-th PAL section
ψ_n	coverage angle of the n-th LSA cabinet (for PALC)
$\tilde{\psi}_n$	n-th partial coverage segment angle of the PAL
ψ_{init}	initial coverage angle of the LSA cabinets

Table 7. Selected venue slice coordinates according to venue 1 from Fig. 2a.

m	x_m / m	y_m / m
1	0	−11
15	7	−11
101	50	−11
122	58.1492	−4.3788
131	58.1492	0.1212
152	66.2984	6.7424
165	66.2984	13.2424
297	0.2984	13.2424

Table 8 Selected venue slice coordinates according to venue 2 from Fig. 2b.

m	x_m / m	y_m / m
1	0	−10
21	10	−10
62	30.4426	−8.4668
231	110.0423	19.8906
246	110.0423	27.3906
466	0.0423	27.3906

Table 9 Splay angles α_n, source-to-receiver distances Δ_n and their product following WST criterion number four for venue 1 using the PALC2 tilt angles.

LSA cabinets	α_n / deg	Δ_n / m	$\alpha_n \cdot \Delta_n$ / (rad · m)
1...2	1.6	62.12	1.73
2...3	1.67	59.48	1.73
3...4	1.72	58.2	1.75
4...5	1.74	58.33	1.77
5...6	1.75	57.62	1.76
6...7	1.79	55.55	1.74
7...8	1.86	53.61	1.74
8...9	1.93	51.8	1.74
9...10	2.13	44.13	1.64
10...11	2.55	36.1	1.61
11...12	3.13	29.4	1.61
12...13	3.84	23.87	1.6
13...14	4.73	19.37	1.6
14...15	5.82	15.77	1.6
15...16	7.12	12.94	1.61

Table 10 Splay angles α_n, source-to-receiver distances Δ_n and their product following WST criterion number four for venue 2 using the PALC2 tilt angles.

LSA cabinets	α_n / deg	Δ_n / m	$\alpha_n \cdot \Delta_n$ / (rad · m)
1...2	1	95.55	1.67
2...3	1.11	86.23	1.67
3...4	1.24	77.71	1.68
4...5	1.37	69.95	1.67
5...6	1.53	62.88	1.68
6...7	1.7	56.47	1.68
7...8	1.89	50.68	1.67
8...9	2.11	45.45	1.67
9...10	2.35	40.75	1.67
10...11	2.62	36.55	1.67
11...12	2.92	32.8	1.67
12...13	3.39	27.6	1.63
13...14	4.12	22.07	1.59
14...15	5.15	17.64	1.59
15...16	6.43	14.16	1.59

Table 11 Tilt angles of the LSA cabinets for the geometry used in Fig. 1 and for venue 1 from Fig. 2a for the different curvings (arc, J, progressive, PALC1, PALC2, MA1, and MA2). Every cabinet of the straight array is tilted by 7 deg.

LSA	γ_n / deg	γ_n / deg	γ_n / deg	γ_n / deg	γ_n / deg	γ_n / deg	γ_n / deg
cabinet	arc	J	prog	PALC1	PALC2	MA1	MA2
1	−2	−1	−2	−1.53	−2.45	−3	−3
2	1	−1	−1.62	1.84	−0.85	−2.5	−2.5
3	4	−1	−0.85	5.2	0.82	−2	−0.5
4	7	−1	0.3	8.55	2.54	−1	0
5	10	−1	1.83	11.88	4.29	0	4
6	13	−1	3.75	15.19	6.04	1	6
7	16	−1	6.05	18.39	7.83	2	10
8	19	4	8.73	21.48	9.69	3	10.5
9	22	9	11.8	24.45	11.62	4	14.5
10	25	14	15.25	27.31	13.75	5	16.5
11	28	19	19.1	30.05	16.3	7	18.5
12	31	24	23.32	32.67	19.43	9	22.5
13	34	29	27.92	35.18	23.27	11	26.5
14	37	34	32.9	37.57	28.01	12	30.5
15	40	39	38.27	39.84	33.83	18	38
16	43	44	44	42	40.95	25.5	45.5

Table 12 Tilt angles of the LSA cabinets for the geometry used in Fig. 1 and for venue 2 from Fig. 2a for the different curvings (arc, J, progressive, PALC1, PALC2, MA1, and MA2). Every cabinet of the straight array is tilted by –4 deg.

LSA	γ_n / deg	γ_n / deg	γ_n / deg	γ_n / deg	γ_n / deg	γ_n / deg	γ_n / deg
cabinet	arc	J	prog	PALC1	PALC2	MA1	MA2
1	−7.14	−7	−7.1	–7.14	−8.24	−9.3	−8.8
2	−4.54	−7	−6.78	−4.03	−7.24	−8.8	−8.3
3	−1.94	−7	−6.13	−0.98	−6.12	−8.3	−7.8
4	0.66	−7	−5.15	2.01	−4.89	−7.8	−7.3
5	3.26	−7	−3.85	4.94	−3.51	−7.3	−5.3
6	5.86	−7	−2.23	7.81	−1.99	−6.8	−4.8
7	8.46	−7	−0.28	10.63	−0.29	−6.3	0.2
8	11.06	−7	2	13.39	1.6	−5.8	3.2
9	13.66	−2.13	4.6	16.09	3.71	−5.3	6.2
10	16.26	2.75	7.53	18.69	6.06	−3.3	9.2
11	18.86	7.63	10.78	21.18	8.68	−1.3	12.2
12	21.46	12.5	14.35	23.56	11.6	0.7	15.2
13	24.06	17.38	18.25	25.83	14.98	2.7	20.2
14	26.66	22.25	22.48	27.97	19.1	4.7	23.2
15	29.26	27.13	27.03	30	24.25	6.7	27.2
16	31.86	32	31.9	31.91	30.68	14.2	30.2

THE AUTHORS


Florian Straube


Frank Schultz


David Albanés Bonillo


Stefan Weinzierl

Florian Straube received the Dipl.-Ing. degree in electrical engineering/communications and information technology from Technische Universität Dresden in cooperation with Klippel GmbH in 2013. Since 2014 he has been working as a research associate at Audio Communication Group at TU Berlin focusing on sound field synthesis and line source array applications for sound reinforcement.

•

Frank Schultz received the M.Sc. in audio communication and technology from Technische Universität Berlin and the Dr.-Ing. degree with distinction from Universität Rostock, in 2011 and 2016, respectively. From 2003–2007 he worked at EVI Audio GmbH/Bosch Communications Systems, Straubing, as an audio DSP engineer. Since 2016 he has been working at sonible GmbH, Graz, as senior R&D engineer for 3D audio. Recent research interests are sound field synthesis applications and acoustic signal processing for loudspeaker arrays. He is currently a visiting postdoc at the Audio Communication Group at Technische Universität Berlin. He is a member of the AES and reviews for the AES and the IEEE.

•

David Albanés Bonillo received the M.Sc. degree in telecommunications engineering with a focus on digital signal processing from the Universidad Europea de Madrid in 2011. Since 2013 he has been working towards the M.Sc. in audio communication and technology from Technische Universität Berlin and is a research assistant at the TU Berlin. His fields of interest are electroacoustics, loudspeaker development, and digital signal processing.

•

Stefan Weinzierl is head of the Audio Communication Group at the Technische Universität Berlin. His activities in research are focused on audio technology, virtual acoustics, room acoustics, and musical acoustics. He is coordinating a master program in Audio Communication and Technology at TU Berlin and teaching Tonmeister students at the University of the Arts (UdK). With a diploma in physics and sound engineering and a two-year study in musicology at UC Berkeley, he received his Ph.D. from TU Berlin. He is coordinating research consortia in the field of virtual acoustics (SEACEN) and music information retrieval (ABC_DJ).

F. Straube, F. Schultz, M. Makarski and S. Weinzierl, "Mixed Analytical-Numerical Filter Design for Optimized Electronic Control of Line Source Arrays"
J. Audio Eng. Soc., vol. 66, no. 9, pp. 690–702, (2018 September.).
DOI: https://doi.org/10.17743/jaes.2018.0043

Mixed Analytical-Numerical Filter Design for Optimized Electronic Control of Line Source Arrays

FLORIAN STRAUBE,[1] *AES Associate Member*, **FRANK SCHULTZ,**[1] *AES Member*,
(florian.straube@tu-berlin.de) (frank.schultz@tu-berlin.de)

MICHAEL MAKARSKI,[2] *AES Member*, **AND STEFAN WEINZIERL**[1]
(michael.makarski@ifaa-akustik.de) (stefan.weinzierl@tu-berlin.de)

[1]*Audio Communication Group, TU Berlin, DE-10587 Berlin, Germany*
[2]*Institute for Acoustics and Audio Technique, DE-52146 Würselen, Germany*

Line source arrays (LSAs) are used for large-scale sound reinforcement aiming at the synthesis of homogeneous sound fields for the whole audio bandwidth. The deployed loudspeaker cabinets are rigged with different tilt angles and/or are electronically controlled in order to provide the intended coverage of the audience zones and to avoid radiation towards the ceiling, reflective walls or residential areas. In this contribution a mixed analytical-numerical approach, referred to as line source array venue slice drive optimization (LAVDO), is introduced for optimizing the individual loudspeakers' driving functions. This method is compared to numerical optimization schemes including least-squares and multiobjective goal attainment approaches. For two standard LSAs in straight and in curved configuration, these temporal frequency domain optimizations are performed for a typical concert venue. It is shown that LAVDO overcomes the non-smooth frequency responses resulting from numerical frequency domain approaches. LAVDO provides smooth amplitude and phase responses of the loudspeakers' driving functions that is essential for the subsequent practical finite impulse response filter design and implementation.

0 INTRODUCTION

For the optimization of the curving and the electronic control of line source arrays (LSAs) for advanced large-scale sound reinforcement there is no standard procedure. In practice, a pure geometric and a pure electronic wavefront shaping, as well as combinations thereof are realized [1]. For LSAs with several individually controlled, small high frequency drivers, electronic beam steering is feasible up to high audio frequencies. While the cabinets of most LSA systems are curved in addition to the electronic beam steering, the cabinets of others are rigged in a straight line.

Gain and delay are the two parameters—sometimes called excitation coefficients, feeding coefficients or driving functions—that have to be ascertained for electronic optimization of the LSA radiation. They are typically computed separately for each frequency. These two parameters can be mathematically considered as the amplitude and phase of a complex frequency-dependent driving function.

The established Wavefront Sculpture Technology [2] consists of five criteria on how to create a homogeneous wavefront based on geometric shaping of uniformly driven LSAs [3]. It does not include criteria for finding optimized driving functions for the individual loudspeakers. As a result, appropriate coupling and equalization filters are still adjusted manually [4].

Least-squares optimization algorithms with Tikhonov regularization are frequently used in sound field synthesis applications for determining the loudspeakers' driving functions. They include methods such as the loudspeaker weight energy method, which minimizes the spatial average error between the desired and the synthesized sound field imposing an energy constraint on the loudspeaker weights [5].

In the field of multi-zone sound field synthesis, the minimization of the spatial average error often comes with a loudspeaker weight energy-like constraint and is linked to the minimization of the sound pressure in the dark zone. Alternatively, the error minimization is linked to the acoustic contrast control, i.e., maximizing the ratio of the average sound pressure in the bright and dark zones [6]. The bright/dark zones correspond to the audience/non-audience zones in large-scale sound reinforcement problems.

In the context of LSA optimization, a least-squares algorithm has been extended by spatial weighting for the control

positions and measures to make the driving robust against small deviations of the LSA characteristics [7]. Also, genetic algorithms have been used for calculating appropriate loudspeaker driving signals [8]. Wave field synthesis as an approach for wavefront shaping within a target listening plane using a contour of loudspeakers has also been proposed as a large-scale sound reinforcement technique [9–11].

Recent, mostly proprietary, software such as Martin Audio Display [12], EAW Resolution 2 [13], d&b ArrayCalc [14], and AFMG FIRmaker [15] offer (numerical) optimization schemes. These approaches yield considerable improvements with respect to homogeneous audience coverage and/or avoidance of high side lobe energy compared to manually adjusted setups. However, the algorithms and their parametrization are rarely publicly documented except in [16–19]. In the cited papers, a multiobjective goal attainment optimization approach [20] is used, i.e., a vector of multivariable functions incorporating the loudspeakers' driving functions as variables are optimized. The objective vector contains the optimization goals, such as the error between the desired and the generated sound field, or the ratio of the sound pressures in the audience and in the non-audience zones, with specified weights for the different objectives.

The present article is focused on the optimization of the individual driving signals of LSAs with subsequent finite impulse response (FIR) filter design. We therefore introduce a mixed analytical-numerical optimization scheme, referred to as line source array venue slice drive optimization (LAVDO). We compare this method to the least-squares approach with Tikhonov regularization applied in [5] and a multiobjective goal attainment approach applied in [18, 19]. LAVDO is meant to overcome the non-smooth frequency responses resulting from numerical frequency domain approaches. Its features, i.e., combining far-field considerations and the multiobjective goal attainment approach for curve fitting optimization across broad frequency ranges, as well as the subsequent practical FIR filter design, are examined.

For optimizing the sound fields at the selected control positions in the venue slice, cf., Fig. 2, goals such as flat magnitude responses, maximizing the sound pressure levels (SPLs) at all audience positions and minimizing the SPLs at all non-audience positions, are pursued. Acoustic simulations based on the complex-directivity point source model [21, 22] including measured far-field loudspeaker directivity data provide the basis for an evaluation of the different optimization approaches.

The article is organized as follows. In Sec. 1 the chosen LSA configuration and the selected exemplary concert venue are presented first of all for convenient variable introduction. The complex-directivity point source model for sound field prediction is briefly recalled in Sec. 2. Two numerical methods and the introduced LAVDO—for optimizing the driving functions of the individual loudspeakers of LSAs—as well as the method for designing practical FIR filters from the calculated driving functions are described in Sec. 3.

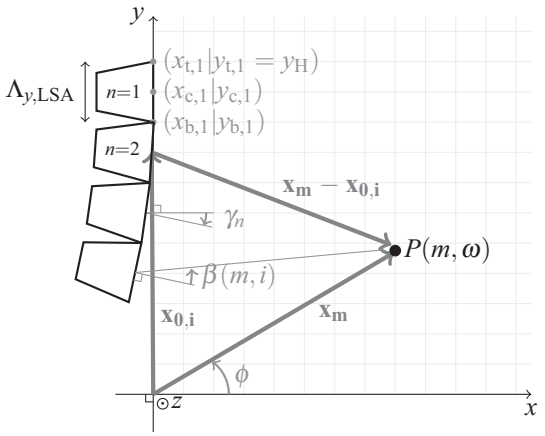

Fig. 1. Schematic sketch of the LSA setup under discussion. A total of $N = 4$ LSA cabinets with the individual height $\Lambda_{y,\mathrm{LSA}} = 0.346$ m is used.

In Sec. 4, the three aforementioned optimization schemes are applied for intended wavefronts based on the control positions in the venue slice. For one optimization goal, the calculated driving functions are presented. The optimization results are discussed and compared in Sec. 5, leading to the conclusion in Sec. 6.

1 SIMULATION SETUP

An LSA setup in straight and in curved configuration is examined for a typical concert venue with audience and non-audience sections given within the *xy*-plane. The sources are characterized by geometric attributes such as the number of cabinets, cabinet dimensions, and tilt angles, as well as electric and acoustic attributes such as the loudspeaker directivity, sensitivity, and the crossover functions. The venues are specified by the source and the receiver positions that are classified as either audience or non-audience positions.

1.1 Line Source Array Setup

The LSA setup and the geometry under discussion are schematically depicted in Fig. 1 for calculating the sound pressure $P(m, \omega)$ at the angular frequency ω and the m-th receiver position characterized by the vector $\mathbf{x_m}$. A total of $N = 4$ LSA cabinets with $n = 1, 2, 3, 4$ is deployed in order to allow for a clear comparison of the optimization methods. The front grille's height $\Lambda_{y,\mathrm{LSA}}$ of a single LSA cabinet is set to 0.346 m resulting in an overall LSA length of 1.384 m. Fixing the mounting height of the LSA, the top position of the first LSA cabinet is $y_{\mathrm{H}} = 2\,\Lambda_{y,\mathrm{LSA}}$, i.e., the LSA is approximately centered around $y = 0$. The individual tilt angles are γ_n, and $\mathbf{x_{0,i}}$ denotes the front grille center position vector of the i-th LSA driver. For the straight LSA $\gamma_n = 0$ holds for all cabinets. For the curved array, the optimized tilt angles $(\gamma_1, \gamma_2, \gamma_3, \gamma_4)^{\mathrm{T}} \approx (6.2^\circ, 6.6^\circ, 7.2^\circ, 8.1^\circ)^{\mathrm{T}}$ were calculated by applying the polygonal audience line curving approach 2 (PALC2) [23] to the considered venue geometry in Fig. 2. The vectors $\mathbf{x_{t,n}}$, $\mathbf{x_{c,n}}$, and $\mathbf{x_{b,n}}$

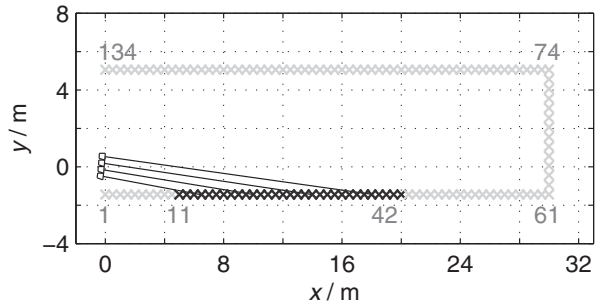

Fig. 2. Venue slice under discussion within the *xy*-plane with audience (black) as well as non-audience/avoid (gray) positions and selected index numbers (change of audience/avoid zone and/or polygonal line's section angle) from *M* receiver positions.

define the top, center, and bottom position of the *n*-th LSA cabinet, respectively. By the radiation angle $\beta(m, i)$, the source-receiver configuration is specified for the *i*-th source and the *m*-th receiver position. ϕ denotes the far-field radiation angle. Further detailed information on the geometric configuration can be found in [24].

Built from three-way cabinets in this article, the chosen LSA consists of $V_{\mathrm{LF}} = 1$, $V_{\mathrm{MF}} = 2$, and $V_{\mathrm{HF}} = 5$ vertically stacked, individually controlled drivers per cabinet for the low, mid, and high frequency band (LF, MF, HF). Twelve- inch, 6.5- inch, and 2.64- inch drivers are used for LF, MF, and HF, respectively. Thus, the LSA consists of a total of $V \cdot N$ sources with $i = 1, 2, \ldots, V \cdot N$ for each frequency band. The so called Active Radiating Factor amounts to 0.61 for LF, 0.72 for MF, and 0.97 for HF following [25].

Using measured loudspeaker directivity data for the sound field predictions and optimizations, the frequency dependent sensitivities $S_{\mathrm{LF}}(i, \omega)$, $S_{\mathrm{MF}}(i, \omega)$, and $S_{\mathrm{HF}}(i, \omega)$ are also measured in order to obtain realistic sound pressure values for vertical radiation. For the frequency band crossover, linear-phase Linkwitz-Riley filters with the transition frequencies of $f_{\mathrm{LF,\,MF}} = 400$ Hz and $f_{\mathrm{MF,\,HF}} = 1.1$ kHz are applied.

1.2 Venue Geometry

A standard concert venue with audience (bright zone, high SPL) and non-audience (dark zone, low SPL) sections is modeled by a venue slice representation in the *xy*-plane considering vertical LSA radiation, cf., Fig. 2. It consists of one audience line (15 m) and four non-audience lines and resembles an elementary sound reinforcement setting for easily interpretable optimization results.

A distance of 0.5 m for adjacent receiver positions was chosen, which corresponds to $M = 134$ considered receiver positions ($m = 1, 2, \ldots, M$). The receiver positions are composed of M_{a} audience positions from the set $\mathcal{M}_{\mathrm{a}}$ and M_{na} non-audience positions from the set $\mathcal{M}_{\mathrm{na}}$ with $M = M_{\mathrm{a}} + M_{\mathrm{na}}$. They are characterized by the position vectors $\mathbf{x_m} = (x_m, y_m, 0)^{\mathrm{T}}$ and are numbered counterclockwise starting from the position directly beneath the LSA (index 1, cf., Fig. 2). Note that the receiver positions have to cover at least ± 90 degree of the main LSA radiation direction referring to the center of a straight LSA in order to avoid severe side lobes resulting from numerical optimization schemes.

2 CALCULATION MODEL

The sound field prediction and optimization are based on the complex-directivity point source model [21, 22]. For predicting the sound pressure

$$P(m, \omega) = \sum_{i=1}^{i=V \cdot N} G(m, i, \omega)\, D(i, \omega) \tag{1}$$

[21, Eq. (5)], [22, Eq. (11)] is used. Eq. (1) considers the sources *i* with a total of *N* LSA cabinets each equipped with *V* loudspeakers in a specified frequency band (LF, MF, HF). $P(m, \omega)$ denotes the sound pressure with the angular frequency ω at the *m*-th receiver position characterized by the vector $\mathbf{x_m}$. $G(m, i, \omega)$ terms the acoustic transfer function from the *i*-th source to the *m*-th receiver position

$$G(m, i, \omega) = p_0\, 10^{\frac{S(i,\omega)}{20}}\, R\,(\beta(m, i), \omega)\, \frac{\mathrm{e}^{-\mathrm{j}\,\frac{\omega}{c}\,|\mathbf{x_m} - \mathbf{x_{0,i}}|}}{|\mathbf{x_m} - \mathbf{x_{0,i}}|}. \tag{2}$$

It is composed of (i) a frequency-band specific far-field radiation pattern $R(\beta(m, i), \omega)$ for the radiation angle $\beta(m, i)$ with the angular frequency ω, (ii) the ideal point source wave propagation $\frac{\mathrm{e}^{-\mathrm{j}\,\frac{\omega}{c}\,|\mathbf{x_m} - \mathbf{x_{0,i}}|}}{|\mathbf{x_m} - \mathbf{x_{0,i}}|}$ with the speed of sound *c* and $\mathrm{j}^2 = -1$, (iii) the reference sound pressure $p_0 = 2 \cdot 10^{-5}$ Pa in air, and (iv) the loudspeaker sensitivity $S(i, \omega)$ specifying the SPL in 1 m distance for 1 W electrical input power.

Utilizing Eq. (1) for the sound field prediction, the calculated sound fields result from the superposition of the impact of the sources *i*. The impact of each source is characterized by the source-receiver propagation characteristics—described by the acoustic transfer function $G(m, i, \omega)$—and by its signal characteristics, i.e., the signal input as well as the electronic filters affecting the input of each source—described by the driving function $D(i, \omega)$.

$$D(i, \omega) = D_{\mathrm{in}}(i, \omega)\, D_{\mathrm{opt}}(i, \omega)\, D_{\mathrm{xo}}(\omega) \tag{3}$$

of the *i*-th source at the angular frequency ω consists of the signal input $D_{\mathrm{in}}(i, \omega)$, the complex optimization filter $D_{\mathrm{opt}}(i, \omega)$—which is to be found and implemented as an FIR filter—and the complex frequency band crossover/high/low pass filters $D_{\mathrm{xo}}(\omega)$. Gain and delay are mathematically considered as the amplitude and phase of these complex functions.

Eq. (1) reads $\mathbf{p}(\omega) = \mathbf{G}(\omega)\, \mathbf{d}(\omega)$ in matrix notation, accounting for all receiver positions *M* at a single angular frequency ω with (i) $\mathbf{p}(\omega)$ denoting the $(M \times 1)$ vector of sound pressures for all considered receiver positions $\mathbf{x_m}$, (ii) $\mathbf{G}(\omega)$ denoting the $(M \times V \cdot N)$ acoustic transfer function matrix from all drivers *i* to all receiver positions *m,* and (iii) $\mathbf{d}(\omega)$ denoting the $(V \cdot N \times 1)$ vector of the complex driving functions for all drivers *i* per angular frequency ω. Then, for a desired sound field $\mathbf{p}_{\mathrm{des}}(\omega)$ at the considered evaluation positions $\mathbf{x_m}$

$$\mathbf{p}_{\mathrm{des}}(\omega) = \mathbf{G}(\omega)\, \mathbf{d}(\omega) \tag{4}$$

has to be solved for the driving functions $\mathbf{d}(\omega)$. Since typically $M > V \cdot N$ in the discussed application, i.e., the number of evaluation positions is larger than the number of individual sources, an ill-posed inverse problem must be analyzed [26, 27]. For the numerical optimization schemes considered in this article, the optimization is performed separately for each frequency.

3 ELECTRONIC CONTROL METHODS FOR SOUND FIELD OPTIMIZATION

In the following section different numerical optimization schemes are discussed which were applied to sound reinforcement with LSAs. Alternatively, the mixed analytical-numerical approach LAVDO is introduced. Their optimization results are examined in Sec. 4. These approaches operate in the frequency domain. They are only focused on the optimization of the loudspeakers' driving functions with subsequent FIR filter generation, without optimization of the LSA curving. The practical FIR filter design from the calculated driving functions is considered in this section as well.

3.1 Least-Squares Optimization with Tikhonov Regularization

In [5] the least-squares optimization with Tikhonov regularization of the driving functions is termed loudspeaker weight energy according to the considered constraint. In order to solve Eq. (4) with respect to the loudspeaker weights, the objective function to be minimized reads

$$\begin{aligned} &\min_{\mathbf{d}(\omega)} \|\mathbf{G}(\omega)\mathbf{d}(\omega) - \mathbf{p}_{\text{des}}(\omega)\|_2^2 \\ &\text{subject to:} \quad \|\mathbf{d}_{\mathbf{opt}}(\omega)\|_2^2 \leq D_{\text{max}}^2 \end{aligned} \tag{5}$$

denoting the squared Euclidean norm $\|\cdot\|_2^2$ [28, Eq. (3.2.13)] and the constraint D_{max}^2 with $D_{\text{max,dB}} = 10\,\text{lg}\,D_{\text{max}}^2$ as the limit for the summed squares of the driving functions' absolute values, i.e., the total energy of the driving functions (cf., [5, Eq. (1)]). The solution is known as

$$\mathbf{d}(\omega, \lambda_{\text{reg}}) = [\mathbf{G}(\omega)^{\text{H}}\mathbf{G}(\omega) + \lambda_{\text{reg}}\mathbf{I}_{V\cdot N}]^{-1}\,\mathbf{G}(\omega)^{\text{H}}\mathbf{p}_{\text{des}}(\omega), \tag{6}$$

with the regularization parameter λ_{reg}. The Hermitian is denoted by $^{\text{H}}$ and $\mathbf{I}_{VN}$ is a $(V \cdot N \times V \cdot N)$ identity matrix. Taking D_{max}^2 into account, λ_{reg} can be found by means of singular value analysis and using Newton's method, cf., [5, Sec. II. B/C].

3.2 Multiobjective Goal Attainment Approach

The multiobjective goal attainment optimization approach [20] is applied in [18, 19]. Its equation is (cf., [20, Eq. (1)] for a generalization)

$$\begin{aligned} &\min_{\zeta, \mathbf{d}(\omega)} \zeta \\ \text{such that:} \quad &\mathbf{F}[\mathbf{d}(\omega)] - \mathbf{w}\,\zeta \leq \mathbf{F}^*[\mathbf{d}(\omega)] \\ \text{subject to:} \quad &|D_{\text{opt}}(i, \omega)| \leq D_{\text{opt,max}}(\omega) \quad \forall i \\ &|D_{\text{opt}}(i, \omega)| \geq D_{\text{opt,min}}(\omega) \quad \forall i \end{aligned} \tag{7}$$

with two exemplary constraints for the maximum $D_{\text{opt,max}}(\omega)$ and the minimum value $D_{\text{opt,min}}(\omega)$ of the amplitudes $|D_{\text{opt}}(i, \omega)|$ of the individual driving functions and with the vector of objective functions

$$\mathbf{F}[\mathbf{d}(\omega)] = \begin{pmatrix} F_1[\mathbf{d}(\omega)] \\ F_2[\mathbf{d}(\omega)] \end{pmatrix} = \begin{pmatrix} E(\omega) \\ L_{p,\text{a,na}}(\omega) \end{pmatrix} \tag{8}$$

that shall incorporate two goals in this case. The vector of objective functions comprises the frequency dependent absolute amplitude error [24, Eq. (16)]

$$E(\omega) = \left\| \mathbf{p}(\omega)_{m\in\mathcal{M}_{\text{a}}} - \mathbf{p}_{\text{des}}(\omega)_{m\in\mathcal{M}_{\text{a}}} \right\|_2^2 \tag{9}$$

between the desired and the generated sound field in the audience zone as well as the frequency dependent ratio of the mean squared sound pressures of the audience and the non-audience zone, given as level

$$L_{p,\text{a,na}}(\omega) = 10\,\text{lg}\left(\frac{\frac{1}{M_{\text{a}}} \left\| \mathbf{p}(\omega)_{m\in\mathcal{M}_{\text{a}}} \right\|_2^2}{\frac{1}{M_{\text{na}}} \left\| \mathbf{p}(\omega)_{m\in\mathcal{M}_{\text{na}}} \right\|_2^2} \right), \tag{10}$$

cf., [24, Eq. (18)]. The latter measure corresponds to the so called acoustic contrast [6, Eq. (16)] established in multi-zone sound field synthesis.

In general, the optimization in Eq. (7) is aimed at minimizing the parameter ζ, i.e., the difference of the objective functions $\mathbf{F}[\mathbf{d}(\omega)]$ and their design goals $\mathbf{F}^*[\mathbf{d}(\omega)]$. Optimizing for one objective typically results in impairing other objectives when using multiobjective goal attainment optimization approaches. Including the weighting vector $\mathbf{w}$ in the optimization allows for balancing the different objectives. In combination with the minimization parameter, the product $\mathbf{w}\,\zeta$ entails that the design goals do not necessarily have to be rigidly met.

3.3 Mixed Analytical-Numerical Approach/LAVDO

Referred to as line source array venue slice drive optimization, abbreviated LAVDO, due to the application of controlling positions from the venue slice, a mixed analytical-numerical approach is introduced here. It is based on the idea of finding meaningful initial solutions analytically and refining them numerically (here using the multiobjective goal attainment optimization approach) in a subsequent step.

Different optimization goals can be included, such as maximizing the ratio of the obtained sound pressures in the audience and in the non-audience zones, flat frequency responses at all audience positions, as well as maximizing the SPLs at all audience positions. In contrast to the aforementioned "complex" optimizations, the amplitudes and the phases are calculated separately using LAVDO in order to clearly distinguish between beam width and beam steering effects. Therefore, the analytically determined initial solutions are found by means of far-field considerations for straight as well as curved LSA configurations.

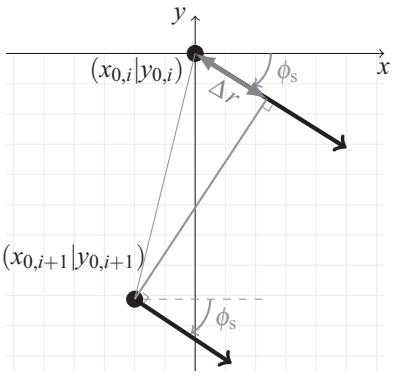

Fig. 3. Sketch of the far-field beam steering for a curved array used for finding an initial optimization solution for the LAVDO approach. It is visualized for two sources and for a beam steered downwards by ϕ_s.

The motivation for LAVDO originates from intending smooth amplitude and smooth phase frequency responses. This smoothness is not ensured using numerical-only approaches with driving functions optimized separately for different frequencies. Smooth frequency responses are necessary for the practical FIR filter design in order to obtain moderate filter lengths and in order to deal with uncertainties of the measurement data and of the geometric source-receiver configuration. Due to the initial solutions of LAVDO, physically unfeasible solutions that may be found by numerical-only optimization schemes do not have to be eliminated by successive post-processing. The approach results in a restricted solution space and exhibits low computational load.

For the initial solutions, the (group) delays of the individual loudspeakers are sought iteratively for every considered frequency at first, i.e., with respect to $e^{j[\omega t+\varphi(i,\omega)]}$ in the time domain. Hence, each angle $\varphi(i, \omega)$ of the complex driving function of the i-th loudspeaker is calculated depending on the steering angle ϕ_s, so that $D_{\mathrm{opt}}(i, \omega) = e^{j\varphi(i,\omega)}$.

For a curved LSA configuration, cf., Fig. 3,

$$\begin{aligned}\frac{\varphi(i,\omega)}{\omega} &= \frac{\Delta r}{c}\\ &= \sin\left(\phi_s - \frac{\pi}{2} + \arctan\left[\frac{y_{0,i+1}-y_{0,i}}{x_{0,i+1}-x_{0,i}}\right]\right)\\ &\quad\times\frac{\sqrt{(x_{0,i+1}-x_{0,i})^2+(y_{0,i+1}-y_{0,i})^2}}{c}\\ &= \frac{\sin\phi_s|y_{0,i+1}-y_{0,i}| - \cos\phi_s|x_{0,i+1}-x_{0,i}|}{c}\end{aligned} \tag{11}$$

holds for downward beam steering and $\varphi(i+1, \omega) = 0$, i.e., only considering the delay difference between two sources by Eq. (11), cf., [29, Sec. 7.8] for a straight array.

According to the different optimization goals,

$$\text{(i)}\qquad \max_{\phi_s} L_{p,\mathrm{a,na}}(\omega, \phi_s) \tag{12}$$

is set for maximizing the ratio of the mean squared sound pressures in the audience and in the non-audience zones, see Eq. (10) for the definition of $L_{p,\mathrm{a,na}}(\omega)$. If flat frequency responses are desired at all audience positions,

$$\text{(ii)}\qquad \max_{\phi_s} \left\| \mathbf{p}(\omega, \phi_s) \right\|_{m\in\mathcal{M}_a,\infty} \tag{13}$$

$$\text{subject to: } \left\| \mathbf{p}(\omega, \phi_s) \right\|_{m\in\mathcal{M}_a,\infty} - \left\| \mathbf{p}(\omega, \phi_s) \right\|_{m\in\mathcal{M}_a,\mathrm{min}} < L_{p,\mathrm{diff}}$$

is computed denoting the maximum norm $\|\cdot\|_\infty$ [28, Eq. (3.2.13)] and defining a minimum norm

$$\left\| \mathbf{p}(\omega, \phi_s) \right\|_{m\in\mathcal{M}_a,\mathrm{min}} = \min_{m\in\mathcal{M}_a} |P_m(\omega, \phi_s)|. \tag{14}$$

Eq. (13) incorporates the constraint that the difference of the maximum SPL and the minimum SPL does not exceed $L_{p,\mathrm{diff}}$, which may amount to, e.g., 6 dB.

Subsequently, if smooth SPL responses are desired at all audience positions, a global magnitude $D_g(\omega)$ is determined for each frequency. This global magnitude is equal for all sources per frequency band and it does not exceed 0 dB. It is computed by adapting $D_g(\omega)$ iteratively regarding the respective calculated maximum SPLs at all audience positions, so that $D_{\mathrm{opt}}(i, \omega) = D_g(\omega)e^{j\varphi(i,\omega)}$. Hence, to achieve a smooth amplitude response, the maximum approved SPL can either be chosen based on a reference frequency, e.g., $f = 1$ kHz, or on a fixed reference SPL, e.g., $L_p = 90\,\mathrm{dB_{SPL}}$.

These initial solutions for the individual driving functions are then smoothed with respect to frequency. In a next step, the amplitudes and unwrapped phases are fitted separately to predetermined curves, such as polynomials

$$|D_{\mathrm{opt}}(i, \omega)| = \sum_{k=0}^{k=K} \nu_{\mathrm{mag},k,i} \left(\frac{\omega}{f_s}\right)^k \tag{15}$$

of the K-th degree for the magnitudes with the k-th curve parameter $\nu_{\mathrm{mag},\,k,i}$ for the i-th source and the sampling frequency f_s. For the phase, the K-th order Fourier series

$$\begin{aligned}\arg\{D_{\mathrm{opt}}(i, \omega)\} = &\sum_{k=0}^{k=K} \nu_{\mathrm{cos},k,i}\ \cos\left(k\,\nu_{\mathrm{fund},i}\,\frac{\omega}{f_s}\right)\\ &+\sum_{k=0}^{k=K} \nu_{\mathrm{sin},k,i}\ \sin\left(k\,\nu_{\mathrm{fund},i}\,\frac{\omega}{f_s}\right),\end{aligned} \tag{16}$$

with the curve parameters $\nu_{\mathrm{cos},\,k,i}$, $\nu_{\mathrm{sin},\,k,i}$, and $\nu_{\mathrm{fund},\,i}$ is used for the considered angular frequency ω and the i-th LSA source. This smoothing limits the solution space regarding different frequencies.

Compared to fitting the FIR filter coefficients directly, a further subsequent processing step, i.e., the filter design, is necessary but the magnitudes and the phases can still be dealt with independently which is one key factor for magnitude and phase-controlled optimization filters. This approach ensures that the effects of magnitude and phase optimization can be physically understood and allows for excluding unfeasible solutions. It also allows to control the dynamic range of the magnitudes and the group delay of the filters separately. The conversion from a logarithmically-spaced to the required linearly-spaced frequency vector is not processed at this stage so that the number of considered

frequencies is kept low with a frequency distribution that is rather perceptually motivated, but it has to be adjusted in a later stage.

Applying the multiobjective goal attainment optimization approach, the final solution is computed, again separately for the driving functions' amplitudes and phases. In contrast to the method in Sec. 3.2, the optimizations are not performed by determining the amplitudes and/or phases for each driver at a discrete frequency. Instead, the curve parameters ν of the fitting functions are sought for all evaluated frequencies ensuring smooth amplitude and phase responses. The smoothness is maintained and while the difference between the goals and the obtained sound fields and driving functions may be improved for several frequencies, it may be impaired for some other frequencies. Forming the $(V \cdot N \times \Psi)$ matrix $\mathbf{D}(\nu_i)$ with the number Ψ of evaluated frequencies that contains the driving functions $\mathbf{d}(\omega)$ for all frequencies, Eq. (7) is for $\nu_i \in \{\nu_{\text{mag},\,k,i}, \nu_{\cos,\,k,i}, \nu_{\sin,\,k,i}, \nu_{\text{fund},\,i}\}$ rewritten as

$$\begin{aligned} & \min_{\zeta,\nu_i} \zeta \\ \text{such that:} \quad & \mathbf{F}[\mathbf{D}(\nu_i)] - \mathbf{w}\,\zeta \leq \mathbf{F}^*[\mathbf{D}(\nu_i)] \\ \text{subject to:} \quad & |D_{\text{opt}}(i,\omega)| \leq D_{\text{opt,max}}(\omega) \quad \forall\omega \\ & |D_{\text{opt}}(i,\omega)| \geq D_{\text{opt,min}}(\omega) \quad \forall\omega. \end{aligned} \tag{17}$$

The vector of objective functions $\mathbf{F}[\mathbf{D}(\nu_i)]$ contains the goals according to Eqs. (12) and (13), respectively. Note that the optimization constraints can be freely chosen in this approach.

3.4 Driving Filter FIR Design

Following the optimization of the individual driving functions, the calculated amplitude and phase frequency responses are implemented by means of FIR filters for practical application to loudspeakers. The filters are designed with the frequency sampling method [30]. Hence, a linearly-spaced frequency vector is required for the inverse discrete Fourier transform. Since it is reasonable to use a logarithmically-spaced frequency vector for the optimizations with respect to computational efficiency and human perception, this vector has to be converted prior to the filter design.

For all optimizations in this article, a logarithmically-spaced frequency, $\frac{1}{12}$ octave resolution vector with $f_{\text{opt,min}} = 100$ Hz and $f_{\text{opt,max}} = 20$ kHz is used. Utilizing measured loudspeaker data for the sound field prediction, the frequency vector is slightly modified by picking those frequencies from the linearly-spaced measurement frequency vector that are nearest to the ones of the logarithmically-spaced optimization vector. This "quasi" logarithmically-spaced vector proved to be more practical with respect to the results and the computational effort than interpolating the linearly-spaced measurement frequency vector in order to obtain a purely logarithmically-spaced one in advance.

4 OPTIMIZATION RESULTS

In this section the three sound field optimization approaches from Sec. 3 are compared based on simulations considering the audience and the non-audience positions in the vertical radiation plane, cf., Fig. 2. The desired sound field depends on the required characteristics in the audience zone, such as flat magnitude responses, a fixed SPL loss per distance doubling or maximum SPL at all positions, as well as in the non-audience zone, such as minimum SPL directed towards ceilings, reflective walls, residential areas or the stage. The performance evaluation, i.e., the visualizations and the technical quality measures, is intentionally not consistently given for all approaches in this section. They are rather individually selected in order to reveal various deficiencies leading to the developed feature set of the LAVDO.

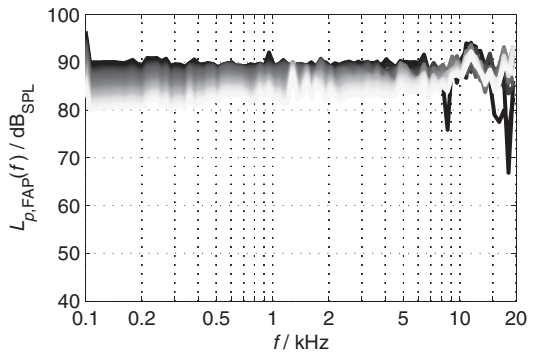

(a) SPL frequency responses at all audience positions

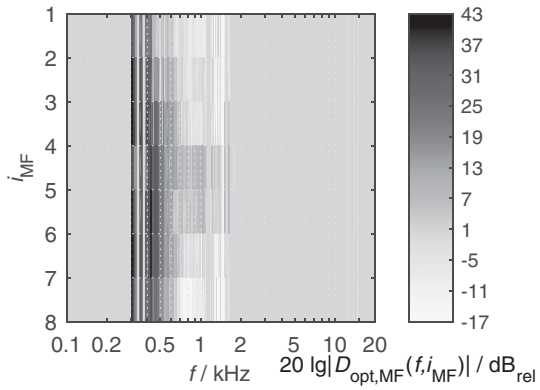

(b) driving function index plot

Fig. 4. Exemplary least-squares optimization with Tikhonov regularization for the straight LSA from Sec. 4.1. SPL frequency responses at all audience positions (a) and driving function index plot (b) for all mid frequency way sources are shown. In the SPL frequency responses at all audience positions, the curves become brighter from the first to the last audience position.

4.1 Least-Squares Optimization with Tikhonov Regularization

For the least-squares optimization with Tikhonov regularization from Sec. 3.1, the sound field $P_{\text{des}}(m, \omega)$ with 3 dB level loss per distance doubling is desired. A target SPL of 90 dB_{SPL} at the first receiver position within the audience zone ($m = 11$) is requested for the venue in Fig. 2.

In Fig. 4 optimization results are shown for a straight LSA configuration and the parameters $D_{\text{max, dB}} = 30$ dB as

the limit for the summed squares of the driving functions' absolute values and $\lambda_{\text{reg, 0}} = 1$ as initial regularization parameter. $D_{\text{max, dB}} = 30$ dB means that the limit for the summed squares of the driving functions' absolute values amounts to 1000, i.e., possible solutions for the driving functions' magnitudes considering three sources could be for example (i) $\sqrt{(1000, 0, 0)}$ or (ii) $\sqrt{(1000/2, 1000/2, 0)}$ or (iii) $\sqrt{(1000/3, 1000/3, 1000/3)}$which corresponds approximately to (i) $(30, -\infty, -\infty)$ dB and (ii) $(27, 27, -\infty)$ dB, and (iii) $(25, 25, 25)$ dB, respectively. These examples reveal that the upper limit of the single driving functions' magnitudes cannot be directly specified by $D_{\text{max, dB}}$ and that the lower limit is not defined at all. The visualizations comprise the SPL frequency responses at all audience positions and the driving function index plot representing the magnitudes over frequency that have to be applied to the individual sources i in order to obtain the optimized sound field [24].

In Fig. 4 it can be observed that the desired wavefront can be well synthesized up to ca. 10 kHz neglecting the level response at the first audience position when using the least-squares algorithm. The driving function index plot reveals that the individual sources, depicted for the mid frequency way in this case, are rather unevenly controlled with respect to the frequency and to the sources, i.e., the frequency responses are not smooth. As the driving functions are calculated separately for each frequency, a variation greater than the chosen 30 dB is possible between different frequencies. Note that the group delays of the driving functions are not visualized as they also suffer from inadequate frequency smoothness analogue to the magnitudes, cf., the results in [24].

4.2 Multiobjective Goal Attainment Approach

The multiobjective goal attainment optimization approach from Sec. 3.2 is applied using

$$\begin{aligned} \mathbf{F}[\mathbf{d}(\omega)] = \begin{pmatrix} E(\omega) \\ L_{p,\text{a,na}}(\omega) \end{pmatrix} &= \begin{pmatrix} 10^{-6}\,\text{Pa}^2 \\ 15\,\text{dB}_{\text{rel}} \end{pmatrix} \\ D_{\text{opt,min,dB}}(\omega) &= -12\,\text{dB}_{\text{rel}} \\ D_{\text{opt,max,dB}}(\omega) &= 0\,\text{dB}_{\text{rel}} \\ \mathbf{w} &= (1, -1/0.1)^{\text{T}} \end{aligned} \tag{18}$$

for a straight LSA configuration. According to Eq. (18), minimum and maximum values are assigned as constraints for the magnitudes of the driving functions, a level difference of 15 dB between the sound pressures in the audience and in the non-audience zone is demanded per frequency, and the minimization of the absolute error between the desired and the synthesized sound field is given a higher weight than the maximization of the acoustic contrast. As in Sec. 4.1 the desired sound field is set to exhibit 3 dB SPL loss per distance doubling. In Fig. 5 the SPL frequency responses at all audience positions, the driving function index plot, and the acoustic contrast $L_{p,\text{a,na}}(f)$ are shown for this exemplary optimization.

In the SPL frequency responses at all audience positions, it can be seen that the desired sound field is well synthesized up to ca. 1 kHz. This frequency approximately

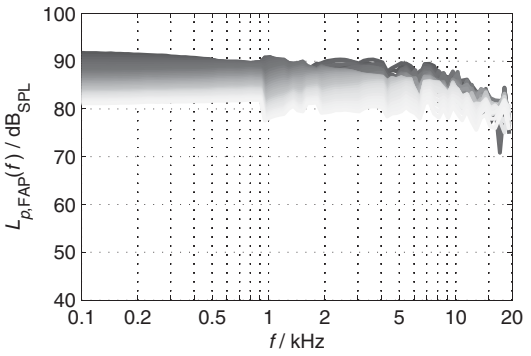

(a) SPL frequency responses at all audience positions

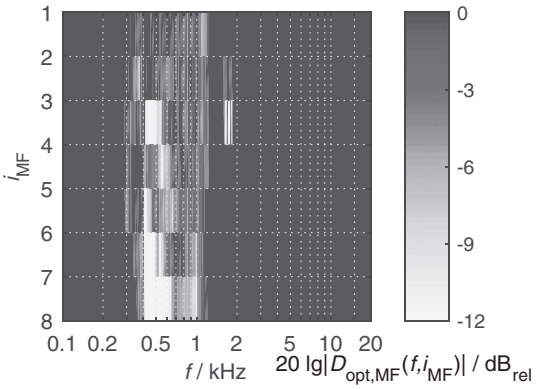

(b) driving function index plot

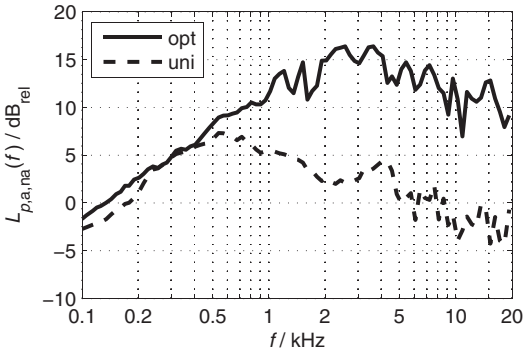

(c) acoustic contrast $L_{p,\text{a,na}}(f)$

Fig. 5. Exemplary multiobjective goal attainment optimization for the straight LSA from Sec. 4.2. SPL frequency responses at all audience positions (a), driving function index plot (b) for all MF sources, and the acoustic contrast $L_{p,\text{a,na}}(f)$ (c) are shown. In the SPL frequency responses at all audience positions, the curves become brighter from the first to the last audience position.

coincides with the MF-HF-crossover frequency. Above that frequency, the SPL loss per distance doubling exceeds 3 dB but the frequency responses are quite flat with a decrease of the maximum SPL above ca. 8 kHz. The behavior in the MF-HF-crossover range is caused by the transition and combination from/of the MF driving function to/and the HF driving function optimization with a different amount of involved loudspeakers. These effects could be decreased by additional post-processing that was not considered for this plot in order to reveal this weakness.

In the main working range of the mid frequency loudspeakers from ca. 300 Hz up to ca. 1.5 kHz, the driving function index plot reveals insufficient level smoothness but the range of the values is restricted to the constrained maximum and minimum value. Compared to the driving functions resulting from the least-squares optimization in Sec. 4.1, the deviation of the magnitudes between the different sources is considerably decreased, yielding a more feasible and economical driving load. Plotting $L_{p,\mathrm{a,na}}(f)$, the desired increase of the acoustic contrast is clearly noticeable for frequencies for which the LSA is capable of directional coverage.

4.3 Mixed Analytical-Numerical Approach/LAVDO

Applying the mixed analytical-numerical approach from Sec. 3.3, referred to as LAVDO, for optimizing the individual loudspeakers' driving functions, there is no need for defining the exact desired sound field analytically. The desired sound field is initially given by the uniformly driven LSA radiation. Each magnitude of the individual sources' driving functions is constrained to $D_{\mathrm{opt,max,\ dB}}(\omega) = 0\,\mathrm{dB_{rel}}$ for the initial solutions and the numerical refinements.

For each parameter set, a straight and a curved LSA configuration are examined. Polynomials of the first degree and Fourier series terms up to the 7th order serve as fitting functions for the numerical refinements of the driving functions' amplitudes and unwrapped phases, respectively. For frequencies $f > 200$ Hz, the optimizations are performed.

Two goals are pursued: (i) achieving a maximum ratio of the average sound pressures in the audience and in the non-audience zones, cf., Eq. (12), and (ii) achieving a constant SPL with a tolerance of ± 3 dB at all audience positions, cf., Eq. (13). For all goals, the weighting factors for the numerical refinements are chosen to 1 for minimizations and –1 for maximizations. The objective function vector for goal (i) is written as

$$\mathbf{F}[\mathbf{D}(\nu_i)] = \begin{pmatrix} \frac{1}{\Psi}\sum_{\omega} \left\| \mathbf{p}(\omega) \right\|_{m\in\mathcal{M}_\mathrm{a}}\Big\|_{\infty} \\ 10\ \lg\left(\frac{1}{\Psi}\sum_{\omega} \frac{\frac{1}{M_\mathrm{a}} \left\| \mathbf{p}(\omega) \right\|_{m\in\mathcal{M}_\mathrm{a}}\Big\|_2^2}{\frac{1}{M_\mathrm{na}} \left\| \mathbf{p}(\omega) \right\|_{m\in\mathcal{M}_\mathrm{na}}\Big\|_2^2} \right) \end{pmatrix} \tag{19}$$

with the maximum norm $\|\cdot\|_\infty$. The first objective is the average of the maximum sound pressures at all audience positions over all frequencies and the second objective function is the average of the ratios of the sound pressures in the audience and non-audience zone over all frequencies, analogue to $L_{p,\mathrm{a,na}}(\omega)$. They are set to 120 $\mathrm{dB_{SPL}}$ and 24 $\mathrm{dB_{rel}}$, respectively. For goal (ii) the objective function vector reads

$$\mathbf{F}[\mathbf{D}(\nu_i)] = \begin{pmatrix} 10\lg\left(\frac{1}{p_0^2 M_\mathrm{a}} \left\| \mathbf{p}(\omega = \omega_\mathrm{ref}) \right\|_{m\in\mathcal{M}_\mathrm{a}}\Big\|_2^2 \right) + 3\,\mathrm{dB} \\ 10\lg\left(\frac{1}{p_0^2 M_\mathrm{a}} \left\| \mathbf{p}(\omega = \omega_\mathrm{ref}) \right\|_{m\in\mathcal{M}_\mathrm{a}}\Big\|_2^2 \right) - 3\,\mathrm{dB} \end{pmatrix} \tag{20}$$

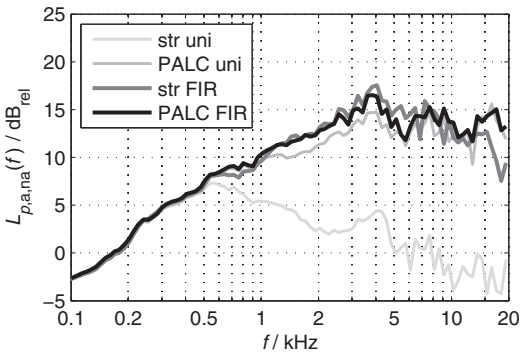

Fig. 6. $L_{p,\mathrm{a,na}}(f)$—the level of the frequency dependent ratio of the mean squared sound pressures of the audience and the non-audience zone—for the straight ("str") and the curved ("PALC") configuration with the tilt angles from Sec. 1.1. Both the values for the uniformly driven ("uni") as well as the optimized ("FIR") LSAs are visualized. The used goal (i) is to achieve maximum acoustic contrast, here 15 dB.

with the reference angular frequency $\omega_\mathrm{ref} = 2\pi f_\mathrm{ref}$ with $f_\mathrm{ref} = 1\,\mathrm{kHz}$. Here, objectives 1 and 2 contain the average SPLs over all audience positions at the reference frequency and the ± 3 dB tolerance.

Comparing the acoustic contrast for the case including its maximization, goal (i), cf., Fig. 6, the ratio of the mean squared sound pressures of the audience and the non-audience zones is considerably higher for the curved and electronically controlled straight array than for the uniformly driven straight array as expected. This is valid for high frequencies for which the LSA does not radiate omnidirectionally. The PALC2 curved LSA further gains slightly increased acoustic contrast by additionally applied optimization filters. $L_{p,\mathrm{a,na}}(f)$ does not differ substantially for the optimized straight and the optimized curved LSA configuration in this rather simple reinforcement scenario. Only small differences within a small band width are observable.

Ensuring SPL frequency responses as flat as possible, cf., SPL frequency responses at all audience positions in Fig. 7, the SPL tolerance of ± 3 dB of goal (ii) can be accomplished up to ca. 4 kHz. Above this frequency, the SPL loss from the first audience positions to the last audience positions exceeds this limit. The maximum SPLs are rather low in favor of the flat frequency responses taking the high frequency level decrease into account and not allowing gains larger than 0 dB.

4.4 LAVDO Driving Functions

In Fig. 8 the transfer functions' levels and group delays are visualized for the LAVDO case from Sec. 4.3 with the goal (ii) of achieving a constant SPL with a tolerance of ± 3 dB at all audience positions. They are shown for a straight LSA configuration.

Low pass characteristics can be observed for the low as well as mid frequency way level in Fig. 8. Compensating for the decreasing SPLs with increasing frequency, high pass analogies are observable for the high frequency way levels. For the frequency transitions between the low and mid

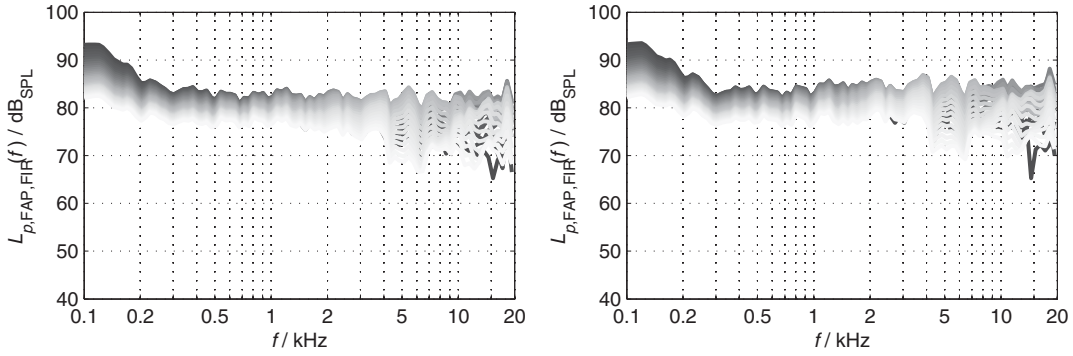

(a) straight LSA (b) curved LSA

Fig. 7. Line source array venue slice drive optimization (LAVDO) with optimization goal (ii): achieve a constant SPL with ±3 dB tolerance at all audience positions. SPL frequency responses at all audience positions (FAP) for the line source array driven with the calculated FIR filters for the straight (a) and curved (b) configuration with the tilt angles from Sec. 1.1 are shown. In the SPL frequency responses at all audience positions, the curves become brighter from the first to the last audience position.

frequency as well as between the mid and high frequency range, the driving functions of both frequency ways affect the SPL frequency responses at the receiver positions. The mid frequency magnitude and phase frequency response values for low frequencies—where the influence of the mid frequency cabinets are small—result from extrapolation of the mid frequency values from the frequencies where the influence of the mid frequency cabinets is significant. Except for a small low frequency range, the group delays do not exceed 6 ms. Note that the extracted pre-delays are not shown for this optimization case.

5 DISCUSSION

In Table 1 the most significant characteristics of the three presented optimization methods in this article are summarized. Considering these, it shows that the least-squares algorithm with Tikhonov regularization and the multiobjective goal attainment method require extensive post-processing and/or re-optimizations for obtaining smooth magnitude and phase frequency responses. This is due to performing the optimizations at discrete frequencies. Although it is possible to include constraints that connect nearby frequencies, the choice of a reference value is not obvious, i.e., which frequency and which amplitude and phase shall serve as the reference. Since these approaches incorporate complex optimizations, combined for the magnitudes and phases, the magnitude and phase effects cannot be clearly distinguished after the optimizations.

Comparing the mid frequency driving functions of the numerical optimization schemes in Figs. 4b and 5b with the driving functions of the presented mixed analytical-numerical approach LAVDO in Fig. 8c, the deviations between the driving function magnitudes for different loudspeakers and for different frequencies can be clearly seen for the numerical methods. For LAVDO, the increased smoothness of the magnitude frequency responses in Fig. 8c is obvious considering different loudspeakers and different frequencies.

Applying the least-squares algorithm with Tikhonov regularization from Sec. 3.1 it is not possible to set constraints on all individual sources but only on several ones together. Therefore, the resulting power loads of the individual drivers must be carefully monitored. This is one considerable drawback of the deployed loudspeaker weight energy algorithm.

With the multiobjective goal attainment approach, separate optimization constraints can be selected for the individual sources and several goals can be pursued weighted according to the intended priority. This includes the practically relevant control of the driver efficiency and the driver power balance by including corresponding constraints. Utilizing the advantages of the multiobjective goal attainment method and reducing the computational costs, the presented mixed analytical-numerical approach LAVDO restricts the solution space in advance, avoiding extensive post-processing and avoiding non-smooth frequency responses.

For all driving function optimization schemes, the choice of the desired sound field or rather the intended wavefront shape is crucial. While analytically exact sound fields may be advantageous for modeled loudspeaker data, the desired sound fields should, in practice, rather be based on a feasible solution, such as, the sound fields generated by a uniformly driven LSA used here or manually pre-adjusted setups. Using measured loudspeaker data, this approach incorporates the specific radiation characteristics of the considered LSA and it does not force the magnitudes and phases to differ significantly from the measured values, i.e., the influence of the FIR filters is kept low. With a low influence of the FIR filters, the impact of the uncertainties of the measurement data and of the geometric source-receiver configuration may also be limited. This approach restricts the freedom of the optimization algorithms resulting in fewer potential solutions and also reduces the amount of physically unrealizable solutions.

For the design of practical FIR filters the chosen frequency resolution is important. A linearly-spaced frequency vector is necessary for performing the inverse discrete

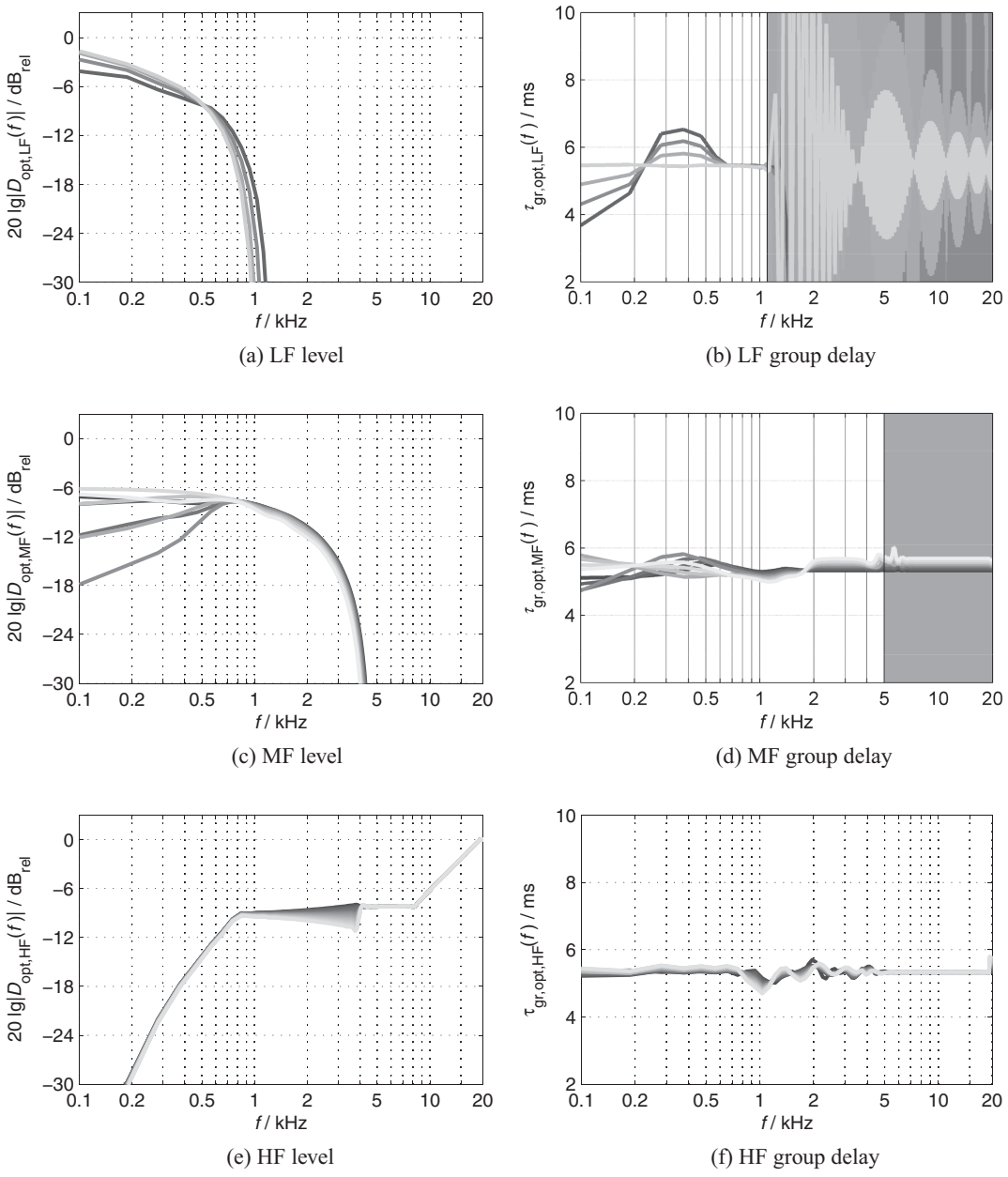

Fig. 8. Driving functions for the line source array venue slice drive optimization (LAVDO) with straight LSA from Fig. 7, left. Level responses (a), (c), (e) and group delays (b), (d), (f) of all loudspeakers of the different frequency bands ((a), (b): low frequency sources, (c), (d): mid frequency sources, (e), (f): high frequency sources) are shown. The optimization goal (ii) is to achieve a constant SPL with ±3 dB tolerance at all audience positions from Sec. 4.3. In the plots, the curves become brighter from the topmost to the bottommost LSA enclosure. Parts of the group delays that are irrelevant due to the working range of the different frequency bands are charted gray.

Fourier transform. Due to performance reasons with respect to the optimization schemes and due to perceptual reasons, it is convenient to cover the audio bandwidth with a logarithmically-spaced frequency vector. The logarithmically-spaced vector thus has to be converted to a linear scale before generating the FIR filter coefficients.

6 CONCLUSION

In this article different optimization approaches for the electronic drive of line source arrays (LSAs) are applied for exemplary sound reinforcement setups. These methods include the least-squares optimization with Tikhonov regularization, the multiobjective goal attainment approach, and the line source array venue slice drive optimization (LAVDO) that is introduced as a mixed analytical-numerical approach in this contribution. Both straight and curved LSA configurations are examined based on measured loudspeaker directivity and sensitivity data. The optimizations are performed for audience and non-audience positions along the vertical venue slice. As a last step, the conversion from the calculated individual loudspeakers' driving functions to practical finite impulse response filters is considered.

Table 1. Comparison of the discussed optimization methods for sound reinforcement with LSAs.

optimization method	least-squares optimization with Tikhonov regularization	multiobjective goal attainment approach	mixed analytical-numerical approach (LAVDO)
optimization goals	only one optimization goal	several optimization goals are possible	several optimization goals are possible
optimization constraints	separate constraints on individual sources are not possible	separate constraints on individual sources are possible	separate constraints on individual sources are possible
power limitation	no limitation of the maximum tolerated electric power of the individual sources	limitation of the maximum tolerated electric power of the individual sources is possible	limitation of the maximum tolerated electric power of the individual sources is possible
load balance	resulting loads must be carefully monitored for practically feasible drive	range of the resulting loads can be easily controlled	range of the resulting loads can be easily controlled
frequency smoothness	cannot be directly controlled	cannot be directly controlled	can be easily controlled
complexity	simple optimization scheme	elaborate optimization scheme	elaborate optimization scheme
computational efficiency	mid load	high load	low load

Smooth amplitude and phase frequency responses are necessary when dealing with uncertainties of the measurement data and of the geometric source-receiver configuration as well as for the FIR filter design in order to obtain moderate filter lengths. The introduced LAVDO approach ensures smooth responses as the magnitudes and phases are fitted separately to predetermined curves. Since the numerical refinement does not operate frequency-wise and since the calculation of the initial solutions is based on analytical considerations excluding physically unfeasible solutions in advance and furthermore allowing broad parameter control, extensive post-processing and/or re-optimizations can be avoided. Therefore LAVDO turns out to be more aim-oriented, more robust and lower-computational than the considered least-squares optimization and the pure multiobjective goal attainment approach.

The optimization results show that the desired sound fields can be realized with straight as well as curved LSA setups. If the array is not geometrically adapted to the audience zone, small source distances are, however, necessary for grating lobe free beam steering up to the highest audio frequencies. Therefore it seems to be reasonable to find a meaningful interaction of geometric and electronic wavefront shaping using LSAs for practical realizations with respect to technical and economical considerations. The electronic influence and hence the applied optimization algorithms can be kept to a manageable level if the LSA geometry is appropriately adapted to the sound reinforcement area.

For the future, it is planned to consider additional LAVDO optimization goals and to combine these within the numerical computation in order that an absolute weighting between the different goals is possible. It is also planned to examine whether the curve fitting within the LAVDO approach should be directly based on the filter coefficients and not on the associated driving functions, i.e., combining the calculation of the driving functions and the subsequent FIR filter design to be one single stage. Wave field synthesis based initial solutions shall be incorporated rather than initial solutions found by far-field considerations.

7 REFERENCES

[1] D. Scheirman, "Large-Scale Loudspeaker Arrays: Past, Present, and Future (Part Two—Electroacoustic Considerations)," presented at the *AES 59th International Conference: Sound Reinforcement Engineering and Technology* (2015 Jul.), conference paper 1-3.

[2] M. Urban, C. Heil, and P. Bauman, "Wavefront Sculpture Technology," *J. Audio Eng. Soc.*, vol. 51, pp. 912–932 (2003 Oct.).

[3] M. S. Ureda, "Analysis of Loudspeaker Line Arrays," *J. Audio Eng. Soc.*, vol. 52, pp. 467–495 (2004 May).

[4] L'Acoustics, "Training Module Variable Curvature Line Source," L'Acoustics (2016).

[5] T. Betlehem and C. Withers, "Sound Field Reproduction with Energy Constraint on Loudspeaker Weights," *IEEE Trans. on Audio, Speech, and Language Processing*, vol. 20, no. 8, pp. 2388–2392 (2012 Oct.).

[6] J.-W. Choi and Y.-H. Kim, "Generation of an Acoustically Bright Zone with an Illuminated Region Using Multiple Sources," *J. Acoust. Soc. Am.*, vol. 111, no. 4, pp. 1695–1700 (2002 Apr.), doi:https://doi.org/10.1121/1.1456926.

[7] G. W. van Beuningen and E. W. Start, "Optimizing Directivity Properties of DSP Controlled Loudspeaker Arrays," *Proc. of the Inst. of Acoustics: Reproduced Sound*, vol. 22, no. 6, pp. 17–37 (2000).

[8] M. Terrell and M. Sandler, "Optimizing the Controls of a Homogenous Loudspeaker Array," presented at the *129th Convention of the Audio Engineering Society* (2010 Nov.), convention paper 8159.

[9] D. de Vries, E. W. Start, and V. G. Valstar, "The Wave Field Synthesis Concept Applied to Sound Reinforcement: Restrictions and Solutions," presented at the *96th*

Convention of the Audio Engineering Society (1994 Feb.), convention paper 3812.

[10] E. W. Start, "Application of Curved Arrays in Wave Field Synthesis," presented at the *100th Convention of the Audio Engineering Society* (1996 May), convention paper 4143.

[11] F. Schultz, G. Firtha, P. Fiala, and S. Spors, "Wave Field Synthesis Driving Functions for Large-Scale Sound Reinforcement Using Line Source Arrays," presented at the *142nd Convention of the Audio Engineering Society* (2017 May), convention paper 9722.

[12] Martin Audio Ltd., "User Guide. Display 2.2, version 3.2," Tech. rep., https://martin-audio.com/downloads/software/Display-2.2-User-Guide-v3.2.pdf, last seen on 2017-08-21 (2017).

[13] Eastern Acoustic Works Inc., "EAW Resolution 2. Help File," Tech. rep., http://eaw.com/docs/3_Manuals/EAW%20Resolution%202%20User%20Guide.pdf, last seen on 2017-08-21 (2017).

[14] d&b Audiotechnik GmbH, "ArrayCalc Simulation Software V8. ArrayProcessing Feature, Technical White Paper," Tech. rep., http://www.dbaudio.com/en/support/downloads/category/download/4195.html, last seen on 2017-08-21 (2017).

[15] AFMG Technologies GmbH, "AFMG FIRmaker. AFMG White Paper," Tech. rep., http://www.afmg-support.eu/SoftwareDownloadBase/FIRmaker/FIRmaker_White_Paper.pdf, last seen on 2017-08-21 (2017).

[16] A. Thompson, "Real World Line Array Optimisation," *Proc. of the Inst. of Acoustics*, vol. 30, no. 6 (2008).

[17] A. Thompson, "Improved Methods for Controlling Touring Loudspeaker Arrays," presented at the *127th Convention of the Audio Engineering Society* (2009 Oct.), convention paper7828.

[18] A. Thompson, J. Baird, and B. Webb, "Numerically Optimized Touring Loudspeaker Arrays—Practical Applications," presented at the *131st Convention of the Audio Engineering Society* (2011 Oct.), convention paper 8511.

[19] S. Feistel, M. Sempf, K. Köhler, and H. Schmalle, "Adapting Loudspeaker Array Radiation to the Venue Using Numerical Optimization of FIR Filters," presented at the *135th Convention of the Audio Engineering Society* (2013 Oct.), convention paper 8937.

[20] F. W. Gembicki and Y. Y. Haimes, "Approach to Performance and Sensitivity Multiobjective Optimization: The Goal Attainment Method," *IEEE Trans. on Automatic Control*, vol. 20, no. 6, pp. 769–771 (1975 Dec.).

[21] D. G. Meyer, "Computer Simulation of Loudspeaker Directivity," *J. Audio Eng. Soc.*, vol. 32, pp. 294–315 (1984 May).

[22] S. Feistel, A. Thompson, and W. Ahnert, "Methods and Limitations of Line Source Simulation," *J. Audio Eng. Soc.*, vol. 57, pp. 379–402 (2009 Jun.).

[23] F. Straube, F. Schultz, D. A. Bonillo, and S. Weinzierl, "An Analytical Approach for Optimizing the Curving of Line Source Arrays," *J. Audio Eng. Soc.*, vol. 66, pp. 4–20 (2018 Jan./Feb.), doi:https://doi.org/10.17743/jaes.2017.0043.

[24] F. Straube, F. Schultz, M. Makarski, S. Spors, and S. Weinzierl, "Evaluation Strategies for the Optimization of Line Source Arrays," presented at the *AES 59th International Conference: Sound Reinforcement Engineering and Technology,* (2015 Jul.), conference paper 2-1.

[25] F. Schultz, F. Straube, and S. Spors, "Discussion of the Wavefront Sculpture Technology Criteria for Straight Line Arrays," presented at the *138th Convention of the Audio Engineering Society* (2015 May), convention paper 9323.

[26] G. A. Deschamps and H. S. Cabayan, "Antenna Synthesis and Solution of Inverse Problems by Regularization Methods," *IEEE Trans. on Antennas and Propagation*, vol. 20, no. 3, pp. 268–274 (1972 May).

[27] Y. Kim and P. Nelson, "Optimal Regularization for Acoustic Source Reconstruction by Inverse Methods," *J. Snd. Vibr.*, vol. 275, no. 3, pp. 463–487 (2004 Aug.).

[28] F. W. J. Olver, D. W. Lozier, R. F. Boisvert, and C. W. Clark, *NIST Handbook of Mathematical Functions*, 1st ed. (Cambridge University Press, Cambridge, 2010).

[29] L. E. Kinsler, A. R. Frey, A. B. Coppens, and J. V. Sanders, *Fundamentals of Acoustics*, 4th ed. (Wiley, New York, 2000).

[30] A. V. Oppenheim, R. W. Schafer, and J. R. Buck, *Discrete-Time Signal Processing*, 2nd ed. (Prentice-Hall, New Jersey, 1999).

THE AUTHORS


Florian Straube


Frank Schultz


Michael Makarski


Stefan Weinzierl

Florian Straube received the Dipl.-Ing. degree in electrical engineering/communications and information technology from TU Dresden in cooperation with Klippel GmbH in 2013. Since 2014 he has been working as a research associate at Audio Communication Group at TU Berlin focusing on sound field synthesis and line source array applications for sound reinforcement.

•

Frank Schultz received the M.Sc. degree from TU Berlin and the Dr.-Ing. degree with distinction from the University of Rostock in 2011 and 2016, respectively. Within postdoctoral research he works with the Audio Communication Group at TU Berlin and the Institute of Electronic Music and Acoustics in Graz. From 2003–2007 he worked in R&D at Bosch Communications Systems and from 2016–2018 at sonible GmbH. Recent research interests are acoustic signal processing for and perceptual evaluation of large-scale sound reinforcement.

•

Michael Makarski received the Dipl.-Ing. degree in electrical engineering in 2001 and the Dr.-Ing. degree from the RWTH Aachen University in 2006. Since 2006, he works as a freelancer with focus on the development of professional loudspeakers, acoustic measurement technique, and acoustic consulting. He is one of the founders of Four Audio GmbH & Co. KG. Since 2007, Four Audio develops and produces DSP solutions, software, and measurement technique for professional audio applications.

•

Stefan Weinzierl is head of the Audio Communication Group at TU Berlin. His activities in research are focused on audio technology, virtual acoustics, room acoustics, and musical acoustics. He is coordinating a master program in audio communication and technology at TU Berlin and teaching Tonmeister students at the University of the Arts (UdK). With a diploma in physics and sound engineering and a two-year study in musicology at UC Berkeley, he received his Ph.D. from TU Berlin. He is coordinating research consortia in the field of virtual acoustics (SEACEN) and music information retrieval (ABC_DJ).